74
9/2/97 JSD (1)

ANL-97/13

Chemical Technology Division

Annual Technical Report

1996

Applying Chemical Innovation to Environmental Problems

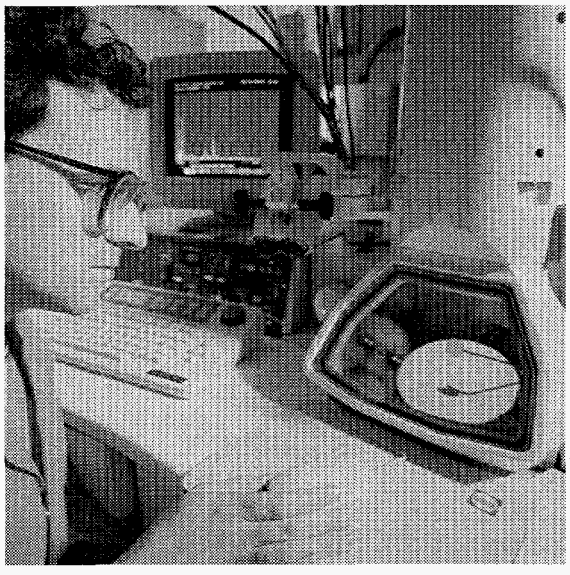

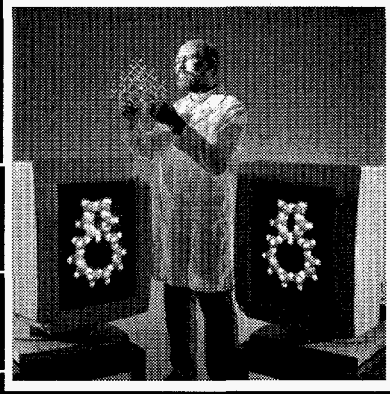

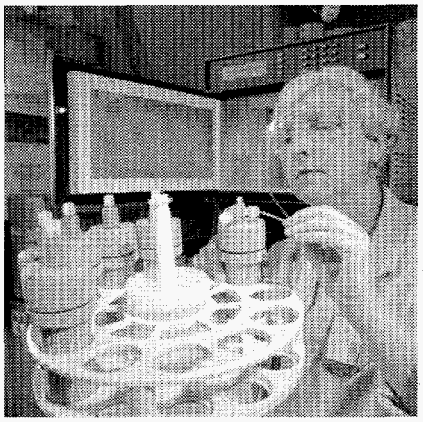

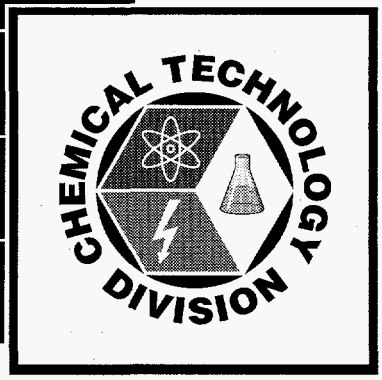

Argonne National Laboratory

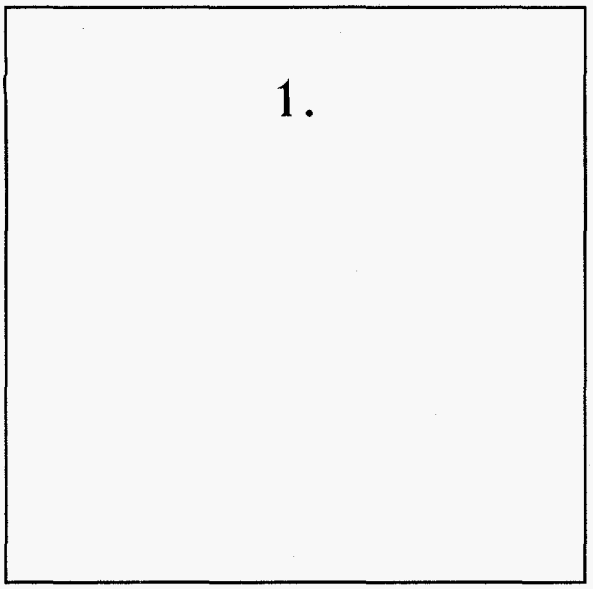

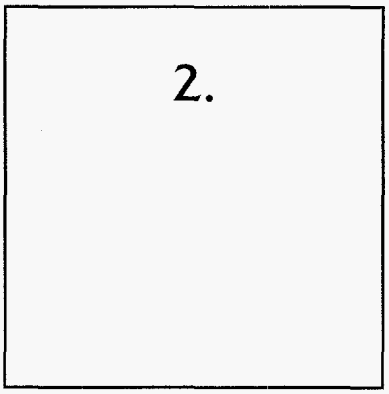

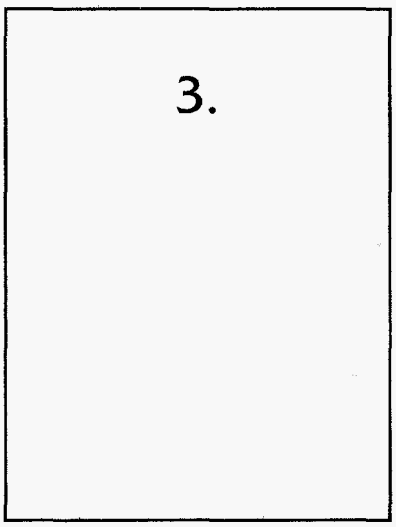

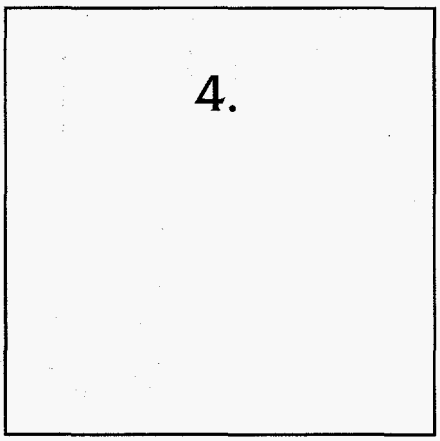

Cover Description

1. Analytical transmission electron microscope used for studying reacted samples of nuclear waste glass and spent fuel in the Waste Management Programs.
2. Molecular models used in theoretical studies of materials properties as part of the Electrochemical Technology and Basic Science Programs.
3. Uranium deposited on cathode by electrometallurgical treatment developed in the Nuclear Technology Programs.
4. Microwave digestion apparatus employed for sample analysis in the Analytical Chemistry Laboratory.

Disclaimer

Printed in the United States of America

This report has been reproduced from the best available copy.

Available to DOE and DOE contractors from the Office of Scientific and Technical Information
P.O. Box 62
Oak Ridge, TN 37831
Prices available from (423) 576-8401, FTS 626-8401

Available to the public from the National Technical Information Service
U.S. Department of Commerce
5285 Port Royal Road
Springfield, VA 22161

ANL-97/13

Argonne National Laboratory
9700 South Cass Avenue
Argonne, IL 60439

1996

Chemical Technology Division

Annual Technical Report

J. J. Laidler — Division Director
K. M. Myles — Associate Division Director
D. W. Green — Associate Division Director
C. C. McPheeters — Associate Division Director

June 1997

TABLE OF CONTENTS

TABLE OF CONTENTS (contd)

TABLE OF CONTENTS (contd)

TABLE OF CONTENTS (contd)

1996

Chemical Technology Division

Annual Technical Report

Abstract

The Chemical Technology (CMT) Division is a diverse technical organization with principal emphases in environmental management and development of advanced energy sources. The Division conducts research and development in three general areas: (1) development of advanced power sources for stationary and transportation applications and for consumer electronics, (2) management of high-level and low-level nuclear wastes and hazardous wastes, and (3) electrometallurgical treatment of spent nuclear fuel. The Division also performs basic research in catalytic chemistry involving molecular energy resources, mechanisms of ion transport in lithium battery electrolytes, materials chemistry of electrified interfaces and molecular sieves, and the theory of materials properties. In addition, the Division operates the Analytical Chemistry Laboratory, which conducts research in analytical chemistry and provides analytical services for programs at Argonne National Laboratory (ANL) and other organizations. Technical highlights of the Division's activities during 1996 are presented.

Summary

Electrochemical Technology

The CMT Division conducts research, development, testing, and technical evaluation studies of advanced power sources for vehicle propulsion, utility load-leveling, and other energy storage applications. The technical management of industrial contracts for the Department of Energy (DOE) is also being carried out on the development of fuel cells for transportation applications.

During the past year, the in-house battery R&D has focused on the lithium-polymer, lithium-ion, and nickel/metal hydride systems. Under a U.S. Advanced Battery Consortium program, the Division is working with 3M Corp. and Hydro-Québec to develop lithium-polymer batteries for transportation applications. These batteries show promise for meeting the demanding performance requirements of electric vehicles and operate at low temperature (typically 60°C). This development effort (proprietary) involves engineering studies, development of electrode materials, and electrochemical characterization of electrodes, cells, and multicell modules.

The lithium-ion battery operates at room temperature and is receiving increased attention as power supplies for consumer electronics and, in the longer term, electric vehicles. Our research on this system has focused on the use of a Li-Mn-O spinel, $LiMn_2O_4$, as a replacement for the present $LiCoO_2$ cathodes. There are concerns about the use of $LiCoO_2$ because of its high cost and safety hazards. The thermal stability of $LiMn_2O_4$ was studied by various *in situ* analytical methods. The data have provided important information on the processes that occur during $LiMn_2O_4$ synthesis and highlight the care that must be taken in controlling temperature to obtain single-phase spinel samples.

The nickel/metal hydride battery is a strong contender to replace the nickel/cadmium battery for transportation applications because of its superior performance and low impedance and the absence of toxic cadmium. However, the present nickel/metal hydride battery has several limitations, including long-term capacity loss caused by corrosion of the metal hydride electrode. A promising material for the metal hydride is La-Ni alloy with a small amount of aluminum. The behavior of selected $LaNi_{5-y}Al_yH_x$ electrodes was studied by extensive electrochemical measurements and *in situ* neutron diffraction measurements of a deuterated electrode during charge-discharge cycles. Electrochemical measurements indicated that the aluminum-containing alloy undergoes a capacity fade associated with the corrosion of aluminum in the alloy. Rietveld analyses of the neutron diffraction data indicated that $LaNi_5$ and its derivatives have a hexagonal space group structure containing two crystallographically distinct nickel sites, Ni(1) and Ni(2). In aluminum-substituted $LaNi_5$, the aluminum substitutes selectively on Ni(2) sites.

The Electrochemical Analysis and Diagnostic Laboratory in CMT includes a test laboratory to conduct battery evaluations under simulated application conditions. During 1996,

performance and life evaluations were conducted for nickel/metal hydride modules fabricated by Ovonic Battery Co. for the U.S. Advanced Battery Consortium and a variety of advanced lead-acid systems for the Electric Power Research Institute. In addition, Ovonic nickel/metal hydride cells were subjected to post-test analysis following life evaluations, and the results helped to identify specific areas where changes in design or the materials of construction would improve cell performance. Examinations were also completed for Commonwealth Edison Co. on lead-acid cells (used for standby power in nuclear generating stations) that had undergone an abrupt capacity fade. The root cause of this problem was identified.

Several types of advanced fuel cell are under development at CMT: high-temperature molten carbonate and solid oxide fuel cells for utility applications, and low-temperature solid oxide fuel cells for transportation applications.

In molten carbonate fuel cells, the present NiO cathodes have dissolution/precipitation problems that limit cell lifetime under pressurized operating conditions, and a search is underway for alternative conductive materials that are stable in the high-temperature (650°C) cell environment. Low electrical resistivity and stable cell performance (over 1700 h in small test cells) have been obtained with a $NiO\text{-}LiFeO_2$ cathode. Another problem with the present molten carbonate fuel cell is segregation of the $Li_2CO_3\text{-}K_2CO_3$ electrolyte. Tests with carbonate-wetted $LiAlO_2$ strips and 100-cm^2 cells indicated that electrolyte segregation could be minimized by use of a $Li_2CO_3\text{-}Na_2CO_3$ electrolyte. Work is also underway to develop materials that will prevent corrosion of the metal hardware in the molten carbonate fuel cell.

In the solid oxide fuel cell, the overpotential at the cathode/electrolyte interface has been recognized as an important limitation on performance. A project has been initiated to investigate which interface features and conditions contribute to cathode polarization in these fuel cells and, consequently, to determine optimal fabrication methods for the production of these cells. Test results indicated that total surface coverage of the electrolyte by the cathode may be a critical factor for improving cathode performance. Improved performance was also linked with increased cathode density near the cathode/electrolyte interface.

Also under development for the transportation application is a low-temperature (450-550°C) solid oxide fuel cell capable of running directly on methanol fuel, with a high tolerance for fuel impurities. Promising test results have been obtained in a cell with a gadolinium-doped ceria electrolyte and a $La_{1-x}Sr_xCo_yFe_{1-y}O_3$ cathode.

To aid the development of fuel cells for transportation applications, CMT staff are developing a fast-response fuel reformer that converts hydrocarbon fuels into a hydrogen-rich gas for use with low-temperature fuel cells (polymer electrolyte and phosphoric acid fuel cells). A bench-top methanol reformer based on partial oxidation has been built and tested. These tests have demonstrated that, with methanol, the reformer operates as anticipated—yielding a product gas of 50% H_2, 20% CO_2, and less than 0.5% CO (remainder H_2O). Test results also indicate that the partial oxidation reformer could serve as a startup burner for a methanol steam reformer and for a thermal management system in a fuel cell power plant for a transit bus. Effort is now being directed toward extending the usefulness of the reformer to paraffinic hydrocarbons.

Systems analysis and modeling of a methanol steam reformer (the type of reformer now being developed by General Motors Corp.) identified problems associated with dynamic power turndown from steady operation, and this shortcoming will need to be addressed by developing suitable control strategies.

A direct-methanol polymer electrolyte fuel cell is under development for small applications requiring a lightweight and easily portable power source. This work is focused on overcoming the two major obstacles to commercialization of this fuel cell: low electrocatalytic activity of the anode catalyst for the methanol oxidation reaction and transport of methanol through the polymer membrane to the cathode compartment.

The CMT Division continued to provide support to the DOE Office of Transportation Technologies and the DOE Office of Buildings Technology in the form of technical management of R&D contracts with industrial developers of fuel cells and related components. Major ongoing projects managed by CMT include contracts with General Motors Corp., Ford Motor Co., Chrysler Corp., and fuel-cell component suppliers.

Hazardous and Mixed Waste Research

A major challenge facing DOE is management of the massive quantity of hazardous and mixed (hazardous/radioactive) waste that has accumulated at various DOE sites as a result of nuclear-defense production and other activities conducted for more than four decades at these sites. A new technology, aqueous biphasic extraction, has been developed at CMT for removal of heavy metals and toxic materials from solid wastes and wastewater streams and is a prime candidate for large-scale application. The extraction systems are generated by combining an aqueous salt solution with an aqueous polymer solution such as polyethylene glycol. Fundamental studies of aqueous biphase formation have led to an equation for predicting the cloud point of polymer-salt solutions. Aqueous biphasic extraction is currently being tested for removing lead from contaminated soil.

A design concept has been developed for an advanced electrochemical system that would destroy nitrate and nitrite from caustic high-level waste. Enhanced efficiency is achieved by the selective separation of sodium nitrate and nitrite from the waste feed by aqueous biphasic extraction, followed by reduction to N_2 in an electrochemical cell.

Staff in CMT are evaluating advanced sol-gel processes for the recovery of fine particles from the aqueous process streams generated in treating high-level tank wastes. Early indications are that sol-gel processes should be capable of recovering more than 99.999% of all particulates in an aqueous waste slurry, with more than 90% of salts (e.g., nitrate, nitrite, sulfate) being diverted to a separate aqueous stream.

The Waste Isolation Pilot Plant (WIPP) in Carlsbad, New Mexico, has been selected as a possible disposal site for transuranic radioactive wastes resulting from defense-related activities at DOE sites. Work for this project in this past year involved determining actinide stability and solubility in various simulated WIPP brines. One finding from these studies is that steady-state concentrations of uranium are established in WIPP brine when carbonate complexation is not

significant. The low steady-state concentrations indicate that uranium phases are being precipitated from solution. These data are being used to test the Actinide Source Term model being developed for the WIPP project.

The interactions of multivalent actinide species with bacteria are being investigated as part of a larger effort to identify key processes that lead to both the immobilization and mobilization of actinide species in subsurface groundwaters on DOE sites. Effort was devoted to determining the interaction of the Pu(IV)-nitrilotriacetic acid (NTA) complex with the NTA-degrading microbe *Chelatobacter heintzii* in aqueous solution. The radiotoxicity of plutonium toward *C. heintzii* was shown to be primarily radiolytic in nature. However, the presence of plutonium did not significantly affect the initial biodegradation of NTA. In time, the plutonium became associated with the biomass through at least two distinguishable mechanisms, depending upon the plutonium concentration. These results point to the importance of biotic processes in the fate of plutonium in the subsurface.

Crystalline silicotitanate is being considered for extracting cesium from aqueous waste streams generated during the processing of high-level wastes at DOE facilities. In CMT several processing options are being studied for separating the extracted cesium from the silicotitanate with the goal of incorporating the cesium into a high-level waste form and the silicotitanate into a low-level waste form. Promising results have been obtained by contacting cesium-loaded silicotitanate with a molten potassium or sodium salt. In another project, phosphate ceramic waste forms are being evaluated for solidifying DOE's mixed low-level radioactive waste. Prototypical samples of the waste form are being tested for radiolytic hydrogen production, an important safety issue for storage and transport of this waste form.

Nuclear Waste Programs

Work is being performed to support programs on the disposal of high-level nuclear waste and spent fuel in the candidate repository site at Yucca Mountain in southwestern Nevada. Several series of laboratory tests are being performed to determine the corrosion behavior of high-level waste glasses upon exposure to liquid water or water vapor. The purpose of these tests is to determine the corrosion behavior of high-level radioactive waste forms under the hydrologically unsaturated conditions anticipated at the proposed Yucca Mountain site. These tests are designed to assist DOE in demonstrating that the Defense Waste Processing Facility (DWPF) and the West Valley Demonstration Project (WVDP) will produce a waste glass product that will perform well in an unsaturated environment typical of what may be expected at Yucca Mountain.

In one series, long-term tests are underway with radioactive sludge-based and simulated nuclear waste glasses having three compositions (SRL 131, 165, and 200). Test conditions include a temperature of 90°C and ratios of glass surface area to water volume (S/V) of 340, 2000, and 20,000 m^{-1}. In tests up to five years at 340 and 2000 m^{-1}, both the radioactive and nonradioactive SRL 131 glasses have reached the stage where the alteration phases affect the corrosion rate, while the SRL 165 and 200 glasses have not yet reached this stage. Also, alteration phases that increase the glass dissolution rate formed after about one year in tests at

20,000 m^{-1} with nonradioactive SRL 200, but have not yet formed with the radioactive counterpart.

In another series, static dissolution tests at S/V ratios of 10 to 20,000 m^{-1} with SRL 131 and 202 glasses have been in progress for six years. The results indicate that more advanced stages of corrosion are attained in tests at high S/V than in tests at low S/V after the same reaction time. Another important finding was that the dissolution rate of the glass increases significantly after certain alteration phases form in tests at 2000 and 20,000 m^{-1}. Other test series are in progress to measure the long-term dissolution rate and study the corrosion behavior of Environmental Assessment glass, which is the benchmark glass for DWPF glasses, and a radioactive glass made from the sludge in DWPF Tank 51.

Long-term drip tests are underway with glasses representative of those that may be produced at DWPF. The data after nine years of testing indicate that insoluble elements, including U, Pu, and Am, are incorporated into alteration phases as the glass reacts and are subsequently released with particulate or colloidal matter as the alteration products spall from the glass. Recent trends have shown that the releases of Pu and Am, while initially quite low compared to those of soluble elements (such as B and Np), eventually are accelerated as the alteration phases spall from the glass surface and enter the test solution. A similar multiyear test series with a WVDP-type glass has indicated that a thorium-rich alteration phase appears to play a substantial role in the corrosion behavior of this glass.

The DOE is examining options for placing surplus plutonium from the weapons program into a form that is unattractive and inaccessible for use by others. As part of this program, CMT has developed an alkali-tin-silicate (ATS) glass into which 5 wt% high-fired plutonium oxide can be dissolved. Various dissolution tests have been performed with this glass, and the results to date have been very encouraging.

Besides the glass studies, long-term tests with unirradiated UO_2 pellets and spent fuel are in progress to determine radionuclide release rates when these materials are exposed to repository-relevant conditions. Results from over 11 years of drip tests with UO_2 pellets indicate that uranium release was rapid during the first one to two years of testing and has remained relatively low in the remaining testing period. The element release patterns indicate that the majority (86-97%) of the released uranium was sorbed or precipitated on the walls of the stainless steel vessel and the Teflon support stand used in testing. From 1 to 12% of the released uranium was present as >5 nm particles suspended in the leachate, with alteration phases such as uranophane and boltwoodite being detected as filter residues. Tests have been ongoing for almost four years with spent fuel samples (ATM-103) under drip conditions. The results indicate that ^{99}Tc release may serve as an indicator of fuel matrix dissolution, that a surface reaction may be the rate-controlling mechanism for fuel reaction under unsaturated conditions, and that through-grain dissolution of the UO_2 fuel matrix may dominate over grain-boundary-enhanced dissolution at this testing time.

Tests were performed to investigate the use of a glass-crystal waste form for treating mixed low-level nuclear and hazardous wastes. Results from Product Consistency Tests and the Toxicity Characteristic Leaching Procedure with glass-crystal composites indicate excellent

durability compared with borosilicate glasses. Also being tested are low-level waste glasses from Pacific Northwest National Laboratory and cement mortar formulations from Applied Innovation Inc.

Separation Science and Technology

The Division's work in separation science and technology is concerned with (1) developing methods for treating radioactive, mixed, and hazardous waste and (2) determining the feasibility of substituting low-enriched uranium for the high-enriched uranium currently used in the production of ^{99}Mo for medical applications.

The main project in the first area involves R&D on solvent extraction processes, namely, TRUEX (transuranic extraction) and CSEX (cesium extraction) combined with SREX (strontium extraction) for the cleanup of acidic nuclear waste solutions. Work on the TRUEX process focused on advising engineers at Idaho National Engineering Laboratory (INEL) on their demonstration of this process on actual high-level waste stored at the site. The demonstration was successfully completed with a 24-stage centrifugal contactor built at ANL. After the demonstration, the test results were analyzed by the Generic TRUEX Model developed in CMT. The actinide removal efficiency in the aqueous raffinate was determined to be 99.97%, so that its alpha activity was 0.12 nCi/g, well below the Nuclear Regulatory Commission requirement of <100 nCi/g for non-transuranic waste. In a collaborative project with the ANL Chemistry Division, workers in CMT are also providing modeling support and testing countercurrent flowsheets for the combined CSEX-SREX process. Testing combined with model calculations indicated that this process has considerable potential for removing ^{137}Cs and ^{90}Sr from acidic waste solution, such as that presently stored at INEL.

In other projects, the Division assisted in the installation, testing, and commissioning of a new evaporator system for treating the underground-storage-tank waste at Oak Ridge National Laboratory; conducted studies on concentrating an aqueous slurry effluent from an incinerator built at Savannah River Site for the combustion of hazardous, low-level radioactive, and mixed wastes; and assisted in the development, fabrication, and startup of waste treatment facilities for liquid transuranic- and organic-containing wastes at Argonne.

A new concept, a continuous countercurrent solid-liquid contactor, was developed for carrying out waste-treatment batch operations where (1) thorough mixing and then separation of liquid and solid phases are essential, and (2) countercurrent movement of the two phases improves process efficiency. A two-stage solid-liquid contactor was tested for application to sludge washing. While the unit was not optimized for sludge washing, the results were much better than one would obtain from simple dilution. Additional work is needed to optimize the system.

A project is ongoing to develop a low-enriched uranium (LEU) target and a processing method for production of ^{99}Mo to be used for medical applications. During the past year, it was demonstrated that irradiated LEU foils can be dissolved in nitric acid alone instead of the current sulfuric/nitric acid mixture, and the barrier metals (Cu, Fe, or Ni) required between the LEU metal foil and target walls are also dissolved by nitric acid alone. The primary consideration for

converting the dissolver solution to nitric acid alone is facilitating waste treatment and disposal. The processing of a fully irradiated LEU metal foil is planned at a facility in Indonesia during 1997. Also under investigation is the basic dissolution of LEU metal targets with alkaline peroxide. An optimized procedure was developed to reduce the hydrogen peroxide consumed per mole of uranium dissolved by use of sequential additions of alkaline peroxide.

Electrometallurgical Treatment Technology

The CMT Division is developing an electrometallurgical process for treatment of spent nuclear fuels. It can handle most types of spent fuel and is especially intended for fuels at risk of chemical reaction with the groundwater in the repository. These "at risk" spent fuels include metal fuels with various cladding and matrix materials, reactive compounds, and highly enriched fuels. The central feature of the electrometallurgical treatment is electrorefining of the spent fuel in a molten salt electrolyte at 500°C. After electrorefining of the spent fuel, the fuel cladding and fission products are placed in two stable waste forms (one a ceramic, the other metal), which are suitable for disposal in a geologic repository. There are no other high-level wastes, and only negligible amounts of low-level waste are generated.

Development of the electrorefining process for deposition of uranium on a solid cathode is continuing. Experiments have been done to test the effectiveness of salt washing for removal of residual fission products from uranium dendrites deposited on the electrorefiner cathode. Salt samples were taken from the surfaces of the cathode product after two sequential washings. The results indicate that this technique holds promise for producing a "pure" uranium product (<1 ppm transuranics and <1 ppm fission products).

In the electrometallurgical treatment, one of the proposed high-level waste streams would be produced by trapping the noble metal fission products in the anodic dissolution baskets in the electrorefiner. Tests of anode baskets with and without a fine-mesh screen showed that both types yield about the same high degree of noble metal retention (about 90%) after the uranium in the spent fuel has been dissolved.

The feasibility of electrometallurgical treatment of oxide and metallic spent fuel has been demonstrated over the past several years. This treatment is now being investigated for use with aluminum alloy fuels, 128 metric tons of which will be shipped to the Savannah River Site over the next 40 years. An engineering-scale (6 kg of aluminum) electrorefiner for handling this type of fuel has been fabricated, and installation and testing will occur in 1997. Another potential application of the electrometallurgical treatment is with uranium fluoride fuel that was dissolved in a mixture of molten fluoride salts as part of the Molten Salt Reactor Experiment (MSRE) conducted at Oak Ridge National Laboratory. A laboratory-scale electrorefiner was fabricated and will be tested with MSRE waste salt in 1997.

An effort is underway to develop an advanced electrorefiner having high throughput (>40 kg uranium per hour) and large batch size (>100 kg). A high throughput electrorefiner is proposed for treating large quantities of spent fuel, such as the N-reactor fuel from the Hanford site. Effort this past year focused on developing a durable beryllia scraper to remove uranium

dendrites from the cathode tubes. This new design of scraper was successfully tested in a high throughput electrorefiner with 0.2-m dia.

In many pyrometallurgical processes for treating spent nuclear fuel, it is necessary to periodically scrub the fission products that accumulate in the molten salt. A nitride enhanced recovery method is being investigated as a means of improving the partitioning of actinide, lanthanide, and transition metal chlorides. This method involves formation of metal nitrides in a molten metal. Thermodynamic equilibrium calculations predicted that this method would decrease metal chloride concentrations to levels below parts per million and would remove strontium, a major fission-product heat source, from the molten salts. In an initial test, lanthanum metal was successfully extracted from molten zinc/Ca_3N_2 by conversion to LaN.

Ceramic and metal waste forms to contain the high-level waste from the electrometallurgical treatment are being developed, along with methods and equipment for isolation of waste components and fabrication of waste forms. The main pieces of isolation equipment are pyrocontactors for the selective redox removal of constituents from process fluids (mainly uranium from electrorefiner electrolyte) and zeolite ion-exchange columns for removal of waste components from the electrolyte. Single-stage pyrocontactors had previously been shown to be effective in conducting redox extractions between molten salt and liquid cadmium; this work was completed, then extended to operation and initial testing of a four-stage countercurrent device this year. Operation of a bench-scale zeolite ion-exchange column has shown the necessity of operation at very low flow rates and identified the advantages of operating at a relatively high temperature (> 525°C).

Those components of the high-level waste that are chemically unaffected by the electrometallurgical process—cladding hulls, zirconium alloying additions, and noble metal fission products—are combined with small amounts of particulate materials from electrolyte filters and melted to form a highly durable metal alloy waste form. Depending on the cladding (stainless steel or Zircaloy), the basic alloy composition is stainless steel-15 wt% zirconium (SS-15Zr) or Zircaloy-8 wt% stainless steel (Zr-8SS). The basic metallurgy of these alloys has been determined, methods and equipment for alloy fabrication have been developed, and physical properties have been measured. Corrosion testing is underway, and metallurgical studies are being completed; future work will emphasize support of waste form fabrication at the Fuel Conditioning Facility of ANL-West, long-term testing, and development of waste form qualification methods.

In routine process operation, it becomes necessary to remove transuranic elements and fission products from the electrorefiner electrolyte. This is done by passing the electrolyte through a zeolite ion-exchange column. The zeolite from the ion exchange column is separated mechanically from excess liquid salt as well as possible, then treated with "anhydrous" zeolite powder to incorporate all salt into the zeolite structure. For plant decommissioning or handling of miscellaneous excess molten salt, the salt can also be occluded directly into the powder. The resulting salt-filled zeolite is made into a sturdy monolithic waste form suitable for geologic disposal by mixing it with glass powder and hot-compacting at a sufficiently high temperature that the glass can flow. Considerable advances in waste form durability have been achieved in the past year by focusing on methods of fabricating the ceramic waste form.

Treatment of Spent Oxide Fuel

The electrometallurgical treatment of spent oxide fuels requires that the metal oxides first be reduced to metals that can be processed in the electrorefiner. A lithium reduction process has been selected to convert the spent oxide fuel into metals. In the process, the spent oxide fuel is reduced by reaction with lithium at 650°C in the presence of molten LiCl.

Laboratory-scale experiments have continued with the goal of better understanding the reduction process. Several areas of the process have been examined: (1) reduction times for different fuel types and sizes, (2) the amount of occluded salt in the uranium product and the amount of Li_2O in the occluded salt, and (3) reactions between Li_2O and ZrO_2 or zirconium with the formation of Li_2ZrO_3.

In the first area, it was found that steel-clad UO_2 pellets, 1.27 cm in length and 0.95 cm in diameter, could be completely reduced in approximately 50 h, whereas unclad pellets of the same dimension could be reduced in 30 h. When UO_2 pellets constitute the feed in the lithium reduction process, the pellet dimensions do not change during reduction. Because of the density difference between UO_2 and uranium, this condition results in the interior of the reduced pellet having voids. These voids are filled with salt that contains dissolved Li_2O. There is concern that the occluded salt may have a Li_2O concentration in excess of 3.3 wt%, a level that would cause incomplete reduction of PuO_2. As part of the second area, measurements of both the amount of occluded salt and its Li_2O content indicated that reduced UO_2 pellets, 0.79 cm in diameter and 1.43 cm in length, retained between 8 and 11% salt based on the mass of the reduced metal, and that this salt contained 8.7 wt% Li_2O. This concentration of Li_2O will have to be lowered, presumably by using smaller feed pellets, in order to effectively reduce PuO_2. Experiments to define an acceptable minimum feed size are in progress. In the third area, it was discovered that after lithium reduction of UO_2-ZrO_2 ceramics, such as exist in the central core region of the Three Mile Island (TMI-2) fuel debris, Li_2ZrO_3 was present in the product. Calculations, supported by experiment, suggest that the formation of Li_2ZrO_3 can be avoided by limiting the Li_2O concentration in the LiCl salt to less than 1.4 wt%.

The reduction salt used in the lithium process must be recycled to minimize the process wastes. This requires removal by electrowinning of the Li_2O that forms in the salt. One of the difficulties encountered in this work has been that the lithium and oxygen recombine in the electrowinning cell to produce Li_2O. This parasitic reaction has been in some cases so efficient as to leave no net lithium production. During this period, work has focused on developing two types of cathodes, liquid bismuth and porous metal, which effectively eliminate this problem. The liquid bismuth cathode prevents the lithium from floating on the salt surface by forming a Li-Bi alloy that keeps the lithium under the salt layer. The alloy effectively lowers the lithium activity in the system by factors of 1000 to 100,000. Experiments have demonstrated that the bismuth cathode is efficient in incorporating the lithium, and that the lithium can be removed from the alloy by electrotransport in a timely manner. The porous metal cathode has some advantages over the bismuth cathode in that the lithium is not alloyed and, hence, does not need an electrotransport step. It also effectively eliminates the need for ceramic components in the system. The porous metal cathode works because the lithium wets the porous metal (stainless steel) and is incorporated into the pores below the salt level. The lithium will not be released

from the cathode under normal operating conditions unless the pore capacity of the cathode is exceeded. Small- and large-scale laboratory experiments have demonstrated the effectiveness of the porous metal cathode.

An engineering-scale series of experiments is in progress to obtain design information and operating experience needed for scaling up the reduction and electrowinning processes to the plant size required for processing DOE oxide spent fuels. To meet this objective, the facility used for these experiments was designed to support the reduction of kilogram quantities of fuel. The engineering-scale demonstration of the reduction of synthetic corium (primarily UO_2 and ZrO_2) and simulated TMI-2 fuel debris was completed in September 1996. Results from this experiment indicate that the reduction of neither the corium nor the clad fuel rod segments was complete. This is believed to be due to an underestimation of reduction times based on the laboratory-scale experiments. The fuel basket, which consisted of an outer shell and an inner screen pouch that held the simulated fuel, worked well. It was possible to remove the fuel pouch containing the reduced product from the basket, allowing the basket to be reused in later experiments.

Basic Chemistry Research

Basic chemistry research is being pursued in several areas: fundamental chemistry associated with catalysis in systems that involve molecular energy resources, mechanisms of ion transport in lithium battery electrolytes, materials chemistry of electrified interfaces (in connection with corrosion and electrochemical devices) and molecular sieve materials, and the theory of materials properties.

Recent research in the catalysis program has focused on the catalytic chemistry of (1) phosphine-modified catalysts for the hydroformylation of olefins in supercritical fluids and (2) the extremely robust polyfluorophthalocyanine catalysts for hydrocarbon activation processes.

The various processes designed to achieve the commercial hydroformylation of olefins are the subject of the program's current efforts in supercritical fluid catalytic processes. Olefin hydroformylation catalysts based on dicobaltoctacarbonyl can be modified with tertiary phosphines to achieve greater stability and higher selectivity. These catalysts are used commercially to produce agricultural chemicals, industrial solvents, and detergents from olefinic feedstocks. Using *in situ* nuclear magnetic resonance (NMR) measurements that for the first time encompass the high pressures and high temperatures of the process, CMT researchers have determined the thermodynamics associated with a key hydride-formation step for the phosphine-modified catalyst.

Research in hydrocarbon activation is aimed at achieving the controlled catalytic functionalization of methane and other hydrocarbons via activation of their C-H bonds. Current research focuses on developing catalytic strategies based on the extremely robust phthalocyanine nucleus. During the past year, CMT researchers synthesized a dimeric oxo-bridged iron complex of a highly fluorinated phthalocyanine ligand and proved it to be an effective catalyst for the epoxidation of olefins and the hydroxylation of alkanes. A high-valent $Fe^{IV}=O$ complex of unusual stability was also prepared and characterized, and the oxidative properties of the oxo

oxygen atom studied. The Fe^{IV}=O complex is an intermediate in the iron porphyrin-catalyzed hydrocarbon oxidation.

Also, in a new initiative associated with the advancement of the lithium-polymer battery, ion transport mechanisms are being investigated by use of the *in situ* spectroscopic techniques developed for the catalysis research. The goal is to investigate the mechanism(s) of ion transport in lithium-polymer electrolyte battery materials by using *in situ* NMR imaging developed in the catalysis research. A persistent problem with the present generation of polymer electrolyte materials is that the bulk of the ionic current is carried by the anion. Accordingly, the electroactive lithium ions are rapidly depleted from the region adjacent to the cathode. This electrolyte depletion limits the active volume of the polymer film that is utilized and results in nonuniform discharge voltages. Nondestructive *in situ* spectroscopic techniques have been developed by CMT researchers for measuring ionic mobilities and the size of the electrolyte depletion zones. Distance resolution of 3 μm has been achieved with the NMR imager. Future work will include determining the effect of plasticizers, temperature, and alterations in the polymer backbone on the lithium ion transport properties.

The Division's materials science program continues to explore corrosion and interfacial electrochemistry and entails (1) development and implementation of *in situ* synchrotron X-ray methods to elucidate issues related to metal/aqueous solution interfaces, (2) theoretical studies of materials that emphasize both method development and application, and (3) integration of theoretical studies with laboratory experiments.

Synchrotron far infrared spectroscopy has been used to probe the influence of the pseudo halides OCN^- and SCN^- on passive film breakdown at the copper/aqueous solution interface. In another study, nickel oxide films deposited on graphite were found to increase the capacitance of the graphite by a factor of four. These films were deposited electrochemically and characterized by synchrotron X-ray absorption spectroscopy. An X-ray scattering study of the deposition of silver on platinum revealed that the silver deposit consisted of randomly distributed microcrystals. A detailed atomistic model of the incipient oxidation/reduction of the Pt(111) single-crystal surface, using synchrotron X-ray scattering measurements, confirmed the long-assumed place-exchange mechanism.

High-temperature/high-pressure measurements of the kinetics of the Cu^{2+}/Cu^{+} charge-transfer reaction between 25 and 100°C showed that the transfer coefficient (α) is independent of temperature ($\alpha = 0.57 \pm 0.04$) and yielded an electron transfer activation energy of 30 kJ/mol. The distance dependence of the coupling of a hydrated copper ion near a copper surface, determined by using extended Hückel theory, will be employed in the calculation of Cu^{2+}/Cu^{+} electron transfer rates carried out at the University of Minnesota for comparison with the experimental measurements made at ANL.

The homogeneous inner-shell electron transfer reaction, $Fe^{3+} + e^- \rightarrow Fe^{2+}$, facilitated by the bridging halide anions F^-, Br^-, and I^-, has been investigated by means of *ab initio* molecular orbital theory. These halide anions were found to give an increased coupling due to a closer approach distance than is possible for an outer-sphere water bridge, in agreement with what had

previously been reported for the inner-shell chloride bridge of the Cu^{2+}/Cu^{+} electron transfer reaction.

The set of reaction energies used to assess the performance of our quantum chemical computational methods has been extended to larger molecules and to a wider variety of systems. This new test set (148 molecules) was used to evaluate the accuracy of various versions of our Gaussian-2 (G2) theory and to compare calculations done with G2 and density functional theory (DFT) methods. While the G2 methods gave the best performance, the much more time-efficient DFT methods have reached the point where they are now an effective alternative for systems with a large number of atoms. The G2 and DFT methods have been employed in tandem to examine proton transfer between acid sites in zeolites and absorbed water molecules. Increasing the water loading in the zeolite from one per site to two or more per site was found to raise the rate of proton transfer.

Analytical Chemistry Laboratory

The Analytical Chemistry Laboratory (ACL) is administratively within CMT, its principal client, but collaborates as a full-cost-recovery service center with many technical divisions and programs at ANL. In addition, the ACL conducts research in analytical chemistry and provides analytical services for governmental, educational, and industrial organizations.

During the past year, ACL was involved in a diverse array of activities, including the following: analyses in support of the ANL project to develop an electrometallurgical treatment for spent nuclear fuels; continuous monitoring of the ANL-West plasma arc furnace developed to treat radioactive waste; characterization of products from the recycling of automobile shredder "fluff"; analyses in support of the development of high-temperature superconductors; testing of a wide variety of oils for their ability to remove radon from air; development of automated methods for real-time analysis of chemical sensor data from environmental samples; preparation and characterization of simulated waste samples in support of the Waste Isolation Pilot Plant; characterization of "orphan" waste materials from ANL that have unknown origins or inadequate documentation or that remain from programs no longer funded; characterization of used laboratory exhaust filters for disposal; testing of new instrumentation in support of a U.S. Army program on the stand-off detection of gaseous plumes; analysis for the U.S. Department of Agriculture of environmental samples under a former grain storage facility; development of analytical procedures that will be used to characterize the lability of transition metals in textile mill wastewater; analysis of U.S. currency bills for the presence of cocaine; analysis of samples from a pilot-scale test of a process to recycle aluminum salt cake; development of a new technology based on solid-phase extraction for radium determination in aqueous samples; development of a Fourier transform infrared sensor that has no moving parts and is extremely rugged and immune to vibrations; radiological characterization of the JANUS Biological Irradiation Facility being decommissioned at ANL; and characterization of samples from dry-storage casks containing spent nuclear fuel.

I

Electrochemical Technology

The ANL Electrochemical Technology Program in CMT undertakes (1) in-house research, development, testing, post-test analysis, and technical evaluation studies of advanced battery and fuel cell systems and (2) support research, technology transfer, and technical management for industrial R&D contracts to develop these systems. During the past year, in-house battery R&D has focused on lithium-polymer, lithium-ion, and nickel/metal hydride systems. The testing, evaluation, and post-test analysis of a variety of advanced batteries (e.g., lead-acid, nickel/metal hydride, sodium/sulfur) fabricated by industrial firms are performed in CMT's Electrochemical Analysis and Diagnostics Laboratory. Potential uses of these battery systems include vehicle propulsion, utility load-leveling, and other energy storage applications. In-house R&D is also being conducted on fuel cells, where the CMT Division continues to be the premier DOE laboratory in fuel-cell technology development. We are engaged in R&D on the solid oxide fuel cell and the molten carbonate fuel cell, which are targeted for utility applications, and we are becoming increasingly involved with R&D on the advanced fuel cell systems for transportation applications.

A. Advanced Battery Research and Development

1. Lithium-Polymer Electrolyte System

a. Project Overview

The lithium-polymer battery (LPB) is a lightweight, high-energy system that can operate at moderate temperatures (typically 60°C). With a polymer electrolyte, this all-solid-state battery can be manufactured by using high-speed film-laminate technology. The battery's low weight translates into high specific energy. The Li/Li^+ redox reaction (negative electrode, -3.0 V) gives the battery its high power. The positive electrode is a reversible chemical host for intercalating lithium cations. Thus, during discharge, the lithium cations insert into the host material with simultaneous electrochemical reduction of the host's closest-neighbor redox sites.

The host structure is highly reversible to both redox and insertion reactions; this allows the lithium cations to exit upon recharge.

As part of the U.S. Advanced Battery Consortium (USABC) program, we are developing the LPB for electric-vehicle applications under a Cooperative Research and Development Agreement (CRADA) with 3M Corp. and Hydro-Québec. Under the CRADA, ANL provides technical support related to all aspects of battery development, including component, cell, and battery testing and characterization; post-test diagnostic analysis; electrochemical cell modeling and battery design; and electrode materials evaluation and optimization.

Component and cell testing and characterization are carried out with electrochemical techniques such as DC methods (e.g., constant current or power discharge, peak power measurements, and current interruptions), Dynamic Stress Tests, and AC impedance methods. The purpose of these investigations is to develop a better understanding of the cell characteristics and to provide the critical information needed to focus the future research efforts on improving and optimizing the LPB performance.

In the post-test studies, the initial focus has been the destructive evaluation of fractured and/or peeled cells by electron and optical microscopy. The investigation of state-of-the-art nondestructive techniques has also begun. These newer methods may provide us with a better means for conducting post-test analysis. The overall goal is to precisely determine the factors affecting the electrochemical performance of cells.

Electrochemical modeling of LPB cells has been initiated to elucidate the phenomena occurring in the cells during operation. The time constant for the lithium transport in the lithium polymer cells is relatively large when compared to liquid electrolyte battery systems. This is a result of the slow ionic transport in the polymer electrolyte and the cathode active material. These phenomena are difficult to separate and examine experimentally because of the long time constant; the composite cathode structure of carbon, electrolyte, and active material; and the thin cell geometry.

b. System Description and Research Directions

Rechargeable lithium batteries with either metallic lithium or lithium carbon as the anode use transition metal oxides as the cathode, for example, oxides of V, Mn, Co, or Ni. These transition metal oxide electrodes have host structures into which lithium can be inserted during electrochemical discharge; the insertion of lithium is accompanied by a concomitant reduction of the transition metal ion. The reverse process occurs during charge.

The structural stability of a host electrode to the repeated insertion and extraction of lithium is undoubtedly one of the key properties for ensuring that a lithium cell operates with good electrochemical efficiency. In transition metal oxides, both stability of the oxygen-ion array and minimum displacements of the transition metal cations in the host are required to ensure good reversibility. Also, structures of transition metal oxide insertion electrodes are, in general, not tolerant to overcharge or overdischarge. It is, therefore, critically important to carefully

control fabrication conditions so that the composition of the electrode corresponds to that of the most-stable host structure of the metal oxide system. Furthermore, cell operating conditions, such as voltage limits and current drain, must be carefully controlled to ensure that the structural integrity of the electrodes is not destroyed on cycling. Materials development within the LPB project is focused on the synthesis and characterization of metal oxide electrodes that offer superior electrochemical behavior to state-of-the-art materials. Results are proprietary.

2. *Lithium-Ion System*

Rechargeable lithium batteries are receiving increased attention as power supplies for consumer electronics, such as lap-top computers, camcorders, and cellular phones, as well as for electric vehicles in the longer term. Of particular interest today are "lithium-ion" batteries, as they are now generally known, which operate at ambient temperature and function by an electrochemical process during which lithium ions are shuttled between two host electrode structures during charge and discharge. In a DOE-supported project, we are investigating the use of Li-Mn-O spinels as a replacement for $LiCoO_2$ cathodes in 4-V rechargeable lithium-ion batteries. There are concerns about the $LiCoO_2$ because of its high cost and safety hazards.

The Li-Mn-O spinel electrodes can be synthesized chemically or electrochemically over a wide compositional range within the $LiMn_2O_4$-$Li_4Mn_5O_{12}$-λ-MnO_2 tie triangle of the Li-Mn-O phase diagram (see Fig. I-1). Of particular significance are the stoichiometric spinels that lie on the tie line between $LiMn_2O_4$ and $Li_4Mn_5O_{12}$; they can be represented by the general formula $Li_{1+\delta}Mn_{2-\delta}O_4$ ($0 \leq \delta \leq 0.33$). Lithium can be extracted from, and reinserted into, $Li_xMn_2O_4$ at

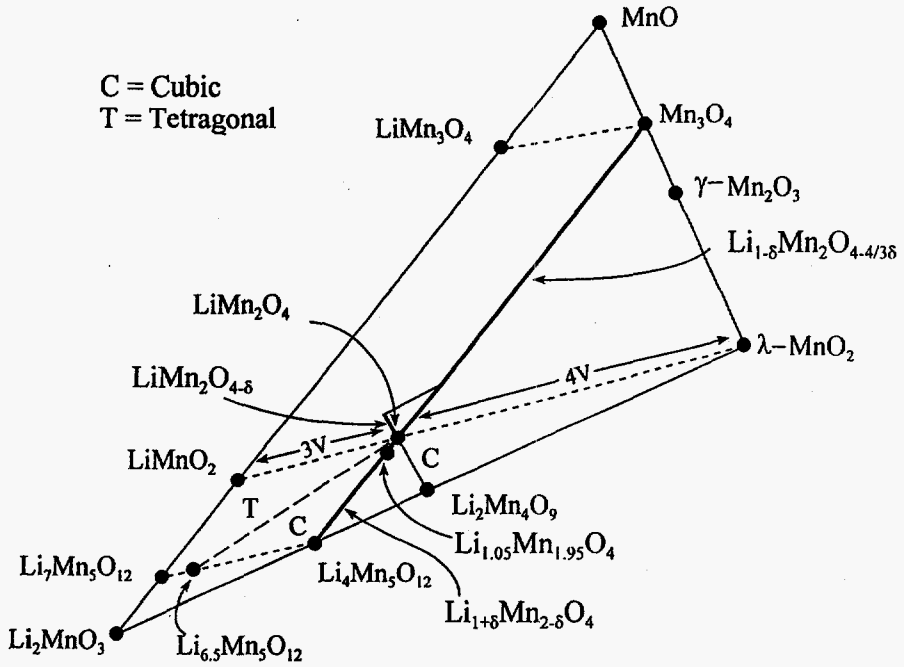

Fig. I-1. Phase Diagram for Li-Mn-O

approximately 4 V vs. metallic lithium over the range $0 \leq x \leq 1$. Therefore, $LiMn_2O_4$ is being considered as a possible alternative cathode material for commercial lithium-ion cells that currently use the significantly more expensive material, $LiCoO_2$. The cycling efficiency of the $LiMn_2O_4$ electrode at 4 V can be improved if a small amount of lithium replaces some manganese on the octahedral sites of the spinel structure, i.e., $Li_{1+\delta}Mn_{2-\delta}O_4$, typically with $0.03 \leq \delta \leq 0.33$.

When synthesizing these electrode materials at elevated temperatures, one must maintain rigid process control because of the wide range of solid solution that exists within the Li-Mn-O family of spinel compounds, and the fact that the composition of the spinel electrode material plays a pivotal role in controlling the rechargeability. In the past, much of the information about the structural stability of the spinel electrodes has been gathered from samples that had been quenched from high temperature or slowly cooled in a furnace. We have investigated the thermal stability of $LiMn_2O_4$ by *in situ* high-temperature X-ray diffraction (XRD), differential thermal analysis (DTA), and thermogravimetric analysis (TGA).

Figure I-2 shows a series of powder XRD patterns of a $LiMn_2O_4$ sample collected as a function of increasing temperature (40°C intervals). These data show that when cubic $LiMn_2O_4$ is heated to 1200°C, a number of discrete phases with different crystallographic structure types form as the temperature is raised:

- A spinel phase with tetragonal symmetry. This is reflected by the splitting of the [311] peak at 36°2θ of the cubic $LiMn_2O_4$ phase into the [311] and [113] peaks of the tetragonal phase at approximately 35 and 36°2θ. A *c/a* ratio of 1.02 was calculated from the lattice parameters of the tetragonal phase at 880°C, which indicates the degree of tetragonal distortion.
- A rock salt phase, Li_2MnO_3, with monoclinic symmetry, in which all the manganese ions are tetravalent. Figure I-2 shows that the Li_2MnO_3 phase exists up to ~1000°C.
- A rock salt phase, $LiMnO_2$, with orthorhombic symmetry, in which all the manganese ions are trivalent. Figure I-2 shows that the $LiMnO_2$ phase exists up to ~1120°C.
- A spinel phase in which a significant number of manganese ions occupy the tetrahedral sites of the spinel structure, as in Mn_3O_4. At 1000°C, this spinel phase has tetragonal symmetry, whereas at 1200°C it has cubic symmetry.

The DTA and TGA data revealed the onset of distinct thermal processes at 780, 915, and 1060°C. Combining the XRD, DTA, and TGA data, we derived a reaction sequence for $LiMn_2O_4$ when heated in air. This sequence falls into three temperature ranges: 780-915°C, ≥915°C, and ~1060°C.

At ~780°C, oxygen is lost from cubic $LiMn_2O_4$. A tetragonal $LiMn_2O_{4-\delta}$ phase is formed with $\delta \approx 0.14$. However, the high-temperature XRD data in Fig. I-2 suggest that oxygen loss from

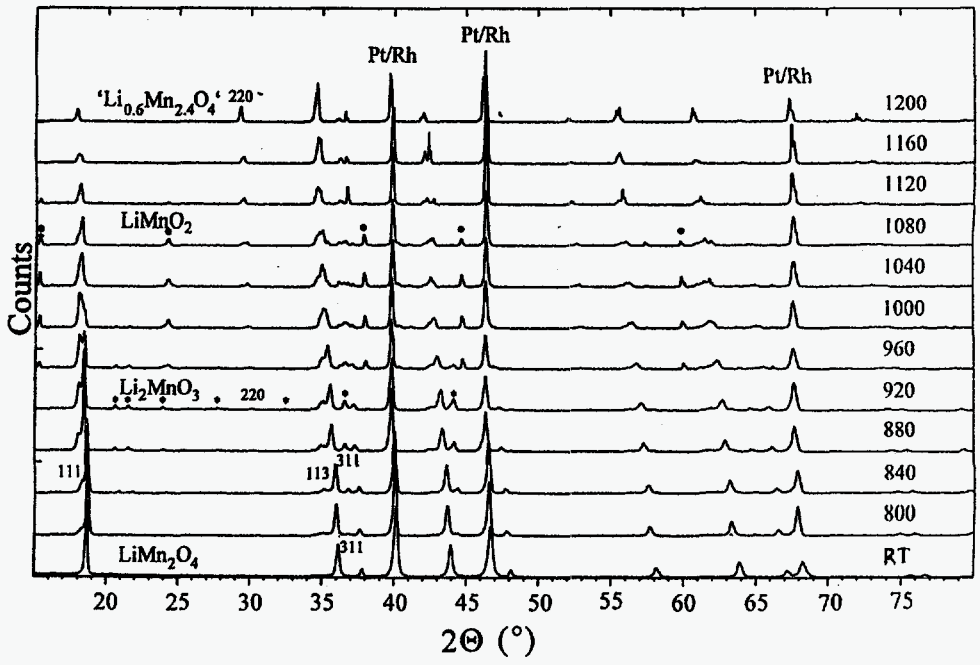

Fig. I-2. X-ray Diffraction Powder Pattern for $LiMn_2O_4$ between Room Temperature and 1200°C. Taken on Pt/Rh heating strip (• denotes $LiMnO_2$ peaks, * denotes Li_2MnO_3 peaks). Temperature (°C) indicated on right-hand side.

the spinel is accompanied by lithium diffusion to the particle surface, where a disproportionation reaction occurs:

$$LiMn_2O_4 \rightarrow \delta\, Li_2MnO_3 + Li_{1-2\delta}Mn_{2-\delta}O_{4-3\delta-\delta'} + \delta'/2\, O_2 \qquad (1)$$

In this reaction no lithia (Li_2O) is lost from the sample; it is all contained by the Li_2MnO_3 ($Li_2O{\bullet}MnO_2$) rock salt phase on the particle surface, which is stable at high temperatures.

Above ~915°C, oxygen is lost rapidly from the sample. In this reaction, the lithium-rich Li_2MnO_3 phase (Li:Mn = 2:1) is consumed by the manganese-rich spinel phase (Li:Mn ≈ 1:2) to produce $LiMnO_2$. In an ideal simplified case, the reaction between the rock salt phase and the spinel phase can be represented by

$$Li_2MnO_3 + LiMn_2O_4 \rightarrow 3\, LiMnO_2 + 1/2\, O_2 \qquad (2)$$

The $LiMnO_2$ phase is stable to approximately 1100°C, after which it is reincorporated into the spinel phase to yield a single-phase spinel product.

The TGA and DTA data indicate a transition at 1060°C, which is attributed to a reversible transition of a tetragonal spinel phase to cubic symmetry. The transition was confirmed

by a powder XRD pattern of the $LiMn_2O_4$ sample after rapid cooling from 1200°C to room temperature. At 1200°C, the pattern can be indexed to a cubic unit cell, whereas after cooling, the pattern can be indexed to a tetragonal unit cell with $c/a = 1.12$. This phenomenon is similar to that observed in hausmannite (Mn_3O_4), a spinel which undergoes a reversible phase transition from tetragonal symmetry ($c/a = 1.16$) to cubic symmetry ($c/a = 1.00$) at 1160°C. The magnitude of the c/a ratio, which reflects the extent of the Jahn-Teller distortion, depends on the concentration of Mn^{3+} ions on the octahedral B sites of the spinel structure; a c/a ratio of 1.12 implies the composition $(Li_{0.6}Mn_{0.4})_{tet}Mn_{2oct}O_4$. In this compound, the manganese ions on the tetrahedral sites are divalent; the manganese ions on the octahedral sites are of mixed Mn^{4+}/Mn^{3+} valence, with an average manganese oxidation state of 3.3.

The transition of the parent cubic $LiMn_2O_4$ spinel to a tetragonal spinel phase requires the loss of both lithia and oxygen. If it is assumed that the final product is a stoichiometric spinel that falls on the $LiMn_2O_4$-Mn_3O_4 tie line (Fig. I-1), then the overall reaction at 1200°C can be represented by

$$LiMn_2O_4 \rightarrow Li_{1-\delta}Mn_2O_{4-4/3\delta} + \delta/2\, Li_2O + 5\delta/12\, O_2 \qquad (3)$$

As δ increases, Mn^{2+} ions replace Li^+ ions on the tetrahedral sites of the spinel structure. If all the lithium could be removed from $LiMn_2O_4$ ($\delta = 1$), the product would be Mn_3O_4. The above data have provided important information on the processes that will occur during $LiMn_2O_4$ synthesis and highlight the care that must be taken in controlling temperature to obtain single-phase spinel samples with a required stoichiometry. Continued development of the Li-Mn-O system is planned.

3. Nickel/Metal Hydride System

The nickel/metal hydride (Ni/MH) battery is a strong contender to replace the nickel/cadmium battery because of its superior performance, low impedance, and absence of toxic cadmium. However, the present Ni/MH battery is limited by hydrogen management problems associated with charge-discharge cycling and self-discharge, active material deterioration, and long-term capacity loss caused by corrosion of the MH electrode. Promising materials that might improve the stability and capacity of the MH electrodes include rare earth alloys, such as $LaNi_5$, preferably with the partial substitution of La or Ni by a small amount of other metals (e.g., Sn, Mn, Co, or Al).[1] However, the role of alloying components is not yet clearly understood. Therefore, we devised a combination of electrochemical and neutron diffraction techniques for *in situ* investigations of Ni/MH cells. With neutron diffraction and analysis, the location of deuterium (a hydrogen isotope) can be identified in the bulk of the metal hydride crystal structure, which is not possible with X-ray diffraction. This coupling of investigative techniques provides a unique tool to study the properties of the alloy electrodes *in situ* with respect to composition, atomic structure, and phase change.

---

[1] M. Latroche, A. Percheron-Guegan, Y. Chabre, C. Poinsignon, and J. Pannetier, *J. Alloys Comp.* **189**, 59-65 (1992).

The Ni/MH cell reaction can be represented by the following simple cell reaction:

$$MH_x + xNiO(OH) = M + xNi(OH)_2 \quad (4)$$

where M denotes a metal-based alloy. A quartz-tube cell was specially designed for the *in situ* neutron diffraction measurements. The design (Fig. I-3) minimized the background scatter caused by cell construction materials, electrolyte, and the presence of remaining protons. Two main features of this cell should be pointed out: (1) the cell uses deuterated components exclusively (hydrogen creates too much scatter), and (2) only the metal-deuteride electrode and a minimal amount of electrolyte are exposed to the neutron beam. A commercial $NiO(OH)/Ni(OH)_2$ electrode was deuterated and used as the positive electrode. The electrolyte was 15 wt% KOD/D_2O. A dry nitrogen purge outside of the quartz tube prevented proton isotope exchange in the cell from the ambient atmosphere. Electrochemical performance tests were made with a different cell design that consisted of plane-parallel or jelly-roll electrode combinations with hydrogen-containing species. The electrochemical properties of the MH electrodes and Ni/MH cells (such as capacity, electrode potential, area specific impedance, and cycle life) were determined at room temperature and ambient pressure by interrupted galvanostatic cycling.

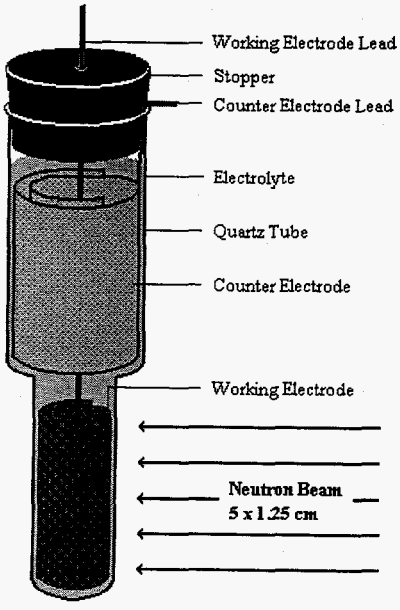

Fig. I-3.

Schematic of Quartz-Tube Cell Used for *In Situ* Neutron Diffraction Measurements

So far, the following alloys have been investigated: $LaNi_5$, $LaNi_{4.88}Al_{0.12}$, and $LaNi_{4.4}Al_{0.6}$. Figure I-4 shows the capacity of the three alloys determined by electrochemical cycling. The $LaNi_5$ electrode had low, but very stable, capacity. The $LaNi_{4.4}Al_{0.6}$ electrode had the highest capacity and exhibited a relatively small capacity drop. The alloy with the lowest concentration of aluminum, $LaNi_{4.88}Al_{0.12}$, however, had an initially high capacity but poor stability. To investigate the capacity-loss mechanism of the $LaNi_{5-y}Al_yH_x$ electrodes, we applied inductively coupled plasma/atomic emission spectrometry to electrolyte solutions taken from the cells during cycling. This method confirmed the hypothesis that the aluminum was corroding and

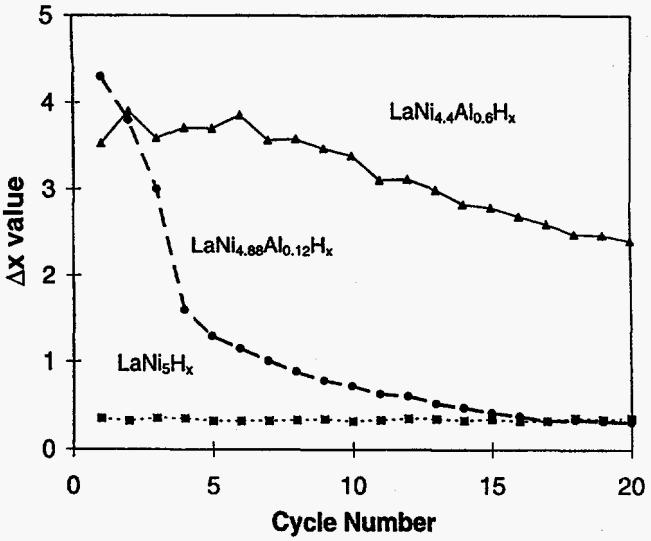

Fig. I-4.

Capacity Loss with Cycling of Candidate Alloys for Metal Hydride Electrodes (Δx = difference between x fully charged and discharged)

migrating out of the metal hydride structure into the caustic electrolyte (no lanthanum or nickel species were detected in the electrolyte).

Neutron diffraction measurements were conducted with the General Purpose Powder Diffractometer at ANL's Intense Pulsed Neutron Source. The quartz-tube cell was exposed to a neutron beam every 30 min during charge and/or discharge, with diffraction patterns and electrochemical data being collected simultaneously. With modern multiphase analysis techniques, scattering from the electrolyte and quartz tube can be modeled as background, leaving only the crystalline nickel mesh support and $LaNi_{5-y}Al_yD_x$ phases to consider. Rietveld profile refinements provide precise data corresponding to phase identification, deuterium and metal atom siting, and phase composition as a function of charge-discharge state.

For accurate refinement of the neutron diffraction data, a H/D ratio of less than 0.02 is required. To verify the deuterated condition of the cell, we developed a Fourier transform infrared (FTIR) technique that monitors the H/D ratio during the deuteration process. With this technique, characteristic absorption peaks of KOD/D_2O appeared at 2650, 2500, and 1200 cm^{-1}, while those of KOH/H_2O were at 3300 and 1650 cm^{-1}. This separation in absorption peaks between hydrogen and deuterium allows an estimation of H/D ratios.

To produce deuterated NiO(OD) electrodes, we cycled two pieces of NiO(OH) electrodes (removed from Ni/Cd cells) in 15% KOD/D_2O solution 16-20 times. The electrolyte was exchanged and analyzed by FTIR every four cycles to determine the remaining hydrogen content of the overall cell. Four samples were taken successively from the cell during the deuterating process. Figure I-5 shows the FTIR spectra of the deuterated solutions. The hydrogen characteristic peak at 3300 cm^{-1} from the first to the fourth sample decreased from 5% H_2O to approximately 0%, indicating the effectiveness of the deuterating technique. Neutron diffraction experiments confirmed this observation. There was no heavy background scattering present in the neutron diffraction patterns.

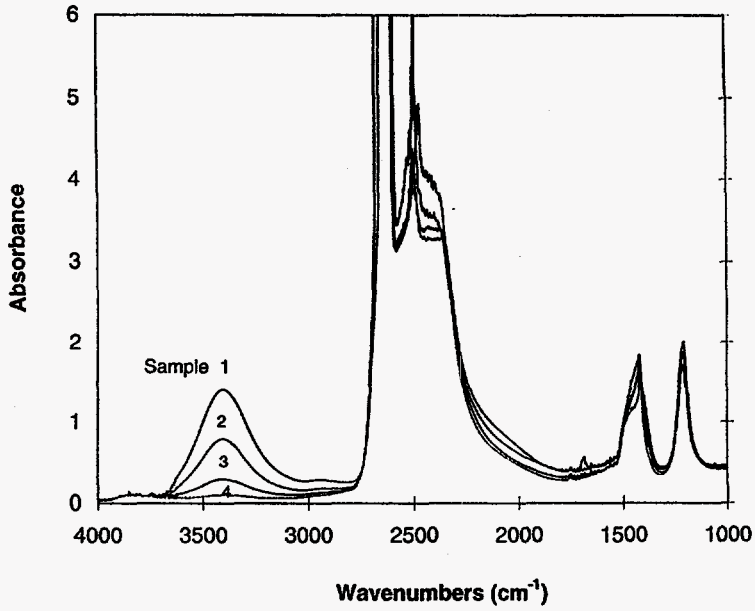

Fig. I-5. Fourier Transform Infrared Spectra of Four Successive Electrolyte Samples during the Deuterating Process

In situ neutron diffraction and Rietveld profile refinements of the neutron powder diffraction data of operating electrochemical cells were also used. The discharge capacity is indicated by the change in the value of x in the formula $LaNi_{5-y}Al_yH_x$. However, the absolute value of x at the end of discharge cannot be easily determined electrochemically. In our work we define Δx as the amount of hydrogen (deuterium) released from the hydride alloy upon electrochemical discharge and designate it to represent the cell capacity. One advantage of neutron diffraction analysis over coulometric calculation is that it can provide an *absolute* value of x. Thus, the discharge capacity observed by neutron diffraction, Δx_N, is the difference between the absolute x values at full charge and discharge.

Figure I-6 is a plot of Δx from electrochemical coulometric data, x from neutron diffraction analysis, and the open-circuit cell voltage as a function of discharge time for $LaNi_{4.4}Al_{0.6}D_x$. The discharge capacity determined by neutron diffraction (Δx_N) is in good agreement with that calculated by coulometry (Δx) during galvanostatic cycling. Note, however, that the x value at the fully discharged point (t = 12:00:00) is not zero, suggesting that deuterium is not completely depleted from the deuterated alloy when the alloy is electrochemically discharged to the cut-off voltage. As a result, Δx from coulometry is different from the x value by neutron diffraction at any given time during discharge (the absolute value of x at the end of charge or discharge cannot be determined from coulometry alone because of competing reactions such as gas evolution and corrosion). At this time, residual uncertainty in the data is too large to quantitatively correlate Δx and x, although the general shapes are in close agreement.

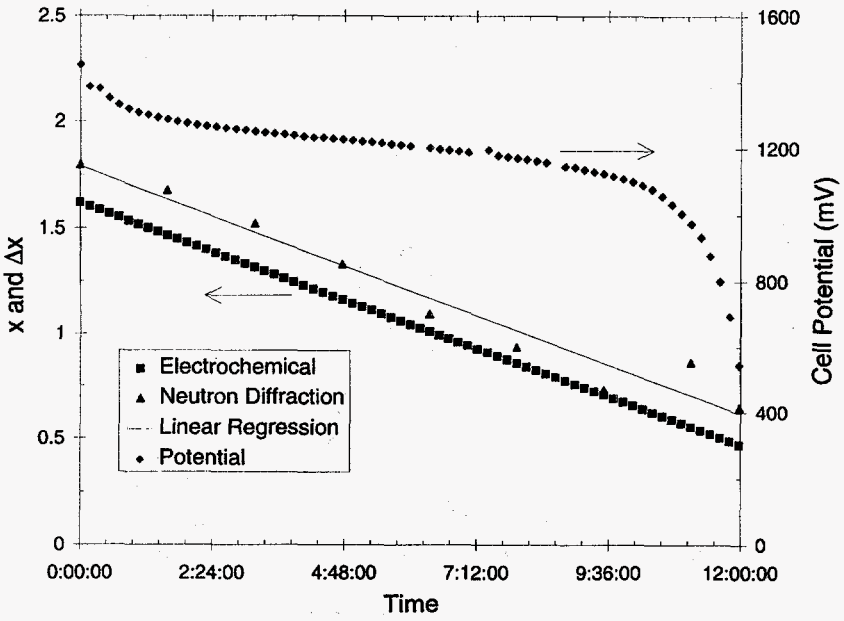

Fig. I-6. Electrochemical Coulometric Data (Δx), Neutron Diffraction Analysis (x), and Open-Circuit Cell Voltage for $LaNi_{4.4}Al_{0.6}D_x$ during Cell Discharge

We have found that $LaNi_5$ and its derivatives have a hexagonal space group (P6/mmm) crystal structure (Fig. I-7) containing two crystallographically distinct nickel sites, Ni(1) and Ni(2).[1] In aluminum-substituted $LaNi_5$, the aluminum substitutes selectively on Ni(2) sites. Deuterides of $LaNi_5D_x$ and its derivatives cover a range of deuterium concentrations (x) from 0.1 to 6.7 per lanthanum atom. In the range $x < \sim 1.0$, the α-phase is the preferred phase, while above this level, the β-phase forms. Under some conditions, both phases will coexist. Deuterium sites for $LaNi_5D_x$ and its derivatives occupy interstitial locations near the Ni(2) sites. For most deuterides, only some of these deuterium sites are occupied.

Refined structural parameters for $LaNi_{4.4}Al_{0.6}$ powder, as well as results from fully charged and discharged cells, indicate that fully charged $LaNi_{4.4}Al_{0.6}D_x$ is ~80 vol% α-$LaNi_{4.4}Al_{0.6}D_{1.3}$ and 20 vol% β-$LaNi_{4.4}Al_{0.6}D_{3.6}$. During continuous *in situ* discharging, the volume fraction of β-phase decreases progressively, eventually giving way to pure α-phase. In the fully discharged state, only α-$LaNi_{4.4}Al_{0.6}D_{0.7}$ is present, i.e., the overall deuterium concentration x = 0.7. This corresponds to a concentration change Δx = 1.1, in agreement with electrochemical measurements. In the coming year, these investigations of the MH electrode behavior will continue.

B. Electrochemical Analysis and Diagnostics Laboratory

The Electrochemical Analysis and Diagnostics Laboratory (EADL) was established at ANL to study advanced battery systems for applications such as electric vehicles (EVs) and

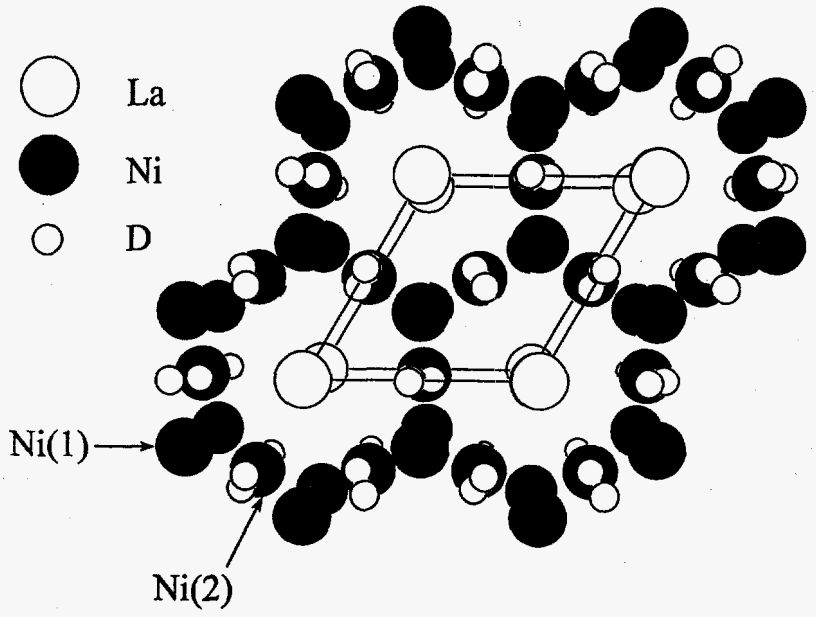

Fig. I-7. Hexagonal Crystal Structure Representation of $LaNi_5D_x$

utility load-leveling. The facilities include a test laboratory to conduct battery experimental evaluations under simulated application conditions and a post-test analysis laboratory to determine, in a protected atmosphere if needed, component compositional changes and failure mechanisms. Evaluations are performed for DOE, the Electric Power Research Institute (EPRI), the U.S. Advanced Battery Consortium (USABC), and others to provide insight into those factors that limit the performance and life of advanced battery systems. The results of these evaluations help identify the most promising R&D approaches for overcoming these limitations and provide battery users, developers, and program managers with a measure of the progress being made in battery R&D programs, a comparison of battery technologies, and basic data for modeling.

1. Performance and Life Evaluations

Performance and life evaluations were continued under a Cooperative Research and Development Agreement (CRADA) with the USABC. This CRADA was initiated in the last quarter of 1992. These evaluations focused on nickel/metal-hydride modules from a USABC battery development contract with Ovonic Battery Co. (OBC). In 1996, EADL activities under this CRADA were expanded to include a study to assess the suitability of modules that have reached the end of their EV-battery lives for other applications such as standby power, uninterruptible power sources, utility load management, and commercial/industrial vehicles (golf carts, fork lift trucks, etc.). A special test plan and procedures had to be developed to simulate operating conditions for these applications. The testing of OBC modules is continuing. Also initiated during this past year was the evaluation of a full-size EV battery pack for Chrysler Corp., constructed with OBC nickel/metal-hydride modules. The results of these tests and analyses will be released by the USABC at a later date.

The Electrochemical Analysis and Diagnostic Laboratory evaluated, for EPRI, advanced lead-acid batteries manufactured by Electrosource, Inc.; Yuasa/Exide, Inc.; and GNB Industrial Battery Co. Of the modules tested, Electrosource modules achieved the highest specific energy, 43 and 36 Wh/kg with discharges at the 3-h rate and under the Dynamic Stress Test (DST), respectively. The peak power capability at 80% depth-of-discharge was calculated with USABC power test data, and the highest value, ~171 W/kg, was obtained for an Electrosource module. However, with the minimum voltage limit (9.0 V) specified by Electrosource, a maximum peak power of only 125 W/kg is achievable, which is less than that of the Yuasa/Exide modules (~130 W/kg). A Yuasa/Exide module (17-Ah unit) attained the longest life (494 cycles) under driving profile discharges (DST to 80% depth-of-discharge). In comparison, the best Electrosource module achieved a DST life of only 76 cycles. One of the Yuasa/Exide modules (50-Ah unit) achieved a life of 113 cycles with 80% depth-of-discharge DST discharges and 203 cycles with a fast charge (15 min to 40% state-of-charge) in the middle of each DST discharge to 120% of its rated capacity. All of the EPRI modules completed their life evaluation in the first seven months of 1996.

Besides performance and lifetime evaluations, the ANL Electrochemical Technology Program has supported the USABC by having representatives on the OBC Nickel/Metal-Hydride Working Group, the Nickel-Based Component Cost Reduction (NBCCR) Group, and the Battery Testing Procedures Tiger Team. The ANL Electrochemical Technology Program has also participated in USABC battery readiness review meetings to verify proper test planning, instrumentation, and data acquisition before the start of unique tests.

2. Post-Test Analysis

A number of OBC nickel/metal-hydride cells have undergone post-test analysis after life evaluations in the EADL. This activity is being sponsored by the USABC to assist OBC staff in identifying and focusing their resources on critical design issues facing their technology. Many of the post-test analyses performed in the EADL have been a joint effort between ANL and OBC. In the DOE "Summary Appraisal Report for FY1995," ANL received special recognition and an overall performance of "excellent"; the EADL test and post-test analyses were acknowledged as contributing greatly to the improved capabilities of the OBC nickel/metal-hydride system and the development techniques to eliminate electrode failures.

Examinations were also completed for Commonwealth Edison Co. on six lead-acid round cells used for standby power requirements at their nuclear generating stations. These cells had exhibited an abrupt capacity loss, which caused the power station to fail its periodic standby power test. Commonwealth Edison asked ANL to identify the root cause(s) for this capacity loss. The results of these examinations revealed a grid corrosion problem that led to a high internal cell resistance and reduced capacity. Additional cells from other utility companies are being sent to the EADL for similar examinations.

In 1997, post-test analyses, as well as performance and life evaluations, will be continued on cells, modules, and batteries for the USABC, Chrysler, and Commonwealth Edison.

C. Fuel Cell Research and Development

All fuel cells convert the chemical energy of fuels such as hydrogen, methane, methanol, ethanol, and other hydrogen-bearing compounds to electricity with little or no pollution and with greater efficiency than heat engines. Fuel cell technology could thus become a significant part of the economy of the U.S. and other countries. Following the U.S. lead, Japan has mounted a major initiative to develop the molten carbonate fuel cell (MCFC) for distributed utility applications. The European Union is concentrating its efforts on development of a solid oxide fuel cell (SOFC) and has reoriented the R&D programs in some of its national laboratories from nuclear to SOFC technology. Furthermore, Daimler-Benz AG in Germany and Toyota Motor Corp. in Japan have begun major programs to explore the potential of the polymer electrolyte fuel cell (PEFC) for automobiles.

Being a pioneer in fuel cell technology since the 1970s, the CMT Division continues to conduct R&D on the MCFC and SOFC for utility applications, a low-temperature SOFC for transportation applications, and the PEFC for portable uses in military applications. Work also continues on an innovative new fuel reformer for converting various hydrocarbon fuels to hydrogen for use in polymer electrolyte fuel cells for transportation applications.

1. *Molten Carbonate Fuel Cells*

At present, the molten carbonate fuel cell consists of a porous nickel anode, a porous nickel oxide cathode, a semi-fluid $(Li,K)_2CO_3 + LiAlO_2$ electrolyte, and a metal bipolar plate. The operating temperature is 650°C. Our MCFC program is engaged in efforts to develop alternative cathodes, develop nonsegregating electrolytes, and improve the corrosion resistance of the cell components. The goal of these efforts is to extend life, increase power density, and decrease cost for the MCFC.

a. Alternative Cathodes

In the present technology, lithiated NiO is used as the cathode. Over the lifetime of the cell, however, Ni^{2+} ions tend to transport to the anode, where they are reduced to metallic Ni.[2] With increased CO_2 partial pressure, the nickel transport increases because of the increased solubility of NiO in the carbonate electrolyte. Although this process is slow in MCFCs operated at atmospheric pressure (100 kPa) and a low CO_2 partial pressure (about 10 kPa), transport of nickel to the anode may be excessive at a higher pressure (e.g., 300 kPa) and a high CO_2 partial pressure (e.g., about 30 kPa). This transport is expected to lead eventually to poor MCFC performance and/or short circuiting.

[2] N. Q. Minh, *J. Power Sources* **24**, 1-19 (1988).

Several alternative cathode compositions have been explored to reduce cathode solubility in the molten salt electrolyte. For example, $LiCoO_2$ has been studied extensively[3-6] as a potential cathode material. The $LiCoO_2$ cathode has a low resistivity, about 1 Ω•cm, and can be used as a direct substitute for NiO. However, the high material cost may prevent large-scale implementation.

We are developing advanced cathodes based on lithium ferrate ($LiFeO_2$), which is attractive because of its low cost and very low solubility in the molten $(Li,K)_2CO_3$ electrolyte.[7] Because of its high resistivity (about 300 Ω•cm at 650°C), however, $LiFeO_2$ cannot be used as a direct substitute for NiO. Cation substitution is, therefore, necessary to decrease resistivity. During 1996, we determined the effect of cation substitution on the resistivity of $LiFeO_2$. As seen in Fig. I-8, the plot of lattice parameter vs. NiO concentration is a smooth curve throughout the entire solid solution range. The results show that NiO forms a continuous solid solution with $LiFeO_2$. As expected, the resistivity of the solid solution is inversely proportional to the NiO concentration. For example, the resistivity of 25 mol% NiO-$LiFeO_2$ is 41 Ω•cm at 650°C. By using a combination of cation substituents, we lowered the resistivity of a $LiFeO_2$-based material (designated Material 1) to 1.3 Ω•cm at 650°C, close to the desired value for an MCFC.

A fibrous cathode of Material 1 was used in a 5 × 5-cm MCFC test at 650°C and high CO_2 partial pressures (30 kPa). The cell potential at 160 mA/cm^2 was determined as a function of time (Fig. I-9). After an initial break-in period, a constant potential of 850 mV was observed for 1700 h. Polarization experiments indicated a small performance degradation at 1706 h. These results show that $LiFeO_2$-based cathodes have good performance and durability at high CO_2 partial pressures.

Low electrical resistivity and stable cell performance represent two important requirements for cathode development. Another requirement is adequate creep strength or resistance to deformation. If the cathode structure is not mechanically stable, cell performance will degrade. We determined the relative creep strength of several potential materials.

---

[3] L. Plomp, E. F. Sitters, J. B. J. Veldhuis, R. C. Makkus, and S. B. van der Molen, "Performance and Dissolution-Precipitation Behavior of Molten Carbonate Fuel Cell Cathodes," Proc. of the Third Int. Symp. on Carbonate Fuel Cell Technology, 183rd Electrochem. Soc. Meeting, Honolulu, HI, May 16-21, 1993, Vol. 93-3, pp. 171-185 (1993).

[4] L. Plomp, R. C. Makkus, E. F. Sitters, and G. Rietveld, "Endurance Issues and Materials Development in Molten Carbonate Fuel Cells," Fuel Cell Seminar Program and Abstracts, San Diego, CA, November 28-December 1, 1994, p. 164 (1994).

[5] B. Bergman, E. Fontes, C. Lagergren, G. Lindbergh, A. Lundblad, S. Schwartz, D. Simonsson, and C. Sylwan, "Swedish Research on MCFC," Fuel Cell Seminar Program and Abstracts, Tucson, AZ, November 29-December 2, 1992, p. 73 (1992).

[6] M. Carewska, S. Scaccia, G. Ghidelli, L. Giorgi and E. Simonetti, "Synthesis and Electronic Conductivity of $LiCoO_2$ Materials for MCFC Alternative Cathodes," Fuel Cell Seminar Program and Abstracts, San Diego, CA, November 28-December 1, 1994, p. 176 (1994).

[7] D. Shores and Y. Qu, "Dissolution of Oxides in Molten Carbonates," Proc. of the Third Int. Symp. on Carbonate Fuel Cell Technology, 183rd Electrochem. Soc. Meeting, Honolulu, HI, May 16-21, 1993, Vol. 93-3, pp. 356-367 (1993).

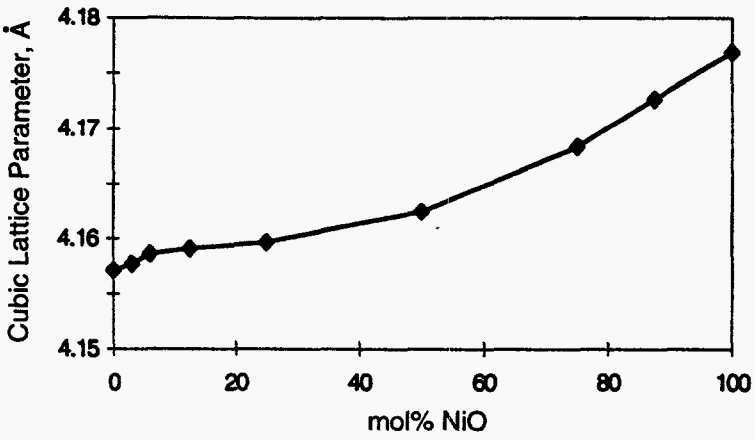

Fig. I-8. Effect of NiO Concentration on Cubic Lattice Parameter in $Li(Fe,Ni)O_2$ Solid Solutions

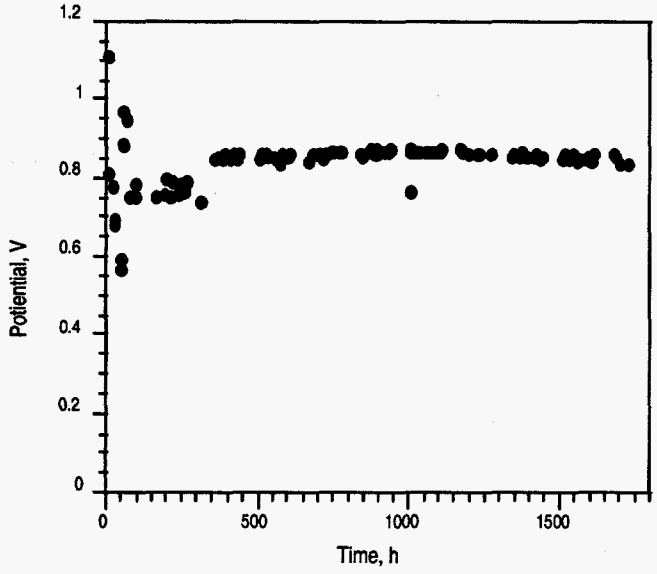

Fig. I-9.

Cell Potential vs. Time for MCFC Containing Material 1 Cathode

Figure I-10 shows a log-log plot of the deformation rate vs. stress at 1000°C for pure $LiFeO_2$, 12.5 mol% NiO-$LiFeO_2$, pure $LiCoO_2$, and 5 mol% Li_2O-NiO. In this figure, the deformation rate was normalized with respect to grain size and stress to the material density, and it was assumed that the deformation rate is controlled by lattice diffusion. The slope of all curves is close to unity, implying that all four materials exhibit the same deformation mechanism (diffusional creep and/or grain boundary sliding). The $LiFeO_2$ has higher deformation rates than lithiated NiO. The $LiCoO_2$ has the highest deformation rate. Doping $LiFeO_2$ with NiO decreased the deformation rate as compared with that of pure $LiFeO_2$. In sum, the $LiFeO_2$, NiO-$LiFeO_2$, and $LiCoO_2$ will compact more than lithiated NiO at the MCFC operating temperature of 650°C. Alternative cathode compositions will continue to be explored.

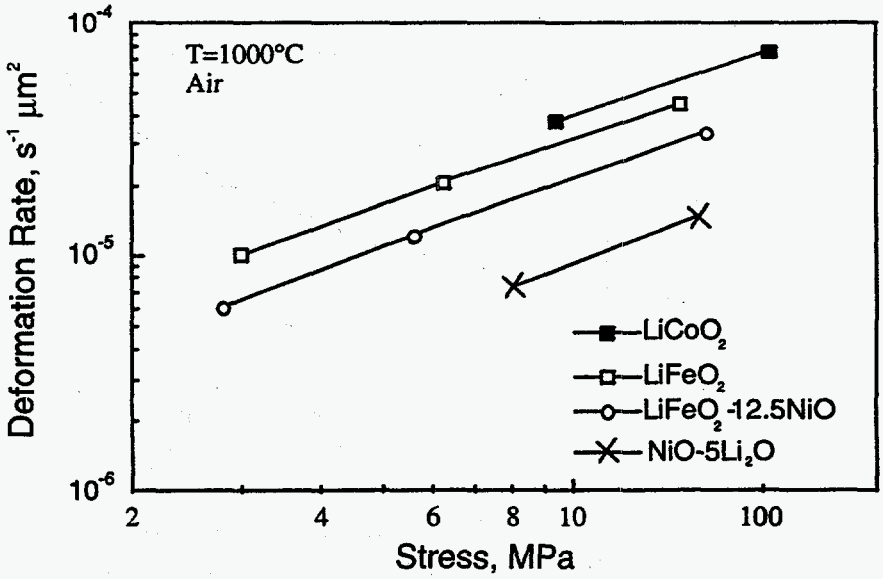

Fig. I-10. Deformation Rate vs. Stress for Four Cathode Materials at 1000°C in Air

b. Nonsegregating Electrolytes

Electrolyte segregation has been reported[8] to occur within both the individual molten carbonate fuel cell and stack of cells. In the cell, the segregation increases the potassium concentration near the cathode, which, in turn, leads to increased cathode solubility and performance decline. In a stack of fuel cells, the high potential difference along the manifold gaskets causes electrolyte migration and cation segregation, which, in turn, leads to severe performance decline of the "end" cells.

An electrolyte is considered nonsegregating when the cations have equal mobilities. With equal cation mobilities, electrolyte migration should also be minimized. We studied cation segregation and electrolyte migration in six electrolyte compositions in the Li_2CO_3-Na_2CO_3 binary system (no potassium present). Two tests were used: carbonate-wetted $LiAlO_2$ strips and 100-cm^2 MCFCs at a current density of 320 mA/cm^2.

For the strip tests, six Li_2CO_3-Na_2CO_3 compositions were evaluated (in mol%): 52/48, 40/60, 60/40, 67/33, 70/30 and 75/25; hereafter, these electrolyte compositions will be referred to as A, B, C, D, E, and F, respectively. Composition A is the eutectic. The carbonate-wetted $LiAlO_2$ strips were submitted to 5-20 V potential gradients, representative of the gasketing strip of an externally manifolded MCFC. The test vessel was purged with a 1:2 O_2/CO_2 gas mixture at ~655°C. After 72 h at 20 V, the potential distribution in the strip had reached equilibrium, and the strip was quenched under load. Two-gram samples were removed from four spots along the 12-cm strip length for analysis by inductively coupled plasma/atomic emission spectroscopy (ICP/AES). Cation ratios and electrolyte fill in each of the spots were calculated.

---

[8] H. R. Kunz, *J. Electrochem. Soc.* **134**, 105 (1987).

The potential distribution for the A, B, C, and D compositions is given in Fig. I-11. Clearly, the change in potential vs. length is lower for Composition D than it is for A. The ICP/AES results present a consistent picture of electrolyte segregation in relation to composition and changes in potential; off-eutectic compositions have reduced segregation. Examination of the Li/Na cation ratios along the strip indicated that Composition D exhibited a small change in composition (hence, cation segregation) at 20 V, while Composition A, the eutectic composition, exhibited significant cation segregation. On the basis of the correlation between the ICP/AES results and the potential variation along the strip, the voltage profiles determined in these tests are reliable indicators of cation segregation. However, the relation between these potentials and carbonate composition is not well understood.

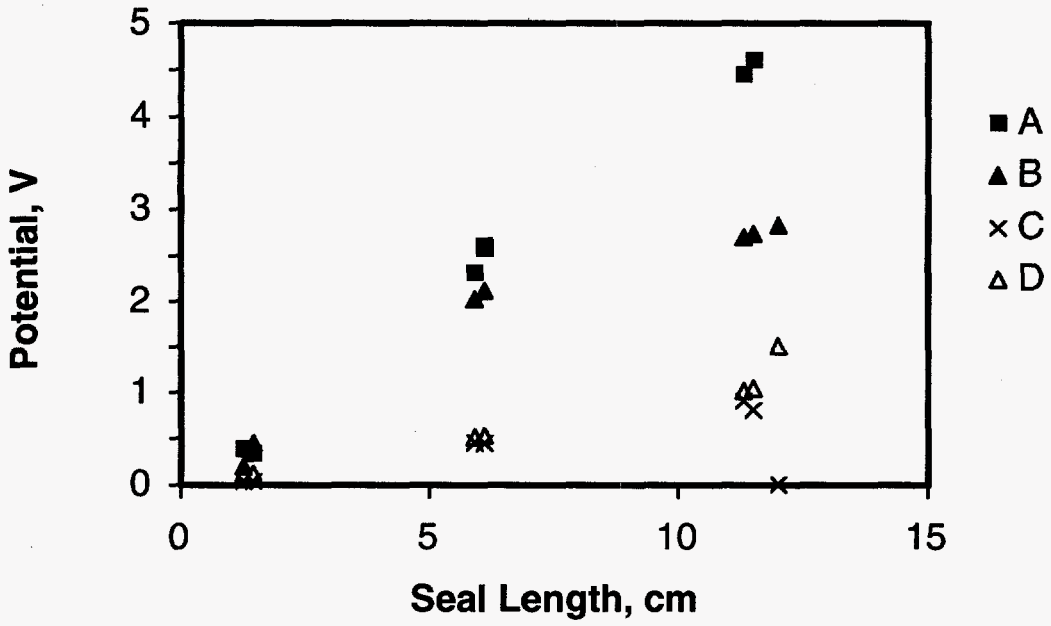

Fig. I-11. Potential Distribution vs. Seal Length of 12-cm Strips Wetted with Li_2CO_3-Na_2CO_3 Electrolyte. Electrolyte compositions (A-D) defined in text.

We also found that electrolyte migration and cation segregation are correlated. The degree of electrolyte migration in the strip is indicated by the variation in "electrolyte fill," given as the carbonate-to-$LiAlO_2$ weight ratio determined at the sample locations along the strip. Similar to cation segregation, the smallest change in electrolyte fill occurs in Composition D. With the other carbonate compositions, the electrolyte migration tends toward the cathode.

Bench-scale (100 cm^2) MCFCs were assembled with standard nickel anodes (6% chromium) and nickel cathodes. Five electrolyte compositions were tested: Compositions A, B, C, D, and 71.5 mol% Li_2CO_3-28.5 mol% Na_2CO_3. Performance data of the bench-scale cells were used to compare the performance of Li/Na electrolyte compositions. Data on cell impedance, cell voltage, electrode performance at various utilizations, and current density operation were collected as a function of time at atmospheric pressure with laboratory standard oxidant and humidified fuel. All cells were operated for at least 500 h at 650°C. For the purposes

of investigating electrolyte segregation, the cells were operated at a current density of 400 mA/cm^2 for at least 0.5 h at the end of the life test. The cells were then rapidly quenched to fix compositional gradients. Metallographic and chemical analyses were used to determine the composition and amount of carbonate in the MCFC components.

Figure I-12 shows the polarization curves for the five MCFCs. These tests are conducted with fuel and oxidant utilizations of 60% and 40%, respectively, at 320 mA/cm^2. The cell tests displayed improved performance as the nonsegregating tendency of the electrolyte increased. For that reason, the cell containing Composition D showed good stability, as indicated by the 0.71 V achieved at 320 mA/cm^2. We know from past research that high current density operation in Li_2CO_3-K_2CO_3 cells leads to early cell shorting,[2] and that electrolyte segregation or solidification presents problems for operation at high current density. These problems did not arise for Composition D. Moreover, the cell impedance remained stable at 0.9-1.0 Ω•cm^2. The 71.5 mol% Li_2CO_3 composition exhibited an even higher cell potential, 0.76 V, at 320 mA/cm^2. Alternative electrolyte compositions will continue to be explored in the next year.

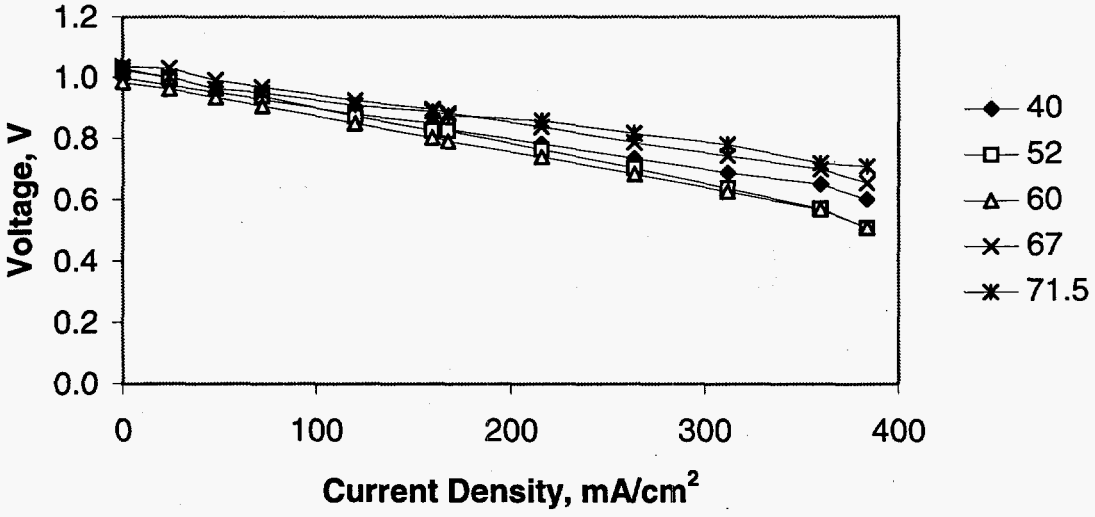

Fig. I-12. Polarization Curves for Bench-Scale MCFCs with Different Li_2CO_3-Na_2CO_3 Electrolyte Compositions. Numbers on far right indicate mole percent of Li_2CO_3 in binary electrolyte.

c. Cell Hardware

The temperature, gas compositions, electrolyte composition, and chemical potential differences in the MCFC lead to corrosion of the metal hardware. Two regions in the MCFC experience high corrosion rates, the bipolar plate and the wet seal area. We are determining the mechanism of this corrosion and investigating methods to mitigate it.

The bipolar plate in the MCFC consists of nickel-clad stainless steel. Here, the nickel-clad side is exposed to the anode compartment, and the bare steel side is exposed to the cathode. A highly resistive oxide scale forms on the steel during cell operation, which lowers cell

performance. Our approach to the corrosion problem is to evaluate dense, adherent coatings which have low bulk and interfacial resistivities. We are currently characterizing the electrical and corrosion properties of thermally cyclable ceramic coatings for steel.

In the conventional MCFC, a portion of the molten $(Li,K)_2CO_3$ + $LiAlO_2$ electrolyte extends beyond the electrode area and forms a wet seal against the stainless steel cell housing. On the fuel side of the MCFC, the wet seal is exposed to high and low oxygen partial pressures simultaneously. Thus, one or more galvanic cells can form, leading to severe corrosion. In turn, the corrosion leads to a poor seal and to rapid decline of cell performance. Only aluminum and aluminum-containing alloys have sufficient corrosion resistance for use in the wet seal. Aluminizing the wet seal surfaces increases their corrosion resistance by increasing the surface aluminum content.

The corrosion behavior of aluminized 310S stainless steel in the wet seal of MCFCs was investigated. Samples from two aluminizing methods were tested: thermal spray and slurry coating. Examination of both types of samples shows that, at 650°C, Fe and Cr diffuse readily into the Al layer. At first this interdiffusion is limited to the interfacial area. With time, iron and chromium aluminides precipitate in the aluminum layer. The slurry-coated layer contains a higher concentration of FeAl and Fe_3Al than does the thermal spray layer. After a 500-h exposure on the anode-side wet seal, the slurry-coated sample displayed greater corrosion damage than did the thermal-sprayed sample. Because of the high iron content, the corrosion protection of the slurry layer is less effective than that of the thermal spray layer. We will continue evaluating the corrosion resistance of the iron and chromium aluminides in the wet seal of the MCFC.

2. *Solid Oxide Fuel Cells*

Present SOFC technology has an oxide-ion-conducting electrolyte material, yttria-stabilized zirconia; a cathode of strontium-doped lanthanum manganite; an anode of nickel/yttria-stabilized zirconia; and a cell interconnect of strontium-doped lanthanum chromite. The typical cell operating temperature is 800-1000°C.

The overpotential at the cathode/electrolyte interface has been recognized as an important limitation on the performance of SOFCs. This project is an effort to gain an improved understanding of which interface features and conditions contribute to cathode polarization in SOFCs and, consequently, to determine optimal fabrication methods for the production of SOFCs with low cathode polarization.

The first part of this project was an effort to determine exactly where the cathode reaction (oxygen reduction) takes place; possibilities include on the porous cathode surface, at the "triple" interface (cathode, electrolyte, and air), or on the electrolyte surface. Whether the reaction is possible at these locations depends on the mixed conductivity in the cathode or electrolyte and on their relative surface areas. Later stages of this project also included a study of the cathode geometry near the electrolyte interface.

a. Electrolyte Doping

To test the role of the electrolyte surface, the mixed conductivity in the electrolyte was altered by ion implantation of manganese. Porous $La_{0.9}Sr_{0.1}MnO_3$ (LSM) cathodes were coated by a slurry process onto this doped surface. Electrochemical testing was performed on 2.5-cm dia cells made with doped and undoped electrolytes. Results from both impedance spectroscopy and polarization testing indicated that the doping failed to significantly change the cathode polarization. Thus, electronic conduction within the electrolyte, if it is involved in the cathode reaction, apparently is adequately provided by manganese diffusion from standard methods of cathode fabrication.

Significant changes in the distribution of manganese were observed after the electrochemical testing. Undoped electrolytes typically caused a small percentage of the adjoining cathode surface to be low in manganese, possibly indicating the presence of lanthanum zirconates. However, when manganese-doped electrolytes were used, the cathode fracture surfaces tended to have uniform manganese contents. Cathodes on the doped substrates also tended to have lower wetting/adhesion to the electrolytes. Thus, the absence of a reaction layer is suggested for doped electrolytes.

In this case, the electrochemical behavior is probably controlled by poor properties or geometry in the rest of the cathode, masking any effect from reaction layers at the interface. Doping of the electrolyte may be a useful strategy for improving interface properties for electrodes in which the electrode structure itself has already been optimized.

b. Cathode Surface vs. Triple Interface

If the air/electrolyte surface is not an important site for oxygen reduction, as indicated from the experiments above, the remaining choices are the cathode surface or the triple interface region. We have tested the role of each of these regions with experiments on two types of cathodes: nonporous and thin film.

When nonporous electrodes are used, the triple interface is effectively eliminated, and oxygen reduction must take place at the cathode surface, with the oxygen ions passing through the cathode. Thus, we tried a number of methods to obtain sufficiently dense and defect-free electrodes to observe the effect of eliminating the triple interface. One method was to prepare dense LSM layers by pressing 200-μm-thick LSM pellets, firing to near full density, and joining these to electrolyte substrates with a thin, slurry-coated LSM layer. Glass sealing material was then used to ensure that the edges of the dense cathodes did not permit air exchange. However, the thickness of these electrodes, as well as the joining and sealing method, made the electrochemical data difficult to interpret.

We, therefore, tried thin-film formation, including coating with nitrate and citrate solutions. Nitrate solutions of LSM tended to create porous thin films, even after reducing-atmosphere sintering treatments. Citrate solutions, on the other hand, tended to have a more favorable decomposition reaction, which allowed denser film formation. By experimenting with citrate solution concentrations, surfactants added, and heating rate, we were able to create films

with adequate density to effectively eliminate the triple interface regions. Films of mixed-conducting materials, including $(La_{0.6}Sr_{0.4})_{0.99}Co_{0.2}Fe_{0.8}O_3$ and $SrFeCo_{0.5}O_3$, have both shown excellent electrochemical performance. Figure I-13 compares cathode resistances with and without a dense mixed-conducting thin film between the porous cathode layer and the zirconia electrolyte; significant improvement is seen when dense thin films are used.

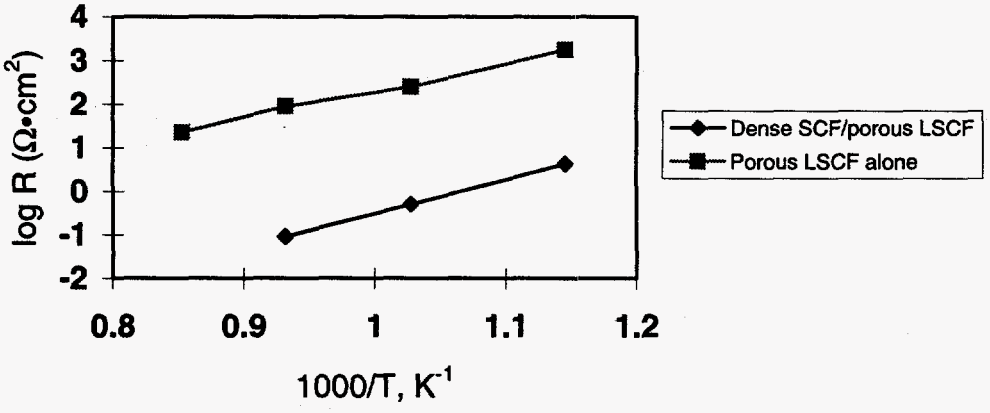

Fig. I-13. Cathode Resistance with and without Dense Mixed-Conducting Film on Zirconia Electrolyte. [SCF = $SrFeCo_{0.5}O_3$ and LSCF = $(La_{0.6}Sr_{0.4})_{0.99}Co_{0.2}Fe_{0.8}O_3$]

These results show that total surface coverage of the electrolyte by the cathode may be a more critical parameter for improving cathode performance than the triple interface distribution. In this case, the cathode surface is the probable site of oxygen reduction, and mixed conductivity within the bulk of the cathode is responsible for distribution of current onto the electrolyte.

c. Cathode Geometry near the Interface

Testing of porous LSM cathodes clearly showed that their performance improves dramatically with cathodic potential conditioning; the cathode polarization at 800°C drops from an initial value of 0.9 to 0.68 $\Omega \cdot cm^2$ after a conditioning period of 60 h at 750 mV. Clear microstructural changes in the cathode were found to accompany this conditioning; in post-test analyses with scanning electron microscopy, an obvious sintering effect was seen that extended outward from contact points to form a sintered disc with a diameter of 30-40 μm; outside this area the porous structure of the LSM appeared unchanged. We were able to find similar sintering enhancements by simply heating the cathodes in reducing atmosphere (6% hydrogen in helium) as opposed to in air. Thus, it appears likely that the reducing potential during conditioning is responsible for the microstructural evolution seen in our cathodes.

By linking improved performance with increased cathode density near the interface, we have shown that current distribution from the cathode to the electrolyte surface may be an important limitation for cell operation. This hypothesis agrees with our dense thin-film results (Fig. I-13).

d. Continuing Work

Currently, our approach focuses on a study of cathodes with two distinct layers, each with specialized functions, in order to eliminate the remaining cathode polarization. This polarization could arise as a result of using inappropriate materials for the various functions of the cathode. For example, while porous LSM may be a good material to catalyze oxygen reduction, when used adjacent to the electrolyte, it may cause polarization due to (1) low surface coverage of the electrolyte, limiting the area available for transfer of oxygen ions, and (2) inadequate ionic conductivity until partially reduced by the cathodic potential, which incurs a polarization penalty. On the other hand, a dense mixed-conducting material may be ideal for the layer in contact with the electrolyte but may not be sufficiently catalytic or have adequate surface area for use in the outer cathode layer. We hope to experimentally verify these observations with our planned study of multilayer cathodes.

3. Transportation Applications

To aid the development of fuel cells for transportation applications, we are developing methods for fuel processing before use in the fuel cell stack, developing a new design of solid oxide fuel cell, and modeling fuel cells and fuel cell systems under various modes of operation.

a. Fuel Processing

The objective of this work is to develop catalytic partial-oxidation reformers for the generation of hydrogen from alcohol and hydrocarbon fuels for use with the low-temperature fuel cells (polymer electrolyte and phosphoric acid fuel cells) being developed for transportation applications. Such fuel processors need to be compact, lightweight, efficient, and capable of rapid startup and good dynamic response.

For the partial-oxidation reforming of methanol, the idealized general reaction is

$$CH_3OH + x(O_2 + 3.76N_2) \rightarrow 2xCO_2 + (1 - 2x)CO + 2H_2 + 3.76xN_2 \quad (\text{for } x \leq 0.5) \qquad (5)$$

where x is the oxygen/methanol molar ratio. This reaction is followed by the water-gas shift reaction to convert the CO to CO_2 and additional hydrogen,

$$CO + H_2O \rightarrow CO_2 + H_2 \qquad (6)$$

Thus, the net idealized reaction can be represented as

$$CH_3OH + x(O_2 + 3.76N_2) + (1 - 2x)H_2O = CO_2 + (3 - 2x)H_2 + 3.76xN_2 \qquad (7)$$

A 10 kW(e) bench-scale reactor has been used extensively for developing the partial-oxidation process for reforming methanol. In this reactor, methanol, air, and water are

injected at the top, and the reaction is initiated with an electrically heated coil. The partially vaporized mixture then continues its reaction in the catalyst zone and exits at the bottom. The product gas contains approximately 50% hydrogen (on a dry basis). To convert the 1-2% carbon monoxide in this gas, a small water-gas shift reactor is installed at the bottom of the reformer. The shift reactor is able to decrease the CO concentration to as low as 0.3%. Figure I-14 shows the product gas composition during a test. The reformate contained 50% H_2, 20% CO_2, and less than 0.5% CO.

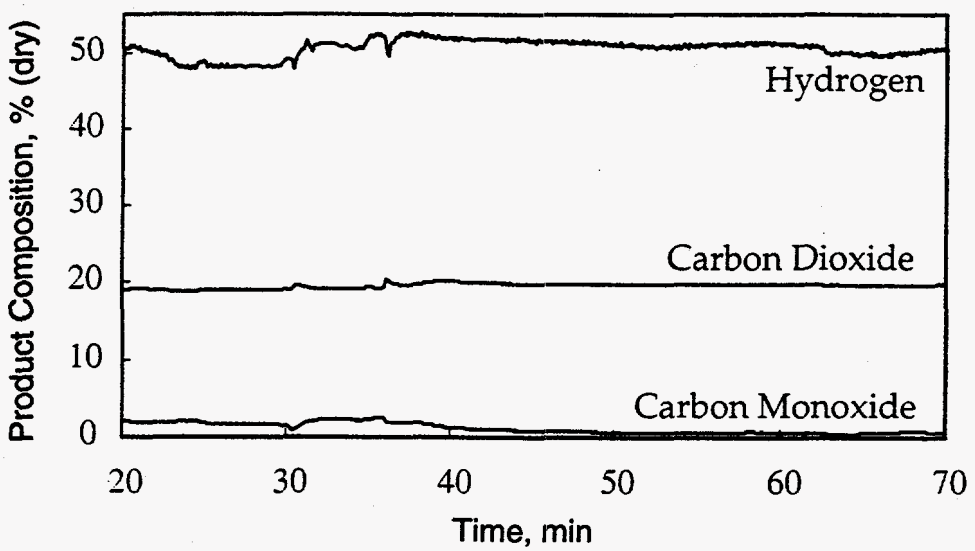

Fig. I-14. Composition of Product Gas from Methanol Partial-Oxidation Reformer and Shift Reactor

In a manner similar to that of Eq. 7, the overall partial oxidation of a paraffinic hydrocarbon to generate hydrogen may be represented by the following equation:

$$C_nH_{n+2} + x(O_2 + 3.76N_2) + (2n - 2x)H_2O = nCO_2 + (3n + 1 - 2x)H_2 + 3.76xN_2 \quad (8)$$

The equilibrium product distribution as a function of temperature is shown in Fig. I-15. Although the highest hydrogen concentration of 50% is possible at 700°C, the level of carbon monoxide is also quite high (20%). This means that extensive post-processing of the reformate would be necessary to reduce the CO to acceptable levels of a few parts per million. Moreover, thermodynamic equilibrium is difficult to attain at these relatively low temperatures. Thus, we are exploring a catalytic pathway for the desired conversion in Eq. 8. As a first step, we are identifying materials that will catalyze the reaction at low temperatures and achieve good product selectivity (high H_2 and low CO and CH_4).

b. Fuel Sulfur Removal and Reformer Startup Burner

Under the sponsorship of the U.S. Department of Transportation and Georgetown University, International Fuel Cells (IFC) is developing a phosphoric acid fuel cell power plant

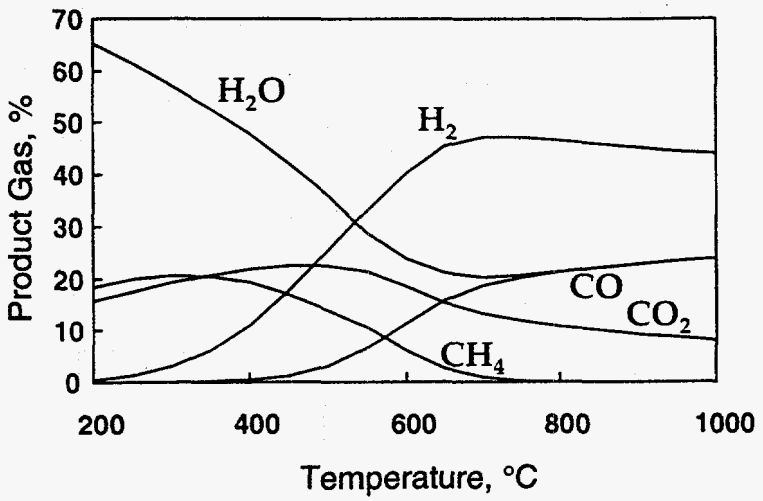

Fig. I-15. Equilibrium Product Composition as Function of Temperature for Partial-Oxidation Reforming of Hydrocarbon Fuels

(100 kW) for a full-size (12-m) transit bus. We were asked by IFC to investigate (1) the removal of sulfur contaminants (which would poison the catalysts used in the methanol steam reformer) present in some methanol fuel, and (2) the potential of the Argonne partial-oxidation reformer for use as startup burners for the methanol steam reformer and the thermal management system in the bus power plant.

Sulfur Contaminant Removal

Commodity methanol by itself contains very little sulfur. Occasionally, however, it may become contaminated with up to about 1% diesel fuel or gasoline in current liquid-fuel distribution systems, which introduces sulfur into the methanol fuel. This sulfur must be removed because of its deleterious effect on the reforming catalysts.

We obtained samples of gasoline and diesel fuels marketed in the Chicago area and analyzed them for the amounts and types of sulfur compounds present in them. The gasoline and diesel transportation fuels were found to contain 550 and 2870 ppm by weight of sulfur, respectively. The sulfur species present were determined to be C1-C4 alkyl-substituted benzothiophenes and 0-C3 alkyl-substituted dibenzothiophenes in a typical diesel fuel, and benzothiophene, methylbenzothiophene, and possibly C1-C3 alkyl-substituted thiophenes in unleaded gasoline. Among the many different adsorbents screened, activated carbons were found to be the most effective in removing these sulfur compounds from methanol that had been contaminated with 1-2% of gasoline or diesel fuel.

Adsorption isotherms as a function of sulfur concentration in methanol were obtained for four commercially available activated carbons: two from Calgon Carbon Corp. and two from Barnebey & Sutcliffe Corp. The results suggest that the benzothiophene and

dibenzothiophene groups exhibit different adsorptivity on the activated carbons, and that the two types of sulfur species compete for the adsorption sites in the activated-carbon pore structure. Packed column tests were also conducted to obtain data on sulfur breakthrough with these activated carbons. Analysis of the data suggested that a granular activated carbon adsorber (the most popular fixed-bed process for adsorption operations) may not be suitable for an on-board application because of the large amount of sorbent required. However, it would be feasible to install such adsorbers at refueling stations, where space and weight are not a critical concern. Used in such a manner, this adsorber can provide insurance against occasional sulfur contamination of commodity methanol.

Startup Burner

The methanol steam reformer in the fuel cell power system for the bus application must be capable of rapid startup. We have investigated the potential for using a suitably modified Argonne partial-oxidation reformer (APOR) as a startup burner for the steam reformer in the IFC fuel cell system, as well as a startup burner for the entire thermal management system in the bus.

The APOR was modified and tested to determine if it could meet IFC's specifications for the reformer startup burner. The APOR was reconfigured with a 1-kW ignition coil and a catalyst bed containing four or five honeycomb disks of 25-mm length each. The results showed that this burner can very quickly ignite the liquid methanol to rapidly heat up the catalyst bed. Subsequently, the partial-oxidation reactions of methanol generate hot (200-300°C), combustible product gas (20-30% H_2 and 10% CO) within the 13 s specified by IFC. A general protocol for the startup burner was derived and sent to IFC. This protocol also applies to the thermal management system burner, with proportional adjustments in air/methanol flows and the ignition coil power. On the basis of limited experimental tests, we concluded that the APOR can be adapted for use as the startup burners for the reformer and the thermal management system of the bus power plant.

c. Direct Methanol Solid Oxide Fuel Cell

The objective of this effort is to develop a solid oxide fuel cell (SOFC) that can operate at 450-550°C (as opposed to the 800-1000°C now required) on methanol and air. At these relatively low temperatures (for an SOFC), the stack materials and designs could be much simpler, and the fuel cell would be attractive for transportation applications.

Last year[9] we reported the results of testing such fuel cells with a thick electrolyte (1.2 mm) of gadolinium-doped ceria, an anode of nickel-ceria cermet, and a cathode of $La_{1-x}Sr_xCo_yFe_{1-y}O_3$ (LSCF). The performance of these cells, while promising, was not adequate for the transportation application. As shown in Fig. I-16, the cell voltage decrease was caused almost equally by the iR drop in the thick electrolyte (~12 $\Omega \cdot cm^2$) and the polarization at the cathode-electrolyte interface (~14 $\Omega \cdot cm^2$). The open-circuit voltage ranged from 980 mV for the

[9] J. J. Laidler et al., *Chemical Technology Division Annual Technical Report, 1995*, Argonne National Laboratory Report ANL-96/10, pp. 22-24 (1996).

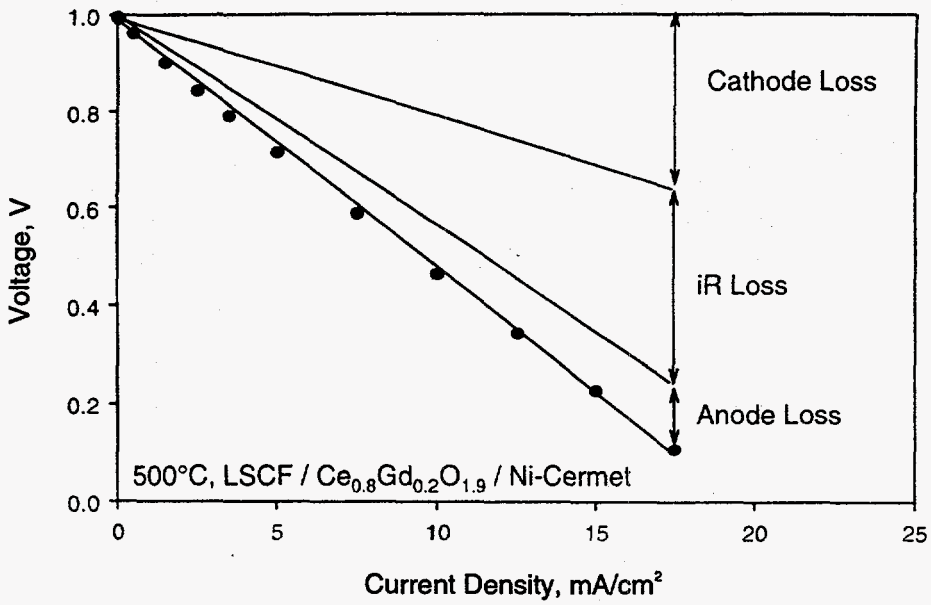

Fig. I-16. Polarization and Resistive Losses in Solid Oxide Fuel Cell at 500°C

thick-electrolyte cells to 800 mV for thinner (~0.5 mm) electrolyte cells. The decrease in open-circuit voltage with decreasing thickness was found to be due to some interconnected porosity in the sintered electrolyte discs. We expect the electrolyte porosity in future cells to be eliminated with improved powders now becoming available from commercial vendors. The iR drop through the electrolyte can be reduced by decreasing the electrolyte thickness and will be a future endeavor.

Effort this past year was also focused on further improving the cathode materials. The performance of the LSCF cathode was improved by developing a new fabrication method that yields a better microstructure. This has reduced the cathode polarization resistance from ~14 to ~6 $\Omega \cdot cm^2$. This resistance, however, is still too high to achieve adequate cell performance at 500°C, for which the polarization needs to be reduced to ~1 $\Omega \cdot cm^2$. New cathode materials and structures have been tested in an attempt to achieve this low polarization. One of the new materials is a two-phase material, which showed a polarization resistance of 1.7 $\Omega \cdot cm^2$ at 500°C and 0.32 $\Omega \cdot cm^2$ at 600°C. Work is in progress to further improve the cathode by modifying the microstructure to achieve the target polarization resistance of ≤ 1 $\Omega \cdot cm^2$ at 500°C.

d. Modeling and Systems Analyses

In this activity, we are developing computer simulations of various configurations of fuel-cell systems for use in transportation applications. The major activity is related to the design and analysis of polymer electrolyte fuel cell systems and components; other fuel cell systems, such as the phosphoric acid fuel cell, are also modeled, as needed. Work this year has focused on dynamic modeling of methanol steam reformers, the type of reformer now being developed by General Motors Corp.

Some early results of the dynamic modeling of a methanol steam reformer heated by a hot gas were presented in last year's report.[10] Those results showed that catalyst tubes with small diameters (1-2 cm) yielded significantly faster reformer startup times, primarily due to improved heat transfer to the catalyst from the hot-gas flow. We have now incorporated the dynamic reformer model in the system simulation and examined the system's dynamics during power transients. Since the steam reforming catalyst degrades rapidly if it overheats, we looked primarily at the problems associated with dynamic power turndown from steady operation at the design power levels.

Three turndown scenarios were analyzed, and the results are shown in Fig. I-17. In the first, the flow rates of both the fuel and air were decreased at a uniform rate from 100% to 50% over 10 s while the fuel utilization in the fuel cell stack was held constant. Figure I-17a shows the temperatures of the process gas entering the catalyst bed in the reformer. Note that the system is not at a new steady state at the end of the first 10 s. The temperature of the process gas at the inlet to the copper-zinc oxide catalyst used in the reforming reaction increases from 130°C to over 350°C in 10 s. This temperature is much higher than what the copper-zinc oxide catalyst can safely tolerate. This is caused by two factors. The hot gas, while having a smaller flow rate, is still delivering heat to the reformer walls, and the walls have a sufficiently high thermal mass to maintain the design temperature but are now delivering heat to a much smaller water/fuel mixture.

The second scenario (Fig. I-17b) was devised to control the reformer inlet temperature. The system configuration was changed so that some of the process water for the reformer would come directly from the coolant water flow. In this scenario, the total water-to-fuel ratio was kept constant. After 10 s, 10% of the process water was supplied from the coolant water tank. Figure I-17b shows that the addition of the cold water easily keeps the water/fuel mixture at the reformer inlet under 200°C.

During the above two scenarios, the system power turndown was matched by a corresponding reduction in fuel gas flow rates such that the fuel utilization was maintained constant. If, however, the fuel utilization were to decrease in the early stages of the power turndown, then the temperature of the hot gas entering the preheater would increase dramatically, necessitating a still greater control over the inlet process gas temperature. Figure I-17c shows the results for such a scenario, in which the fuel utilization is suddenly decreased from the design level of 85% to 25% at 1 s into the run, and is then increased to 85% over the next 9 s as the gas flow rate is reduced. The water quench of the second scenario is also used. This simulation shows that the process gas inlet temperature increases to over 360°C in the first 9 s and is still rising at that time. Thus, the cold-water mixing that was effective in the second scenario is no longer adequate to control the reformer catalyst temperature within acceptable values if the fuel utilization is allowed to drop, even if for a very short time.

[10] J. J. Laidler et al., *Chemical Technology Division Annual Technical Report, 1995*, Argonne National Laboratory Report ANL-96/10, p. 35 (1996).

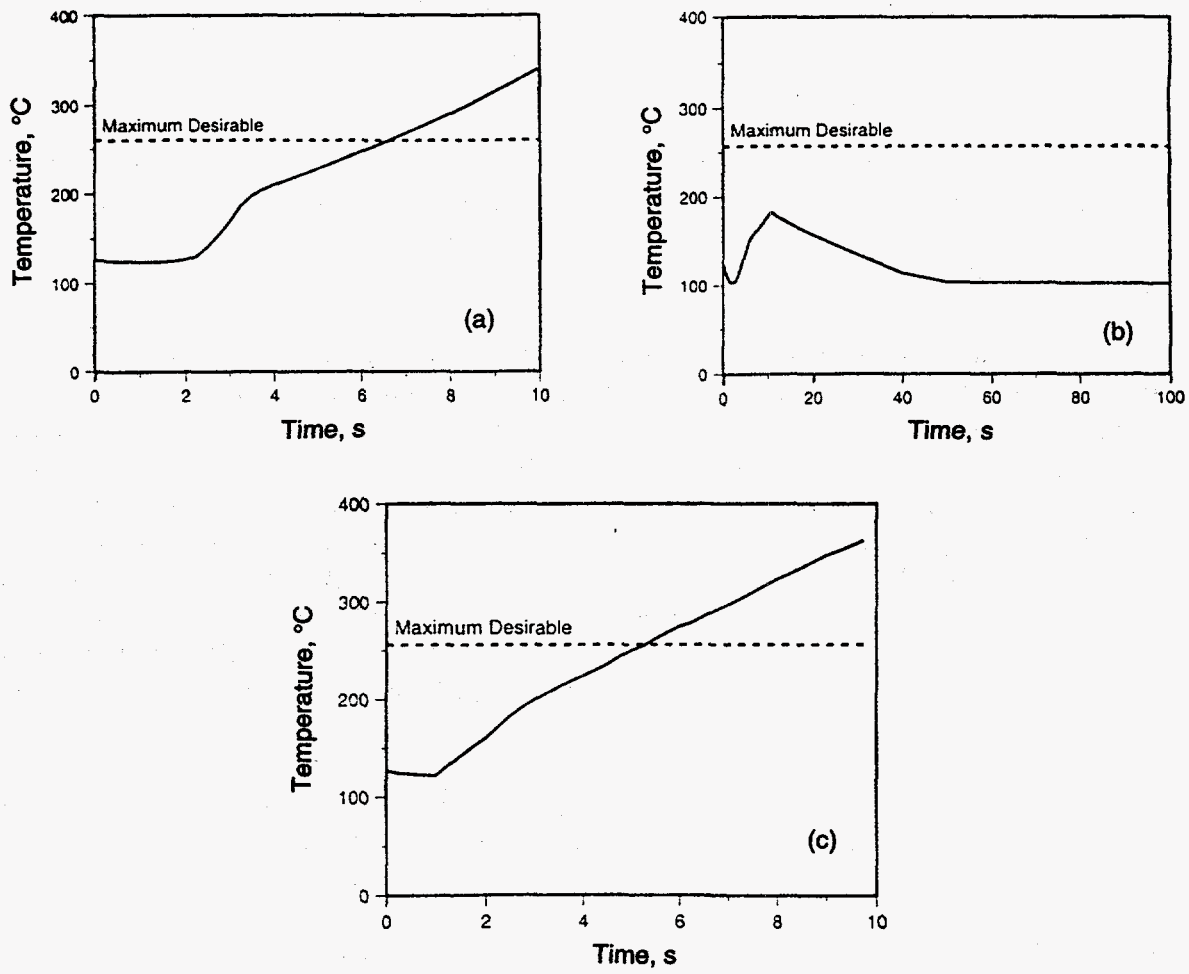

Fig. I-17. Temperatures of Methanol Steam Reformer during Power Turndown Transients: (a) Power Turndown to 50% of Full Load with Constant Fuel Utilization; (b) Same as in (a) but with 10% Cold Water Added to Process Gas; (c) Same as in (b) but with Decreased Fuel Utilization during the First 10 s of Power Transient

In practice, fuel cells are being considered for use in hybrid systems, where an energy storage subsystem, such as a battery, would be used for load leveling. Even so, because of the highly variable driving situations, there will be instances when the power from the fuel cell subsystem must be turned down. Our analyses have shown that a hot-gas-heated steam reformer is not well suited to transient operation, and this shortcoming will need to be addressed by developing suitable control strategies.

4. *Direct Methanol Polymer Electrolyte Fuel Cells*

The direct methanol fuel cell (DMFC) is an attractive power source for portable applications due to the high energy density of methanol, the portability and ease of distribution of liquid rather than gaseous fuel, and elimination of the need for a bulky, power-consuming fuel

reformer. Solid polymer proton-conducting membranes, such as Nafion (made by DuPont), have received much attention for use in DMFCs since they are highly conductive at low temperatures (60-100°C), thermally and chemically stable, and noncorrosive. Two major obstacles to commercialization of the proton-conducting DMFC are low electrocatalytic activity of the anode catalyst for the methanol oxidation reaction and transport of methanol through the membrane to the cathode compartment. Methanol crossover not only lowers fuel utilization but also depolarizes the cathode catalyst, decreasing the cell operating voltage by as much as 250 mV.

Methanol transport through a proton-conducting membrane can occur by two mechanisms. The dominant mechanism at low current densities and at methanol concentrations below 2 M is diffusion of methanol through the hydrophilic pores of the membrane due to the concentration gradient. Methanol is also transported as part of the solvation sphere of the proton (electroosmotic drag). The ratio of methanol molecules to water molecules solvating the proton is identical to their concentration ratio in solution. Therefore, electroosmotic drag of methanol becomes a significant factor at methanol concentrations greater than 2 M and is most likely responsible for the DMFC performance decline previously seen at methanol concentrations above 4 M. Elimination of electroosmotic drag would allow the use of higher concentrations of methanol, which would improve the kinetics for methanol electrooxidation and decrease the volume of water needed in the system.

Electroosmotic drag of methanol may be eliminated entirely by reversing the direction of ionic conduction in the DMFC such that ions are transported from the cathode to the anode. The product of the cathodic oxygen reduction reaction in a basic environment is the hydroxide ion. Transport of the hydroxide ion can be accomplished by using an anion exchange membrane. An additional advantage of working in the basic environment provided by a hydroxide ion conductor is a decrease in the formation of poisoning intermediates in the methanol oxidation reaction. This decrease leads to much higher rates for the methanol oxidation reaction in basic solutions as compared to acidic solutions. The cathodic oxygen reduction also causes less polarization loss in the basic electrolyte.

This concept of using a hydroxide-ion-conducting membrane to reduce methanol crossover in a DMFC was pioneered in CMT. Fuel cells based on hydroxide-conducting membranes that are commercially available have been fabricated and are being tested for their performance as DMFCs and for their methanol crossover rates. Figure I-18 shows typical performance and compares the methanol crossover rates for the hydroxide-ion-conducting cells to the rates for proton-conducting cells operating at 60°C on 2 M methanol. This figure illustrates that the methanol crossover rate is reduced by 86% with a hydroxide-ion-conducting membrane. At this point, the current densities obtainable with cells based on hydroxide-ion-conducting membranes are approximately an order of magnitude lower than those obtainable with Nafion-membrane cells. These lower current densities reflect poor utilization of the platinum-based catalyst caused by inadequate contact of the catalyst with the membrane. Catalyst utilization will be improved by polymerizing the monomers of the membrane around the catalyst particles on either side of a membrane that was prepared in-house.

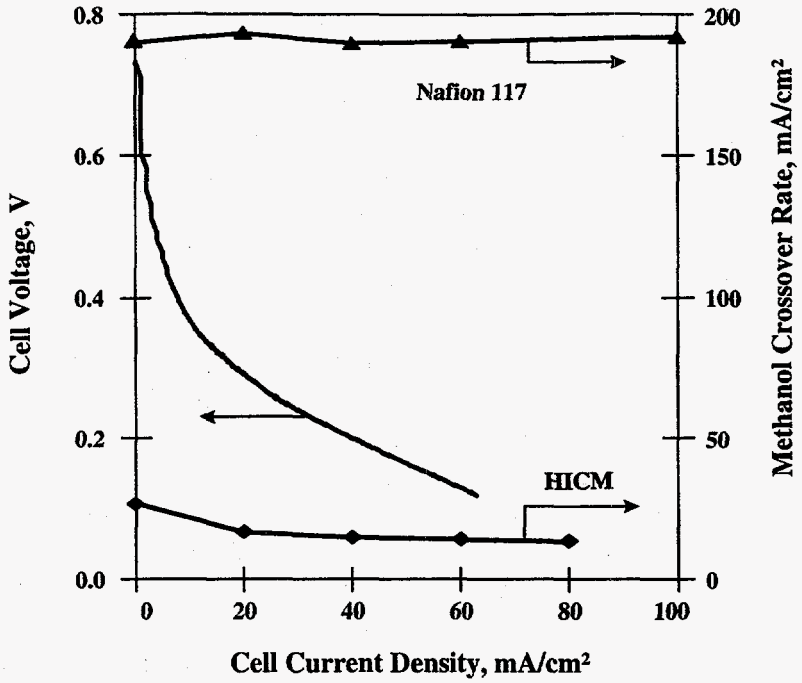

Fig. I-18. Methanol Crossover Rates for Fuel Cells with Hydroxide-Ion-Conducting Membrane (HICM) and Proton-Conducting Electrolyte (Nafion 117)

5. Technical Management

The CMT Division, through the ANL Electrochemical Technology Program, provides support to the DOE Office of Transportation Technologies and to the DOE Office of Buildings Technology in the form of technical management of R&D contracts with industrial developers of fuel cells and related components. In this capacity, we prepare work statements, evaluate proposals, and conduct progress reviews. Major ongoing projects managed by CMT include DOE contracts with General Motors Corp., Ford Motor Co., Chrysler Corp., and fuel-cell component suppliers.

The DOE/General Motors project managed by the Electrochemical Technology Program completed the second year of a three-year contract ($35 million) to develop a 50-kW methanol-fueled PEFC system for automotive applications. During 1996, two 30-kW PEFC stacks were built and tested by Ballard Power Systems (under a subcontract to General Motors). These stacks achieved the target power density set for 1996 (300 W/L). General Motors also made significant progress in fuel processing technology with the development of a low-cost, low-temperature catalytic combustor for a 30-kW methanol steam reformer. General Motors also began the scaleup of a partial oxidation reformer for methanol to a size suitable for a 50-kW fuel cell; this effort represents a successful technology transfer from ANL, where the concept was developed, to General Motors.

The Electrochemical Technology Program also manages two DOE contracts with project teams headed by Ford and Chrysler to develop PEFC propulsion systems for passenger cars fueled directly by hydrogen carried on board the vehicle. In 1996, Phase I of the DOE/Ford project was completed with the assembly and testing of several 10-kW PEFC stacks; the project targets for a specific power of 280 W/kg and 0.25 mg Pt/cm^2 catalyst loading were achieved. Two of Ford's fuel cell suppliers, International Fuel Cells and Mechanical Technology, Inc., were selected to proceed into Phase II. The Phase II deliverable scheduled for 1997 is an integrated power system with a 50-kW PEFC stack having a specific power of 370 W/kg and a stack catalyst loading of 0.25 mg/cm^2.

Chrysler also completed the second year of a three-year contract ($15 million) to develop a PEFC propulsion system by using a design-to-cost approach. During 1996, AlliedSignal developed an advanced PEFC stack design with a specific power and power density of 620 W/kg and 620 W/L, respectively, which exceeded the performance goals. AlliedSignal also completed initial development of lightweight bipolar plates made from carbon-coated metal and conductive plastic. On the basis of AlliedSignal's design-to-cost analysis, the projected cost for their PEFC was reduced by an order of magnitude, to $73/kW and $50/kW for the carbon-coated metal and conductive-plastic bipolar plates, respectively.

The Electrochemical Technology Program also continues to manage a DOE contract with Arthur D. Little, Inc. (ADL) to develop a partial-oxidation fuel reformer that can be carried on board a vehicle to reform gasoline into a hydrogen-rich gas of sufficient purity for a PEFC. The effort in 1996 builds upon the 1995 successful demonstration of a compact 50-kW fuel reformer optimized for ethanol fuel. During 1996, ADL developed and initiated testing of their 50-kW fuel reformer for gasoline.

The Electrochemical Technology Program undertook the management of six new contracts ($5 million) that were awarded by DOE during 1996. Energy Partners, Texas A&M University, and International Fuel Cells were awarded contracts to incorporate innovative designs and materials into small fuel cell stack prototypes and advance the state-of-the-art in PEFC technology. AlliedSignal, ADL, and Vairex Corp. were awarded contracts to develop integrated compressor/expander technologies for supplying pressurized air to fuel cells with the objective of improving the overall energy efficiency of the PEFC system. An expander is used with all three compressor concepts to recover energy in the pressurized exhaust gas stream and thereby enhance the overall efficiency of the fuel cell system.

II

Hazardous and Mixed Waste Research

A major challenge facing the Department of Energy (DOE) is management of the massive quantity of hazardous and mixed (hazardous/radioactive) waste that has accumulated at various DOE sites as a result of nuclear-defense production conducted for more than four decades at these sites. Cleanup and disposal of this waste in an environmentally sound and cost-effective manner is now a major DOE mission. In addition, minimization of hazardous waste production and safe and efficient management of any hazardous waste that is produced are becoming increasingly important considerations in the commercial sector. We are investigating a variety of approaches aimed at treating and disposing of hazardous and mixed wastes in support of DOE's waste management mission. In addition, we are investigating whether the technologies developed for DOE applications could also be used for hazardous waste minimization in industry.

A. Development of Aqueous Biphasic Extraction Processes

Aqueous biphasic extraction (ABE) processes offer the potential for highly selective separations at low cost. This countercurrent extraction technique involves selective partitioning of either dissolved solutes or ultrafine particulates between two immiscible aqueous phases. The extraction systems are generated by combining an aqueous salt solution with an aqueous polymer solution such as polyethylene glycol (PEG).

We have examined a wide range of potential applications for ABE, including the treatment of solid and liquid nuclear wastes, decontamination of soils, and processing of mineral ores. We have also conducted fundamental studies of solution microstructure, using small angle neutron scattering (SANS), in an effort to better understand the physicochemical mechanism of aqueous biphase formation. Summarized below are recent results from the fundamental studies as well as a study of lead removal from soil.

1. Fundamental Studies of Aqueous Biphase Formation

From earlier SANS measurements of PEG/salt solutions,[1] we know that the presence of various biphase-forming salts (e.g., Na_2CO_3, Na_2SO_4, and Na_3PO_4) leads to the formation of PEG aggregates whose length increases with increasing salt concentration up to the consolute point. Our recent analysis of the effects of electrolytes on the cloud points of PEG in H_2O and D_2O suggests that the PEG phase behavior in solution is entropy driven, and that increased structuring of water by lyotropic ions provides the driving force behind polymer aggregation and phase separation.

We have also found that the cloud point lowering of PEG by inorganic salts correlates linearly with the change in water entropy upon the addition of electrolytes.[1] Salt effects on cloud points and biphase formation follow the well-known Hofmeister series.[1] Anions leading to increased structuring of water lower the cloud point. This is illustrated in Fig. II-1, in which the cloud points for solution containing 10 wt% PEG-10,000 are plotted as a function of salt type and concentrations. The data can be described by the following equation in which the salt effects are additive:

$$T_{cp} = T_{cp}^{\circ} + \sum \alpha_i C_i \qquad (1)$$

where T_{cp} is the cloud point of the polymer-salt solution, and α_i is the slope of the straight line relating the change in cloud point with the concentration (C_i) of salt i. The cloud point of the salt-free polymer solution (T_{cp}°) can be estimated by extrapolating the straight-line fit of the data to zero salt concentration. Analysis of systems containing mixtures of salts has shown that, within experimental error, the anion effects are additive.

We have begun to expand our studies to include the effects of polymer structure (e.g., linear versus branched) and polymer type on cloud points and biphase formation. Thus far, we have found that the effects of biphase-forming salts on the cloud points of branched PEG-10,000 and polyvinylpyrrolidone correlate linearly with salt concentration in a manner similar to that observed for PEG (see Fig. II-1).

The α_i values for the linear and branched PEGs are very similar, implying that the conformation of the polymer chain (e.g., linear or branched) is not the dominant factor in salt-induced clouding and aqueous biphase formation. This contradicts the view of Karlstrom,[2] who presented a thermodynamic model for predicting critical solution temperatures in polyethylene oxide/salt solutions. The model was based on the assumption that the temperature-dependent conformation of polyethylene oxide and its effects on the van der Waals attraction between polyethylene oxide molecules are predominantly responsible for the observed phase diagrams.

---

[1] P. Thiyagarajan, D. J. Chaiko, and R. P. Hjelm, Jr., *Macromolecules* **28**, 7730 (1995).

[2] G. Karlstrom, *J. Phys. Chem.* **89**, 4962 (1985).

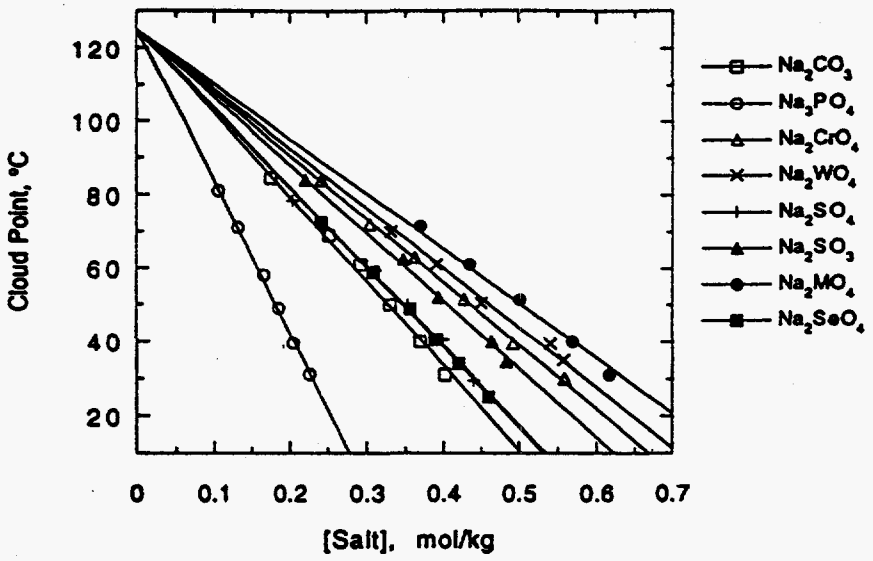

Fig. II-1. Effects of Salt Type and Concentration on the Cloud Point of Polyethylene Glycol with Molecular Weight of 10,000 (PEG-10,000)

Our analysis of cloud point effects has also included the influence of polymer concentration, temperature, and their relationships. We are now able to predict phase diagrams for PEGs with only two to three initial data points. In the near future, we hope to expand these studies to include cation effects.

2. *Removal of Lead from Contaminated Soils*

The removal of heavy metal contaminants from clay-rich soils would achieve significant volume reduction in cleanup efforts. However, it is beyond the capabilities of traditional soil washing techniques. During 1996, we began a study to determine the feasibility of using ABE technology for removal of lead from clay-rich soils. The sources of the two contaminated soil samples used in the ABE studies are two inactive firing ranges at ANL.

The treatment flowsheet includes a combination of conventional particle-classification technologies together with the treatment of the fine-particle-size fraction by the ABE process. Conventional particle classification of the soil samples was carried out by Metcalf & Eddy, Inc. The soil samples were classified according to size and density. The major fraction of the soil (-150 mesh) had lead concentrations ranging from 500 to 1400 mg Pb/kg, which is above industrial cleanup standards (e.g., 400 mg Pb/kg). Two continuous countercurrent ABE runs were completed in 1996. An additional two extraction runs are scheduled for early 1997 to examine the effects of humate removal before the soil is fed into the ABE system. Analytical data from the two completed extraction runs are not yet available.

B. Advanced Electrochemical Systems for Nitrate/Nitrite Destruction

Many of the aqueous wastes that have accumulated from DOE defense operations have high nitrate and nitrite concentrations, which present a disposal problem. For example, if treated by high-temperature vitrification, these wastes will generate significant quantities of nitrogen oxides. In collaboration with JGC Corp. (Oarai Nuclear Research Center), we have developed a design concept of an advanced electrochemical system for the destruction of nitrate and nitrite from caustic high-level waste. Enhanced efficiency is achieved by the selective separation of sodium nitrate and nitrite from the waste feed by ABE followed by reduction to N_2 in a divided electrochemical cell. The ABE system produces feed solutions for the cathode and anode compartments of the electrochemical cells that are at equal osmotic pressure, thereby stabilizing the cell membrane.

A schematic diagram of the treatment system is shown in Fig. II-2. A continuous countercurrent extraction system utilizing PEG treats a salt solution feed and produces a purified nitrate/nitrite stream. Before this stream enters the cathode compartment, the PEG is recovered for recycle by cloud point extraction. The caustic salt solution, depleted in nitrate and nitrite, is fed into the anode compartment. The ABE pretreatment step enables the production of a relatively pure sodium hydroxide stream that is free of unwanted ions such as aluminate. In addition, slow poisoning and corrosion of the cathode by chemical species such as chromate and HF are avoided by use of the caustic solutions generated in the ABE pretreatment step. The flowsheet allows the combination of nitrate destruction and salt splitting in a single treatment system and does not generate hydrogen gas as a byproduct of the electrochemical reduction.

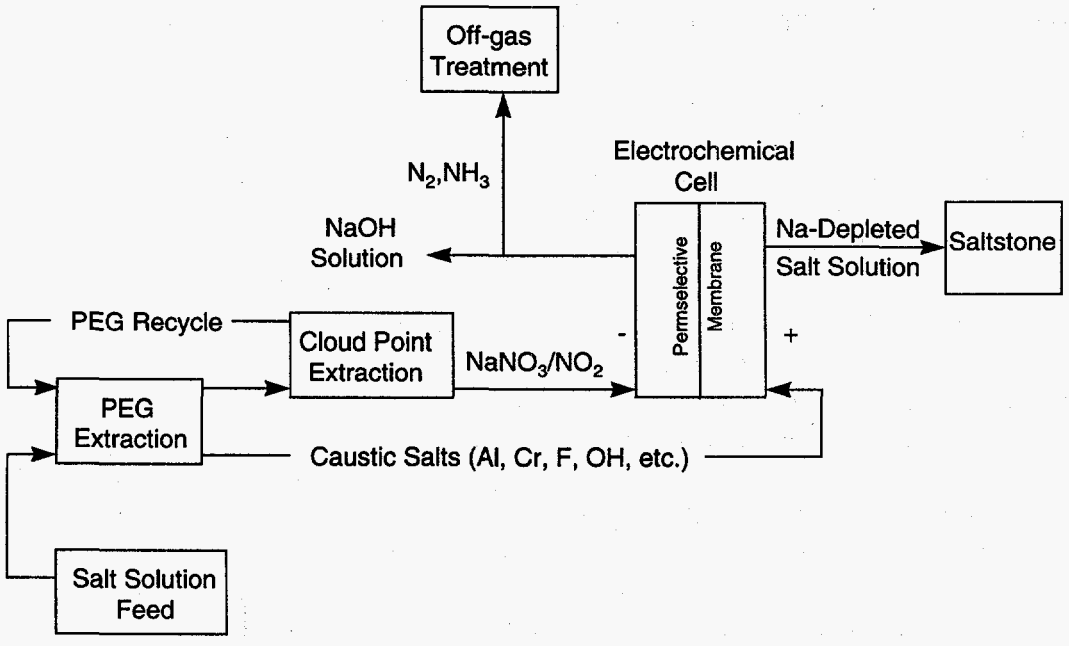

Fig. II-2. Schematic Flowsheet for Nitrate and Nitrite Destruction from Caustic High-Level Waste

Preliminary results from bench-scale tests have shown that the electrochemical flowsheet in Fig. II-2 is capable of achieving >95% efficiency with N_2 gas as the primary reduction product. Further work is needed to collect more detailed mass-balance and energy-balance data for cost analysis. We are currently seeking funding to complete an evaluation of this promising technology.

C. Solid/Liquid Separation by Sol-Gel Approach

The recovery of fine particles from aqueous process streams remains one of the more difficult and expensive operations in the treatment of high-level tank wastes, such as those at the DOE Hanford site. The baseline technology for solid/liquid separation currently includes filtration. In an effort to find a less costly and more effective approach, we are evaluating advanced sol-gel processes for separating and recovering particulates from both acidic and highly caustic waste slurries. Early indications are that sol-gel processes would be capable of recovering more than 99.99% of all particulates in a slurry, including colloidal species, with more than 90% recovery of salts in a separate aqueous stream. The sol-gel approach combines the aqueous waste slurry with an alkali silicate (as an aqueous solution or a dry powder) and a gelling agent. While the gel ages, a process called "syneresis" occurs, in which the liquid held within the pores of the gel is spontaneously exuded from the gel. The choice of gelling agent, the presence of water soluble salts, the pH, and the temperature can significantly affect both the rate of syneresis and the amount of liquid recovered.

During the wet processing stage, the gel contains a high degree of porosity (50 to 70%) and a large, average pore size. Particles that are larger than the pore size are physically trapped within the gel. We have also observed that particles smaller than the pore size act as nucleation sites and become immobilized in a three-dimensional SiO_2 network. Thus, nearly complete recovery of particulates and colloids from high-level waste streams can be achieved.

In initial laboratory tests, neutralized current acid waste (NCAW), a Hanford tank waste simulant, was spiked with 20 wt% of micron-sized powders (Fe_2O_3 or zeolite) and treated by the sol-gel process. The results showed, contrary to previous expectations, that it is possible to form a silica gel monolith under highly caustic conditions. The NCAW simulant used in these tests contained 4 M hydroxide, and the pH did not decrease significantly during silica gel formation. A number of commercially available gelling agents were capable of producing a silica gel monolith in the presence of the tank waste simulant. A reduction of pH to below 10 was not required to form the gel, as suggested in the literature.[3,4]

In preliminary tests, equal volumes of the spiked NCAW simulant and Kasil 6 (a commercial potassium silicate solution) were combined with a gelling agent. The aqueous liquor generated during syneresis was collected and analyzed by either ion chromatography or inductively coupled plasma/atomic emission spectroscopy, and a mass balance of the various

[3] R. K. Iler, *The Chemistry of Silica*, John Wiley and Sons, New York (1979).

[4] C. J. Brinker and G. W. Sherer, *Sol-Gel Science*, Academic Press, New York (1990).

ionic species was calculated. Table II-1 gives the mass-balance results for several of the salts originally present in the NCAW simulant. Results from the analysis of the mother liquor by filtration at 0.02 μm and examination of the filter by electron microscopy indicated nearly complete recovery of the solids in the silica gel monolith; no zeolite or iron oxide particles were found in the filters. As shown by Table II-1, however, the process conditions have not yet been optimized with respect to salt recovery.

Table II-1. Mass Balance of Salt Partitioning from NCAW Simulant during the Sol-Gel Process for Solid/Liquid Separation

Ionic Species	Salt Recovery in Mother Liquor, wt%
Nitrate	96.1
Nitrite	91.2
Sulfate	89.3
Sodium	75.7
Potassium	71.1
Rubidium	98.1

The sol-gel process allows dry silica monoliths with high solids loading (e.g., 40-50 wt% or higher) to be produced for use as a feedstock to a glass melter. The high solids loading means that the sol-gel process would have a negligible impact on the final volume of borosilicate glass required for disposal of high-level waste.

D. Actinide Stability/Solubility in Waste Isolation Pilot Plant (WIPP) Brine

The Waste Isolation Pilot Plant (WIPP) in Carlsbad, New Mexico, has been selected as a possible disposal site for transuranic radioactive wastes resulting from defense-related activities at DOE sites. The CMT Division is providing experimental data for the WIPP project on actinide solubility and oxidation-state distribution in simulated WIPP brine. These data are being used to test and challenge the Actinide Source Term (AST) model being developed for the WIPP project. Additionally, our empirical solubility measurements will serve as a backup for the AST program should solubility data from more fundamental studies be unavailable.

The goals of the stability/solubility experiments are to establish the oxidation-state stability and solubility of U(VI), Np(VI), and Pu(VI) in WIPP-relevant brine. Experiments were performed with a starting actinide concentration of ~10^{-4} M in several simulated WIPP brines: G-Seep at pH 5 and 7, ERDA-6 at pH 8 with carbonate, and ERDA-6 at pH 10 with and without carbonate present. All experiments were conducted at 25°C in an oxygen-free environment with

a hydrogen atmosphere of ~1000 torr (~0.1 MPa). The reaction vessel was a 1-L polypropylene bottle placed inside of a Hastelloy C-276 pressure vessel. Gas and liquid sampling was done periodically, without removing the atmosphere, through the ball valve on the vessel. Analyses performed included gas chromatography (gas phase), alpha scintillation counting (for plutonium), gamma counting (for neptunium), inductively coupled plasma/mass spectroscopy, and absorption spectrometry. Duration of the experiment is expected to be ~1 yr.

The results obtained to date (150 days) have fallen into two categories. First, in several experiments, the actinide(VI) oxidation state has been found to persist as a stable, truly dissolved species. This occurred with Pu(VI) in ERDA-6 brine with and without carbonate present, Np(VI) in ERDA-6 with carbonate, and U(VI) in G-Seep at pH 5 and in ERDA-6 at pH 10 with carbonate. As an example, Fig. II-3 shows the persistence of the U(VI) species in ERDA-6 brine at pH 10 with carbonate. As deduced from the top spectrum in Fig. II-4, a U(VI)-carbonate complex formed during this test. Also shown in Fig. II-4 is the spectrum obtained for G-Seep brine at pH 5, which indicates that a U(VI)-aqo/chloride complex formed during this test. The starting ~0.1 mM actinide concentrations in these experiments were below saturation. Factors that led to the continued high actinide concentrations during testing were carbonate complexation, low pH, and redox stability.

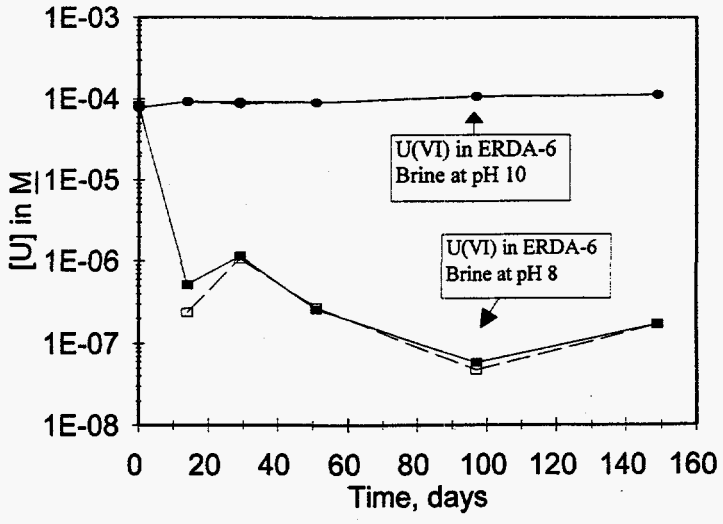

Fig. II-3. Concentration of Uranium as a Function of Time for Uranium in ERDA-6 Brine at pH 8 and pH 10 with Carbonate (filled symbols, unfiltered; open symbols, samples passed through 0.2 μm filters)

In the second category of results, the actinide(VI) oxidation state was found to have a low steady-state solubility. This occurred with uranium in G-Seep at pH 7 and in ERDA-6 with carbonate at pH 8, as well as with neptunium in ERDA-6 at pH 10 with no carbonate. Final actinide concentrations decreased from ~0.1 mM at the start of the experiment to a value that was typically two or three orders of magnitude lower (e.g., see Fig. II-3 for uranium in ERDA-6 at

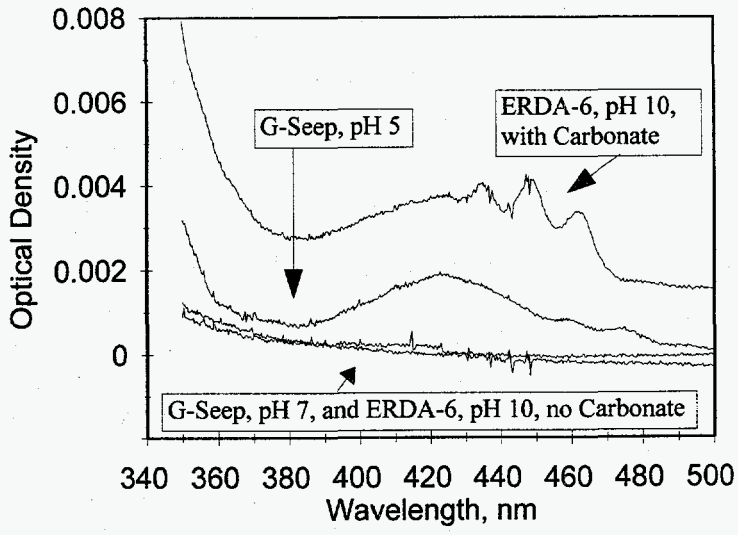

Fig. II-4. Absorption Spectra for Uranium in WIPP Brine after 149 Days of Testing

pH 8). This suggests that actinide phases are being formed, and steady-state actinide concentrations are established in these brines.

Redox instability was also noted. For both Np(VI) and Pu(VI) in G-Seep (i.e., at low pH), actinide(V) species were observed. For neptunium, reduction to Np(V) was rapid and complete, so the contribution to long-term solubility from the Np(VI) species can be discounted. For Pu(VI), reduction was slow and appeared to be linked to autoradiolytic effects.

The presence of chelating agents (citrate, oxalate, and ethylenediaminetetraacetic acid) was qualitatively evaluated. Organics destabilized the actinide(VI) oxidation state in WIPP brine, leading to the reduction of actinide(VI) to form organic complexes of lower oxidation state [e.g., Np(V) and Pu(IV/V) organic complexes] or the precipitation of actinide phases. Complexation with carbonate decreased the reduction rate but did not prevent net reduction of the actinide. Further work is needed to quantify the redox effects noted.

E. Microbiological-Actinide Interactions in the Subsurface

The speciation (i.e., complexation, oxidation state, and aggregation) of radionuclides is being investigated under conditions relevant to subsurface groundwaters on DOE lands. Past practices at DOE facilities have resulted in the contamination of subsurface aquifers with mixtures of organic compounds and radionuclides. An important class of mixed contaminants includes co-disposed actinides and organic chelating agents, such as nitrilotriacetic acid (NTA). The presence of strong complexing agents in subsurface environments can increase dissolved actinide concentrations, leading to enhanced radionuclide migration in groundwater.

Efforts during the past year were continued to identify the key interactions between plutonium-organic complexes and bacteria in the subsurface. The degradation of NTA by *C. heintzii* is a relatively well-understood "model" system that is being used to investigate actinide-microbiological interactions. The *C. heintzii* bacterium is an NTA degrader that is representative of aerobic bacteria being considered for *in situ* bioremediation. Recent emphasis has been on determining the radiotoxicity of plutonium toward *C. heintzii* and conducting experimental work to develop a basis for modeling actinide-microbiological interactions in the subsurface. This work is being done to establish the key interactions that lead to the mobilization and immobilization of plutonium in the subsurface and is part of a multi-laboratory effort involving collaborations with Pacific Northwest National Laboratory and Northwestern University.

During the past year, the radiotoxicity of plutonium toward *C. heintzii* was examined in three sets of experiments. First, gamma irradiation experiments were performed at room temperature with the *C. heintzii* suspended in high-purity water or 0.01 M PIPES [1,4-piperazinebis(ethane-sulfonic) acid] buffer medium. Five milliliters of the suspended bacteria was placed in glass tubes, then irradiated at a rate of ~ 2×10^5 rad/h for up to one day. Second, plutonium experiments were performed in PIPES buffer (pH ~ 6.2) at room temperature in the concentration range of 10^{-4} to 10^{-9} M Pu-239 with 0.2 mM NTA present in solution. Third, experiments were also performed with Pu-242 under conditions that were otherwise identical with the Pu-239 studies. In all cases, cell viability was established by plate counts of the colony-forming units.

In the gamma irradiation experiments, exposure of *C. heintzii* to 18.5×10^3 rad of gamma radiation killed over 99% of the bacteria. This is typical of procaryotic cells in oxygenated systems. No differences in radiotoxicity were noted between the microbes suspended in high-purity water compared with those suspended in 0.01 M PIPES buffer. In the Pu-239 experiments, significant toxicity effects were noted at plutonium concentrations greater than ~ 0.001 mM (see Fig. II-5). When Pu-242 was used instead of Pu-239, the cell death rate was primarily proportional to the activity of the plutonium rather than its concentration. Thus, the toxicity is considered radiolytic rather than chemical in nature when the plutonium exists as a Pu-NTA complex. The dose-to-solution ratio in the plutonium concentration experiments was, however, far less than that needed to cause cell death in the gamma experiments. This suggests that the observed association of plutonium with the bacteria was a necessary step in the loss of cell viability in that alpha particle deposition in the vicinity of the cell, or in the cell itself, was needed to account for the toxicity observed. The strong association between *C. heintzii* and plutonium was attributed to two mechanisms. At plutonium concentrations $\leq 10^{-4}$ mM, bioassociation was rapid and occurred even in the presence of NTA as a complexant. At higher plutonium concentrations, the association of plutonium with the biomass was slow and attributed to the destabilization of the Pu-NTA complex and subsequent plutonium polymer formation. The NTA tied up in the Pu-NTA complex was not biodegradable.

The second area of progress was in modeling the degradation of NTA by *C. heintzii*. A biodegradation model is being developed at Northwestern University. Initially, an assessment of data needs for the model system was made. Experiments were then performed to develop the

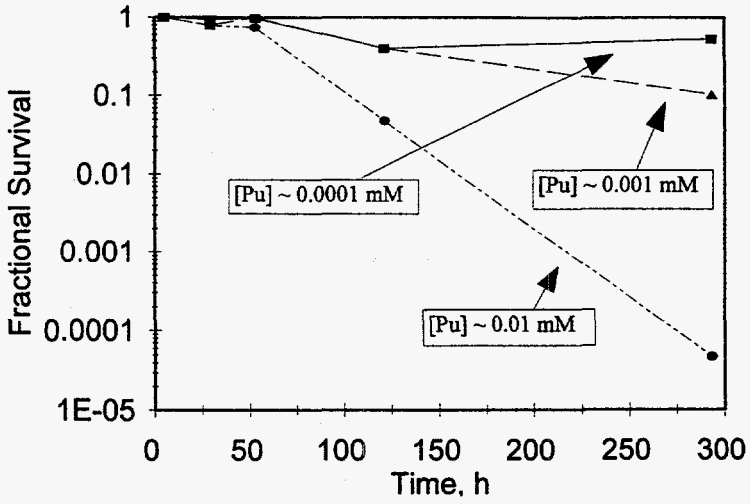

Fig. II-5. Effect of Plutonium-239 Concentration on the Survival (based on colony-forming units) of *C. heintzii*

needed database and mechanistic understanding. The most important accomplishments of this work were (1) establishing the relationship between biomass and net NTA degradation, (2) determining the role of oxygen availability in limiting/facilitating cell growth, (3) measuring ammonia production as a result of biodegradation, and (4) deriving a quantitative correlation between mineralization rates and NTA degradation. Additionally, two mass-balance studies (for nitrogen and carbon) were performed to further define the degradation mechanism. The nitrogen mass-balance studies showed that NTA is primarily converted to ammonium by *C. heintzii*. The carbon mass-balance studies showed that mineralization of NTA to carbon dioxide was incomplete, and a lag time occurred between NTA degradation and CO_2 production. The carbon could be accounted for as partly in the cell and partly in a dissolved organic species. It is thus important to rely on NTA degradation rather than CO_2 formation to measure degradation kinetics. All of these results have led to improvements in the ability to model the *C. heintzii*-NTA system.

Future efforts will expand this work to include actinides besides plutonium (e.g., Np and U) and anaerobic, as well as other aerobic, biosystems.

F. Separation of Cesium from Crystalline Silicotitanates

Crystalline silicotitanates (CSTs) are inorganic ion exchangers, jointly developed by Sandia National Laboratories, Texas A&M University, and UOP, Inc. These materials are being considered for extracting cesium from aqueous waste streams generated during the processing of high-level waste at DOE facilities. Once loaded with cesium, the preferred option would be to directly incorporate the cesium-loaded CST (Cs-CST) into a borosilicate glass waste form. However, this option may increase the volume of solidified high-level waste because of the titanium loading limit in borosilicate glass and the relatively high concentration of titanium in

CST. Alternatives are, therefore, being investigated for incorporating the extracted cesium into borosilicate glass. We are investigating several processing options for separating the extracted cesium from the CST with the goal of incorporating the cesium into a high-level waste form and the CST into a low-level waste form.

Our approach is to contact the Cs-CST with a molten potassium or sodium salt in which the CST is insoluble. Sodium or potassium cations in the molten salt are expected to exchange with cesium cations in the Cs-CST, with the final distribution of cesium between the CST and the salt being proportional to the ratio of cesium to total alkali (cesium plus sodium or potassium) in the system. The molten salt plus Cs-CST mixture is then cooled to resolidify the salt, which now contains most of the cesium. This solidified mixture is contacted with an aqueous solution to dissolve and, hence, separate the cesium-enriched salt from the insoluble CST. Important criteria for selection of candidate salts were that the salt had to melt at a relatively low temperature (<400°C), and both the cation and the anion had to be compatible with existing borosilicate glass compositions being considered for waste disposal. We sought to identify conditions under which sufficient quantities of cesium can be recovered in the aqueous phase so that the insoluble solid, containing most of the CST, can be processed as low-level waste.

Scoping experiments using salts such as KNO_3, $NaNO_3$, KOH, NaOH, and NaO_2CH were conducted at various temperatures ranging up to 700°C and salt:Cs-CST weight ratios ranging from 0.5:1 to 10:1. The highest cesium recoveries were observed under conditions in which the crystalline structure of the CST was altered by thermal or chemical processes. The processing conditions necessary for this alteration differed widely for the various salts tested. For example, with KOH, significant cesium recovery (~80%) was observed at 200°C, whereas with KNO_3, considerably higher processing temperatures, 700°C, were required to achieve comparable cesium recovery. Also, partial dissolution of the CST occurred in the presence of KOH, whereas the CST was chemically inert and underwent thermal decomposition in the presence of KNO_3.

As illustrated in Fig. II-6, cesium recoveries increased as the ratio of KOH to Cs-CST (i.e., potassium to cesium) was increased. Recoveries as high as >97% were observed for a KOH:Cs-CST weight ratio of 4.2:1. As shown in Table II-2, the K/Cs ratio in the solid phase after processing is approximately equal to the initial K/Cs ratio. Although we have shown that the KOH process is able to separate cesium from the CST, significant quantities of certain elements present in the CST, including titanium, appear in the aqueous phase. Work is currently focusing on identifying processing conditions which minimize the transfer of titanium to the aqueous phase.

G. Testing of Phosphate Ceramic Waste Forms

In collaboration with the Energy Technology Division, we are investigating phosphate ceramic waste forms as one option for solidifying DOE's mixed low-level radioactive waste. Because these waste forms contain hydrogen atoms (e.g., in the form of pure water or water of crystallization), the radiolytic production and accumulation of hydrogen gas constitute an

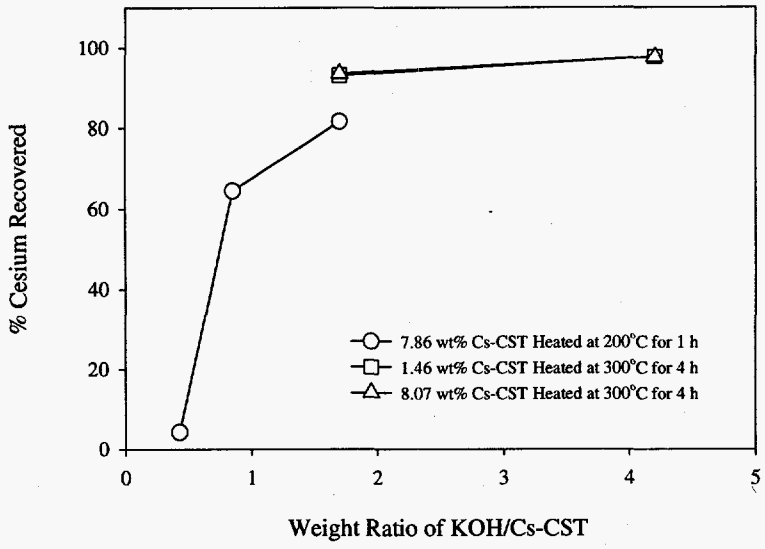

Fig. II-6. Cesium Recovery as Function of KOH/Cs-CST Weight Ratio

Table II-2. Weight Ratio of KOH/Cs-CST before and after Processing

Initial Cesium Loading, wt%	Initial Weight Ratio of KOH/Cs-CST	Weight Ratio K/Cs before Melt Contact	Weight Ratio K/Cs of Recovered Solid
1.46	1.7	80.6	71.9
1.46	4.25	204	244
8.07	1.7	16.4	12.9
8.07	4.25	0.38	0.43

important safety issue for storage and transportation operations. The objective of this study was to quantify the rate of radiolytic hydrogen production by measuring "G-values" (i.e., number of molecules produced or depleted per 100 eV of gamma radiation deposited in the sample) when prototypical samples of the waste form material were irradiated in a gamma radiation field.

The test matrix for the irradiations was designed to allow us to measure the gas generation and depletion when samples of magnesium potassium phosphate, with and without a fly ash waste stimulant, were each irradiated in helium and air atmospheres. The samples were irradiated in sealed pressure vessels for sufficient time to achieve a dose of greater than 10^8 rad. Inductively coupled plasma/mass spectrometry was used to determine the gas generation and depletion in the vessels during irradiation. The G-values were calculated from the gas production and depletion ($\Delta\mu$mol of gas) as follows:

$$G = (\Delta\mu\text{mol of gas})/(\text{sample wt-g})\bullet(\text{dose-rad})\bullet(9.65 \times 10^5) \quad (2)$$

The test results are summarized in Table II-3. In addition to the hydrogen production under all four test conditions, the results indicate significant depletion of the oxygen in the vessels that were filled with air. Much of this oxygen appears in the form of CO and CO_2. The "missing" oxygen is probably due to the formation of water and other condensable molecules. These results provide a basis for initial assessments of the significance of radiolytic gas generation and depletion in applications of phosphate ceramics for radioactive waste stabilization/solidification. The future work, which will be conducted principally in ANL's Energy Technology Division, will focus on scaleup of the production processes for the phosphate ceramic waste form and demonstration of these processes with real mixed waste.

Table II-3. Generation (+) and Depletion (-) of Gases from Irradiation of Magnesium Potassium Phosphate (MKP) with and without Fly Ash (FA)[a]

	MKP		MKP-FA	
Species	Air	Helium	Air	Helium
H_2	+1.45E-2	+4.73E-2	+2.0E-2	+2.66E-2
O_2	-7.25E-2	–	-9.22E-2	–
CO	+0.42E-2	+0.15E-2	+0.53E-2	+0.24E-2
CO_2	+3.03E-2	+0.81E-2	+5.37E-2	+0.85E-2

[a]Number of molecules per 100 eV gamma irradiation (G-values).

III

Nuclear Waste Management

Before nuclear waste can be buried in a geologic repository, its corrosion behavior over long time frames must be known. In the CMT nuclear waste programs, a variety of laboratory tests with simulated and fully radioactive waste glasses are performed to obtain corrosion information that is used to support development of a geologic repository in an unsaturated environment similar to that expected for the candidate site at Yucca Mountain in southwestern Nevada. These tests are primarily directed at determining the interactions between groundwater and various nuclear waste forms, including high-level waste glasses and spent nuclear fuel, under unsaturated conditions. Tests are also underway to support development of vitrified forms of low-level waste generated at the DOE Hanford site, as well as glasses for the disposal of surplus plutonium and plutonium-bearing wastes.

A. Preparation of Review Documents

In this effort, we are compiling and interpreting previously published data that address the effects of several important parameters on the reactions between glass and repository groundwater. Over the last several years, critical reviews were completed on the effects of temperature, glass composition, radiation, and ratio of glass surface area to water volume (S/V) on glass reaction, as well as the status of glass reaction modeling. Two more critical reviews will be completed in the future: one on the effects of unsaturated conditions on glass durability, and the other on the corrosion behavior of natural analogues to the waste glass.

B. Testing of High-Level Waste Glasses

Projects have been ongoing for many years to support DOE in efforts to qualify vitrified high-level nuclear wastes for geologic disposal. The work has been aimed primarily at glass compositions similar to those to be produced at the Savannah River Site in the Defense Waste Processing Facility (DWPF) and at the West Valley Demonstration Project (WVDP). In this work, important information is being gathered on the reaction of the glass waste forms with

groundwater. This information is useful to performance assessments in which the long-term behavior of glass exposed to water must be known.

1. Static Tests of Savannah River Glass

The transuranic elements in high-level nuclear waste require a stable final waste form for a long time frame (>10,000 years). The chosen vitrification material, borosilicate glass, will confine the transuranic elements, and understanding its corrosion mechanism is important to evaluate the behavior of glass destined for a repository in contact with water. The behavior of glass scheduled for production at the DWPF must be evaluated experimentally. However, the time frame for opening a repository site obviously excludes any long-term experimentation that would involve hundreds of years of data collection. Thus, the corrosion behavior must be experimentally evaluated in a more realistic time frame. The glass corrosion mechanism is being studied by varying physical parameters to accelerate the glass reaction. The variation of the S/V ratio is one parameter used jointly with elevated temperature to accelerate glass reaction.

Static dissolution tests with simulated high-level waste glasses that may be produced at the DWPF are in progress at various S/V ratios and 90°C. The objectives are to (1) compare the corrosion behavior of three fully radioactive glasses with that of analogous nonradioactive glasses, (2) determine the effects of S/V on the corrosion behavior of radionuclide-doped glasses and on the disposition of released radionuclides, (3) measure the long-term dissolution rate and study the corrosion behavior of Environmental Assessment (EA) glass, which is the benchmark glass for DWPF glasses, and (4) measure the long-term dissolution rate and study the corrosion behavior of radioactive glass made from the sludge in DWPF Tank 51. Results from these ongoing tests are summarized below.

a. Corrosion Behavior of Fully Radioactive vs. Simulated Glasses

Static dissolution tests with fully radioactive glasses (SRL 131, SRL 165, and SRL 200 frits plus actual DWPF sludge) and nonradioactive homologues are being conducted at 90°C and S/V ratios of 340, 2000, and 20,000 m^{-1} to determine the effect of radionuclides on the glass dissolution and the rates of elemental release. Each S/V is designed to provide information on the different stages of glass reaction. The S/V ratios of 340, 2000, and 20,000 m^{-1} provide information regarding the initial, interim, and long-term stages of glass reaction, respectively. The corrosion mechanism of the glass is inferred from the release rate of the glass matrix elements (Li, Na, B, and Si) and the radionuclides, solution pH, and alteration phases that form on the glass surface. Tests have been in progress for up to 1820 days.

The following observations were made from the test results obtained to date. The dissolution rates of the fully radioactive glasses are similar to those of the corresponding nonradioactive glasses in tests at low S/V (340 and 2000 m^{-1}) and at short test duration (365 days). After five years of testing at 340 and 2000 m^{-1}, both the radioactive and nonradioactive SRL 131 glasses have reached the stage where the alteration phases affect the corrosion rate, while the SRL 165 and 200 glasses have not yet reached this stage. Alteration phases that increase the glass dissolution rates form after about one year in tests at 20,000 m^{-1} with the nonradioactive SRL 200 glasses, but not in the tests with the fully radioactive glasses.

Also, at 20,000 m^{-1}, the leachate solutions in tests with radioactive glasses do not become saturated with respect to those alteration phases that form with nonradioactive glasses. Small compositional differences between the radioactive and nonradioactive glasses and radiolysis of the air and solution in the tests with the fully radioactive glass result in solutions that have lower pH values (differences of between 0.5 and 1.0 pH unit). The concentration of acid produced as a result of radiolysis has been calculated with Geochemist's Workbench™ (Ref. 1), and acidification alone cannot account for the large difference in the leachate solutions for the SRL 200 glass. Furthermore, the calculations of the solution chemistry with the Geochemist's Workbench™ have failed to completely account for the difference in pH between the leachate solutions from the radioactive and nonradioactive glasses. The pH difference is probably due to a combination of radiolysis and compositional effects in the tests with SRL 200 glass, although this remains to be confirmed.

b. Effects of S/V

Static dissolution tests are being conducted at 90°C with glasses made from SRL 131 and 202 frits at S/V ratios of 10, 340, 2000, and 20,000 m^{-1}. The objective is to assess the effect of the S/V on the glass corrosion behavior and the release of radionuclides. Tests completed through six years show that, while the results of tests at different S/V cannot be compared directly because of differences in the pH values, more advanced stages of corrosion are attained in tests at high S/V than in tests at low S/V after the same reaction time. This is because the leachate solutions become highly concentrated in waste form species and alteration phases develop faster in tests at high S/V. The disposition of radionuclides is determined primarily by their solution chemistries. Both Pu and Am are sparingly soluble in the alkaline solutions generated during these tests, while U and Np are moderately soluble. Significant amounts of these actinides become associated with colloidal material that is settled out of solution over time. The solubility of technetium is high in short-term tests but decreases in long-term tests (>1 year) in which the Eh decreases.

An important finding from these tests is that the dissolution rate of the glass increases significantly after certain alteration phases form in tests at 2000 and 20,000 m^{-1}. We have analyzed the results of tests at 20,000 m^{-1} in which rate-affecting phases formed to determine if the long-term dissolution rates are consistent with the model of glass corrosion currently used to calculate long-term behavior.[2] From that model, the dissolution rate after rate-affecting phases form will be constant if those phases precipitate at a rate that is much higher than the glass dissolution rate, so that the assemblage of alteration phases maintains a constant orthosilicic acid activity in the solution. The extent of glass dissolution in our tests was calculated based on the accumulation of boron in solution. The glass particles were modeled as spheres, and the dissolution rate was expressed in terms of the decrease in the radius of the spheres. The test results were adjusted to take into account the effect on the boron release of the loss of surface area as the glass dissolves. This analysis showed that the glass dissolution rate decreased with the test duration and was not constant. This suggests that a different process

---

[1] C. M. Bethke et al., *Geochemist's Workbench*, University of Illinois, Champaign-Urbana, IL (1994).

[2] B. P. McGrail and D. K. Peeler, *Evaluation of the Single-Pass Flow-Through Test to Support a Low-Activity Waste Specification*, Pacific Northwest Laboratory Report PNL-10746 (1995).

influences the dissolution behavior at long reaction times. For example, the precipitation rate of the alteration phases may decrease over time. Nevertheless, the dissolution rate calculated with the current model after alteration phases form provides an upper limit to the dissolution rate under these conditions.

c. Long-Term Corrosion Behavior of Environmental Assessment Glass

We have conducted static dissolution tests at S/V ratios of 2000 and 20,000 m^{-1} and 90°C with the EA glass to measure its corrosion rate in the presence of alteration phases. The behavior of the EA glass in a 7-day Product Consistency Test (PCT) is the benchmark for waste glasses produced at the DWPF. An understanding of the long-term corrosion behavior of the EA glass will provide insight into the possible relationship between corrosion behavior measured in short-term tests such as the PCT and long-term corrosion behavior. Alteration phases that increase the glass dissolution rate (including analcime, gmelinite, and sodium aluminum silicate hydrates) formed within one year in tests conducted at an S/V of 2000 m^{-1} and within 14 days in tests at 20,000 m^{-1}. Similar alteration phases formed in vapor hydration tests at 70–200°C. The glass dissolution rate in the presence of these alteration phases was initially about 0.2 g/(m^2•d) at both S/V ratios, based on the accumulation of boron, but decreased over time (see Sec. III.B.1.b). The decrease may be due to the accumulation of an alteration layer at the glass surface, a decrease in the precipitation rate of the alteration phases, or some other effect on the rate-limiting step as yet unidentified. Other tests are needed to further evaluate why the dissolution slows with reaction time.

d. Long-Term Corrosion Behavior of Tank 51 Sludge-Based Glass

Static dissolution tests are being conducted with a radioactive glass made during a demonstration of the DWPF process (sludge from Tank 51 at Hanford) and with a nonradioactive homologue glass. The objective is to measure the long-term dissolution rate of the sludge-based glass and to determine if alteration phases that increase the dissolution rate form under the same test conditions as occur for other DWPF glasses. Tests are being conducted at 90°C and S/V ratios of 2000 and 20,000 m^{-1}. The test results indicate that the Tank 51 radioactive glass reacts slower than the nonradioactive glass through the longest test durations completed to date (400 days), and it exhibits less corrosion than SRL 202-based glass, which has a similar composition to the Tank 51 glass (see Sec. III.B.1.b). Alteration phases are expected to form after about one year in tests conducted at 20,000 m^{-1} for the SRL 202-based glass. However, after 400 days, no evidence was found of alteration phase formation in the Tank 51 glass. Testing continues.

2. *Drip Tests of Savannah River Glass*

Unsaturated Glass Tests, designated the N2 tests, were initiated in February 1986 on actinide- and technetium-doped SRL 165, a DWPF glass. These tests are still in progress, and the test solutions have been sampled intermittently over the ensuing period of nearly nine years, with regular sampling at 26-week intervals since December 1993. Designed to simulate potential conditions at the proposed Yucca Mountain Repository, in these tests groundwater representative of the site (EJ-13 water) is slowly dripped onto waste glass samples at 90°C in a closed stainless steel vessel. Periodic analysis of the leachate water is performed to monitor release of glass

components, including actinides. Details of the test procedure and test results can be found elsewhere.[3,4] Particulate and colloidal materials released to solution are also analyzed with analytical transmission electron microscopy (AEM) and by sequential filtering with alpha-spectroscopy (for transuranic content). These combined data indicate that insoluble elements, including U, Pu, and Am, are incorporated into alteration phases as the glass reacts and are subsequently released with particulate or colloidal matter as the alteration products spall from the glass. Recent trends have shown that the releases of Pu and Am, while initially quite low compared to those of soluble elements (such as B and Np), eventually are accelerated as the alteration phases in which they are entrained spall from the glass surface and enter the test solution.[3] Ultimately, the release of these actinides will be determined by the transport of the particulates suspended in solution.

An example of the apparent role of colloids in actinide release appears in Fig. III-1. Here, the cumulative normalized release of the elements B, Np, Pu, and Am from one of the three ongoing tests in the N2 series displays a behavior that is best explained by a release of particulate material to solution. The soluble elements B and Np were initially released at a substantially greater rate than the relatively insoluble elements Pu and Am. At later times (after ~8 yr), the spallation of alteration phases, some of which have incorporated Pu and Am, led to total release of these elements, approaching the level expected from congruent dissolution of the glass. We have confirmed through sequential filtering that more than 80% of the Pu and Am, but very little of the Np, in solution from the N2 series are trapped on a 0.1 μm filter. Some of the potential actinide-bearing alteration phases have been observed with AEM. Many of these particles have small (<1 μm) linear dimensions and high surface areas that are characteristic of colloids. The role of colloids in actinide release will continue to be investigated as testing proceeds.

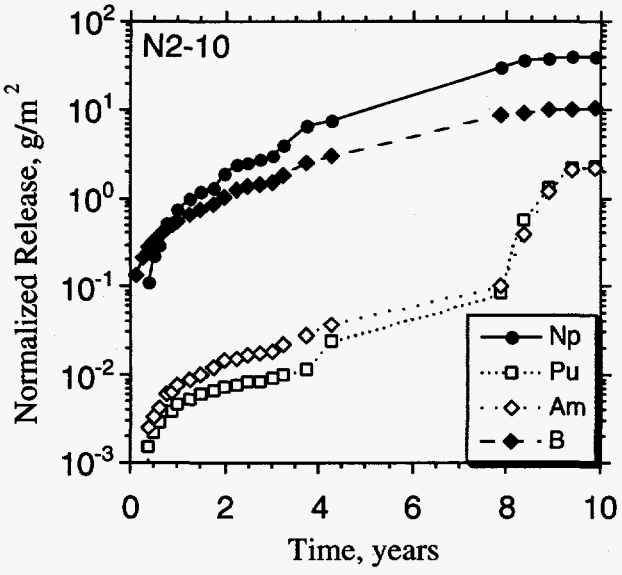

Fig. III-1.

Cumulative Normalized Release of the Elements B, Np, Pu, and Am from Test in the N2 Series. The sudden increase in the release of the insoluble elements Pu and Am shortly after 400 weeks is strong evidence of the role of colloids in the release of these elements from the waste package. The curves are a guide to the eye.

[3] J. A. Fortner and J. K. Bates, *Mater. Res. Soc. Symp. Proc.* **412**, 205-211 (1996).

[4] J. A. Fortner, S. F. Wolf, E. C. Buck, C. J. Mertz, and J. K. Bates, "Solution-Borne Colloids from Drip Tests Using Actinide-Doped and Fully-Radioactive Waste Glasses," to appear in Proc. of the Mater. Res. Soc.

3. Drip Tests of West Valley Glass

Unsaturated Glass Tests, designated the N3 tests, are also being conducted with an actinide- and technetium-doped ATM-10 glass. These tests, begun in July 1987, are similar to the N2 tests described in Sec. III.B.2, and remain ongoing with regular sampling at 26-week intervals. The ATM-10 glass is a former reference glass for the WVDP, and its composition differs only slightly from the present WVDP reference glass.

The ATM-10 glass, like other West Valley glasses, contains substantial thorium, which has been found to cause extensive formation of the actinide-bearing phase brockite (nominally, $CaThPO_4$). Release of actinide elements, besides neptunium, is controlled by their incorporation into alteration phases, which may subsequently spall from the glass and become suspended in solution. A fragment of alteration clay from the surface of one of the reacted glass samples from the N3 series was examined with AEM. The alteration clay was found to be an interesting composite of smectite clay with copious amounts of brockite, plus an amorphous thorium-titanium-iron silicate similar to the mineral thorutite (nominally, $[Th,U,Ca]Ti_2O_6$).[3] Thorium-rich alteration phases appear to play a substantial role in the corrosion behavior of the glass, as the element thorium is released to the test solution at a rate nearly three orders of magnitude lower than the release rates of the water soluble elements Li and B.[3,4]

4. Immobilization of Plutonium Glass

Several alternatives are being considered by DOE for the long-term disposal of surplus plutonium resulting from the dismantlement of nuclear weapons and the cleanup of weapon production sites. One such alternative is immobilization, where the plutonium would be fixed into a glass or ceramic waste form that meets safety and security objectives. Argonne is participating in this national program by (1) developing an alkali-tin-silicate (ATS) glass for the immobilization of plutonium and (2) corrosion testing of glass and ceramic material prepared both at Argonne and at other DOE laboratories for plutonium immobilization.

In 1995, we developed an ATS glass that can accommodate a high plutonium loading (more than 5 wt%) and yet is durable under conditions likely to accelerate glass reactions during long-term storage.[5] This year, a more systematic approach was used to gain a better understanding of the ATS glass composition and the interactions among glass components. The ATS glass includes the following components: Li_2O, Na_2O, K_2O, Cs_2O, ZnO, B_2O_3, Al_2O_3, SiO_2, TiO_2, SnO_2, ZrO_2, C, and Gd_2O_3. In this glass, B, Al, Si, and possibly Zr are "network formers"; Ti, Zn (if in two-fold coordination with oxygen), Al, Zr, and Th have intermediate structural roles that depend on their concentration; and Sn, Th, Li, Zn, Na, K, and Cs act as "network modifiers."[6] The exact roles some of these elements play in the ATS glass depend, in part, on the

[5] J. K. Bates, A. J. G. Ellison, J. W. Emery, and J. C. Hoh, *Mater. Res. Soc. Symp. Proc.* **412**, 57-64 (1996).

[6] W. D. Kingery, H. K. Bowen, and D. R. Uhlmann, *Introduction to Ceramics*, John Wiley & Sons, New York (1976).

concentration of each element and the interactions between an element of interest and the other elements in the glass.[7]

On the basis of this systematic evaluation of the glass, a clear, stable ATS glass containing 5 wt% plutonium (named "P5") was prepared. This glass is currently undergoing testing to characterize the long-term corrosion behavior; tests include a standard leach test (MCC-1), Product Consistency Tests (PCT-A and PCT-B), and the ANL vapor hydration test (VHT). Both the MCC-1 (3 days at 90°C) and the PCT-A tests (7 days at 90°C) have been terminated. Results indicate that durability of the P5 glass is better than the EA reference glass (Sec. III.B.1.c) and is similar to the ATS glass (named "P10") that was prepared in 1995.[5] All vapor hydration tests (exposure to vapor-saturated air at 200°C up to 56 days) for the P5 glass have been terminated; analyses indicated that a hydrated water layer formed on the glass surface, but no alteration phases were seen. The solution and solids from PCT-B with P10 glass were analyzed after one year of testing. No significant reaction had occurred, and the release rates for both Pu and Gd were comparable.

In addition to the ATS glass development and testing, we are involved in the characterization and corrosion testing of ceramic waste forms prepared by Lawrence Livermore National Laboratory (LLNL) and glass waste forms prepared by Pacific Northwest National Laboratory (PNNL). The ceramic samples submitted by LLNL are being characterized by AEM to help determine the phase compositions, microstructures, and plutonium oxidation state of the material. This analysis will aid LLNL in developing new ceramic materials.

Corrosion testing of the ceramic and glasses follows the same test matrix as the ATS glass described above. For the ceramic waste form, standard PCT-A (90°C for 7 days) and MCC-1 (90°C for 3 days) tests have been completed, and the results are being analyzed; PCT-B tests are underway. One long-term (35 days at 200°C) VHT has been completed, and alteration products have been found on the ceramic surface but have not as yet been analyzed.

A lanthanide borosilicate glass, also known as LaBS glass, is being considered for the disposition of surplus weapons plutonium and plutonium scraps. This glass is based upon Löffler-type glasses, is chemically durable, and can dissolve substantial amounts of plutonium as well as the neutron absorbers Gd and Hf.

Vapor hydration tests on the LaBS glass have been performed through 14 days. Optical analysis indicated that alteration products are forming on the surface of this glass. Characterization of these phases will continue. Product Consistency Tests have been initiated in triplicate at an S/V ratio of 2000 m^{-1} for the 7 day tests (modified version of the PCT-A) with the LaBS and ARM-1 (reference) glasses. Eight PCT-B tests for the LaBS glass were initiated at an S/V ratio of 20,000 m^{-1} and for test durations through 728 days. Results will be reported next year.

---

[7] F. Farges, G. E. Brown, Jr., A. Navrotsky, H. Gan, and J. J. Rehr, *Geochim. Cosmochim. Acta* **60**, 3039-3053 (1996).

5. Use of Energy Loss Spectrometry to Analyze Glasses

In the static dissolution and vapor hydration tests, boron release is frequently used as a measure of glass corrosion. The determination of boron content can be difficult owing to the low energy of the B-K X-ray and the relatively poor resolution of X-ray detectors. However, electron spectroscopy has much better energy resolution and is an effective method for detecting the B-K absorption edge. Combined with the small-probe capability of transmission electron microscopy, electron energy loss spectroscopy can be used to detect and quantify boron at levels down to a few parts per million. This technique can be employed to probe changes in boron across a reacted zone in the glass or to determine the nature of phase segregation. Figure III-2 illustrates our ability to detect boron with electron energy loss spectroscopy. The plot shows the boron peaks through the reacted layer of a Hanford glass (depths of 10, 40, and 100 nm). In the future, we intend to use this technique to help understand the nature of phase-separated glasses.

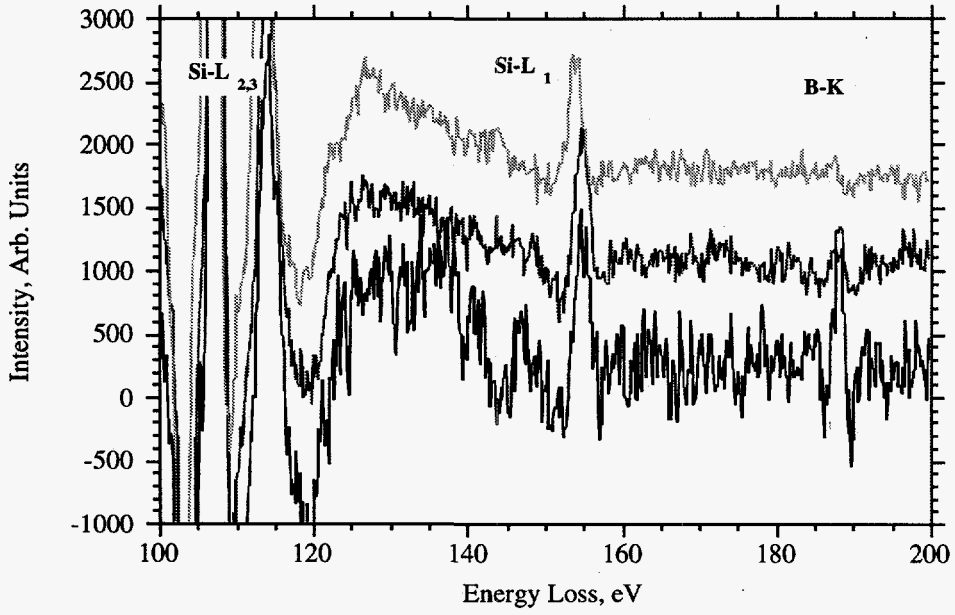

Fig. III-2. Electron Energy Loss Spectra of Reacted Layer of Hanford Glass at Depths of 10 nm (top spectrum), 40 nm (middle), and 100 nm (bottom)

C. Testing of Spent Fuel

Spent nuclear fuel contained in an engineered barrier system surrounded by consolidated volcanic tuff is the current reference design for the potential repository at Yucca Mountain. This multiple barrier system will be designed to limit the radionuclide release from the spent fuel. Long-term tests with both unirradiated UO_2 and spent fuel are in progress to determine the behavior of, and the radionuclide release from, spent fuel under unsaturated conditions.

1. Unsaturated Tests with UO_2 Samples

The objective of this program is to evaluate the reaction of unirradiated Zircaloy-clad UO_2 pellets after exposure to dripping EJ-13 water at 90°C. Results from these tests will be used to characterize the dissolution behavior of UO_2, formation of alteration phases, and rates and mechanisms of uranium release. These tests will also serve as a pilot study for drip tests with spent nuclear fuel.

Drip tests of UO_2 pellets in a stainless steel test vessel supported by a Teflon stand are continuing into their twelfth year. Uranium release from the UO_2 samples was rapid from one to two years of testing, followed by relatively low rates of release over the 2- to 11-yr period. The rapid release period could be correlated with an episode of preferential corrosion along UO_2 grain boundaries and the subsequent spallation of micrometer- to submicrometer-sized UO_{2+x} particles (where $0 \geq x \leq 1$) from the sample surfaces. Electron microscopy and optical examinations of cross-sectioned samples revealed a reaction front that penetrated into the samples an average of two to four grains (~10 to 20 μm) ahead of the exposed external sample surface, but this front varied from regions with little visible corrosion to regions where penetration occurred to a depth of approximately ten grains. After approximately two years of reaction, the formation of a dense mat of alteration phases enveloped the loosened UO_{2+x} grains. This resulted in a reduction of particulate spallation and a lowering of uranium release rates.

A preliminary examination of sample PMP8U-2, reacted for eight years, revealed that ~80 mg of uranium was incorporated into the alteration phases that had formed on the UO_2 sample and Zircaloy cladding surfaces. This amount far exceeded the 5 mg (cumulative) that was recovered after successive nitric acid strips of the leachate solution collected from the bottom of the test vessel. An additional ~780 mg of uranium remained *in situ* as undissolved UO_{2+x} cores that had undergone some corrosion along their grain boundaries. The remainder of the pellet (29,166-mg total sample weight, 25,709 mg of which is uranium) did not show evidence of alteration under examination with scanning electron microscopy/energy dispersive X-ray spectroscopy.

The normalized uranium release rates from the 2- to 11-yr period are variable but generally average between 0.1 and 0.3 mg/(m^2•d), no change from last year's results.[8] An analysis of the size-fractioned release patterns during this period indicates that the majority (86 to 97%) of the released uranium was sorbed or precipitated on the walls of the stainless steel test vessel and the Teflon support stand. From 1 to 12% was present as >5 nm particles suspended in the leachate after filtering, with alteration phases such as uranophane [$Ca(UO_2)(SiO_3)(OH)_2$•$5H_2O$)] and boltwoodite [$(Na,K)(UO_2)(SiO_4)(H_3O)$•$H_2O$] being detected as filter residues. Less than 2% of the total uranium could be attributed to dissolved uranium or particles that passed through a filter with 5-nm pore sizes. This percentage indicates a uranium concentration of 4×10^{-6} M for the leachate collected from the bottom of the test vessel. Testing will continue.

[8] J. J. Laidler et al., *Chemical Technology Division Annual Technical Report, 1995*, Argonne National Laboratory Report ANL-96/10, p. 56 (1996).

2. Unsaturated Tests with Spent Fuel Samples

To qualify the potential Yucca Mountain site for licensing, information is needed on the corrosion behavior of spent fuel under unsaturated and oxidizing conditions at 90°C. Laboratory testing of spent fuel under unsaturated conditions, i.e., with limited water present, provides the information necessary to determine the magnitude of the potential radionuclide source term at the boundary of the fuel cladding after the cladding has failed and water as vapor or liquid contacts the fuel. It also provides insight on the nature of spent fuel reaction under these conditions. Summarized below are the results from drip tests (0.75 mL of EJ-13 groundwater every 3.5 days) with a spent fuel sample (ATM-103) after 3.7 yr.

Several observations have been made from testing to date. First, the ^{99}Tc "interval release fraction" (the ratio of the material released in a given interval to that originally present) has not changed over the course of 3.7 years of reaction and is over 100 times greater than the uranium release. The ^{99}Tc cumulative release fraction is over 2%. Most of the released uranium has been redeposited on the fuel as alteration products. Second, the outer yellow alteration layer that has formed on the fuel can be easily manipulated, but a thinner yellow layer immediately adjacent to the fuel is denser and adheres tenaciously to the fuel surface. Both layers have been identified as sodium boltwoodite, a uranyl silicate structurally related to uranophane type minerals (Sec. III.C.3). Examination of these alteration products showed that the fuel reaction forming the denser layer had been "through" the fuel grain. Third, the ATM-103 fuel fragments are extremely friable and disintegrate under examination. This indicates that reaction has proceeded along all the fuel grains, resulting in a higher reaction surface area as a function of time. In the 3.7 yr of testing, fuel reaction had thus proceeded along grain boundaries as well as through the fuel grains, with the latter being the major reaction route.

The release of technetium is important because it is one of the five fission products (Tc, Ru, Mo, Rh, and Pd) that are incorporated into metallic particles known as the ε-phase in spent fuel. These particles are homogeneously dispersed in the ATM-103 fuel matrix. The constant values for the ^{99}Tc interval release fractions as a function of time suggest that ^{99}Tc release is an indicator of the minimum extent of the spent fuel reaction, and that the alteration products do not prevent further reaction.

The disintegration and ^{99}Tc release behavior of the ATM-103 fuel suggest that a surface reaction is rate controlling. In this surface reaction, oxidants supplied from alpha radiolysis of water play an important role. Within a thin film of water ($\leq$100 μm estimated) on the spent fuel surface, a steady-state concentration of H_2O_2 exists, as well as other radiolysis products. With the use of appropriate Eh/pH diagrams, the oxidation potential at the fuel surface is estimated to be as high as 0.6 V since ruthenium, which requires an Eh of 0.6 V, has dissolved and is being incorporated into alteration products.

We examined four other mechanisms to determine if they might be rate controlling: solubility-limited dissolution, oxygen diffusion, oxidant formation, and growth of alteration layer. Since radionuclide release did not decrease as a function of time, solubility-limited dissolution of the alteration products was excluded. For oxygen transport (i.e., diffusion) to control the rate of the spent fuel reaction and the associated release of technetium, the

dependence of the ^{99}Tc release should be one-half order. The best fit for ^{99}Tc cumulative release as a function of time, however, appears to be a linear curve. Oxygen diffusion thus does not seem to be rate controlling. The formation of oxidants by radiolysis was not rate controlling since, even in a reducing environment, radiolysis supplied sufficient oxidants to oxidize spent fuel. However, if the rate of a surface reaction is higher than the rate of oxidant formation, the latter rate could be rate controlling. For the growth of alteration products to control the reaction rate, radionuclide release should be constant or should increase as the surface area increases, but no increase was found in the ^{99}Tc release fractions as a function of time, although the surface area did increase. Thus, a surface reaction appears to be the most likely rate-controlling mechanism.

Our conclusions from these drip tests are as follows. First, the ^{99}Tc interval release fractions provide a lower limit for the spent fuel reaction. This is supported by the friability of an ATM-103 fuel fragment after less than four years of reaction. Second, oxidation of the elements in the ε-phase suggests that the oxidizing potential at the fuel surface may be as high as 0.6 V, with a likely oxidant being H_2O_2, a product of alpha radiolysis of water. Third, the ^{99}Tc release indicates that a surface reaction may be the rate-controlling mechanism for fuel reaction under unsaturated conditions. Testing will continue.

3. Characterization of Reacted Spent Fuel Samples

The ε-ruthenium metallic phase is known to form during burnup of UO_2 fuel in a nuclear reactor. This phase contains several 4d group transition elements, one of which is technetium. Owing to its long half-life, technetium is a radionuclide of special concern when evaluating the long-term performance of a geologic repository. Using small-particle handling techniques combined with ultramicrotomy, we have prepared thin sections of corroded spent UO_2 nuclear fuel that contain the ε-phases. They were extremely small spherical particles, around 20-50 nm in diameter. Nonetheless, we were able to determine their structure with electron diffraction and to quantify the relative concentrations of the 4d elements in the particles with electron energy loss spectroscopy. Many of the phases appeared weathered, and the total amount of Tc and Mo in the phase was lower than that reported by other investigators[9] who have examined the fuel before corrosion testing. Within the vicinity of some ε-phases, we found plutonium-rich regions. Further studies will be conducted on these particles next year.

The spent fuel from the drip tests (Sec. III.C.2) was examined by AEM. After 3.7 yr of reaction in EJ-13 water at 90°C, this spent fuel was found to have altered primarily to a uranyl silicate; sodium boltwoodite, $Na[(UO_2)(SiO_3OH)](H_2O)$ (~80 vol%); and β-uranophane, $Ca[(UO_2)_2(SiO_3OH)_2](H_2O)_5$ (~10-20 vol%). At 1.8 yr, a Cs-Mo-U(VI) phase was also recovered from the test stand. An alteration layer, approximately 20-40 mm thick, had formed on the fuel surface. The inner ~10 mm of this layer is due to the iso-volumetric replacement of the fuel by sodium boltwoodite, whereas the outer 20-30 mm represents uranium transport out of the replacement volume. Of the 250 mg of fuel that has reacted (based on technetium release), approximately 180 mg (80%) is derived from the replacement layer and ~70 mg (20%) from dissolution of the fuel along grain boundaries. Through-grain dissolution of the UO_2 fuel matrix

[9] L. E. Thomas and R. J. Guenther, *Mater. Res. Soc. Symp. Proc.* **127**, 293-300 (1989).

appears to predominate over grain-boundary-enhanced dissolution at this stage of reaction. The density of the alteration layer indicates that the layer probably contains only ~50% of the 250 mg U lost from the fuel, and another ~50% may be held up elsewhere.

D. Vitrification of Low-Level Waste

1. *Development and Testing of Glass-Crystal Composite*

The safe disposal of radioactive and toxic waste elements requires the development of durable waste forms that effectively isolate these components from the biosphere. Glass-crystal composite (GCC) waste forms, composed of crystals encapsulated in a glass matrix, were evaluated for their potential use in the disposal of mixed low-level nuclear and hazardous waste materials. Crystal formation was induced from the melts by the proper blending of the simulated waste streams; addition of chemical additives such as Zr, Ti, and P; and slow cooling of the molten samples from the 1400 ± 100°C melting temperatures. The formation of the iron-rich spinels was the primary requirement for the high melting temperatures, which may conceivably be reduced with lower metal content melts. This study showed that hazardous elements such as U, Pu, Sr (analogue for ^{90}Sr), Cr, Cd, Pb, As, Ba, and Ni can be incorporated into corrosion-resistant crystal phases such as zirconolite [$CaZrTi_2O_7$], perovskite [$(Ca,Na,Fe,Ce,Sr)TiO_3$], apatite [$Ca_5(PO_4)_3(F,Cl,OH)$], monazite [$(Ce,Th)PO_4$], and spinel [$(Mg,Fe,Zn,Mn,Ni)(Al,Fe,Cr,Ti)_2O_4$]. Since these phases also can incorporate Fe, P, and F in their structures, they also show promise in processing of waste streams containing large proportions of components that are only slightly soluble in most silicate glasses (e.g., transition metals, phosphorus, and halides).

Results from Product Consistency Tests at 90°C (7, 28, and 91 days) indicate that silicon release from the GCCs was significantly lower than that of both EA and SRL 202U borosilicate waste glasses. Silicon is primarily contained within the glassy fraction of the GCCs, so its low release reflects a durable matrix. Samples also display minimal development of alteration products on their surfaces, further indicating that the GCCs are resistant to aqueous corrosion. Normalized uranium release rates for zirconolite-, monazite-, and apatite-bearing samples are between 100- and 300-fold lower than those which characterize the SRL 202U borosilicate glass. This high degree of uranium retention is primarily a result of the durable crystalline phases but also is aided by the durable nature of the glass matrix. Test results from the Toxicity Characteristic Leaching Procedure (TCLP) for eight toxic metals (Ag, As, Ba, Cd, Cr, Hg, Pb, and Se) also indicate release concentrations well below the Environmental Protection Agency limits for toxic waste declassification, despite waste loadings of many elements that were in the percent range.

In summary, the GCCs combine advantageous features of the excellent durability exhibited by predominantly crystalline waste forms, such as Synroc, with the ease in processing offered by use of commercially available vitrification facilities. Processing parameters are relatively flexible, allowing GCCs with high durabilities to be produced with minimum processing requirements and additives. Due to funding limitations, no future work is planned on this project.

2. Testing of Glass Waste Forms for Low-Level Waste

Several glasses developed at Pacific Northwest National Laboratory as part of the Hanford low-level waste glass project were evaluated at ANL. In particular, two glasses were extensively tested, LD6-5412 and FLLW-1. The LD6-5412 glass was tested to characterize its corrosion behavior and to provide data for a computer model of the corrosion behavior of sodium-rich borosilicate glasses. The FLLW-1 glass was tested to characterize the corrosion behavior of a sodium-rich borosilicate glass that contains Nd, Sn, Se, Th, U and Zr. These are surrogates for important radionuclides that will be present in the Hanford low-level waste stream. The behavior of these elements during corrosion of the glass must be understood to model the long-term performance of a waste disposal site.

Product Consistency Tests and VHTs were conducted to highlight different aspects of the glass corrosion reaction. Long-term PCTs with LD6-5412 glass were conducted to measure the corrosion rate as the glass and solution approached saturation. The PCTs and VHTs have been completed through two years: several sets of data show that sodium is released from this glass at a higher rate than Si or B, and that it is released by an ion exchange process that is diffusion controlled. Results of PCTs show that the dissolution rate is quite low [$<1 \times 10^{-4}$ g/(m^2•d)] before the formation of alteration phases, but much higher after the formation of alteration phases [>0.5 g/(m^2•d) at 90°C and >0.09 g/(m^2•d) at 70°C]. For comparison, results from other tests in the presence of alteration products (VHT and accelerated dissolution tests) yield a rate of about 2 g/(m^2•d). Therefore, the formation of alteration phases leads to a dramatic increase in the dissolution rate of LD6-5412 glass in PCTs conducted at both 70 and 90°C.

Results from PCTs with FLLW-1 show that the normalized mass loss values of Na and B are generally higher than those of Si and Al, and that the values of U, Nd, and Th are lowest. Vapor hydration tests were used to accelerate the corrosion of FLLW-1 glass and thereby generate alteration phases. Sodium-depleted layers were present in samples of the glass reacted in VHTs conducted at 200°C. The growth of the sodium-depleted layer is probably controlled by the diffusion of water into the glass. Alteration phases (herschelite and boltwoodite) also formed on the surface of the glass during VHTs conducted at 200°C for 120 and 182 days. Several of the surrogates were incorporated into the alteration phases. The boltwoodite ($Na_2UO_2SiO•H_2O$) contains Sn in addition to U, and the herschelite ($Na_4Al_4Si_8O_{24}•12H_2O$) contains Zr, Nd, Sn, Th, and U. These results show that alteration phases will be important in the disposition of radionuclides during corrosion of low-level waste glasses.

Other PCTs and VHTs with LD6-5412 and FLLW-1 glasses are in progress. These will be completed next year, and the results will be used to describe the corrosion behavior of these glasses and the disposition of radionuclides.

E. Characterization of Cement Mortar Formulations

Leach tests have been conducted on cement mortar formulations from Applied Innovation Inc. The objective is to elucidate the capacities of these formulations to retain radioactive elements from radioactive waste, toxic waste, and mixed waste. If successful, these Portland

cement-based mortars could find wide applications in the immobilization and containment of radioactive, toxic, and mixed wastes. We have determined the leachability indices of mortars containing Tc, Cs, Sr, transuranic elements, and hazardous metals. These mortars were subjected to the American Nuclear Society ANS 16.1 test, and the leachates were analyzed by using inductively coupled plasma/mass spectroscopic and gamma spectroscopic analyses. The Nuclear Regulatory Commission has suggested that a low-level waste form should have an effective diffusivity of less than 1×10^{-6} cm^2/s or a leachability index of 6. Thus, only leachability index values of 6 or greater are acceptable for a low-level waste form. Test results for Cs and Sr, hazardous metals, and other radionuclides in soil and sulfide sludge wastes that were cured for 30 days showed that the leachability indices for these elements are higher than those reported in the literature.[10] Radioactive cement mortars were prepared by using soil and low-level waste sulfide sludge (11-50 wt% in mortar) generated by ANL Waste Management Operations and demonstrated leachability indices for Tc, Cs, Ni, U, Se, As, and Cd of 15, 14, 21, 22, 15, 18, and 18, respectively. These excellent results are attributed to the reducing nature of the waste stream itself. They are encouraging for the development of materials for immobilization of low-level waste. Furthermore, the preliminary test of the mortars as a function of curing time (30 to 190 days) showed no significant differences in the leachability indices as a function of curing time. The next series of studies will yield information on higher loading than 50 wt% and the leachability of radionuclides and hazardous metals in mortar prepared with a variety of low-level wastes.

[10] "Measurement of the Leachability of Solidified Low-Level Radioactive Wastes," American Nuclear Society Standards Committee Working Group ANS-16.1 (June 20, 1984).

IV

Separation Science and Technology

The Division's work in separation science and technology during the past year was in two areas:

- Treatment of radioactive, mixed, and hazardous waste
- Substitution of low-enriched uranium for high-enriched uranium in the production of ^{99}Mo

The main project in the first area involves R&D on solvent extraction processes, namely, TRUEX (transuranic extraction) and CSEX (cesium extraction) combined with SREX (strontium extraction). These processes are designed for the cleanup of acidic nuclear waste solutions. In another project, we are assisting in the development of an evaporator/concentrator system for treating low-level radioactive waste at Oak Ridge National Laboratory (ORNL) and Savannah River Site. We also continue to provide technical support for ANL's Waste Management Organization; our major task in 1996 was starting up waste treatment facilities for liquid transuranic (TRU) waste and organic-containing wastes.

In the second area, we are developing a low-enriched uranium target and a processing method for production of ^{99}Mo to be used for medical applications.

A. Solvent Extraction Technology

Although our separation science and technology activities have broadened into other areas, solvent extraction R&D remains a significant fraction of our development work. The TRUEX solvent extraction process is capable of recovering TRU elements from nuclear waste solutions containing a wide range of nitric acid and nitrate salt concentrations. The TRUEX extractant is octyl(phenyl)-N,N-diisobutylcarbamoylmethylphosphine oxide, which is combined with tributyl phosphate and a diluent to formulate the TRUEX solvent. The Generic TRUEX Model (GTM) was developed in the CMT Division for designing TRUEX flowsheets for specific waste streams. The TRUEX flowsheet includes multistage extraction/scrub sections that recover

and purify the TRU elements from the waste streams and multistage strip sections that separate TRU elements from each other and the solvent.

Work during the past year was focused on advising engineers at Idaho National Engineering Laboratory (INEL) on their demonstration of the TRUEX process on actual high-level waste stored at the site. The demonstration was run with a 24-stage centrifugal contactor built at ANL. The GTM was used following the run as a means to better understand the test results. In a collaborative project with the ANL Chemistry Division, we are also providing engineering and modeling support and testing countercurrent flowsheets for the combined CSEX-SREX process, which was invented in the ANL Chemistry Division. This solvent extraction process is applicable to removing ^{137}Cs and ^{90}Sr from acidic waste solution, such as that presently stored at INEL.

1. Demonstration of TRUEX Flowsheet

We provided support for INEL at the Idaho Chemical Processing Plant as they tested the TRUEX solvent-extraction process in an ANL-designed centrifugal contactor using actual sodium-bearing waste. In this effort, we reviewed the INEL test plan and analyzed it with the GTM, reviewed the final test plans and equipment setup and then witnessed the test at INEL, and analyzed the test results with the GTM.

The TRUEX test was done in a 24-stage "minicontactor" (2-cm dia rotor) designed, built, and tested at Argonne. It is now located in a shielded-cell facility at Idaho (Fig. IV-1), where actual sodium-bearing waste can be brought in for flowsheet tests. The unit has already been used to test flowsheets for the TRUEX process, as well as the cobalt dicarbollide and phosphine oxide processes. The minicontactor has been modified at Idaho so that it is easy to switch between these processes. However, when we reviewed the INEL cleanup procedure, it appeared that the high flow rates used for contactor cleanup could force water up into the motor bearings in some contactor stages. This concern was reinforced when, in preparation for the TRUEX test, one of the contactor motors (the last stage, stage 24) was found not to be turning. Because of its simple design, the motor/rotor assembly was removed and replaced by remote operation in only 30 min. After this was done, the test was carried out as planned and went very smoothly. Analysis of the test results indicated that another stage, the scrub feed, also had a motor that was not turning. Based on this experience, the contactor operating procedure at INEL is being modified to ensure that this does not happen again. In spite of this problem, the test was a success because actinide removal efficiency in the aqueous raffinate was 99.97%, so that its alpha activity was 0.12 nCi/g, well below the Nuclear Regulatory Commission requirement of below 100 nCi/g for non-TRU waste. In the next year, we will be supporting INEL as they test the SREX process (see Sec. IV.A.2) in the minicontactor using sodium-bearing waste.

2. Demonstration of CSEX/SREX Flowsheet

Over the past several years, we have been working with the ANL Chemistry Division on the development and demonstration of new flowsheets for the cleanup of nuclear waste. This year, the CSEX-SREX flowsheet was demonstrated. This process is attractive because combining

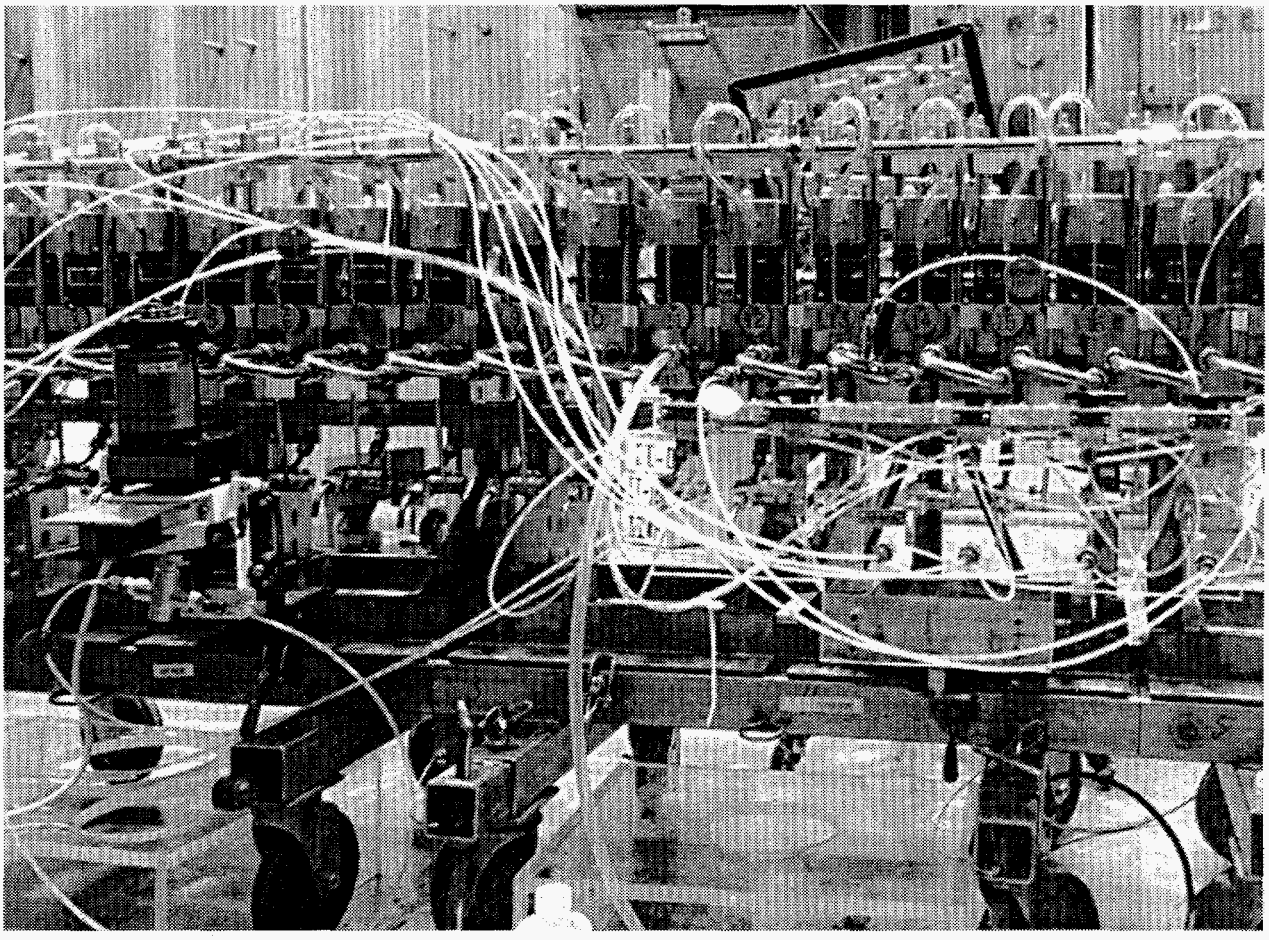

Fig. IV-1. The 24-Stage CMT Minicontactor in Shielded-Cell Facility at INEL

the SREX (strontium extraction) and CSEX (cesium extraction) extractants reduces the number of steps in the pretreatment of the acidic nuclear waste from Idaho and Hanford, while the overall process is made more effective. Pretreatment will greatly reduce the amount of nuclear waste that has to be vitrified with an attendant major reduction in waste disposal costs. The CSEX/SREX process was carried out in a multistage 2-cm minicontactor of the Argonne design. The minicontactor is a good device for testing solvent extraction flowsheets because it allows process evaluation under conditions very close to those that might be expected in a full-scale plant. Thus, if the process runs well in the minicontactor, one can be reasonably sure that it will work in a full-scale plant.

The CSEX-SREX demonstration used the flowsheet shown in Fig. IV-2 for separating Cs and Sr from a simulated sample of zirconia calcined waste at INEL. A demonstration was quite successful since the desired decontamination factor of 10^4 in the aqueous raffinate was achieved for both Sr and Cs. In fact, based on model analysis, the decontamination factors for Cs and Sr were 1.1×10^7 and 1.4×10^8, respectively. The model used was the SASSE (Spreadsheet Algorithm for Stagewise Solvent Extraction) worksheet from the GTM, along with measured values for the distribution coefficients of the various metal ions. The experimental data and model curve, given in Fig. IV-3 for strontium, show that, in the extraction section (moving from

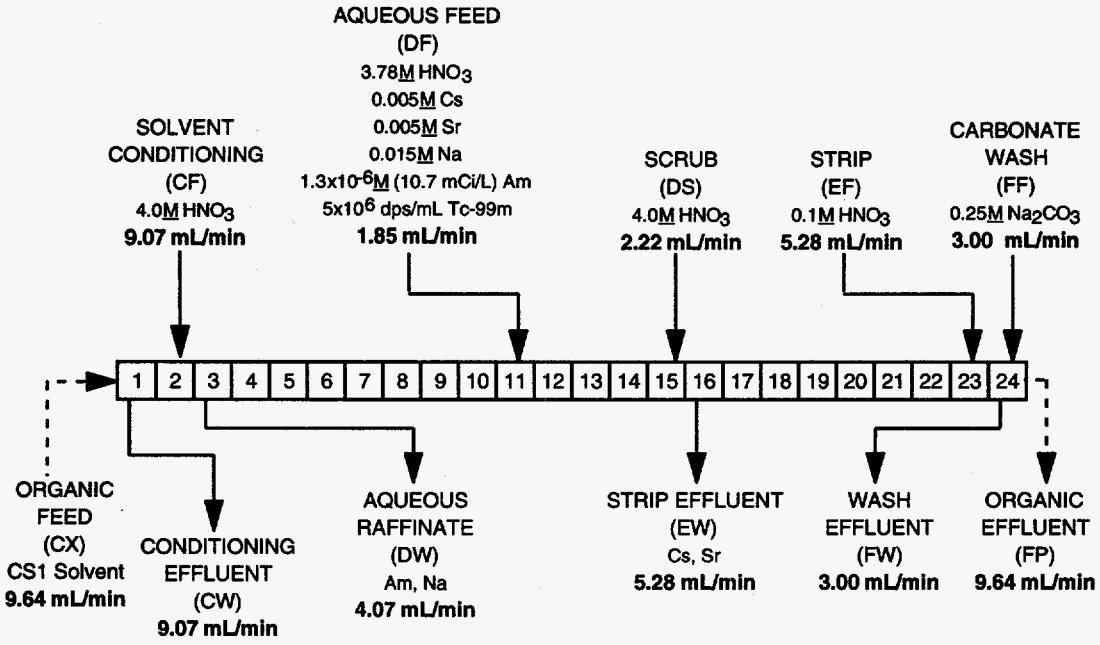

Fig. IV-2. Flowsheet for Demonstration of the CSEX-SREX Process

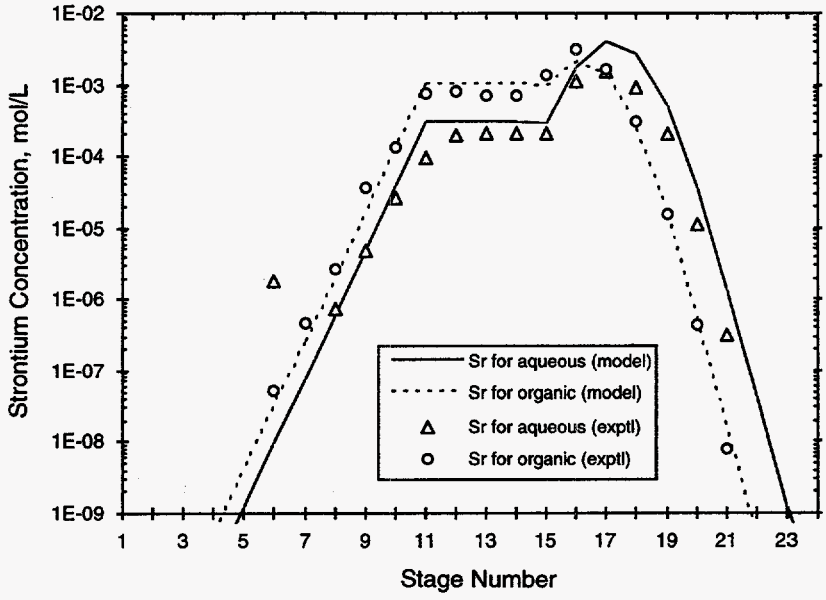

Fig. IV-3. Stage-to-Stage Concentrations for Strontium in the Aqueous and Organic Phases during CSEX-SREX Demonstration

stage 11 to 3), the model curve follows the experimental data downward until the strontium concentration becomes too low to measure. Since 100% extraction efficiency was assumed in the model calculations, the good agreement here confirms that this assumption was appropriate. Other results indicate that the americium was scrubbed out of the solvent in the scrub section as

expected, and that the technetium was pinched between the extraction and scrub sections. Thus, while further work is needed to resolve all flowsheet issues, this successful first test of the CSEX-SREX process in a multistage centrifugal contactor is very encouraging.

B. Advanced Evaporator Technology

The new evaporator system (capacity of 340 L/h) fabricated for ORNL to process its underground-storage-tank waste was installed, tested, and put into service in 1996. Our involvement in this past year included reviewing run plans, writing operational procedures, and suggesting modifications to solve problems as they arose. Given that the system is now fully functional and operating to specifications, our involvement in this project has been completed.

The Savannah River Site has built a Consolidated Incinerator Facility for the combustion of a wide range of hazardous, low-level-radioactive, and mixed wastes. To minimize the amount of waste generated by this facility, Savannah River Site is pursuing an approach of combining fly ash with a scrubber-blowdown solution, evaporating the mixture, then converting the evaporator bottoms into concrete for disposal. A battery of evaporation studies was completed at CMT to help characterize the evaporation process and specify suitable evaporator equipment for this application. A simulated sample of dilute blowdown feed was concentrated in a laboratory-scale evaporator (from 0.08 to 1.5 wt% solids), and the bottoms were mixed with fly ash in a number of combinations, then further concentrated (up to 35 wt% dissolved solids) in evaporation tests.

The tests identified possible problems with scaling, foaming, and high viscosity in certain feeds, but none of these problems appears insurmountable. Provided low fly-ash concentrations are used (<10 wt%), the blowdown solution can be concentrated up to 30 wt% dissolved solids in a traditional evaporator. Higher fly-ash concentrations would require some form of agitated concentrator. A number of evaporator technologies have been suggested as possible for this application, but much depends on the form that the fly ash takes and its concentration in the evaporator feed. Discussions are underway for further testing once the feed composition for an evaporator system can be more clearly predicted.

C. Technical Support to ANL Waste Management

The CMT Division has developed a process to treat TRU wastes generated at ANL because there is currently no disposal site available that will accept these wastes. The process removes the TRU component from solution by magnetite precipitation.[1] A glovebox to treat these wastes by the magnetite precipitation process has been purchased and installed. Startup and systems operability have been successfully demonstrated, and the system is scheduled to begin treating actual wastes by February 1997.

---

[1] J. J. Laidler et al., *Chemical Technology Division Annual Technical Report, 1995*, Argonne National Laboratory Report ANL-96/10, p. 66 (1996).

Mixed wastes (that is, wastes that are both radioactive and hazardous) also have limited disposal options. Therefore, a photo-oxidation system was purchased to treat flammable, radioactive wastes at ANL. This system uses a combination of ultra-violet light and hydrogen peroxide to convert flammable organic constituents into salts, carbon dioxide, and water. The resultant brine can be treated in the existing evaporator/concentrator system at ANL, and the solid product can be disposed of under existing regulations. This system has been installed, and CMT personnel are assisting in startup testing.

D. Production of Molybdenum-99 from Low-Enriched Uranium

Molybdenum-99 ($t_{1/2}$ = 66.02 h) decays by beta emission to ^{99m}Tc ($t_{1/2}$ = 6.02 h). The latter nuclide is used in many nuclear medicine applications. For clinical use, it is prepared first in the form of pertechnetate ion (TcO_4^-) and then suitably changed to other chemical forms, depending upon the intended application. The TcO_4^- is washed from an alumina-column generator that contains the parent ^{99}Mo. This washing is accomplished by elution with a saline solution. Much of the world's supply of ^{99}Mo is produced from fissioning of high-enriched uranium (HEU).

The Reduced Enrichment for Research and Test Reactors (RERTR) program has been active for 19 years at ANL and many countries throughout the world. Its objective is to modify reactor and fuel designs so that reactors could switch from HEU to low-enriched uranium (LEU) with no or little loss in flux or cycle time. Many reactors have converted to LEU, and many more are in the process. While conversions of reactor fuel have proceeded, the amount of HEU being exported from the United States for use in ^{99}Mo production has become an ever more visible proliferation concern.

As a part of the RERTR program, we are studying two LEU target designs, uranium metal foil and uranium silicide (U_3Si_2). At present, either UO_2 or various UAl_x alloys are used in HEU targets. The silicide fuel is being developed as the LEU substitute for UAl_x alloys, and the uranium metal foil is being primarily developed as the LEU substitute for UO_2. We are also looking into the possibility of substituting the LEU metal foil target for all current HEU targets.

1. *Cintichem Processing of LEU Targets*

The Cintichem process produces, recovers, and purifies ^{99}Mo from HEU targets that consist of a thin coating of UO_2 on the inside of a cylindrical target, which is also used as a dissolver vessel for the irradiated HEU. Our R&D effort is focused on modifying the target and the recovery and purification procedures so that they can be used to process LEU targets consisting of uranium metal foil that is 0.13-mm thick. Irradiation testing of the LEU metal targets during 1996 showed that a thin metal barrier was required between the LEU metal foil and the target walls. The barriers sorb fission-recoil atoms that are released from the fissioning of ^{235}U during neutron irradiation. The high energy released by the fission products causes localized melting of the matrix and diffusion of atoms between the uranium and the metal contacting it. This diffusion causes bonding of the uranium foil to the target walls, which makes it impossible

to remove the foil from the target.[2] Through a literature study, we determined that three metals (Ni, Cu, and Fe) would likely be suitable barrier materials for the Cintichem target based on their mechanical, nuclear, and chemical properties. To perform their function, these barriers need to be about 10-μm thick.

It is our objective in switching to LEU to maintain the process for molybdenum recovery and separation from uranium (and its fission and absorption products) as close as possible to the current Cintichem process. It is also our goal to make improvements to the process that will mitigate any economic detriment resulting from conversion to LEU. Argonne National Laboratory and the University of Illinois at Urbana-Champaign are collaborating with the National Atomic Energy Agency (BATAN) of Indonesia to develop and demonstrate the use of LEU targets in the Cintichem process. During 1996, we focused on four technical areas:

- Designing equipment and procedures for dissolving irradiated LEU foils in a shielded cell,
- Testing the effects on foil dissolution and ^{99}Mo recovery and purity when the LEU foil is dissolved in nitric acid alone, rather than in the sulfuric/nitric acid mixture currently used,
- Measuring decontamination factors for radionuclide impurities in each purification step, and
- Testing the effects of adding barrier materials to the LEU metal-foil target.

In early 1997, we plan to demonstrate processing a fully irradiated LEU metal foil at the PUSPIPTEK Radioisotope Production Center in Serpong, Indonesia.

a. Dissolution of LEU Foil and Barriers

The design of the dissolver for the process demonstrations at PUSPIPTEK is such that it can be held and heated in equipment already in use with the current HEU target/dissolver. Procedures for dissolving the LEU foil are also being developed with current equipment and methods in mind. After demonstrating that LEU foil can be substituted for the current target, we will design a dissolver that is optimized for long-term use for foil dissolution. During 1996, we demonstrated that (1) the dissolver solution can be nitric acid alone instead of the current sulfuric/nitric acid mixture, and (2) barrier metals of Cu, Fe, or Ni on the U foil are also dissolved by nitric acid.

The primary consideration for converting the dissolver solution to nitric acid alone is facilitating waste treatment and disposal. Sulfate in the acidic waste solution from the ^{99}Mo

[2] G. L. Hofman, T. C. Wiencek, E. L. Wood, J. L. Snelgrove, A. Suripto, H. Nasution, D. Lufti-Amin, and A. Coogo, "Irradiation Tests of ^{99}Mo Isotope Production Targets Employing Uranium Metal Foils," Presented at the XIX Int. Reduced Enrichment for Research and Testing Reactors Meeting, Seoul, Korea, October 6-10, 1996.

recovery step complicates uranium recovery, waste volume reduction, and waste disposal.[3] Therefore, removal of sulfuric acid from the dissolver solution is likely to significantly reduce total processing costs. The dissolution rate of an 18-g piece of LEU foil was determined to be essentially identical in 8 M HNO_3 as in a solution containing 3 M HNO_3 and 2 M H_2SO_4.

The overall reactions for metal barriers of Cu, Ni, and Fe dissolved with nitric acid alone are the following:

$$Cu/Ni + 8/3\,HNO_3 \rightarrow Cu/Ni(NO_3)_2 + 4/3\,H_2O + 2/3\,NO\,(\uparrow) \quad (1)$$

$$Fe + 4HNO_3 \rightarrow Fe(NO_3)_3 + 2H_2O + NO\,(\uparrow) \quad (2)$$

Dissolution rates for these three metals were measured over a variety of conditions in a covered, but unsealed, centrifuge tube in a constant-temperature bath. The results indicate that all three metals dissolve faster than uranium; nickel is about five times faster, copper is ~200 times faster, and iron is ~600 times faster. Equations 1 and 2 and the ideal gas law were used in calculating the dissolution pressure for a two-sided barrier on a typical 18-g uranium-foil target (barrier dimensions of 76 x 102 x 0.010 mm), a dissolver temperature of 103°C, and a gas volume of 282 mL. The results indicate that the final dissolver pressure for Cu, Fe, and Ni increased by 158, 241, and 172 kPa (23, 35, and 25 psi), respectively, over that for uranium alone. It was concluded that the dissolver pressure will be increased about 10% by the presence of a two-sided barrier. This pressure increase is within the design limits of the stainless-steel dissolver, so that any of these three barrier materials can be used without affecting the operation of the uranium-foil dissolver.

The dissolver design and operation were changed to accommodate the uranium foil, including the addition of (1) simple operations that are easy to do in a remote-maintenance facility, (2) heat removal from the irradiated LEU foil, and (3) a cold trap with high dissolver pressures. Figure IV-4 shows the correlation between pressure generated in the dissolver from NO gas formation and the mass of uranium dissolved. The correlation was used to predict the safety of the current cold trap for containment of the gas generated from a full-size (18-g) LEU foil at operating (103°C) and ambient (25°C) temperatures. The results indicate safe operation at all operating conditions for 20 g or less uranium.

Future work will include testing the improved dissolver in PUSPIPTEK and then designing the production dissolver.

[3] E. P. Gause, L. G. Stang, D. R. Dougherty, E. Veakis, and J. Smalley, *Characterization of the Radioactive Large Quantity Waste Package of the Union Carbide Corporation*, Department of Nuclear Energy, Brookhaven National Laboratory Informal Report BNL-NUREG-30247R (July 1982).

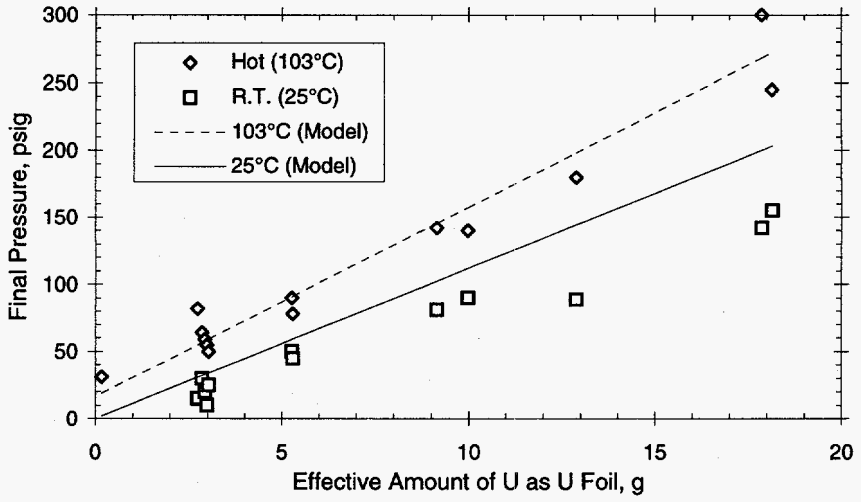

Fig. IV-4. Effect of Uranium Mass on Final Dissolver Pressure at Room Temperature and 103°C

b. Molybdenum-99 Recovery and Purification

Following dissolution, molybdenum is recovered from the solution by its precipitation with α-benzoin oxime (α-BO). Precipitation of Mo(VI) by α-BO is a standard analytical method for molybdenum.[4-6] This standard procedure requires molybdenum in 1 M sulfuric acid. Molybdenum precipitation is quantitative (>99.99%), and the precipitate contains very little impurity. In previous tests, we found that molybdenum can also be precipitated with α-BO from a nitric acid solution.[7,8] However, we still needed to show that use of nitric acid alone as a dissolver solution would not degrade the ^{99}Mo product. Several experiments with irradiated-LEU tracer and with ^{99}Mo tracer were run to determine the effects of replacing sulfuric acid with an equivalent amount of HNO_3. A comparison of the results with and without sulfuric acid showed that eliminating sulfuric acid did not significantly affect either molybdenum recovery or radioisotope decontamination. Most of the decontamination is done in the precipitation of molybdenum with α-BO, and the following purifications are polishing steps. The polishing steps are commercially sensitive and cannot be discussed in an open-literature publication; the target

---

4 W. T. Elwell and D. F. Wood, *Analytical Chemistry of Molybdenum and Tungsten*, Pergamon Press, Oxford, pp. 40-41 (1971).

5 G. A. Parker, *Analytical Chemistry of Molybdenum*, Springer-Verlag, Berlin, pp. 146-147 (1983).

6 A. I. Busev, *Analytical Chemistry of Molybdenum*, trans. J. Schmorak, Humphrey Science Publishers, Ann Arbor, MI, pp. 30-31 (1969).

7 D. Wu, B. A. Buchholz, S. Landsberger, and G. F. Vandegrift, "Processing of LEU Targets for Mo Production–Testing and Modification of the Cintichem Process," Proc. of the XVIII Int. Reduced Enrichment for Research and Testing Reactors Meeting, Paris, France, September 17-21, 1995, paper no. 3-3 (May 1996).

8 D. Wu, S. Landsberger, and G. F. Vandegrift, "Application of Neutron Activation Analysis in a Fission Molybdenum Separation Study," *J. Radioanal. Nucl. Chem.*, in press.

and the initial molybdenum-recovery step were patented in the 1970s.[9,10] Although these results are encouraging, we must note that our small-scale experiments only indicate chemical behavior; verification of this behavior will require full-scale demonstrations using fully irradiated uranium-foil targets.

The allowed radiochemical impurity levels in ^{99}Mo product are very low, ranging from 0.1 to 10^{-7} μCi/mCi-^{99}Mo. Therefore, each purification step must work effectively. The gamma-emitting isotopes that need to be analyzed in the ^{99}Mo product are tabulated in Table IV-1. By using the ORIGEN2 computer code, we calculated the activities of these radioisotopes in an 18-g LEU target at 24 h after discharge from an Indonesian reactor (RGS-GAS), following a 120-h irradiation at full power (second column of Table IV-1). Columns 3 through 5 contain decontamination factors measured in our tracer experiments for each processing step, the α-BO precipitation and two polishing steps (purifications 1 and 2). The predicted impurity levels in units of μCi/mCi-^{99}Mo in the irradiated LEU target are listed in the last column. The calculations show that, except for ^{103}Ru, the desired radioisotopic decontamination levels can be met easily. Because ^{103}Ru contamination is not a concern in the current Cintichem product from HEU targets and because substitution of LEU will not affect the fission yield, this ^{103}Ru result may indicate a limitation of our tracer experiments more than a problem with LEU substitution.

Development of LEU metal-foil targets has led to the use of thin (10 μm) metal barriers between the uranium foil and the target walls. Three metals (Cu, Fe, and Ni) were selected as primary candidates for the barrier material on the basis of their physical, chemical, and nuclear properties.

The nuclear properties of interest are the radioisotopes generated in the barrier during target irradiation and their activity levels, which must be removed from molybdenum during processing. By the use of ORIGEN2, we calculated the radioisotopes generated in Fe, Ni, and Cu barriers during LEU target irradiations in the RGS-GAS reactor. The results of these calculations show that only a copper barrier would generate enough radioactivity to be of concern. For its primary absorption product, ^{64}Cu, to be less than 0.1 μCi/mCi-^{99}Mo in the molybdenum product, its overall decontamination factor must be >3100.

Neither the barrier materials nor their neutron-activation products are reported to interfere with the precipitation of molybdenum by α-BO. Experiments were run to verify the noninterference of these metal ions by using solutions prepared to simulate dissolving the barrier-clad uranium foil in nitric acid. In the same experiments, we measured the amount of each barrier metal that carried with the molybdenum precipitate. Table IV-2 shows the results of these experiments. The molybdenum recovery was high for all experiments, as were the measured decontamination factors. It is likely that the differences in the decontamination factors are more

[9] H. Arino, H. H. Kramer, J. J. McGovern, and A. K. Thornton, "Production of High Purity Fission Product Molybdenum-99," U.S. Patent 3,799,883 (1974).

[10] H. Arino, F. J. Cosolito, K. D. George, and A. K. Thornton, "Preparation of a Primary Target for the Production of Fission Products in a Nuclear Reactor," U.S. Patent 3,940,318 (1976).

Table IV-1. Calculated Impurity Levels of a Fully Irradiated LEU Target and the ^{99}Mo Product[a]

Nuclide	Calculated Target Activity, Ci	Measured Decontamination Factors[b]			Calculated Product Impurity Level, μCi/mCi-^{99}Mo
		Precipitation	Purification 1	Purification 2	
Ba-140	292	>516	>162	>165	<3.6E-05
Ce-141	121	>1116	328	419	<1.3E-06
Ce-143	685	>3354	313	641	<1.7E-06
I-131	186	51	28	41	5.3E-03
I-133	628	91	35	51	6.3E-03
I-135	104	121	38	43	8.8E-04
La-140	224	>2409	>104	>149	<1.0E-05
Mo-99	697	1.04	1.05	1.08	—
Nb-95	4.7	4	>13	>9.5	<1.7E-02
Nb-97	480	11	56	1410	9.2E-04
Nd-147	119	208	>62	>59	<2.6E-04
Np-239	1610	>1770	>247	>333	<1.9E-05
Pm-151	45	103	>16	>21	<2.1E-03
Rh-105	102	>276	>34	>46	<4.0E-04
Ru-103	54	113	1.3	3.7	1.7E-01
Sb-127	13.6	>41	1.3	>10	<4.3E-02
Sr-89	65.7	—	—	—	<2.3E-07[c]
Sr-90	0.39	—	—	—	<1.4E-09[c]
Sr-91	209	>3452	235	>586	<7.4E-07
Sr-92	2.65	>2101	>71	>63	<4.7E-07
Te/I-132	464	>5083	327	657	<7.1E-07
Y-93	258	>1294	511	822	<8.0E-07
Zr-95	70	13	27	>49	<6.8E-03
Zr-97	447	17	23	>41	<4.6E-02

[a]Basis is an 18-g LEU target, 24 h after discharge from the RGS-GAS reactor, following a 120-h irradiation at full power.
[b]Ratio of activity in the molybdenum solution before and after treatment.
[c]Predicted from ^{91}Sr behavior.

Table IV-2. Effects of Barrier Materials on α-BO Precipitation[a]

	Cu	Fe	Ni
Molybdenum Recovery, %	99 ± 3	96 ± 3	96 ± 3
Decontamination Factors	1680	258	660

[a]Solution contained 0.75M HNO_3, 1.5M $UO_2(NO_3)_2$, and the concentration of Cu, Ni, or Fe corresponding to a 10-μm barrier on either side of the uranium foil.

an indication of how well the precipitate was washed in each experiment rather than chemical differences in the barrier-metal ions.

The decontamination factors measured for Fe and Ni are more than high enough to meet impurity requirements for the molybdenum product. However, the removal of ^{64}Cu may require additional decontamination, since the measured value after α-BO precipitation (Table IV-2) is below the required value of >3100. For this reason, we tested the removal of copper by two polishing steps; these tests showed that the overall decontamination factor for the

two polishing steps should be >10,000. A combination of all three steps should, therefore, effectively reduce ^{64}Cu contamination to well below regulatory concern.

In the future, we will continue to assist BATAN researchers at the PUSPIPTEK Radioisotope Production Center, who are preparing to demonstrate the Cintichem process on a fully irradiated LEU target. Our collaboration with BATAN is vital to developing and validating this process. A series of full-scale demonstrations of the process will begin early in 1997.

2. Basic Processing of U_3Si_2 Targets

Over the last several years, processing of uranium silicide fuels has been under development as an LEU substitute for ^{99}Mo production. The LEU silicide is aimed to replace the UAl_x in the HEU dissolution process used throughout the world.[11,12] Replacement of UAl_x with U_3Si_2 targets requires development of an aggressive dissolution process. Unlike UAl_x, U_3Si_2 does not readily dissolve in base. In acid dissolution tests run in Canada, silica gel was precipitated, and the ^{99}Mo was recovered from the solution in very low yield.[13]

We employ a two-step process to dissolve the silicide targets. First, the aluminum alloy cladding and matrix aluminum are dissolved in 3 M NaOH-3 M $NaNO_3$. Then the dispersed U_3Si_2 particles are dissolved in a mixture of 5 M H_2O_2 and 0.1-2 M NaOH. The procedure to remove the aluminum cladding was developed in the fifties at ORNL,[14] and slight variations of it are practiced all over the world. It has worked well for removing cladding from nonirradiated, unannealed ("cold") targets, as well as thermally annealed and irradiated targets. However, the aluminum powder in the fuel meat of the thermally annealed and irradiated targets does not completely dissolve after the cladding is removed. Also, the silicide particles do not disperse but remain in the form of a thin wafer. The annealed targets require approximately double the time of the cold targets to dissolve the matrix aluminum and disperse the particles. After the U_3Si_2 particles disperse, they dissolve readily, as in the cold targets.

During 1996, effort continued on developing a process for dissolving silicide targets with alkaline peroxide solutions and recovering pure ^{99}Mo. The dissolution rate model developed in this study was used to evaluate the effects of hydrogen peroxide concentration, base concentration, and operating conditions. The results provide fundamental knowledge for use in dissolver-system design. Additional effort is needed on developing improved mechanical means to break up the fuel meat wafer and/or finding more powerful dissolution reagents. However,

---

[11] J. Salacz, "Reprocessing of Irradiated U-235 for the Production of Mo-99, I-131, and Xe-133 Radioisotopes," in *Fission Molybdenum for Medical Use, Proceedings of the Technical Committee*, International Atomic Energy Agency, Karlsruhe, Germany, IAEA-TECDOC-515, pp. 149-154 (1987).

[12] R. O. Marques, P. R. Cristini, H. Fernandez, and D. Marziale, "Operation of the Installation for Fission Mo-99 Production in Argentina," in *Fission Molybdenum for Medical Use, Proceedings of the Technical Committee*, International Atomic Energy Agency, Karlsruhe, Germany, IAEA-TECDOC-515, pp. 23-33 (1987).

[13] K. A. Burrill and R. J. Harrison, "Development of the Mo-99 Process at CRNL," in *Fission Molybdenum for Medical Use, Proceedings of the Technical Committee*, International Atomic Energy Agency, Karlsruhe, Germany, IAEA-TECDOC-515, pp. 35-46 (1987).

[14] S. Stroller and R. Richards, Eds., *Reactor Handbook: Fuel Reprocessing*, Interscience Publishers, New York (1961).

because of (1) the inherent problems in dissolving the silicide fuel, (2) the potential problems that dissolved silicate is likely to cause in the molybdenum recovery step, and (3) the relatively high degree of success achieved with LEU foil dissolution in base, development of the U_3Si_2 process is being suspended to concentrate limited resources on metal foil targets.

3. Basic Dissolution of LEU Metal Targets

Since 1995, dissolution of LEU metal foil with alkaline peroxide has been studied as an option for ^{99}Mo production as a replacement for processing of the HEU aluminide targets. An LEU-foil dissolution kinetics model was proposed in the same year.[15] During 1996, work was focused on reducing the consumption of hydrogen peroxide during uranium foil dissolution in alkaline peroxide solution and optimizing the uranium dissolution process.

Dissolution of uranium metal in alkaline hydrogen peroxide involves a complex process in which hydrogen peroxide is consumed by several competing reactions. The uranium surface catalyzes H_2O_2 autodestruction; the rate is orders of magnitude less without the foil present. As a result, a tremendous amount of hydrogen peroxide is consumed during uranium metal dissolution, leading to increased process waste and creating problems in process control. Thus, better understanding the kinetics of hydrogen peroxide decomposition has become a very important factor for reducing the hydrogen peroxide consumption during uranium dissolution. The consumption of hydrogen peroxide essentially follows the kinetic trend of uranium dissolution and can be divided into two regimes, depending on the hydroxide concentration. In the high-base regime (above 0.2 M), the equilibrium H_2O_2 concentration solely controls the rate of H_2O_2 disappearance. In other words, the rate of peroxide decomposition is independent of base concentration. While in the low-base regime (below 0.2 M), the H_2O_2 and OH^- concentrations affect the rate of peroxide decomposition. Based on the above experimental observations, an empirical kinetics model for the overall disappearance of hydrogen peroxide (R_p) was developed:

$$R_p = A_p \exp\left(-\frac{E_a}{RT}\right)\left(\frac{K_a[OH^-]^{n''}}{1+K_a[OH^-]^{n''}}\right)[H_2O_2]^n_{equilibrium} \qquad (3)$$

where A_p is the pre-exponential factor in the Arrhenius equation, E_a is the activation energy, R is the gas constant, T is the temperature, K_a is the equilibrium constant, n and n" are constants, and brackets indicate concentration of the specified compound.

Values for K_a, n, and n" were determined to be 20.4, 0.25, and 2, respectively, from the previous uranium dissolution model.[15] The following values were obtained from experimental data: $A_p = 5.06 \times 10^7$ and $E_a = 76.4 \pm 10\%$ kJ/mol. Equation 3 fits the experimental data fairly well for much of the data, as shown in Fig. IV-5. However, this model underestimates the rate of hydrogen peroxide decomposition by 6 to 98% over the entire regime of base concentrations studied.

[15] D. Dong and G. F. Vandegrift, *Nucl. Sci. Eng.* **124**, 473-481 (1996).

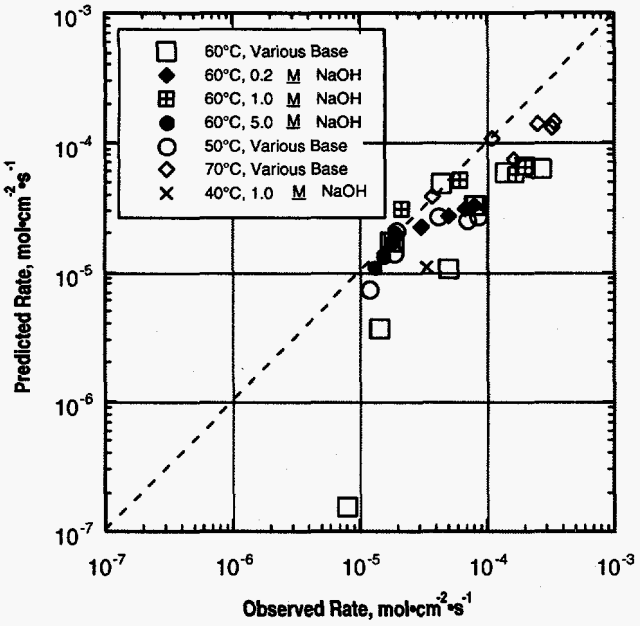

Fig. IV-5.

Predicted Rates versus Observed Rates for Depletion of H_2O_2

In an open, batch-type reactor, most of the available hydrogen peroxide is consumed by unwanted auto-decomposition. In single-batch processing, the hydrogen peroxide consumption ratio (HPCR, moles of hydrogen peroxide consumed per mole of uranium dissolved) was determined to be approximately 600. It is critical in this development effort to reduce the consumption of hydrogen peroxide to make the process practical. An optimized procedure has been proposed to reduce the HPCR by using sequential additions of alkaline peroxide. In this sequential procedure, multi-batch processing was employed to replace single-batch processing and thereby avoid decomposition of the hydrogen peroxide that remained in the reactor. Results in a laboratory-scale reactor showed that the HPCR could be reduced from 100 to 5 times the stoichiometric ratio for uranium dissolution. Because a large number of small-volume additions was actually used in this optimized procedure to frequently replace the dissolving solution or continuously replenish hydrogen peroxide, it opens up the possibility of substituting a plug flow reactor for the multi-batch reactor configuration in the dissolver system.

The HPCR was further reduced by optimizing the dissolution parameters. To that end, we performed a series of experiments to correlate the sodium hydroxide concentration with the uranium dissolution rate and HPCR. The results showed that both the HPCR and the dissolution time were reduced when the base concentrations increased from 0.1 to 5 M. The effect of dissolution temperature on the uranium dissolution consumption and dissolution time was also determined. As expected, the dissolution time was reduced as temperature increased from 50 to 85°C. However, the HPCR was minimized at 70°C. This probably is due to the competing reactions of uranium dissolution and hydrogen peroxide decomposition, each being affected differently by temperature changes. The conclusions of this study are that (1) HPCR can be reduced by a factor of ~20 by using a multi-stage batch reactor, (2) the optimum composition and temperature are 5.0 M H_2O_2/1.5 M NaOH and 70°C, respectively, and (3) significant challenges, such as reactor size and resident time, still need to be resolved.

The use of barrier materials must also be addressed for basic dissolution of LEU-foil targets. Since neither Ni, Cu, nor Fe will dissolve in NaOH or $NaOH/H_2O_2$, another metal needed to be found. A literature review was undertaken to choose metals that would have the mechanical and chemical attributes suitable for barriers. Important chemical properties were (1) ease of dissolution, (2) noninterference with the recovery of molybdenum from the dissolution, and (3) noninterference with the purification of the ^{99}Mo product. Other important factors were (1) the ability to be electroplated or electroless plated on uranium or to be made into foils, (2) low absorption yield of radioisotopes during target irradiation, and (3) low cost. The following elements were found to dissolve in alkaline hydroxide solutions: Al, Zn, Be, Ga, Sn, As, Nb, and Ta. Also, Ge and Re, although not amphoteric, are reported to dissolve readily in dilute hydrogen peroxide, and chromium may be amphoteric, but this is unclear in the literature. Of the metals exhibiting ease of dissolution, aluminum forms intermetallic compounds during irradiation and is, therefore, unsuitable; the toxicity of beryllium metal and the low melting point of gallium may preclude their use; and arsenic is classified as a nonmetal and may not have sufficient metallic properties to be made into a foil. Future work is needed to select barrier materials for targets to be processed by dissolution in base. Zinc will be the first barrier metal tested.

Future work on the dissolution of uranium metal foil will include (1) selecting the proper barrier material, (2) designing the dissolver/off-gas system, and (3) integrating ^{99}Mo recovery and purification steps to the dissolution.

E. Solid-Liquid Contactor

A new concept, a continuous countercurrent solid-liquid contactor, was developed for carrying out processes where (1) thorough mixing and then separation of liquid and solid phases are essential, and (2) countercurrent movement of the two phases improves process efficiency. The unit would do for solid-liquid extraction what the centrifugal contactor has done for liquid-liquid extraction. As shown in the schematic in Fig. IV-6, each stage of the solid-liquid contactor consists of an annular mixing zone and an interstage channel. The annular mixing zone provides good contact between the liquid and the solids. The channel between stages has a steep angle relative to the horizon so that there is countercurrent flow of the liquid and the solid particles. In general, the solid-liquid contactor is designed so that particles cannot settle out. Because it provides continuous countercurrent operation and can have many stages, the solid-liquid contactor can be operated continuously at high separation factors for complex solid-liquid flowsheets.

A two-stage solid-liquid contactor was tested for application to sludge washing. Countercurrent flow of sludge and wash water was achieved at a sludge-to-liquid flow ratio of 1.5. The key to successful operation was (1) good mixing in the contactor zone and (2) the countercurrent flow of solids and liquid in the interstage channel. Based on a test using a simulated sample of Hanford tank C-103 sludge, the interstage channel in the sludge-washing device was found to have a capacity of 80 L of wash water/($h \cdot m^2$). The dissolved solids in the washed sludge were reduced by 60%, where only a 40% reduction would have been expected based on dilution by the wash water. Only 4% of the particulate solids in the sludge

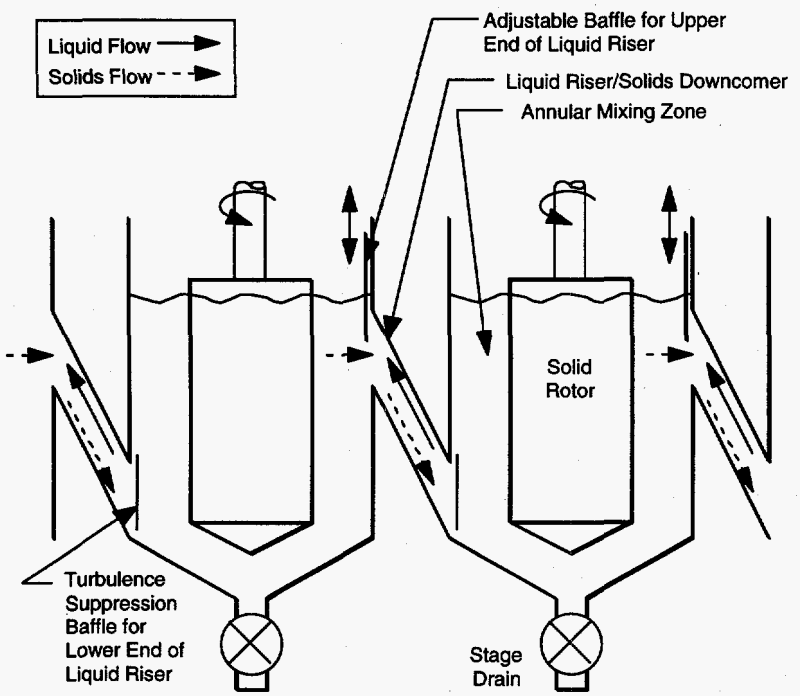

Fig. IV-6. Schematic of Two Stages in Continuous Countercurrent Solid-Liquid Contactor

feed was carried over with effluent wash water. While the unit was not optimized for sludge washing, the results were much better than one would obtain from simple dilution. Additional work is needed to optimize the system.

The solid-liquid contactor is applicable to other batch operations besides sludge washing—for example, Sr and Cs removal from tank supernatants at the Savannah River Plant. Processes to extract these elements are currently being performed in large mixing/settling tanks and could be run more efficiently in a continuous countercurrent mode. Given the right equipment, weeks of settling could become minutes. Countercurrent, multistage equilibrations would also require that less reagent be added and would thus reduce effluent volumes. Another promising application is using a sorbent in a multistage solid-liquid contactor to remove both Sr and Cs from supernatants as they are being transferred from the tanks at Hanford. Supernatant could be washed from sludge in one section; the resultant solution could be contacted with a sorbent to remove Cs and Sr in a second section; and the loaded sorbent could be combined with the sludge stream heading for storage or vitrification. Likewise, a precipitation section could be followed by a solids-washing section, followed by a solids-dissolution section.

V

Electrometallurgical Treatment Technology

The CMT Division is developing an electrometallurgical process for treatment of spent nuclear fuels for disposal in a geological repository. It is capable of handling most types of spent fuel and is especially intended for fuels at risk of chemical reaction with the groundwater in the repository. These "at risk" spent fuels include metal fuels with various cladding and matrix materials, reactive compounds, and highly enriched fuels. The central feature of the electrometallurgical treatment is electrorefining of the spent fuel in a molten salt electrolyte at 500°C (773 K). The LiCl-KCl eutectic electrolyte is formulated to contain about 2 mol% UCl_3. When a potential is applied between the anode and cathode, uranium, active fission products, and transuranic (TRU) elements dissolve at the anode, while pure uranium product is deposited on a solid cathode. The fission products and TRU elements are left behind to accumulate, either in the anodic dissolution basket (more noble fission products) or in the molten salt electrolyte (active fission products and TRU elements). The TRU elements and more active fission products may be extracted by passing the molten salt through anhydrous zeolite. The loaded zeolite may then be combined with a suitable glass frit and hot pressed to make a stable waste form for repository disposal. Fuel cladding, assembly hardware, and the noble metal fission products left in the anodic dissolution basket are melted together to form a Zr-Fe-based metal waste form for repository disposal. The TRU elements could also be placed in this metal waste form for disposal.

All the electrorefining process steps were developed in laboratory-scale experiments and have now been demonstrated at the engineering scale (10-kg batch size). Past work also demonstrated the feasibility of using this process for treatment of N-Reactor fuel (Zircaloy-clad uranium), single-pass reactor fuel (aluminum-clad uranium), and Experimental Breeder Reactor-II fuel (steel-clad uranium alloy). Select topics from the electrometallurgical programs in CMT are discussed below.

A. Electrorefining Process Development

Development of the uranium electrorefining process continues, with emphasis on producing a very pure uranium product, retaining the noble metal fission products in the anode baskets, and developing a new method for recovering chemically active fission products.

1. *Treatment to Produce Pure Uranium*

In the proposed electrometallurgical treatment of metallic spent fuels, an electrorefiner will be used to separate uranium from the fuel cladding, TRU elements, and fission products. Producing a pure uranium product will reduce the high-level waste volume from treating the spent nuclear fuel, thereby resulting in large savings in waste disposal costs. The uranium cathode deposit that will be produced from electrorefining metallic spent fuels will contain a small amount of TRU and fission product elements as chlorides in the salt adhering to the deposited uranium. These chlorides can be removed from the deposit by washing the uranium in molten salt that is in contact with lithium dissolved in a molten metal.

To test the effectiveness of the molten salt washing, a cathode product containing high concentrations of rare earths was used. These rare earths provide a measure of the effectiveness of the molten-salt washing in removing fission products and TRU elements. The uranium and rare earth concentrations (Ce, Nd, and Y) in the salt from the cathode deposit at the start of the experiment were 0.11 and 2.1 wt%, respectively.

In the experimental setup, a steel basket was used to hold the cathode product in the molten salt, which was contained by a steel vessel. Vanes provided at the bottom of the basket forced salt through the uranium bed, and screens at the top and bottom of the basket retained the uranium dendrites. An inverted steel cup, attached to the bottom of the basket, was provided for a Cd-Li alloy. When installed in the washing vessel, the cup was positioned in the cadmium pool. The cup was inverted to ensure slow diffusion of lithium into the cadmium pool, and vanes were attached to the cup to mix the cadmium.

Chemical analysis of filtered salt and cadmium samples that were taken from the washing vessel before the test indicated that the cadmium in the vessel already contained about 115 g lithium. Thus, no Cd-Li alloy was used in the first washing test, and the steel cup with the cadmium mixer was left off the assembly. The duration of the first washing test was 26 h, and the rotation speed of the wash assembly was 75 rpm. The direction of rotation caused salt to flow into the bottom of the steel basket, through the cathode deposit, and out the top. At the end of the test, the deposit was removed for sampling. The cathode deposit from the first experiment was reloaded in the wash assembly for the second experiment. The second washing was conducted with the Cd-Li alloy in the steel cup.

Table V-1 shows the results from chemical analysis of salt samples taken from the deposit before washing, after the first wash, and after the second wash. Before washing, samples were taken from the outer and inner surfaces of the deposit (top to bottom). After washing,

Table V-1. Elements Measured[a] in Salt Coating the Solid Cathode Deposit Used in the Washing Experiments

Average Concentration of Elements in Salt Samples, wt%			
	Before Salt Washing	After Washing 1	After Washing 2
Uranium	0.107	0.080	0.041
Cadmium	0.188	0.045	<0.08
Cerium	0.869	<0.014	<0.008
Potassium	26.43	26.91	26.94
Lithium	7.96	7.71	7.61
Neodymium	1.02	<0.018	<0.006
Yttrium	0.176	<0.016	<0.001
Zirconium	<0.01	<0.004	<0.001

[a]Analyzed with inductively coupled plasma/atomic emission spectroscopy.

samples were taken from top to bottom of the basket that was used to rotate the cathode deposit in the molten salt.

As shown in Table V-1, the concentrations of Nd and Ce in the salt phase from the deposit were reduced from 1.02 and 0.869 wt% to <0.006 and <0.008 wt%, respectively, after two washings in the molten salt. The Y and U concentrations were reduced from 0.176 and 0.107 wt% to <0.001 and 0.041 wt%, respectively. The above results indicate that the technique that is being developed in these experiments shows promise for producing a "pure" uranium product (defined as <1 ppm TRU elements and <1 ppm fission products). Similar washing tests are planned for the granular uranium cathode product from the high-throughput electrorefiner (see Sec. V.C). The salt content of the granular uranium product (1 to 5 wt% salt) is much less than that (57 wt% salt) for the deposit used in this washing test.

2. *Retention of Noble Metals in Anode Baskets*

One of the proposed high-level waste streams in the electrometallurgical treatment of spent nuclear fuel is produced by trapping the noble metal fission products in the anodic dissolution baskets. The purpose of this effort was to determine the effect of a 0.45-V voltage cutoff on the retention of zirconium and noble metals in the anode baskets and to determine whether metal screens are needed to retain the noble metals in the anodic dissolution baskets after electrotransport of the uranium to the cathode. In this experiment, simulated fuel was dissolved with three anode baskets: two were lined with fine-mesh screen (200 and 325 mesh steel screen, respectively), and no retainer screen was used in the third basket. Chemical analyses of samples from the anode baskets were used to measure the quantity of elements retained in the baskets.

The simulated fuel dissolved in this experiment was a steel-clad uranium-zirconium-fissium alloy (87.1 wt% U, 11.5 wt% Zr, 0.7 wt% Mo, 0.4 wt% Ru, 0.2 wt% Pd, and 0.1 wt% Rh) that had been chopped into small segments. The initial weights of material loaded in the anodic dissolution baskets were 6.37 kg of uranium, 0.84 kg of zirconium, 0.10 kg of noble metals, and 1.66 kg of steel cladding.

The chemical analysis results indicate that the following materials were retained in the cladding hulls for the basket with no screen retainer: 5% of the uranium, 100% of the zirconium, 99% of the molybdenum, 60% of the palladium, 100% of the rhodium, and 92% of the ruthenium. These results indicate that 92% of the noble metals was retained in the anodic dissolution basket. The noble metal retention in the anodic dissolution baskets with the retainer screens was about the same as that measured in the basket with no retainer screen.

If the noble metal fission products in spent metal fuel show retention characteristics similar to the above for the noble metals in the uranium-zirconium-fissium unirradiated fuel, these results indicate that a high retention (greater than 90%) of the noble metal fission products can be expected in the anodic dissolution baskets. Tests are now needed with actual spent fuel.

3. Nitride Enhanced Recovery

In many pyrometallurgical processes for treating spent nuclear fuel, it is necessary to periodically scrub the fission products that accumulate in the molten salt. Typical approaches include chemical reduction into a liquid metal. The objective of this project is to investigate a means of enhancing the partitioning of actinide, lanthanide, and transition metal chlorides by forming metal nitrides in a molten metal. Thermodynamic equilibrium calculations predict that this approach would decrease metal chloride concentrations in the molten salt to sub-ppm levels. The same calculations also indicate that this approach can be used to scrub strontium, a major fission-product heat source, from molten salts. The metal nitrides can then be converted to oxides. If successfully demonstrated, this approach has potential application for (1) removing fission products from chloride salts used in treating metallic fuel, (2) removing fission products from the fuel and flush salts used in the Molten Salt Reactor Experiment (MSRE, see Sec. V.B.2), and (3) removing fission products from fluoride salts used in treating aluminum-based spent reactor fuel.

In the early 1970s, precipitation of uranium nitride from molten Zn-Mg was examined as an alternative to removing the uranium by distillation of the Zn-Mg. Scoping experiments confirmed that a bed of calcium nitride placed in molten Zn-Mg-U was converted to uranium nitride, thus separating the uranium from the molten Zn-Mg. However, only 50% of the nitride bed was converted to uranium nitride. Because the uranium concentration in the molten Zn-Mg-U was high, distillation of the Zn-Mg was selected as the preferred means to separate the uranium. This work is an extension of that earlier work.

In development of the nitride enhanced recovery process, we began by selecting candidate metal nitride beds and molten metals for compatibility screening tests. The screening criteria were: (1) the initial and converted metal nitride beds must not react with the molten metal, and

(2) the conversion of the nitride bed must be thermodynamically favored. The selection of candidates was based primarily upon the analysis of published phase diagrams. Next, we experimentally tested compatibility by adding the selected metal nitrides to various molten metals. Samples of the molten metal were then analyzed for degradation products from the metal nitride. Results from the initial compatibility screening tests are given in Table V-2. The low values for percent nitride reacted confirm our phase diagram analyses that these metal nitride/molten metal systems should be compatible.

Table V-2. Results of Metal-Nitride Compatibility Experiment

Metal-Nitride Combination	Nitride Conc., ppm	% Nitride Reacted
Zn-Ca_3N_2	45	2.41
Zn-Li_3N	150	3.78
Zn-BN	< 20	0.36
Sn-Li_3N	90	2.27
Bi-BN	< 20	0.36

The work performed in the 1970s at ANL indicated that Ca_3N_2 could be used to extract uranium from zinc. Therefore, in the initial test of nitride enhanced recovery, lanthanum metal was extracted from molten zinc/Ca_3N_2 by conversion to LaN. In this test, after 24 hours, 96% of the lanthanum was removed from the molten zinc and converted to an insoluble nitride.

Owing to the promising results in the two-phase (molten metal/metal nitride) tests, a preliminary three-phase test was conducted in which $LaCl_3$ was extracted from a LiCl-KCl eutectic salt by using a Ca_3N_2 bed in molten zinc. First, a control test in which the molten salt was contacted with molten zinc without the nitride bed confirmed that there is very little partitioning of the lanthanum into the molten zinc. Next, Ca_3N_2 was added directly to the molten zinc and not allowed to contact the molten salt. Analysis of the molten salt showed that the $LaCl_3$ concentration was reduced from 1 to 0.7 wt%, which corresponds to a 7.5% conversion of the Ca_3N_2 bed. We believe that this low conversion was largely due to the fact that the molten mixture in the test cell was not stirred. A modified cell that will allow better stirring has been fabricated, and the test will be repeated. We also plan to follow a similar series of two-phase and three-phase tests for the promising systems identified in the compatibility screening tests.

B. Alternative Process Applications

The feasibility of electrometallurgical treatment of oxide and metallic spent fuels has been demonstrated in the research done for this program over the past several years. We are now exploring application of this process to other types of spent fuel, including aluminum-alloy fuels and MSRE fuel.

1. Aluminum-Based Spent Fuels

The U.S. Department of Energy faces a dilemma concerning spent aluminum-matrix reactor fuel. Over the next forty years, 128 metric tons of spent aluminum-matrix fuel will be shipped to the Savannah River Site from U.S. and foreign research reactors. When originally fabricated, this fuel contained over 55 metric tons of uranium at an average enrichment of approximately 20%. Some of this fuel is now corroding in wet storage and must be stabilized. In the past, this fuel would be processed in the Savannah River canyons. However, these facilities will be decommissioned in 2005 under current planning.

Earlier this year a task team was formed to recommend to DOE a technical strategy for the treatment, packaging, and disposal of aluminum-based spent nuclear fuel. Electrometallurgical treatment was the recommended backup option to disposition by direct disposal. Electrometallurgical treatment was viewed very favorably by the task team because it has the potential to separate Al and U from the spent fuel, thus greatly reducing the amount of high-level waste.

Reducing the amount of high-level waste and recovering valuable highly enriched uranium add a significant economic incentive for applying electrometallurgical treatment to aluminum-based fuels. As the DOE task team noted, this reduces the cost of high-level waste disposal by $200 million, as compared to direct disposal. By far the largest reduction in high-level waste comes from removing the aluminum, which constitutes about 90% of the volume of the spent fuel. The highly enriched uranium that can be recovered from the foreign and domestic research reactor fuel has an approximate commercial value of over $400 million.

a. Electrometallurgical Process Flowsheet

A diagram of the electrometallurgical process for treating aluminum-based fuels is shown in Fig. V-1. The entire process will be performed in an inert atmosphere enclosure located in a shielded facility. The process operations are grouped into three types of operations: (1) head end steps, (2) electrorefining and consolidation steps, and (3) oxidation and glass-forming steps.

In the first process operation, the end hardware for the fuel assembly is removed; the fuel is then sorted and compacted. Next the fuel is melted in an enclosed tilt-pour furnace. Because silicon forms very stable intermetallic compounds with uranium and enhances the separation of Al and U, silicon is added to the molten fuel at this point. The molten fuel is cast into shapes that will form anodes in the next (electrorefining) step of the process. In the melting step the volatile fission products (Cs, Rb, Br, and I) will vaporize. These volatile species will thus be trapped in a fibrous aluminosilicate (fiberfrax) trap above the molten metal.[1] After casting of the anodes, the trap material is compressed and added to a glass melter. Because the entire process is conducted in an inert atmosphere enclosure, the Xe and Kr fission gases can be captured in cryogenic traps as part of the purification system of the enclosure.

[1] D. Hampson, R. Frye, and J. Rizzie, *Nucl. Metall.* **15**, 57-76 (1969).

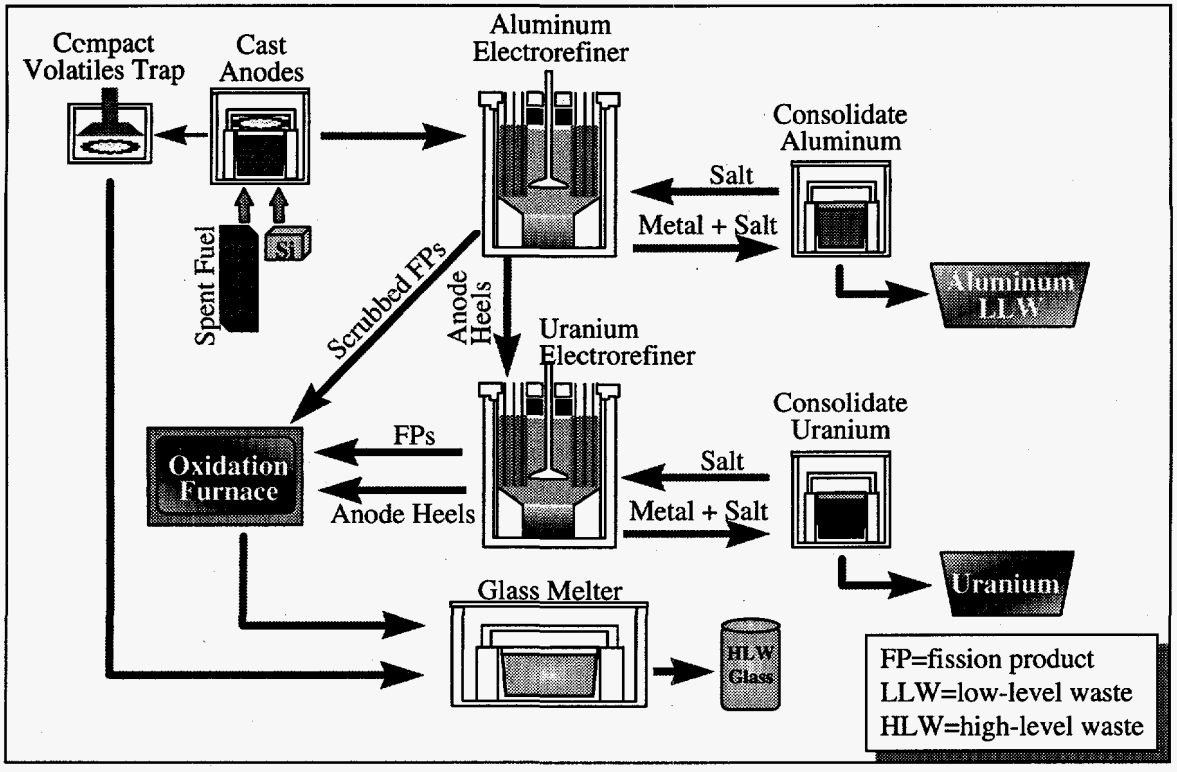

Fig. V-1. Flowsheet for Electrometallurgical Treatment of Aluminum-Based Fuels

The second process operation includes aluminum electrorefining and uranium electrorefining. Both the aluminum and uranium electrorefiners will employ a high throughput design developed at ANL.[2] The anodes formed from the molten fuel are mounted in a circular array and are rotated in a channel between two cylindrical cathodes. Dendritic uranium or aluminum deposits at the cathode and then is removed from the cathode by scrapers attached to the anode baskets. The dendrites then sink to the bottom of the electrorefiner, where they are collected. When all the aluminum or uranium has been electrorefined out of the anodes, the current is turned off, the dendrites are compressed, and the dendrites are removed from the electrorefiner.

Because some salt will adhere to the dendritic products from the aluminum and uranium electrorefiners, a melting step is necessary to coalesce these metals into ingots. Because the melting point of the salt is below that of aluminum and uranium, the salt can be poured off after cooling the melt below the melting point of metal yet above the melting point of the salt. The salt is then returned to the respective electrorefiner, and the consolidated aluminum or uranium ingots can be disposed of as low-level waste or sold to fuel fabricators.

[2] E. C. Gay, W. E. Miller, and J. J. Laidler, "Proposed High Throughput Electrorefining Treatment of Spent N-Reactor Fuel," Presented at the Am. Nucl. Soc. Meeting on DOE Spent Nuclear Fuel and Fissile Material Management, Reno, NV, June 16-20, 1996.

Over time there will be a buildup of alkaline earth fluorides in the aluminum electrorefiner and rare earth and TRU-containing fluorides in the uranium electrorefiner. Eventually this buildup will result in an undesirable carryover into the electrorefiner product. Thus, it will be necessary to periodically scrub these metal fluorides from the salt or discard the salt. Salt scrubbing is the preferred choice because it will allow a single batch of salt to be used in each electrorefiner for the entire campaign.

In the third process operation, the scrubbed alkaline earths, rare earths, and TRUs are converted to oxides along with the metal that remains in the anode after uranium electrorefining. The conversion is performed in an air oxidation furnace.[3] Also, a small glass melter will be used to melt the oxide powder from the oxidation furnace, together with the compressed aluminosilicate trap and additional glass formers. The intent is to formulate a glass within the specifications of the Defense Waste Processing Facility glass. A concerted effort has been made to minimize waste volumes throughout the process by adding only glass-forming oxides (fibrous aluminosilicate) and silicon, which is converted to silica in the oxidation furnace. Alumina and silica are components of defense waste glass. The glass can then be poured into waste canisters that will later be bundled into a waste package.

b. Development Status

Many of the process steps have already been successfully demonstrated in related programs. Uranium has been transported to a solid cathode in a high-throughput electrorefiner, and rare earths have been scrubbed by chemical reduction with lithium. The melting, casting, and consolidation steps were demonstrated much earlier as part of the Melt Refining Process at ANL.[1] Aluminum has been electrorefined on a laboratory scale (aluminum batch size of 2 g), though not under high-throughput conditions. Additionally, an aluminum deposit has been successfully consolidated by melting. An engineering-scale (6 kg of aluminum), high-throughput aluminum electrorefiner has been fabricated, and installation and testing will occur in 1997. In addition to high-throughput aluminum electrorefining, development work continues on scrubbing the alkaline earth fission products out of the aluminum electrorefiner salt, incorporating the oxides into a suitable glass waste form, and improving the head-end melting step.

2. *Waste Salt from Molten Salt Reactor Experiment*

a. Background

In the 1960s, Oak Ridge National Laboratory (ORNL) operated a reactor that used a uranium fluoride fuel that was dissolved in a mixture of molten fluoride salts. In the Molten Salt Reactor Experiment (MSRE), the initial charge loaded as fuel was ^{235}U, but this was later changed to ^{233}U. The reactor achieved criticality on June 1, 1965, and was operated until December 12, 1969. As designed, the reactor had a fuel salt containing the uranium and a flush

---

[3] W. E. Miller, G. J. Bernstein, R. M. Fryer, R. F. Malecha, M. A. Slawecki, and R. C. Paul, *The EBR-II Skull Reclamation Process. Part III: Skull Oxidation Equipment*, Argonne National Laboratory Report ANL-7338 (1967).

salt that did not. At the end of the test, the fuel salt was drained, and the reactor vessel and piping were rinsed with the flush salt. Both fuel and flush salts were stored in three criticality-safe storage tanks.

Tests at ORNL found that the irradiation of the solid salt produces fluorine radicals, which could then combine to form F_2, which diffuses to the salt surface and escapes. A procedure was initiated and carried out until 1990 for annual annealing of the stored solid salt to reduce the release of this radiolytic fluorine.

Almost from the beginning of the salt storage, some migration of fissile materials, notably U as UF_6, was detected. Uranium-233 contains small amounts of ^{232}U, which decays with a 70 yr half-life. One of the products in its decay chain is ^{208}Tl, whose decay emits a 2.6 MeV gamma ray. Therefore, migration of uranium from the tanks has been accompanied by the spread of radioactivity. This led to the formation of a cleanup task force at ORNL, which is in the process of evaluating procedures for dealing with the problem created by the fuel salt decomposition. A task assigned to ANL is evaluation of electrometallurgical separation methods to decontaminate and recover the ^{233}U and to render the balance of the salt into acceptable waste forms.

b. Preparation for Process Demonstration

Last year we discussed the flowsheet for the process.[4] This year we have been building the laboratory apparatus and procuring feedstock for demonstrating the process. The radioactive fluoride fuel salt was simulated by using a blend of nonradioactive salts that simulate the matrix salt LiF-BeF_2-ZrF_4 and actinide and fission product activities. About 8 kg of this salt was made up by blending and melting the constituents and removing insoluble constituents. This feedstock has been chemically analyzed and characterized.

The MSRE waste salt treatment is based on the reduction of the fluoride salt constituents by lithium alloy. This is done electrochemically in a series of four steps using lithium alloy as the anode and collecting the process products on cathodes. In the first reduction, noble metals and zirconium in the salt are transported onto a solid cathode. In the second reduction, uranium, TRU elements, the remaining zirconium, and some rare earths are separated from the matrix salt in a liquid bismuth cathode. (This is treated in a second electrorefiner to purify and isolate the ^{233}U.) In the third and fourth reductions, rare earths, alkaline earths, thorium, cesium, and barium are separated from the matrix salt in liquid bismuth cathodes. This leaves the matrix salt essentially devoid of activity (to be treated to make a low-level waste of fluorapatite) and at about the same volume as the feedstock.

There are two candidates for the anode alloy, Li_3Bi and Li_3Sb. Both alloys are initially solid at the process operating temperature 600°C (873 K). When lithium is electrochemically removed from Li_3Bi, the material changes to a liquid-solid state. When lithium

[4] J. J. Laidler et al., *Chemical Technology Division Annual Technical Report, 1995*, Argonne National Laboratory Report ANL-96/10, p. 81 (1996).

is removed from Li_3Sb, the material remains solid. Our laboratory-scale electrorefiner is designed to handle both alternatives. Part of our work is to select which of these alloys is most suitable for the production process. A number of factors will enter into the selection: (1) ease of preparation of the alloy and shaping into anodes, (2) electrochemical behavior, and (3) ease of recovery of spent anodes since this material will be recycled to make new anodes (by adding lithium) for the next batch cycle.

During the past year, approximately 530 g of the Li_3Bi compound was generated in a tilt-pour casting furnace. The Li_3Bi compound was generated by combining and melting pure lithium and bismuth metals in a tantalum crucible and then casting the product into a round-bottomed stainless steel mold at room temperature. Five "charge-melt" cycles were performed to add the lithium incrementally to the bismuth, with subsequent alloying at 500°C (723 K). After the final charge of lithium was added, the furnace was heated to ~1200°C (~1473 K) and held at that temperature for ~20 min, and the molten material was poured into a stainless steel casting mold. The Li_3Bi was recovered easily (~531 g recovered), and no damage was observed on the tantalum crucible. Figure V-2 shows a photograph of the final product.

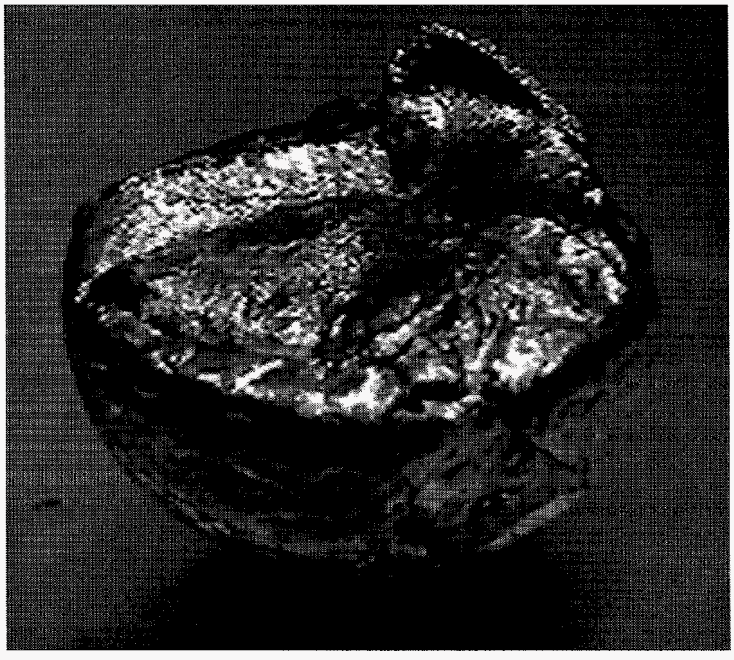

Fig. V-2. Ingot of Li_3Bi Generated by Pouring Molten Li-Bi Alloy. The top surface diameter is ~7 cm.

For the MSRE salt treatment demonstration, the laboratory-scale electrorefining cell that was used in the past for chloride salts was not suitable. A new cell suitable for work with fluoride salts at operating temperatures up to 750°C (1023 K) has been procured. Figure V-3 is a schematic representation of the new cell. The crucible which contains the salt hangs from the lower flange; the internal diameter of this containment crucible is 20 cm. The upper flange

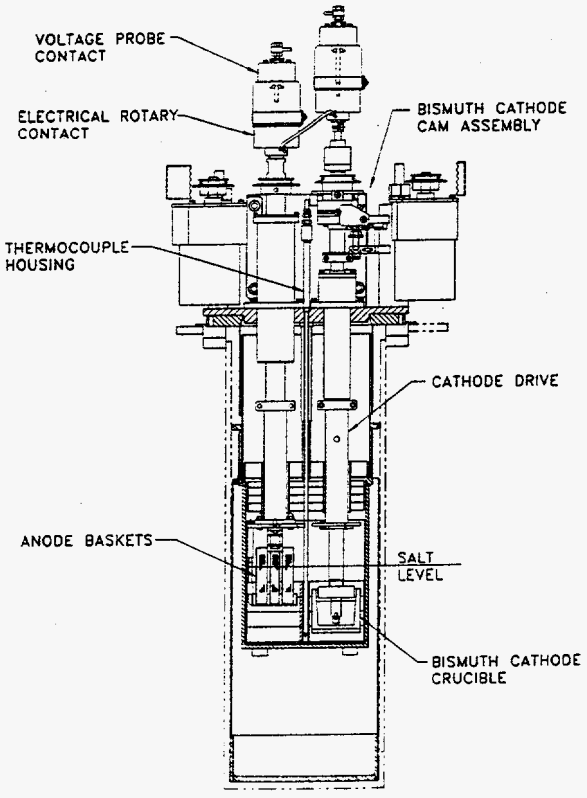

Fig. V-3.

The Anode and Bismuth Cathode Designed for Treating MSRE Salt

supports the drives, the mixer, cell anode, and cell cathode. This upper flange is attached to a lift (not shown on sketch). The lift is used to raise and lower the cell working parts while the cell crucible containing the liquid salt remains fixed. The crucible is located in a heated furnace well that is part of the containment boundary of a high-purity argon atmosphere glovebox. The operating temperature range of the cell is 600-750°C (873-1023 K).

During the past year, all the parts for the electrorefiner cell were procured, and the cell was assembled and mechanically operated at room temperature outside the glovebox. Any deficiencies that were found were corrected. The cell has now been reassembled inside the glovebox (Fig. V-4). Testing of the MSRE waste salt treatment with this cell will begin in 1997.

C. Testing of Advanced Electrorefiner Concepts

An effort is underway to develop an advanced electrorefiner having high throughput (>40 kg uranium per hour) and large batch size (>100 kg). The high throughput electrorefiner (HTER) is proposed for treating large quantities of spent fuel, such as the N-reactor fuel from the Hanford site. A 0.2-m (8-in.) dia HTER was employed to determine the operating characteristics of a new beryllia scraper design. These scrapers are used to remove uranium dendrites from the cathode tubes. The dendrites are knocked off of the cathode tubes and into a collection vessel as the anodic dissolution baskets are rotated. The baskets are rotated in channels formed by the concentric cathode tubes. The new scrapers were designed to be more durable than earlier scrapers. Steel scrapers were also tested as an alternative to the beryllia scrapers.

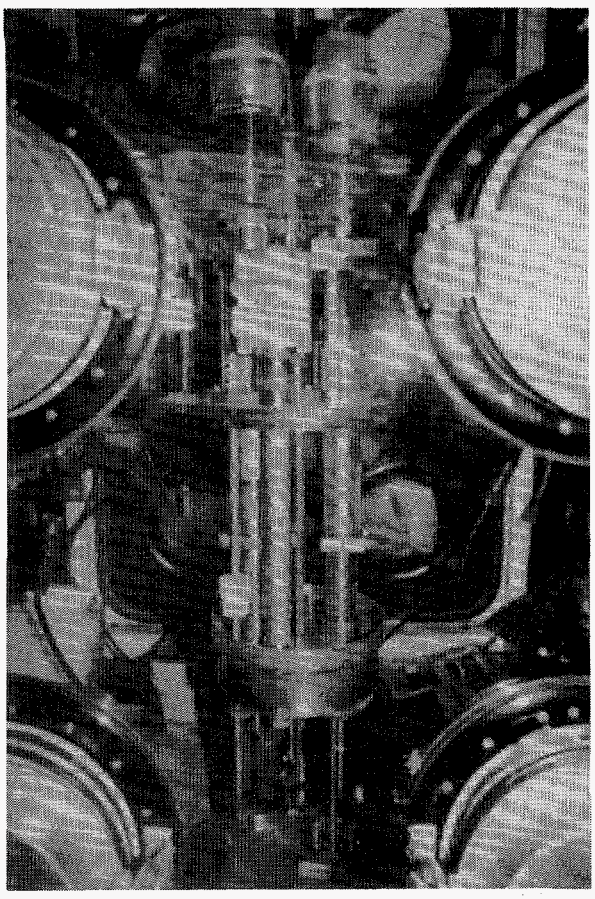

Fig. V-4.

Glovebox Installation of Electrorefining Cell Designed for Treating MSRE Salt

For the scraper tests, four anodic dissolution baskets were bolted to a steel plate, which was attached to the anode shaft of the electrorefiner. A steel ring was attached to the bottom of the anode baskets to provide a more rigid structure. The beryllia scraper was attached to the anode assembly with a steel bar.

Steel-clad uranium-zirconium-fissium (U-Zr-Fs) fuel was chopped into segments (0.5-cm dia, 0.63-cm length), which were anodically dissolved in three runs with the 0.2-m HTER. The average anodic dissolution current was 30.7, 34.0, and 35.5 A for Runs 186, 187, and 188, respectively. The cutoff voltage for these tests was 0.45 V. Under these operating conditions, retention of 100% of the zirconium and greater than 90% of the noble metals in the anodic dissolution baskets was expected.

The results for Run 186 showed that an estimated 0.804 kg of uranium was anodically dissolved in 14.2 h, with a dissolution efficiency of 62%. It appears that about 38% of the electricity passed through intermittent short circuits that were formed in the electrorefiner. Approximately 543 Ah of electricity was required to dissolve a kilogram of uranium, and the uranium dissolution-electrodeposition rate was 57 g of uranium per hour.

Run 187 was a continuation of Run 186. Post-test examination of the HTER electrodes after Run 187 indicated that uranium had bridged between the cathode tube support bars and the bottom of the anodic dissolution baskets (at the lower end of the scraper support rod). This result has implications for the planned design of a 0.6-m (25-in.) dia HTER. This will be the size of the first scaled-up HTER in CMT.

The purpose of Run 188 was to determine the effect on performance of the steel ring that was attached to the bottom of the anodic dissolution baskets in Runs 186 and 187. This ring was removed from the baskets for Run 188. The operating conditions for these tests were nearly the same. For Run 188, 565 Ah of electricity was needed to dissolve the uranium. The dissolution-electrodeposition rate for this run was 63 g of uranium per hour, which is slightly higher than the rate for Run 186. Based on these tests, the steel ring attached to the bottom of the anodic dissolution baskets showed no effect on performance. Thus, the steel ring may be used to provide a more rigid anode structure if needed, without decreasing the uranium dissolution-electrodeposition rate.

Steel scrapers were used in Run 193. Steel scrapers are being investigated as an alternative to beryllia scrapers because of the lower expected cost and lower maintenance required for the metal scrapers. As expected, more electrical short circuits were formed with the metal scrapers. Approximately 1000 Ah was required to dissolve a kilogram of uranium with the steel scrapers, almost double the current required to dissolve one kilogram of uranium in the runs with beryllia scrapers. However, a lower cell resistance was measured with the metal scrapers (about 3 mΩ for the steel scrapers, compared with about 7 mΩ for the beryllia scrapers). This lower resistance permitted higher current operation at a given voltage. Consequently, the uranium dissolution-electrodeposition rates were about the same with the beryllia and metal scrapers (about 60 g of uranium per hour in Runs 186, 188, and 193).

Based on the results from the scraper tests, the following observations and recommendations were made:

1. No chips, cracks, or breaks in the beryllia scrapers were observed with the new beryllia scraper design that was used in Runs 186 through 188. This scraper design is recommended for the 0.6-m (25-in.) dia HTER.
2. The cathode tube support bars should be provided with a ceramic insulator to eliminate electrical short circuits that may be formed by uranium electrodepositing on the bars and bridging to the anode.
3. Scrapers should be provided for coverage of all cathode tube surfaces on which uranium could electrodeposit and bridge to some component on the anode to form a short circuit.
4. A steel ring may be attached to the anode baskets (below the surface of the electrolyte) to provide a more rigid structure. This is an important feature when the anode baskets are scaled up for a full-length N-Reactor fuel element.

5. Both beryllia and metal scrapers show promise for use in the HTER. Further testing is needed to determine the best scraper for various applications.

D. Waste Form Development

High-level wastes from the electrometallurgical treatment of spent nuclear fuel include remnants of the fuel cladding, alloying zirconium from the fuel, TRU elements, and fission products. These wastes are incorporated into two waste forms. The cladding, zirconium, and the least easily oxidized fission products are unchanged by the electrometallurgical treatment. They are removed from the electrorefiner and melted to make a durable stainless steel–zirconium alloy waste form. The TRU elements and the most easily oxidized fission products accumulate in the process salt. These salt-borne wastes are removed and incorporated into the crystal structure of zeolite A; the resulting zeolite is made into a composite ceramic waste form with borosilicate glass. Fission products and TRU elements from the salt are removed into zeolite in an ion exchange column. Because it is desirable to avoid placing uranium chloride into the zeolite along with the fission products and TRU elements, uranium chloride is temporarily removed by means of a pyrocontactor before the salt is passed through the zeolite column. In the pyrocontactor, uranium chloride is reduced to uranium metal, which dissolves in a cadmium stream. After the TRU elements and fission products are removed by the zeolite column, the uranium is re-oxidized into the returning salt, which is then ready for further electrorefining operations, and the cadmium is completely recycled. Progress made in development of the ceramic and metal waste forms is summarized below.

1. Waste Isolation

a. Zeolite Ion-Exchange Column

The salt-borne fission products from the electrometallurgical treatment of spent fuel are incorporated into zeolite A by ion exchange. The ion exchange is accomplished by contacting the salt with zeolite in a column. The fission products in the salt are exchanged with mobile cations in the zeolite. The exchange process is given by the following reaction:

$$FP(Cl)_n + nM(zeolite) = FP(zeolite) + nMCl \quad (1)$$

where FP is a fission product, and M is Li or K. In the past year, we began testing to determine the feasibility of using a zeolite ion-exchange column to remove fission products from molten electrorefiner salt. The first tests were conducted with a bench-scale column (30-cm length, up to 5-cm dia) to establish the approximate operating conditions for sorption of fission products.

The pelletized zeolite A (from UOP Corp.) chosen for initial tests was dehydrated under flowing dry nitrogen and pre-loaded with LiCl-KCl eutectic salt. The pre-loading with LiCl-KCl accomplishes several objectives. First, it exchanges the sodium in the zeolite for Li and K, thus preventing accumulation of sodium in the effluent salt, which is to be recycled to the electrorefiner for reuse. Second, it fills the zeolite structure with chloride, which displaces any

residual water that would otherwise be transferred to the effluent salt. Finally, it provides a way to control the Li/K ratio in the column zeolite and, thus, in the recycled salt. Passing a large excess of LiCl-KCl salt through zeolite in a column proved to be an effective way of pre-loading.

Column ion-exchange tests with simulated waste salt have been conducted at temperatures of 450°C (723 K), 500°C (773 K), and 550°C (823 K) and at several flow rates between 0.1 and 3.3 cm/min. The effluent salt composition from a typical column test is plotted versus time in Fig. V-5. The test was run at 450°C (723 K) and a linear salt flow rate of 0.5 cm/min. In this figure, the fission product concentration in the effluent salt is normalized to the concentration in the inlet salt; the amount of salt that has been treated is shown as the number of grams of salt that has passed through the entire column per gram of dehydrated bed zeolite. The point where fission products are observed in the effluent salt, which is called "breakthrough," defines the amount of salt that can be treated by the zeolite under a particular set of operating conditions, provided the aspect ratio of the column is not too small to allow for substantial uptake of fission products. In Fig. V-5, breakthrough occurs after 2.5 g of salt has been treated per gram of zeolite in the column, but in tests with slower flows and higher temperatures, as much as 3.5 g of salt could be treated per gram of zeolite. Somewhat higher capacities are expected as optimization of the operating conditions proceeds.

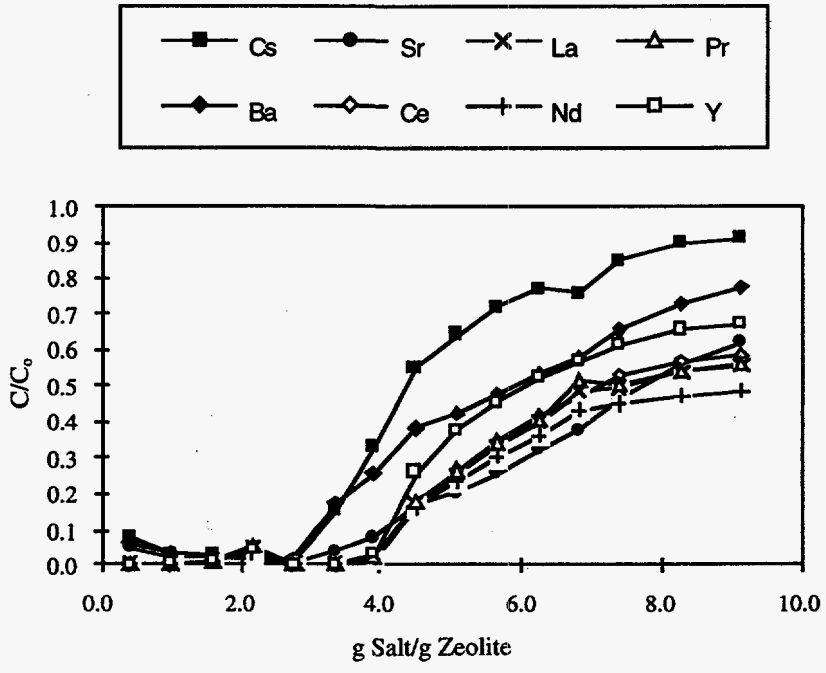

Fig. V-5. Breakthrough Curves for Fission Products in Tests of Zeolite Ion-Exchange Column at 450°C (723 K) and 0.5 cm/min

Both the salt flow rate and temperature were found to affect breakthrough. At 450°C (723 K) and a flow rate of 3.3 cm/min, breakthrough occurred very rapidly for all fission products (between 0.5 and 0.9 g salt/g zeolite), approximately when the salt initially in the

column had been displaced by waste salt. At 0.7 cm/min, breakthrough of Cs, Ba, and Sr occurred nearly simultaneously after 1.7 g of salt had been treated per gram of zeolite; the rare earth cations lagged slightly. At a salt flow rate of 0.5 cm/min, breakthrough of cesium and the alkaline earths occurred after 1.9 g of salt had been treated per gram of zeolite.

A comparison of breakthrough data for temperatures of 450°C (723 K) and 540°C (813 K) indicated that the column temperature has a strong effect on performance. A greater quantity of salt was treated at the higher temperature. For example, at 450°C and a salt flow rate of 1.0 cm/min, breakthrough was observed after 3.3 g of salt had been treated, compared with 2.0 g at 540°C and a similar flow rate. Similar tests are planned with a variety of salt and column compositions.

b. Pyrocontactor

Pyrocontactors are high-temperature centrifugal contactors that provide intense mixing in an annular mixing region to effect chemical reactions between solutes in molten salt and liquid cadmium alloys. They also provide clean separation of these streams in a separating zone. Previous work[5] with a single-stage pyrocontactor used cerium as a stand-in for uranium, lanthanum for plutonium, and yttrium for rare earths, because of the similarity of the relative separation factors among these elements. These tests demonstrated effective separation of lanthanum from yttrium in a salt containing lanthanum and yttrium chlorides by reduction with cerium in cadmium. Thus, it should be possible to use the pyrocontactor to separate the uranium from the fission products contained in the electrorefiner spent salt.

This year, a multistage (four-stage) pyrocontactor was built and tested. The pyrocontactor unit has rotors of 4-cm dia in housings of 6.4-cm dia. The housings were drilled into a single block of 304 stainless steel; flow between stages was obtained via drilled internal passages. Liquid metal enters the unit through one end stage, passes through each successive stage, and exits the unit from the other end stage. Molten salt flows through each stage in the opposite direction, i.e., in countercurrent flow to the liquid metal.

Tests to date included (1) feeding cadmium metal and LiCl-KCl eutectic salt to the pyrocontactor from metal and salt tanks by means of an improved flow path and flow control mechanism (metered flow of pressurized gas), (2) single-component tests reacting Ce in Cd with $CdCl_2$ in salt, and (3) multi-component tests reacting Ce in Cd with $LaCl_3$ and YCl_3 in salt. Good separation of metal and salt phases was demonstrated during these tests. However, the extraction efficiency could not be determined in the multistage tests because cerium was oxidized as a result of an air leak into the glovebox. The glovebox and all its systems have been repaired and are fully functional, and we expect to resume successful testing with the highly reactive rare earths, just as was done with the single-stage unit.

---

[5] J. J. Laidler et al., *Chemical Technology Division Annual Technical Report, 1994*, Argonne National Laboratory Report ANL-95/24, p. 95 (1995).

2. Metal Waste Form

a. Introduction

Stainless steel-zirconium (SS-Zr) alloys have been developed to immobilize radioactive fission products isolated during the electrometallurgical treatment of spent nuclear fuel. The SS-Zr waste form alloys comprise spent fuel cladding, noble metal fission products, and in some cases, zirconium metal from alloy nuclear fuels. Since the cladding typically represents 85 to 99 wt% of the metal wastes from electrometallurgical treatment, SS-Zr alloys may be generated by using the cladding as the principal alloying component, thus minimizing the waste form volume.

This approach gave rise to the parallel development of two nominal compositions for the metal waste form: (1) stainless steel-15 wt% zirconium (SS-15Zr) for stainless steel-clad fuel and (2) Zircaloy-8 wt% stainless steel (Zr-8SS) for Zircaloy-clad fuel. The electrometallurgical process is being demonstrated with spent fuel from the Experimental Breeder Reactor-II (EBR-II), which includes driver fuel and blanket fuel. The driver fuel contains Type 316 and D9 stainless steel cladding, and the blanket fuel has Type 304 stainless steel cladding. Therefore, the metal waste form for EBR-II will be SS-15Zr. Other fuel types that are being evaluated for electrometallurgical treatment have Zircaloy cladding; the metal waste form alloy for these fuels would be Zr-8SS.

The content of noble metal fission products in a metal waste form depends upon the accumulated burnup of the processed fuel. The designation "noble metal" means a metallic element that is inert, or electrochemically noble, in the electrorefiner system; the cladding and zirconium are also noble metals. The noble metal fission products that will be included in SS-Zr waste form alloys include isotopes of Ru, Rh, Re, Pd, Zr, Nb, and Tc.

b. Alloy Preparation

Experiments were carried out to characterize the SS-15Zr and Zr-8SS alloy waste forms. For these experiments, small-scale (approximately 20 g) and large-scale (3 kg) alloys were prepared with different zirconium and noble metal compositions. The simulated waste-form alloys were used to quantify the corrosion behavior, mechanical strength, and thermophysical properties of the waste form alloys.

The small-scale alloys were prepared by melting stainless steel and zirconium metal at 1600°C (1873 K) in yttria (Y_2O_3) crucibles under an argon atmosphere for 1 to 2 h and cooling slowly (approximately 6°C/min) during solidification. Alloys made with this cooling rate will be referred to as "as-cooled" specimens. The small-scale SS-Zr alloys are used for basic microstructural characterization and corrosion test specimens.

The large-scale alloys were generated in a tilt-pour induction furnace connected to an inert atmosphere glovebox. The furnace consists of two hot zones within a single furnace chamber. The melting hot zone is a tilt-pour induction furnace with a graphite susceptor and a

maximum rated temperature of 2200°C (2473 K). The lower hot zone is a graphite element furnace with a maximum rated temperature of 1600°C (1873 K) that is used for preheating casting molds.

A typical alloying experiment for a SS-15Zr alloy proceeds as follows: (1) the melting furnace is slowly (approximately 6°C/min) heated to 1600°C (1873 K); (2) if the metal is to be cast, the casting mold is pre-heated to 800°C (1073 K); (3) the alloy melt is held at 1600°C (1873 K) for approximately 1 h; and (4) the melt is either cooled slowly (approximately 6°C/min) in the yttria crucible or poured into the casting mold. In preparation of SS-15Zr alloys, the molten alloy was either (1) cast into single-cavity graphite casting molds to generate 8-cm dia slugs, (2) cast into four-cavity graphite casting molds to generate 3-cm dia rods, or (3) cooled at a controlled rate in the melt crucible to generate 10-cm dia ingots.

c. Sample Microstructure

Typical "as-cooled" microstructures of the SS-15Zr and Zr-8SS waste form alloys are shown in Fig. V-6. The SS-15Zr alloy contains a two-phase eutectic structure in which the major phases are an iron-rich solid solution designated as ferrite, or α-Fe(Cr,Ni), and an intermetallic designated as a Laves phase, or $Zr(Fe,Cr,Ni)_{2+x}$. The Zr-8SS alloy is a multiphase structure with a primary zirconium metal phase, or α-Zr, surrounded by a three-phase eutectic network containing $Zr_2(Fe,Ni)$ and $Zr(Fe,Cr)_2$ intermetallics and α-Zr metal. The SS-15Zr alloy was investigated first because the initial metal waste forms to be generated will be from EBR-II.

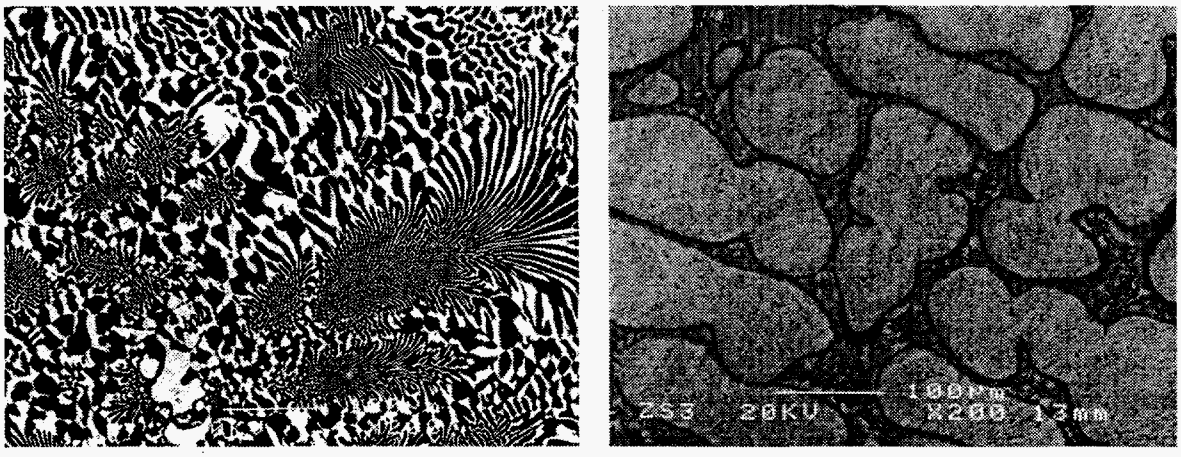

(a) SS-15Zr (b) Zr-8SS

——100 μm

Fig. V-6. Typical Microstructures of As-cooled SS-Zr Alloys: (a) SS-15Zr Containing the α-Fe Solution (dark) and the $Zr(Fe,Cr,Ni)_{2+x}$ Intermetallic (bright) and (b) Zr-8SS Containing α-Zr Surrounded by a Complex Matrix Containing $Zr_2(Fe,Ni)$, $Zr(Fe,Cr)_2$, and α-Zr.

A series of high-temperature annealing experiments was conducted to evaluate the microstructural stability of the SS-15Zr alloy. Preliminary results indicated that the Laves phase

is metastable and transforms into $Zr_6(Fe,Cr,Ni)_{23}$ during high temperature annealing. An equilibrium microstructure of the SS-15Zr alloy may be similar to that shown in Fig. V-7. Although understanding this phase transformation is important for full understanding of the alloy behavior, initial corrosion tests indicate that this transformation has negligible impact on the corrosion behavior of the SS-15Zr alloy.

Fig. V-7. Microstructure of SS-15Zr Alloy Annealed at 1600°C (1873 K). Examples of the $Zr_6(Fe,Cr,Ni)_{23}$ intermetallic (dark gray) are indicated by three white arrows.

Ruthenium, molybdenum, silver, and palladium are used as representative elements to study the distribution of noble metal fission products in the waste form alloys. This study revealed that, in as-cast and annealed SS-15Zr alloys with 4 wt% noble metal, ruthenium, palladium, and silver are predominantly in the intermetallic phases. Molybdenum shows a preference for ferrite but is present in all phases. In Zr-8SS (plus 4 wt% noble metal), palladium was observed in the $Zr_2(Fe,Ni)$ intermetallic, ruthenium was found in all phases with a slight preference for $Zr_2(Fe,Ni)$, and the distribution of Ag and Mo was not determined conclusively. The important point here is that the noble metals are distributed in the SS-Zr alloy phases; no new noble metal-induced phases are found anywhere. Therefore, the retention capability of the SS-Zr alloys for noble metal fission products is dominated by the behavior of the alloy matrix.

d. Corrosion Testing

Three types of corrosion tests are used to characterize the behavior of the SS-Zr alloys. The general corrosion behavior is measured through water immersion tests that use simulated J-13 well water (representative of the groundwater at the proposed high-level nuclear

waste repository site at Yucca Mountain, NV). Electrochemical linear polarization methods are used to measure low corrosion rates and investigate galvanic and localized corrosion phenomena. Finally, vapor hydration testing is an aggressive, accelerated corrosion test method used to examine the durability of the waste form alloys under severe conditions.

The immersion test method is based on the MCC-1 static leach test developed for glass-based waste forms. Disk-shaped metal specimens (15.9-mm dia, 3-mm thick) were polished and immersed in the J-13 solution contained in a sealed Teflon vessel. The sealed vessel was placed in an oven at 90°C (363 K). After over 10,000 h, the measured mass difference for an immersed specimen was typically within the resolution of the measurement (±0.0001 g), and the surface of the specimen was still very shiny, with only a slight tarnish in some cases. These findings indicate that this standard test is not aggressive enough to quantify the corrosion behavior of the SS-Zr alloys.

The electrochemical linear polarization method was used to determine corrosion rates of metal waste-form specimens in J-13 solution of different pH's (2 4, 7, and 10); this technique can measure very low corrosion rates in a short-duration test. The measured corrosion rates are compared in Fig. V-8 for the waste form alloys, commercial zirconium and stainless steel, and selected candidate waste canister materials. The corrosion rates at pH = 7 for the two waste form alloys are similar to the measured rates for the stainless steel (Type 316) and zirconium metal. They are also similar to the rate for Incoloy 825, lower than the rate for copper, and two orders of magnitude lower than the rate for mild steel. Copper and mild steel are waste canister materials that are designed to corrode in service. Incoloy 825 is a low-corrosion waste canister material. Corrosion rates for the Zr-8SS are not significantly affected by pH variations, but increasing acidity increases the corrosion rates for the SS-15Zr and the stainless steel; these increased rates, however, are still relatively low.

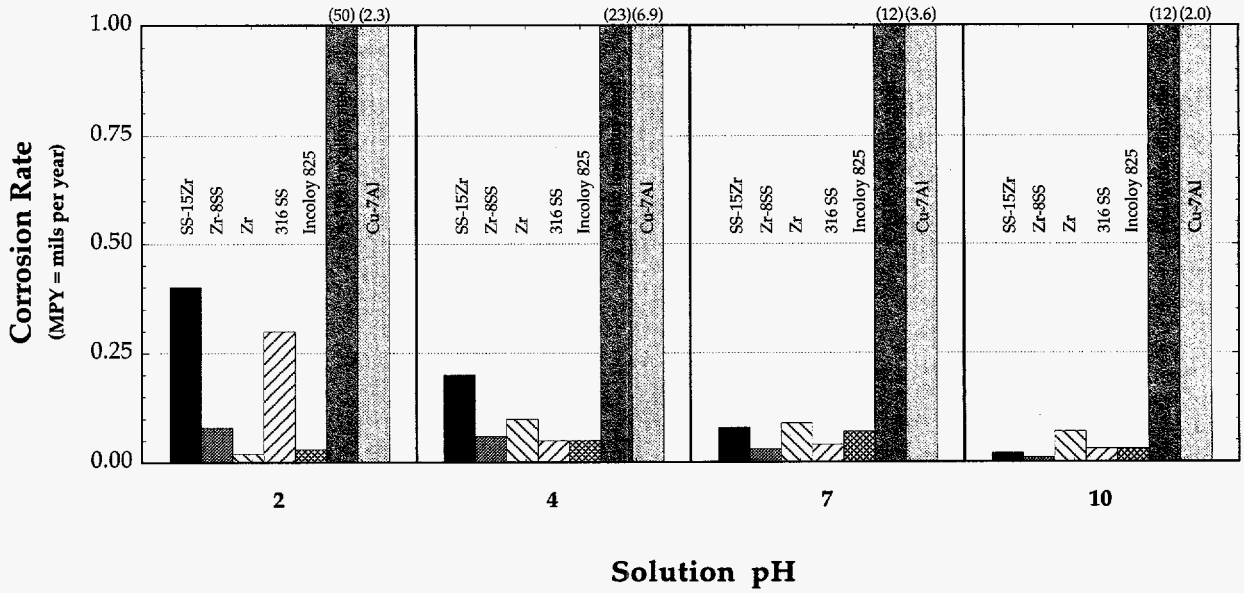

Fig. V-8. Corrosion Rates Measured at Various pH Values by the Linear Polarization Method

In the vapor hydration test, dime-sized monolith specimens of the metal waste form were suspended in a stainless steel container in saturated vapor at 200°C (473 K) for various times. The exposed specimens were weighed after the test to determine mass differences and were examined by scanning and transmission electron microscopy. Chemical durability was measured by (1) the thickness of the surface reaction layer, or alteration layer, and (2) the amount and nature of secondary phases formed on specimen surfaces. Borosilicate glasses typically have alteration layers greater than 100-μm thick after a 56-day test. The alteration layer thickness present on the metal waste form alloys was much lower, approximately 1 μm after 56 days. The mineral hematite (Fe_2O_3) was detected on the SS-15Zr waste forms, whereas monoclinic ZrO_2 was identified on the Zr-8SS waste forms. These test results appear promising.

e. Physical Properties

The physical properties of the waste form alloys must be measured to provide a consistent data base that enables the effective modeling of waste form behavior over the extended lifetime of a repository. Numerous physical and thermophysical properties have thus been measured for the waste form alloys. In general, the SS-15Zr material is very strong with favorable thermal properties. It has low tensile ductility and resistance to impact fracture for a metal. (Many of the measurements on the SS-15Zr alloy were carried out at the Thermophysical Properties Research Laboratory at Purdue University.) The Zr-8SS alloy has not been as extensively examined as the SS-15Zr, but efforts are continuing toward gathering a similar set of data.

f. Future Work

Future development efforts on the metal waste form will continue to focus on behavior characterization, with an added emphasis on waste form qualification. The characterization of the metallurgy and physical properties is nearly complete for the SS-15Zr alloy, and a similar characterization will be done for the Zr-8SS alloy in this coming year. Waste form qualification is a long-term task that involves demonstrating that the waste form will perform acceptably in its final resting place: a high-level nuclear waste repository. This is an especially difficult task because there is as yet no firm definition of acceptable performance, and the location, characteristics, and guidelines of the high-level repository for this waste form have yet to be determined. Therefore, our working assumption for the next year is that the metal waste form must compare favorably with other high-level waste forms, such as borosilicate glass. In addition, test protocols for the metal waste canister materials will be examined, and relevant test methods will be implemented.

3. *Ceramic Waste Form*

a. Introduction

The ceramic waste form is being developed to contain salt-borne fission products from the electrometallurgical treatment of spent fuel; it is a composite formed from a mixture of salt-loaded zeolite A and a glass powder or frit. The zeolite contains the fission products within

its structure. The glass serves as a binder which holds the crystalline phase together, providing structural integrity and "formability." In addition to the fission products, the zeolite contains within its structure the major constituents of the salt, namely, lithium, potassium, and chloride. The fission products are typically incorporated into the zeolite by ion exchange or, alternatively, by simple blending of zeolite and waste salt. Development of ceramic waste forms is being carried out first with zeolite powders; as more column materials become available, they are being investigated to identify any differences that may exist. We are also evaluating the relative performance of waste forms made by converting zeolite to sodalite.

b. Fabrication

Ceramic waste forms fabricated by hot isostatic pressing (HIP) techniques are being developed. The fabrication involves dehydration of the zeolite, blending of zeolite and salt, mixing of the salt-loaded zeolite with glass, and consolidation via a HIP process. Currently, two types of zeolite A powders are being investigated: Na-zeolite and Ca/Na-zeolite.

Zeolite powder, as received from UOP Corp. (Des Plaines, IL), can contain up to 25 wt% of water, which must be removed prior to subsequent operations. We remove this water by heating the powder in flowing dry nitrogen. However, work with zeolite powders showed that the framework structure of the zeolite is destroyed if the material is heated too rapidly. To avoid structural degradation, the thermal profile includes a sequence of four steps in which the temperature of the zeolite is increased to four preselected values and held constant at those temperatures for 16 h each. The four hold temperatures are 150°C (423 K), 200°C (473 K), 350°C (623 K), and 525°C (798 K). This thermal profile was found to effectively dry the zeolite without damaging the crystal structure.

In one of the most critical steps in waste form preparation, dehydrated zeolite and simulated waste salt powders are combined in a high temperature blender to sorb fission products and chlorides into the zeolite crystal framework. It is desirable to place all of the salt within the zeolite structure prior to consolidation because free chloride is expected to be leached rapidly and may affect the structure of the glass. The following quality assurance technique has been developed to evaluate the effectiveness of blending the two powders: the blended zeolite is washed with deionized water for one minute, then the wash water is analyzed for chloride content. Any salt in the wash water is considered "free salt" that was not sorbed by the zeolite. Free salt levels of approximately 0.05 wt% of total sample are commonly achieved with a heating profile that incorporates a 20-h soak at 500°C (773 K) and rapid heating and cooling rates (20°C/min on average). This free salt level represents an order of magnitude improvement over the past year.

The composition of the salt used in nearly all samples tested this year is shown in Table V-3. The minor constituents are added to molten LiCl-KCl eutectic salt at 500°C (773 K). Before testing, the molten salt is then quenched, crushed, and ground to particle sizes less than 50 μm. All handling/processing of this salt is done in either purified helium or argon gloveboxes to ensure that it does not absorb unacceptable levels of moisture.

Table V-3. Nominal Composition of Simulated Waste Salt

Compound	Weight Percent
LiCl-KCl-eut.	89.3
CsCl	2.3
$BaCl_2$	1.0
$SrCl_2$	0.4
$CeCl_3$	2.0
$LaCl_3$	0.6
$NdCl_3$	3.2
$PrCl_3$	0.8
YCl_3	0.1
KI	0.3

Blended zeolites are made at various levels of salt loading, expressed as the number, n, of chloride ions per nominal unit cell of zeolite ($M_{12}Al_{12}Si_{12}O_{48}$•nMCl). Salt loadings which have been investigated include n = 3.2, 4.0, 7.5, 9.5, and 10.0 chloride ions per nominal unit cell (Cl^-/u.c.). The 3.2 and 4.0 Cl^-/u.c. loadings are appropriate for making sodalite-glass composites, and the higher loadings are suitable for zeolite-glass composites. The more compact sodalite structure has approximately one-third the chloride-retention capacity of zeolite A.

Glass powders are added to the zeolite at room temperature after the blending operation is complete. Glass and blended zeolite are mixed with a rotating blade mill to combine the powders and break up agglomerates that may exist. Adequate mixing is achieved in less than 5 min of milling. The hydrophilic nature of blended zeolite necessitates conducting the milling/mixing operation in a purified argon atmosphere.

All of the glass powders under investigation as potential binders are commercially available from either Bayer Corp. (Baltimore, MD) or Corning Inc. (Corning, NY). The glass compositions studied are listed in Table V-4.

In the HIP process, the mixture of glass and blended zeolite (or pre-converted sodalite, as described below) powders is loaded into Type 304 stainless steel canisters. These canisters serve as dies for forming the composite ceramics and also provide an outer containment for the waste form. The powders are pressed into the canisters by use of a uniaxial cold press in thin layers; this step produces an unsintered bulk density of approximately 65% solids. Lower unsintered densities result in nonuniform products, which contain relatively large amounts of open porosity in the final composite. The loaded canisters are heated and evacuated to remove air and moisture, then sealed and hot pressed.

Table V-4. Glass Compositions Studied in HIP Processing of Ceramic Waste Forms

Glass ID[a]	Oxide Type and Nominal Content (wt%, major constituents)										
	Al	B	Ca	K	Li	Mg	Na	Si	Sr	Zn	Pb
D	—[b]	23.3	20.0	—	—	—	10.4	46.3	—	—	—
E	6.8	19.1	—	0.5	—	—	7.1	66.5	—	—	—
B	9.7	13.9	13.5	0.8	—	0.4	6.6	55.0	0.1	—	—
C	8.0	9.0	7.1	1.1	1.7	3.3	2.2	59.1	8.5	—	—
A	6.0	9.7	11.2	1.0	—	—	3.0	61.0	8.1	—	—
MCH	9.1	18.9	12.7	0.8	—	0.4	6.1	51.8	0.1	—	—
c10	1.0	—	—	6.0	—	—	8.0	63.0	—	—	22.0
c80	1.0	—	5.0	—	—	4.0	17.0	73.0	—	—	—
c120	2.0	—	—	9.0	—	—	4.0	56.0	—	—	29.0
c211	2.0	9.0	—	7.0	—	—	7.0	65.0	—	7.0	—
c1990	—	—	—	12.0	2.0	—	5.0	41.0	—	—	40.0
c2473	1.0	—	—	—	—	—	16.0	67.0	—	12.0	—
c7056	3.0	18.0	—	9.0	1.0	—	1.0	68.0	—	—	—
c7720	1.0	15.0	—	—	—	—	4.0	74.0	—	—	6.0
c7800	6.0	11.0	1.0	1.0	—	—	7.0	72.0	—	—	—
c9025	4.0	12.0	—	6.0	3.0	—	5.0	68.0	—	—	—

[a]Glasses A through E are from Bayer; MCH is an in-house composition derived from glass B; all others are from Corning.
[b]Hyphen indicates element not present.

In this past year, we have developed leach-resistant and rugged composite ceramics from both zeolite-glass and sodalite-glass mixtures. Consolidation of the zeolite composites requires a careful thermal treatment process because zeolite A will convert to sodalite (or other phases) if held too long at temperatures above 600°C (873 K). The zeolite structure is capable of accommodating approximately three times more waste salt than the sodalite structure; if the simulated waste salt loading is >4.0 Cl^-/u.c., the zeolite structure must be maintained during pressing to prevent the release of salt. The zeolite A structure was retained during pressing when the "two-step" thermal profile shown in Fig. V-9 (first step from 0 to 0.75 h, second step from 0.75 to ~2 h, then cooling) was employed. This HIP cycle yields greatly improved bulk density for zeolite-glass composites, which enhances the leach resistance and structural integrity of the composite ceramics.

Because the sodalite structure is much more thermally robust than zeolite A, the maximum pressing temperature for sodalite composites is higher, and simpler thermal and pressure profiles can be employed. Development of a sodalite composite has led to the addition

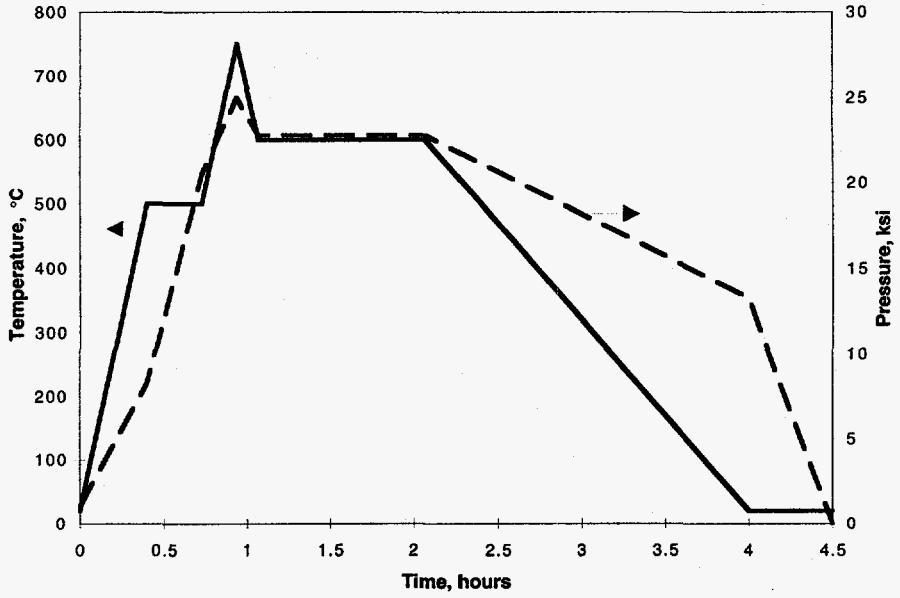

Fig. V-9. Hot Isostatic Pressing Cycle Used for Waste Forms of Zeolite-Glass Ceramic

of a separate thermal step prior to the HIP cycle. Blended zeolite with a chloride loading of less than 4 Cl^-/u.c. is converted to sodalite by heating to >700°C (973 K). In initial HIP experiments, this conversion was done *in situ*; however, this consistently yielded sodalite-glass composites with significant levels of free salt detectable by X-ray diffraction. When the zeolite was heated to >700°C (973 K) to cause the transformation to occur prior to the HIP step, "phase pure" (to X-ray diffraction) sodalite-glass composites were produced. This pre-HIP conversion has resulted in a marked increase in leach resistance. Composites made with pre-converted sodalite release less than 15% of the amount of cesium released by sodalite composites converted *in situ*.

Before more extensive testing of the final product, the post-HIP samples are put through four rapid screening tests to determine HIP conditions that provide good ceramics. First, X-ray diffraction is used to detect any new phases that may have been formed during the HIP process. Second, sample density is determined by Archimedes method, in which 1-octanol is used as the displaced fluid. Third, in conjunction with the density measurement, porosity is determined by intrusion of the 1-octanol into the ceramic. Finally, standard leach tests (MCC-1) are used to measure the leach resistance of the ceramic. In these tests, the ceramic is placed in a sealed Teflon vessel containing deionized water and heated for three days at 90°C (363 K). Ion-specific electrode analysis of chloride content in the leachate and measurement of mass lost by the ceramic pellet give rapid turnaround times. Superior samples are submitted for longer-term testing and more extensive analysis. Because it tends to be the most weakly held fission product, cesium is also used as a marker for the leach resistance of the waste forms.

Of the glasses listed in Table V-4, four (E, B, c7056, and c7800) yielded ceramic composites with superior leach resistance in the 3-day MCC-1 tests. The compositions of these four glasses are fairly similar. In the case of zeolite-glass composites, the type of zeolite used in

blending, whether of the Na or Ca/Na type, does not appear to strongly affect leach resistance. Retention of cesium is similar for all zeolite-glass composites for a particular glass composition. Sodalite-glass composites have been made from only Na-zeolites. The sodalite composites show perhaps slightly improved cesium retention relative to the zeolite-glass composites.

c. Testing and Characterization

Leach tests of 28-day duration have been completed for nine composites, all of which contained 50 wt% glass E. Five of these composites were prepared from Ca/Na-zeolite blended with 7.5 Cl^-/u.c. and four from pre-converted sodalite containing 3.2 Cl^-/u.c. The X-ray diffraction patterns of all these composites were consistent with either a zeolite A or sodalite structure, but not a mixture. The leach tests were conducted at 90°C (363 K) with deionized water as the leachant. The leachates were analyzed for chloride, the matrix elements (Al, Si, and B), and fission products (Cs, Sr, Ba, La, Ce, Nd, Pr, and Y). The results are given in terms of the normalized release rate (NRR):

$$NRR = C_i \bullet V/(f_i \bullet SA \bullet d) \quad (2)$$

where C_i is the concentration of the element in the leachate (g/mL), V is the volume (mL), f_i is the fraction of the element in the solid, SA is the surface area (m^2), and d is the duration of the test in days.

The NRR was less than 1 g/(m^2•d) for all elements in both types of composite, as shown in Table V-5. The NRR for the various elements varied slightly with the crystalline structure. Zeolite-glass composites had lower releases of divalent (Ba and Sr) and trivalent ions (Ce and Nd), whereas sodalite composites had lower releases of cesium. The releases of matrix elements (Al, B, and Si) were similar for both types of composites.

Three leach tests of 56-day duration were also completed. The same trends were present as in the 28-day tests. Also, the NRR decreased with time, indicating that the major fraction of fission products is released in the initial segment of the tests. Additional tests on a larger number of samples are required to fully determine the waste form behavior.

Neutron and X-ray powder diffraction of zeolite waste form composites is being employed for correlating structure features with cation release and phase transformations during processing. To date, the following conclusions have been reached. Zeolite composites tend to exhibit strong long-range cation ordering. Zeolite composites that have relatively high mass fractions of lithium crystallize in a single-phase structure with nearly absolute long-range ordering of cations, largely on the basis of size. On the other hand, mixtures prepared from Na-zeolite A with relatively large retained fractions of sodium are typically two phase: one phase similar to that present in high lithium compositions, the other phase very similar to unreacted Na-zeolite A. A less clear situation pertains when Ca/Na-zeolite A is used as starting material. For these mixtures there appears to be some degree of long-range ordering of cations, but not nearly as marked as the high lithium (Na-zeolite A) compositions.

Table V-5. Normalized Release Rates [g/(m^2•d)] for Composites in 28-Day Leach Tests

	Composite with Ca/Na-Zeolite[a]		Composite with Pre-converted Sodalite[b]	
	Avg.	Stand. Dev.	Avg.	Stand. Dev.
Al	0.23	0.02	0.25	0.03
Ba	0.01	0.01	0.07	0.03
B	0.26	0.24[c]	0.19	0.03
Ce	0.02	0.01	0.05	0.01
Cs	0.52	0.08	0.14	0.05
Nd	0.02	0.01	0.08	0.02
Si	0.18	0.04	0.19	0.03
Sr	0.06	0.05	0.61	0.14
Cl	0.65	0.26	0.40	0.06

[a]Five composites made from standard glass-bonded Ca/Na-zeolite A with 7.5 Cl^-/u.c.
[b]Four composites made from pre-converted sodalite with 3.2 Cl^-/u.c.
[c]One of the composites had an anomalously high release rate for boron.

Equipment has been designed, assembled, and tested for fabricating a plutonium-containing ceramic waste form. The new equipment included a 16-blade stirrer for blending small quantities of plutonium-containing salt and zeolite, along with a uniaxial press for use in the furnace well of a glovebox. Tests showed that chloride ion was incorporated into the zeolite as well with the new stirrer as it was with the conventional tumbling blender. Leach test results of composites pressed with the new uniaxial press are comparable to those pressed with the conventional hot uniaxial press. Plutonium-containing samples will be tested to determine the effect of actinides on the performance of the ceramic waste forms.

d. Future Work

Future development of the ceramic waste form will focus on the development of the phases present in the composite material for isolation and immobilization of the TRU and fission product elements; additives will be evaluated to see if major improvements can be readily made. At the same time, some optimization of the waste form materials and fabrication processes will be carried out with a view to producing products as good as, or slightly better than, the present waste forms in a more economical manner. Fabrication will be extended to include column material containing higher concentrations of fission products and an additional binder phase. New test methods are being developed to accelerate the leaching process, to examine the role the different phases play in waste form properties, and to determine the structure of the various phases in the waste form at a fundamental level. A more extensive long-term characterization and testing program is being implemented; these latter two activities are in support of future waste form qualification.

VI

Treatment of Spent Oxide Fuel

Many different types of spent nuclear fuels are now in storage at several Department of Energy sites. Some of these spent fuels cannot be placed directly in a geological repository, without treatment, because of their chemical reactivity, the presence of hazardous materials, or difficulty of characterization. Electrometallurgical treatment of these spent fuels would convert this large variety of fuel types into well-characterized waste forms, and it would remove the difficulties associated with chemical reactivity and hazardous materials. An additional benefit would be separation of the uranium to a low-level waste stream, thus greatly reducing the volume of material destined for a geological repository.

The electrometallurgical treatment of spent oxide fuels requires that the oxides first be reduced to metals that can be processed in an electrorefiner. A lithium reduction process has been selected to convert the spent oxide fuels into metals.[1] In this process, the spent oxide fuel is reduced by reaction with lithium at 650°C in the presence of molten LiCl. The Li_2O formed during the reduction process is soluble in the salt. The spent salt and lithium are recycled after the Li_2O is electrochemically reduced. The oxygen is liberated as a gas at an inert anode. The reduced metal components of the spent fuel are separated from the LiCl salt and introduced into an electrorefiner. The electrorefining step separates the uranium into a pure product. The uranium product may be enriched for recycle or converted to a suitable form for storage or disposal as low-level waste. The TRU elements can be converted, with the fission products, into a ceramic waste form suitable for geological disposal.

The feasibility of all the steps of the process has been confirmed in small-scale experiments (below 0.5-kg simulated spent fuel). Recent work has concentrated on understanding and improving the chemistry of the lithium reduction process, improving the design of electrodes used for electrowinning lithium oxide, and testing these improvements in engineering-scale experiments using up to 10 kg of simulated fuel.

---

[1] J. J. Laidler et al., *Chemical Technology Division Annual Technical Report, 1994*, Argonne National Laboratory Report ANL-95/24, pp. 101-102 (1995).

A. Process Chemistry

Laboratory-scale experiments have been conducted to investigate the following issues in the lithium reduction process: (1) reduction times for different fuel types, fuel configurations, and basket designs, (2) behavior of zirconium compounds formed in the reduction vessel, (3) amount of occluded salt in the reduction product and the Li_2O concentration of that occluded salt, and (4) interaction of rare-earth oxides with the reduction salt. As part of this work, the reduction process is being evaluated for its application to fuel debris from the accident involving the Three Mile Island-2 (TMI-2) reactor.

1. Reduction Times

Several reduction experiments were done with clad and unclad UO_2 pellets (unirradiated) at 650°C to determine the reduction rates. Stainless-steel-clad fuel pins, 0.95 cm in diameter, were cut into sections, 0.63 cm and 1.27 cm in length, and reduced. Individual sections were periodically taken out of the reduction vessel, sectioned longitudinally, polished, and examined under an optical microscope to determine the extent of reduction. The Li_2O concentrations in the salt were also measured to track the extent of reduction.

Metallographic examination of the cross sections from the 1.27-cm pellets after 10, 30, and 50 h revealed that approximately 50-60 h is required for complete reduction of clad pellets when one end of the pellet is capped. The reduction proceeded mainly from the open end, although some reduction occurred radially inward from the cladding/pellet interface. With both ends open, the 1.27-cm pellets were only partially reduced after 30 h and completely reduced in 50 h. In the case of the 0.63-cm pellets, reduction was complete in 30 h. The completely reduced pellets contained a characteristically interconnected void structure in the cross-sectional view. From these experiments, it is apparent that the reduction time is a strong function of the fuel size.

Tests were also conducted with unclad pellets, 0.79 cm in diameter and 1.27 cm in length. These pellets were easily reduced in 30 h because their reduction can proceed radially inward and longitudinally from the ends. From the reduction standpoint, this is analogous to the reduction of 0.63-cm clad pellets with both ends open. Future experiments will focus on determining the optimum size of fuel and the loading characteristics of the fuel (e.g., basket design).

2. Formation of Li_2ZrO_3

Reactor safety programs in other ANL divisions have studied core melting accidents, and they have produced a synthetic molten-core material, which has been dubbed "corium." Synthetic corium is a mixture of predominantly UO_2 and ZrO_2 produced by the thermite reaction of U, Zr, Fe_2O_3, and Cr_2O_3. The nominal composition of the corium is 58 wt% UO_2, 11 wt% ZrO_2, 14 wt% Zr, 14 wt% Fe, and 3 wt% Cr. Corium was selected to represent the ceramic phase, $(U,Zr)O_2$, present in the TMI-2 debris. Laboratory-scale reductions of corium were done with lithium in LiCl at 650°C to determine the extent of reduction and understand the process

chemistry. The results were used as a basis for performing the same reductions on an engineering scale (see Sec. VI.C).

For the laboratory-scale reductions, the corium particles were sieved through a 40-mesh screen, and only the particles larger than 40 mesh were used. The largest particle size was approximately 1 cm. Reduction of the screened corium particles was done by stirring the molten salt with the particles contained in a screened basket. Periodically, salt samples were drawn from the melt and analyzed for their Li_2O concentration to track the extent of reduction. In the first experiment, the Li_2O concentration of the salt reached a plateau value of 1.45 wt% in about 24 h, while complete reduction would have resulted in a Li_2O concentration of 2.5 wt%. This suggested the formation of a mixed-oxide compound (Li_2O-ZrO_2). This hypothesis was confirmed by the X-ray diffraction (XRD) pattern of the reduced product, which showed the presence of both uranium and Li_2ZrO_3. Further calculations showed that Li_2ZrO_3 formation is thermodynamically favored if the Li_2O concentration exceeds 1.30-1.45 wt% in the reduction salt, according to the following reaction equilibrium:

$$4Li_{(salt)} + Li_2ZrO_{3(c)} = 3Li_2O_{(salt)} + Zr_{(c)} \quad (1)$$

To verify the above calculations, an additional experiment was performed where fine ZrO_2 particles were reduced with lithium in LiCl at 650°C. In this experiment, the concentration of the Li_2O formed during reduction was limited to 1 wt%. The results indicated that all the ZrO_2 was reduced to zirconium. There was no evidence of Li_2ZrO_3 formation. A similar experiment was performed with corium, where the Li_2O concentration in the reduction salt was limited to 1 wt% to determine if complete reduction was achieved. In this case, the XRD pattern of the reduced product did contain the Li_2ZrO_3 peaks, in addition to the metallic peaks. The amount of Li_2ZrO_3 formed in this experiment may have been marginally less than the amount formed in an earlier experiment where the Li_2O concentration in the reduction salt was 1.45 wt%.

The differences in the reduction behavior of fine ZrO_2 particles and corium may be attributable to the differences in particle size and loading of the reactants. Good mixing was achieved with fine ZrO_2 particles because they were directly stirred along with the salt. In contrast, the packed bed of corium particles in the basket developed local concentration gradients, leading to the formation of Li_2ZrO_3. However, formation of Li_2ZrO_3 in corium is likely to be limited to localized regions of low fluid flow when the Li_2O concentration in the bulk salt is maintained at 1 wt%. Further experiments will be done to investigate the effect of bulk stirring on fluid flow under various process conditions (e.g., different fuel particle size and basket configurations).

3. *Occluded Salt in Reduced Metal*

In another set of experiments, the amount of salt occluded in the reduced metal and the Li_2O concentration in that occluded salt were determined. These results allowed us to estimate the extent of UCl_3 losses expected in the electrorefiner as a consequence of salt carryover from the reduction vessel and the effect of occluded salt on a partial reduction product of PuO_2 in the fuel (i.e., Pu_2O_3).

The reduced metal contains some occluded salt. In addition, the occluded salt may contain a higher concentration of Li_2O than the bulk salt because the counter-diffusion of Li_2O out of fuel pellets is much slower than the diffusion of lithium into the pellets during the reduction process. High concentrations of Li_2O in occluded salt can lead to incomplete reduction of Pu_2O_3 in the interior of the fuel pellets at 650°C if the Li_2O concentration exceeds 3.5 wt%. The presence of Li_2O in the reduced metal also leads to losses in the electrorefiner, where UCl_3 is converted to UO_2 as follows:

$$UCl_{3(salt)} + 2Li_2O_{(salt)} = UO_{2(c)} + 3LiCl_{(salt)} + Li_{(salt)} \quad (2)$$

It may, therefore, be necessary to wash the reduced metal in pure LiCl to reduce the concentration of Li_2O in the occluded salt. Experiments were designed to determine the amount of occluded salt, its Li_2O concentration, and the effectiveness of a wash step.

In one experiment, UO_2 pellets (without cladding), 0.79 cm in diameter and 1.43 cm in length, were placed in a 60-mesh basket and reduced with lithium in LiCl for 48 h at 650°C. After the reduction was complete, the salt was drained from the reduced metal, and the occluded salt in the reduced metal was calculated by measuring the mass of the reduced product. The product was then ground to fine pieces and soaked in pure LiCl at 650°C for 6 h (salt wash step) to extract the Li_2O from the occluded salt and determine its concentration. In another experiment, a similar procedure was followed with the exception that the reduced metal was not ground before being washed in pure LiCl. This was designed to provide information on the effectiveness of the salt wash step if the reduced metal were washed with pure LiCl without grinding.

In the experiments with UO_2 pellets, the amount of entrained salt varied between 8 and 11% by mass of reduced metal. In similar experiments with corium particles, the amount of entrained salt was measured to be about 20% by mass of the product. Therefore, the total amount of entrained salt strongly depends on the size and morphology of the reduction product. The size and morphology of the reduction product, in turn, depend on the size and morphology of the incoming fuel. In the experiments with UO_2 pellets, a large fraction of the entrained salt was occluded. The occluded salt in these pellets was found to be saturated in Li_2O (~8.7 wt%), while the Li_2O concentration in the bulk salt was only 2.5 wt%. The salt wash was only partially effective in removing the Li_2O from the occluded salt when the reduced product was not ground. Hence, the effectiveness of the salt wash step depends on the size and morphology of the reduced metal particles. Future experiments will investigate the effect of particle size and cladding on the buildup of Li_2O in occluded salt. This will provide information on the optimum particle size and fuel characteristics for achieving the desired reduction product and Li_2O distribution.

4. Rare Earth Interactions

Laboratory-scale experiments are underway to study the chemistry of rare earth oxides in the reduction salt. The prior experiments[2] with rare earth fission products, done in the presence

[2] J. J. Laidler et al., *Chemical Technology Division Annual Technical Report, 1995*, Argonne National Laboratory Report ANL-96/10, pp. 103-104 (1996).

of excess lithium in the reduction salt, proved that soluble mixed oxides of rare earths (Ce, Nd, Eu, Sm, etc.) are formed during the lithium reduction of spent oxide fuel, and these oxides account for the observed presence of rare earths in the reduction salt. During this past year, similar experiments were conducted without excess lithium, and this led to an even better understanding of the behavior of rare earth oxides in LiCl.

The experimental results indicated that the absence of excess lithium does not affect the total amount of neodymium in the salt phase, but it does reduce the total amount of cerium in the salt phase. This is because the Ce-O system is characterized by multiple oxide phases, and the stable oxide phase in equilibrium with the salt phase is determined by the oxygen potential established in the melt. In the presence of excess lithium, the Li-Li_2O couple controls the oxygen potential, and Ce_2O_3 is the stable phase. In the absence of lithium, cerium oxides richer in oxygen than Ce_2O_3 (CeO_x with x greater than 1.5) coexist with Ce_2O_3 and, consequently, reduce the activity of Ce_2O_3 and hence the concentration of cerium-bearing species in the salt, according to the following reaction equilibria:

$$CeO_{x(c)} + Li_2O_{(salt)} = LiCeO_{2(salt)} + O_{2(g)} \quad (3)$$

$$CeO_{x(c)} + Li_2O_{(salt)} = Li_3CeO_{3(salt)} + O_{2(g)} \quad (4)$$

Future experiments will focus on the mutual interactions of the rare earths in the salt phase and the effect of these interactions on the concentrations of rare earths in the salt phase.

B. Electrowinning Development

An economic and environmentally acceptable process for the reduction of oxide fuels to metals involves two separate steps: (1) the chemical reduction of the fuel, with the concomitant production of lithium oxide, and (2) the electrochemical regeneration of the spent salt by the reduction of the lithium oxide to produce lithium metal reductant. The latter process is the subject of this work.

The CMT Division has done many tests of lithium oxide electrolysis on a laboratory scale (~0.1 L of molten salt) and two experiments on an engineering scale (~50 L of salt). A very wide range of geometries and materials was involved in these tests, but one common factor in all tests was the use of porous and/or dense ceramics. These ceramic components were used as either shrouds to direct the flow of oxygen and lithium or as containers to hold liquid metals (Li and Li-Bi).

Natural convection can play an important role in the performance of an electrowinning cell. Since natural convection is difficult to predict on scaleup, it is evident that the results from the small cells used in the laboratory experiments are not universally applicable for development of large cells. This difficulty was addressed by the completion of a Large Laboratory Scale (LLS) cell facility. In this facility, it is now possible to test cells that are half the radial dimensions of

the engineering-scale cells. This allows not only more representative convection conditions but also more typical electrode arrangements.

One of the primary problems encountered in this development effort has involved the recombination of the lithium and oxygen in the electrowinning cell to produce Li_2O. This parasitic reaction has been, in some tests, so efficient as to leave no net lithium production. During this period, work has been focused on the development of two types of cathodes, liquid bismuth and porous metal, both of which effectively eliminate this problem. Experiments are also in progress to find an alternative to the present platinum anode.

1. Bismuth Cathodes

Thirteen laboratory-scale experiments were conducted to gain experience with various cell configurations and to verify the basic theory and usefulness of molten bismuth cathodes for the collection of lithium during electrowinning. By forming intermetallic compounds, the bismuth cathode is able to reduce the chemical activity of lithium in the LiCl salt by factors of 1,000 to 100,000. This reduced activity significantly enhances the lifetime of lithium-sensitive anode materials for the electrowinning cell. In addition, the use of the heavy metal, bismuth (density = 9.56 g/cm^3), allows the lithium (density = 0.43 g/cm^3) to form an intermetallic compound that is heavier than the LiCl salt (density = 1.48 g/cm^3). The intermetallic can be collected in an environment protected to various degrees (depending on the electrowinning cell construction) from the oxygen bubbles given off and present near the anode. (See Figs. VI-1a and -1b for two typical laboratory cell designs.) This protection from the oxygen retards the major

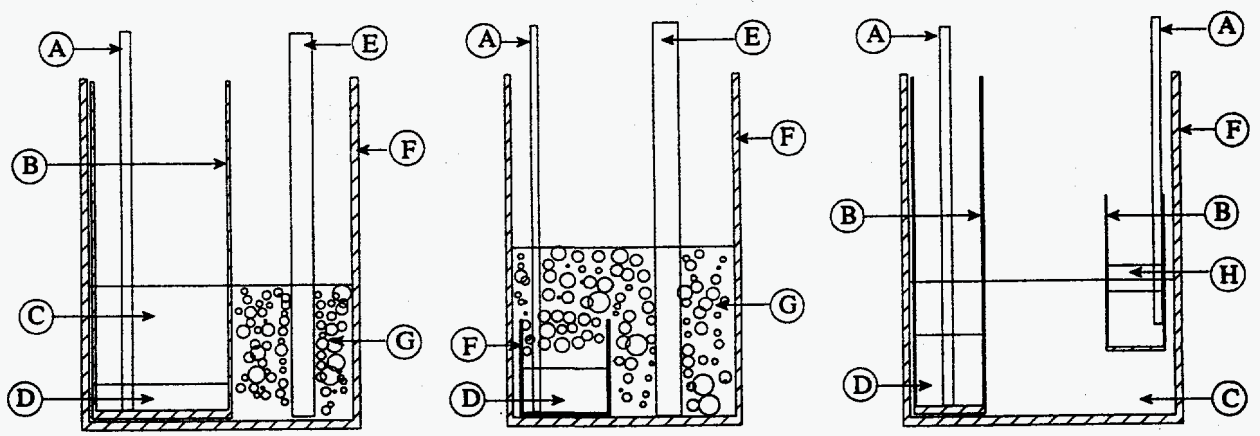

Fig. VI-1. Designs of Electrowinning Cell for Laboratory-Scale Tests

chemical shorting reaction, which can significantly reduce the efficiency of the electrowinning process:

$$4\,Li + O_2 = 2Li_2O \quad (5)$$

One of the major disadvantages of introducing a molten metal cathode such as bismuth into the electrowinning process is the addition of the necessary extra step to remove and collect the lithium from the bismuth pool so that it can be transported and used in the reduction process. (Figure VI-1c shows a laboratory cell design that collects the lithium by use of a second porous crucible.) Another disadvantage is the requirement in some cell designs that ceramic insulators be used below the salt level. These ceramics may be porous or have high density but do not have the structural strength and durability to provide confidence for long-term operation in engineering-scale or larger tests. Furthermore, manufacturing size restrictions of the ceramic components may require the use of multiple electrodes on process scaleup rather than being able to take advantage of economies of scale.

The laboratory-scale experiments were based on variations of two conceptual designs, and most were run in two steps: (1) collection of lithium in the bismuth pool cathode from the electrowinning of lithium oxide and (2) the electrotransport of the lithium from the bismuth pool to form free lithium on the LiCl salt surface. The two concepts differ in the container used for the bismuth pool. One concept uses a high-density magnesia crucible that has either holes above the bismuth level or the top cut off to allow the salt to exchange freely between the anode and cathode regions (Fig.VI-1b). In the other concept, porous magnesia crucibles (70 to 85% dense) are used to contain the bismuth (Fig.VI-1a). The porous barrier allows migration of the salt ions but does not allow oxygen gas bubbles or the bismuth to cross the porous barrier.

The results of the experiments indicated that the use of a bismuth cathode, in general, would protect lithium-sensitive anode materials from lithium attack and may be scalable to larger experiments. However, protecting the anode materials from lithium attack during the electrotransport step still requires that the lithium-sensitive materials be removed from the LiCl salt. The experimental results also indicated that the penalty for adding an additional step to the process may not be too great in that the electrotransport step may require only about 10% additional time compared to the electrowinning step. The added electrotransport step may also provide a convenient quantitative measure of the amount of lithium produced during the electrowinning step. Without the electrotransport step, it may be difficult to assure that the amount of lithium produced is sufficient for the next reduction step.

Five cells with liquid bismuth cathodes were also run in the LLS facility. These cells generally functioned well as long as both the Li-Bi and Li were totally contained in porous magnesia containers. When the containers were open to the salt, the bismuth became dispersed in the salt, apparently as very fine particulate Li-Bi alloy. It appeared that the magnesia was significantly attacked by lithium. The crucibles were dark gray to black through their cross sections, presumably due to partial reduction of the magnesia. Future plans include the procurement and testing of porous yttria or beryllia crucibles as containers for the bismuth because these oxides are thermodynamically more stable than magnesia.

2. Porous Metal Cathodes

The Li-Bi thermodynamic data that were used as a foundation for the choice of bismuth as the cathode were generated at ANL in the 1960s by transporting lithium between a porous stainless steel electrode and a bismuth electrode. It seemed evident that the same type of porous stainless steel cathode could be used directly in the lithia reduction cell instead of depositing lithium in the bismuth. Lithium wets the porous stainless steel cathode and is incorporated into the pores below the salt level. Hence, the lithium does not float to the surface and recombine with oxygen. This type of cathode also eliminates the need for ceramic liners or crucibles.

Three porous cathode designs have been used to date. The first design used stacked discs of screen (40 and 16 mesh). This cathode produced lithium, but this lithium was not homogeneously distributed within the structure because of the mix of small and large pores. A second type of cathode was fabricated by wrapping 40-mesh screen on a steel rod. This electrode exhibited a generally uniform-appearing deposit of lithium, as would be expected from the relatively uniform small pore size. Finally, a cathode was fabricated by making a cylindrical container of 16-mesh screen and packing it with small rings of fine stainless steel wire. The pore distribution of this electrode was undefined, but after cell operation it was totally filled with lithium (determined by cutting the electrode open).

A foam metal material is more appropriate for the cathode than the screen because it has a greater open porosity and a more uniform pore size. The first foam metal obtained for the cathode application (purchased from Astro-Met Inc.) has a nominal pore size of 150-200 μm and has a total porosity of approximately 95%. By comparison, the screen cathodes typically have about 60% porosity and a much less uniform pore distribution. Calculations given later indicate that this foam material will permit electrodes to retain all lithium metal for heights exceeding 0.5 m.

At the outset of the testing with porous cathodes, it was anticipated that the mechanism of lithium incorporation into the electrode would be to first deposit lithium on the outer surface, followed by transport of this lithium to the interior of the cathode by either surface migration or by capillarity. New experimental evidence indicates that the process may be different under some conditions. In particular, when a cell is shut off after a few ampere-hours current, the cathode has no visible lithium metal on the outer surface, but it does have lithium inside. The salt that drains from this cathode has dissolved lithium metal. The fact that the salt inside the cathode has significant lithium metal in solution without lithium metal being present on the cathode surface implies a reaction that is limited by the surface reaction kinetics. It may be due to the initial oxide layer on the cathode and will change once the oxide surface layer has been reduced. While further experiments will be necessary, the observed phenomena may be significant for new cathode startup.

These tests have forced a revision to a commonly assumed characteristic of an operating cell. It had been believed that when lithium metal is present in the cathode, the entire salt bath will be at unit activity of lithium. However, the CMT experiments indicate that the bulk of the salt is essentially devoid of lithium metal until the external potential is removed. This has been

demonstrated by analysis of salt samples for lithium metal and for combined lithium metal plus lithium oxide. Without the external potential, the lithium begins to dissolve and brings the lithium activity of the bulk salt to unity. This phenomenon has been qualitatively observed, but the kinetics of the process have not been measured.

Containment of lithium in the porous cathode is a concern for large electrolysis cells. The driving force for the removal of lithium when the cathode is lifted from the salt is gravity; when the cathode is submerged in the salt, the driving force is buoyancy. Since the density of the salt is about 1.5 g/cm^3, and that of lithium metal is about 0.5 g/cm^3, the driving force to "float" the lithium out of a submerged cathode is twice that to cause it to drain when removed from the salt. Surface tension causes the cathode to retain lithium. A force balance for a pore at the surface of the cathode yields the pressure, P, required to remove lithium,

$$P = 4\gamma_{Li}/D \tag{6}$$

where γ_{Li} is the surface tension of lithium, and D is the pore diameter. This is equated to the pressure generated by buoyancy,

$$P = (\rho_{LiCl} - \rho_{Li})\, g \cdot h \tag{7}$$

where g is the acceleration of gravity, h is the cathode height, and ρ_i is the density of the species identified in the subscript. The maximum height for a cathode is thus given by

$$h = 4\gamma_{Li}/D(\rho_{LiCl} - \rho_{Li})\, g \tag{8}$$

Substituting measured values for the surface tension and densities in Eq. 8 and assuming D = 200 μm yield h = 0.66 m. Clearly, the height for a cathode that will retain lithium is reasonable. Consequently, the cathode may be removed from the electrowinning vessel and transferred to the reduction vessel with no lithium loss. This provides not only an easy transfer method but also a method whereby the salt in the reduction vessel may be saturated with lithium while the lithium metal is completely contained. However, if it becomes desirable to extract some lithium from the cathode (e.g., to increase the speed of the reduction process), this step may be done in a controlled manner by electrotransporting the lithium to the vessel wall, fuel basket, etc. Engineering-scale tests of the porous cathode concept are planned.

3. Ceramic Anodes

In addition to the improved understanding of cell operation and the advances in cathode development, progress has been made on anodes. The platinum anode is not only expensive but is very rapidly attacked by lithium. No stable metals exist in the anode environment, and substitutes must be in the form of oxides because of the release of oxygen on the surface. Candidate materials must be either thermodynamically stable or kinetically stable. To date, the only thermodynamically stable material indicated by experiment is magnetite (Fe_3O_4); its

stability was inferred from postmortem examination of small-scale cells. Other oxides that appear promising are antimony-doped tin oxide and lithium-doped nickel oxide.

Use of ceramics for the anode faces two problems: (1) economic fabrication of long slender rods and (2) handling of long slender rods to avoid breakage from mechanical and thermal shock. These problems may have been solved by a novel application of technology developed by thermocouple fabricators. Powder is packed into a metal tube, and the tube is swaged down on the powder to a packed density as high as 99% of theoretical. It is then possible to fire the powder-in-tube configuration to obtain sintering. The anode is then a metal-sheathed ceramic rod and may be handled, transported, and stored with little concern for breakage. The metal will be consumed by the process during operation. Power leads may be clamped or welded to the sheath, and the high-surface-area interface between the ceramic and tube will minimize the voltage drop at the metal/ceramic interface.

The mechanical properties of the ceramic have been improved by the use of "crack-arrestors," shards of inert ceramic that are homogeneously dispersed in the anode structure. These act to block or divert the propagation of cracks within the ceramic body. In one test, 20 vol% of MgO shard in NiO yielded a ceramic piece that survived repeated removal from an 800°C furnace and quenching immediately under water. The combination of crack arrestors and the new fabrication method should yield a useful anode structure.

C. Engineering-Scale Experiments

The purpose of the engineering-scale experiments is to obtain design information and operating experience needed for scaling up the reduction and electrowinning processes to plant sizes required for processing DOE spent oxide fuels. To meet this objective, the facility used for these experiments was designed to support the reduction of kilogram quantities of fuel. The engineering-scale facility consists of three major components: the reduction vessel, the electrochemical vessel, and the casting station. The reduction vessel holds the salt, fuel, and lithium during the reduction step; the electrochemical vessel holds the molten salt during the electrowinning stage; and the casting station provides a means to cast the salt into ingots for storage between process steps. The molten salt and lithium are transferred among these three components through heated transfer lines. All of the equipment is enclosed in a large (7.6 x 2.4 x 2.6 m) argon atmosphere glovebox; the facility is qualified to handle limited quantities of plutonium and other transuranics. Figure VI-2 is a cutaway view of the engineering-scale equipment.

The first engineering-scale demonstration of the reduction of simulated TMI-2 fuel debris (designated ES-3) was completed in September 1996. The ES-3 experiment had three principal goals: (1) to investigate the reduction of synthetic corium, representing material from the melted central region of the TMI-2 core, (2) to investigate the reduction of clad fuel rod segments, representing material from undamaged and partially damaged regions of the TMI-2 core, and (3) to test a new fuel basket assembly prototypical of one designed for use in the future electrorefiners. The two reductions were carried out in series, starting with the reduction of

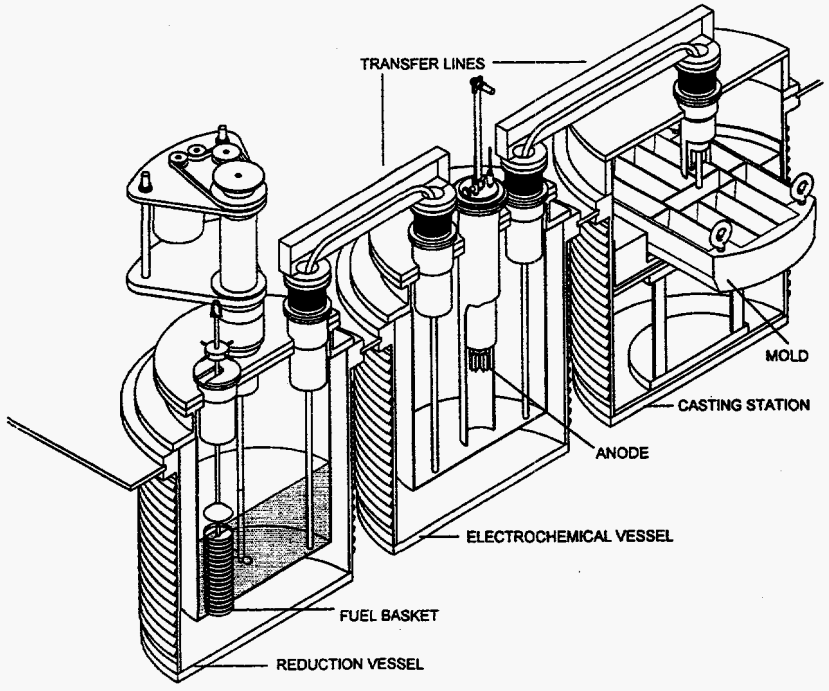

Fig. VI-2. Cutaway View of Components in Engineering-Scale Facility

corium followed by the reduction of the fuel rod segments. After both reductions were completed, the salt was cast into ingots for storage until required for the next experiment.

The first reduction step, that of material simulating debris from the central melt region of the core, was carried out for 30 h. Four kilograms of synthetic corium, consisting primarily of a $(U,Zr)O_2$ matrix, was reduced in a vessel containing 0.4 kg lithium in 77 kg of LiCl. The corium was contained in a newly designed fuel basket assembly consisting of a rigid outer basket containing an inner fuel pouch. This inner pouch (4.5 x 7.6 x 41 cm) was made of 40-mesh stainless steel screen and was designed to be removed from the fuel basket after the reduction. It was also designed such that it could be easily separated from the solidified salt and reduced metal product, simplifying product recovery. Prior to being loaded into the fuel pouch, the corium was passed through a 40-mesh screen, preventing particles smaller than 40 mesh from being placed into the fuel pouch.

The second reduction step, that of fuel rod segments representing material from the peripheral regions of the TMI-2 core, was carried out for 47 h. For this part of the demonstration, 2.5 kg of stainless-steel clad UO_2 fuel rods, cut into 1-cm segments, was reduced with 0.26 kg of lithium in the same 77 kg of LiCl. The fuel rod segments were contained in a fuel basket assembly identical in design to that used to hold the corium.

The extent of the reduction of the corium and fuel rod segments in ES-3 was estimated by qualitative and quantitative techniques. The rate of change and absolute value of the Li_2O concentration in the bulk salt were used to make a quantitative estimate of the extent of the

reduction for both materials. In addition, selected fuel rod segments were cut or crushed to qualitatively evaluate the extent of the reduction based on the presence of visibly unreduced UO_2. The available data indicate that the reduction of both the corium and fuel rod segments was incomplete. The corium reduction was estimated, with reasonable certainty, as being 80% complete. Estimating the extent of the reduction for the fuel rod segments was complicated by unexpected variations in the Li_2O concentration in bulk salt samples; at most this reduction appears to have been 20% complete.

Although a tear in the fuel pouch containing corium led to the loss of some of the reduced product, the concept of a removable fuel pouch was successfully demonstrated. It was possible to remove the fuel pouch from the fuel basket, allowing the fuel basket to be reused in later experiments, and the reduced product was easily separated from the pouch. Analysis of the pouch tear will be used to modify the design of future pouches. The fuel pouch containing the cut fuel rod segments performed as designed.

Results from ES-3 indicated that the laboratory-scale experiments used in planning ES-3 underestimated the time required to complete the reductions of corium and fuel rod segments. One explanation for this problem is that the laboratory-scale experiments employed fuel basket geometries (cylindrical) that did not accurately reproduce the geometry of the ES-3 fuel pouch (rectangular). Specifically, the transport of lithium to the fuel in the laboratory-scale experiments may have been faster than in ES-3. Additional laboratory-scale experiments concerning the relationship among basket geometry, fuel particle size, and reduction rate are planned in support of the follow-on engineering-scale experiments.

VII

Basic Chemistry Research

Basic chemistry research is being pursued in several areas: fundamental chemistry associated with catalyses in systems that involve molecular energy resources, mechanisms of ion transport in lithium battery electrolytes, materials chemistry of electrified interfaces (in connection with corrosion and electrochemical devices) and molecular sieve materials, and the theory of materials properties.

A. Chemical Sciences Research

In situ spectroscopic and mechanistic techniques are being employed to scrutinize and improve the reaction chemistry of industrially important processes. Recent research encompasses investigation of (1) phosphine-modified catalysts for the hydroformylation of olefins in supercritical fluids, (2) extremely robust polyfluorophthalocyanine catalysts for hydrocarbon activation processes, and (3) lithium-polymer battery materials.

1. Catalytic Chemistry in Supercritical Fluids

Supercritical fluids (CO_2 or water) offer environmentally benign alternatives to toxic organic solvents frequently used in homogeneous catalysis. An additional advantage is the elimination of energy-intensive distillations necessary for product separations and catalyst recovery from organic solvents. Our efforts have focused upon the development of homogeneous cobalt oxo catalyst systems (phosphine-modified and unmodified) in supercritical carbon dioxide.

The oxo process, in which homogeneous catalysts are used for the hydroformylation of olefins, is one of the largest industrial processes used worldwide today. In this process, carbon monoxide and hydrogen react with an olefin to selectively produce the desired linear isomers of aldehydes:

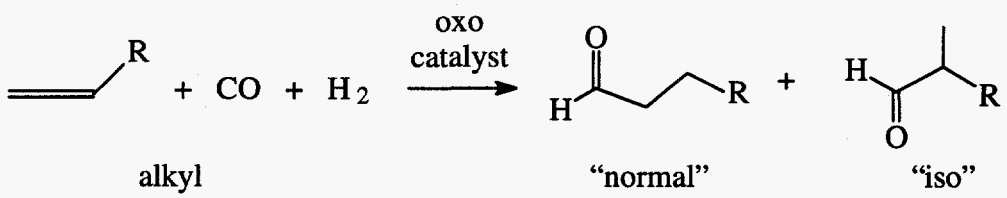

(1)

where R indicates an alkyl group. The linear "normal" isomers in Eq. 1 are desired over the branched "iso" products. Oxo products are used in detergents, plastics, and agricultural chemicals. The capacities of homogeneous oxo processes exceeded 6.6 million tons per year in 1995.[1]

While rhodium catalysts account for most of the C_4 hydroformylation products, oxo reactions producing C_5 and higher products are dominated by cobalt over rhodium catalysts by a ratio of 9 to 1. The primary advantage of cobalt catalysts over rhodium is their better reactivity toward internally branched olefins. The thermal stability of the cobalt catalysts is also desirable as high temperatures are required for separating high-molecular-weight products by distillation. Phosphine-modified cobalt catalysts greatly improve the ratio of normal-to-iso products (versus unmodified) and now account for 0.7 million tons of products per year.

Currently, we are examining phosphine-substituted cobalt carbonyl catalysts in conventional organic solvents and in supercritical carbon dioxide by nuclear magnetic resonance (NMR) spectroscopy.[2,3] Using our toroid NMR detector[4] (see Fig. VII-1), we are able to monitor catalytic reactions *in situ* under the high pressures and temperatures at which the oxo process is commercially operated.

The phosphine-substituted cobalt system has been examined in a variety of solvents. These solvents include cyclohexane, benzene, dioxane, 2-methylpropanol, supercritical carbon dioxide ($scCO_2$), and $scCO_2$/toluene mixtures. The cobalt system examined most extensively by us has been $Co_2(n\text{-}Bu_3P)_2(CO)_6$, a Shell-type catalyst. High-pressure/high-temperature experiments have allowed the observation of precatalytic species involved in hydroformylation. When $Co_2(n\text{-}Bu_3P)_2(CO)_6$ is placed under the conditions of high CO and H_2 pressures, at least two equilibria are observed:

$$\underset{\text{[dimer]}}{Co_2(n\text{-}Bu_3P)_2(CO)_6} + CO \rightleftharpoons \underset{\text{[cation]}}{[Co(n\text{-}Bu_3P)_2(CO)_3]}\underset{\text{[anion]}}{[Co(CO)_4]} \qquad (2)$$

---

[1] M. Beller et al., *J. Mol. Catal. A* **104**, 17-85 (1995).

[2] J. W. Rathke, R. J. Klingler, R. E. Gerald, K. W. Kramarz, and K. Woelk, *Prog. Nucl. Magn. Reson. Spectrosc.*, in press.

[3] K. W. Kramarz, R. J. Klingler, and J. W. Rathke, "*In Situ* NMR Spectroscopy Studies of Hydroformylation Catalysts Using High Pressure Toroid Probes," Abstracts of the Sixth International Conference on the Chemistry of the Platinum Group Metals, University of York, p. 48 (1996).

[4] J. W. Rathke, *J. Magn. Reson.* **85**, 150 (1989).

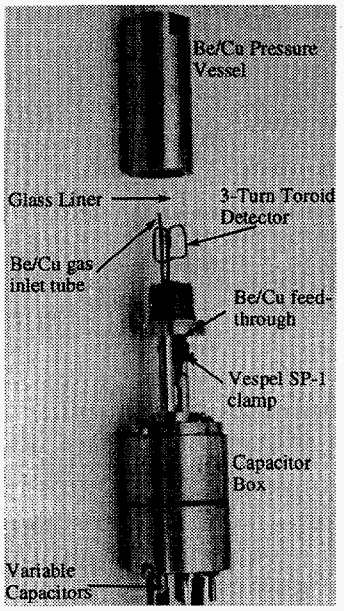

Fig. VII-1.

View of Interior of High-Pressure Toroid NMR Probe

$$Co_2(n\text{-}Bu_3P)_2(CO)_6 + H_2 \rightleftharpoons 2\ HCo(n\text{-}Bu_3P)(CO)_3 \quad (3)$$
[hydride]

In the n-Bu_3P-substituted case, the equilibrium measurements of precatalytic species (dimer and hydride) are complicated by a disproportionation reaction of the dimer to form $[Co(n\text{-}Bu_3P)_2(CO)_3][Co(CO)_4]$, a catalytically "inert" salt. The salt formation shown in Eq. 2 becomes more favorable as solvent polarity increases (cyclohexane < benzene < dioxane < i-butanol). This equilibrium is undesirable, especially in the $scCO_2$/toluene mixtures. The dimer, $Co_2(n\text{-}Bu_3P)_2(CO)_6$, is moderately soluble in $scCO_2$/toluene. However, upon addition of CO, the dimer precipitates out of the fluid, presumably as the salt. In the absence of CO, the hydride is unstable at the temperatures required to form it from the dimer. Experiments are underway to determine if salt formation can be retarded by more electron-withdrawing phosphine ligands.

The ^{31}P NMR spectra in Fig. VII-2 illustrate the temperature dependence (100–175°C) of the equilibria (dioxane solvent) in Eqs. 2 and 3. In these spectra, the hydride is observed to be undergoing a dynamic process at higher temperatures; the ^{31}P resonance for the hydride broadens significantly at higher temperatures relative to the other ^{31}P resonances. Increased CO pressure does not sharpen the resonance, and the broadening is reversible with temperature. This rules out any broadening due to decomposition of the hydride at higher temperatures.

Proton transfer (H^+) between the hydride and the tetracarbonyl anion to form the tetracarbonyl hydride, $HCo(CO)_4$, is an unlikely candidate for the dynamic process as this process is thermodynamically uphill by more than 7 pK_a units. The pK_a of $HCo(n\text{-}Bu_3P)(CO)_3$ has not been reported in the literature; however, we do know that the pK_a of $HCo(CO)_4$ is 0, and the pK_a of the triphenylphosphine hydride analog, $HCo(Ph_3P)(CO)_3$, is 7. The pK_a of $HCo(n\text{-}Bu_3P)(CO)_3$ can thus be approximated as ≈10, given the difference in pK_a's of Ph_3P and

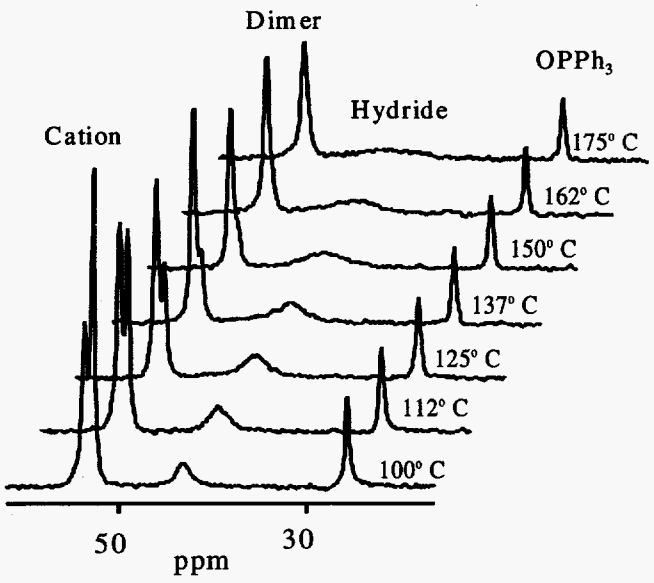

Fig. VII-2.

Series of ^{31}P NMR Spectra of Species Present from Reaction of Shell-Type Catalyst $Co_2(n\text{-}Bu_3P)_2(CO)_6$ as Function of Temperature under High Pressures of CO and H_2 ($OPPh_3$ = triphenylphosphine oxide, an integration standard)

n-Bu_3P and the reported effects of phosphine basicity on transition metal phosphine hydrides.[5,6] Hydride transfer (H^-) to the $[Co(n\text{-}Bu_3P)_2(CO)_3]^+$ can also be ruled out for the dynamic process since the observed line width of the cation's ^{31}P resonance does not broaden as the hydride's does with temperature (Fig. VII-2).

The broadening of the hydride ^{31}P NMR resonance may be due to the lability of the phosphine ligand at higher temperatures. We are examining the exchange reactions of the phosphine ligands by introducing free *n*-Bu_3P into these systems. Other phosphine-substituted dimers [PR_3, where R = $-CH_3$, $-CF_3C_6H_4$, and $-C_6(CF_3)_2H_3$] are under investigation. The exchange of phosphine ligands between $Co_2(n\text{-}Bu_3P)_2(CO)_6$ and $Co_2(Me_3P)_2(CO)_6$ has already been observed to be facile at temperatures below 100°C. Additionally, the presence of a small amount of $\bullet Co(n\text{-}Bu_3P)(CO)_3$ radical (or less likely, a Co^{2+} species) can be implied from the observation that at high temperature, in the presence of the dimer, the ^{31}P resonance of free *n*-Bu_3P broadens while the resonance of the dimer remains narrow. This is consistent with a facile exchange of the free phosphine with a small amount of radical species. The hydride broadening could be due to a related process involving hydrogen atom exchange with such a radical. Future studies will attempt to confirm the formation of neutral radical or Co^{2+} species and continue the development of a phosphine-modified cobalt hydroformylation process in $scCO_2$.

---

[5] S. S. Kristánjansdóttir and J. R. Norton, in *Transition Metal Hydrides: Recent Advances in Theory and Experiment*, Ed., A. Dedieu, VCH, New York, pp. 309-359 (1992).

[6] C. Masters, *Homogeneous Transition-Metal Catalysis: A Gentle Art*, Chapman and Hall, London, p. 116 (1981).

2. Hydrocarbon Activation Chemistry

Selective functionalization of hydrocarbons remains one of the most challenging areas of research for organometallic chemists.[7,8] Because the structures of the homogeneous catalysts are better defined and more easily characterized than the heterogeneous catalysts, major advances in our understanding of catalytic hydrocarbon activations have come mostly from studies in homogeneous rather than heterogeneous systems. In addition, the uniformity of the "catalyst sites" in homogeneous solutions makes these catalysts more likely to exhibit a product selectivity. We have chosen metallophthalocyanines (MPc) as the catalyst because of their high thermal stability and their similarity in structure to porphyrins, which are the prosthetic groups of heme enzymes that catalyze the autoxidation of hydrocarbons in biological systems.[9]

In an earlier study of the activation of hydrocarbons by rhodium phthalocyanines, we demonstrated that the reaction proceeds by a radical mechanism initiated by the abstraction of a hydrogen atom by a RhPc radical.[10,11] We have extended our study to investigating (FPc)Fe-catalyzed oxidation of hydrocarbons [where FPc^{2-} = dianion of 1,4,8,11,15,18,22,25-octakis(trifluoromethyl)phthalocyanine]. The dimeric $[(FPc)Fe]_2(\mu\text{-}O)$ was found to catalyze the oxidation of 3-methylpentane by *tert*-butyl hydroperoxide in 3-methylpentane/methylene chloride solution (1:1 molar ratio) at ambient temperatures to yield 3-methyl-3-pentanol and 3-methyl-2-pentanone, with catalyst turnovers of 150 and 70, respectively.

It is well known that high-valent iron-oxo complexes, namely, (FPc)Fe=O and $[(FPc)Fe{=}O]^+$, are likely reaction intermediates in iron-catalyzed oxidation reactions. We thus decided to direct our initial study toward the preparation and characterization of these iron-oxo complexes and the transfer of the oxo atoms to various substrates.

We have observed that the μ-oxo atom of $[(FPc)Fe]_2(\mu\text{-}O)$ is transferred to trimethylphosphine (PMe_3) and triphenylphosphine (PPh_3). In the latter case, a nitrogen base is required to induce the oxidation. With 1-methylimidazole (mim) as the base, the stepwise formation of $(mim)_2[(FPc)Fe]_2(\mu\text{-}O)$ and (FPc)Fe=O and the subsequent transfer of the μ-oxo ligand of the latter to PPh_3 have been observed:

$$[(FPc)Fe]_2(\mu\text{-}O) + 2\ mim \rightleftharpoons (mim)_2[(FPc)Fe]_2(\mu\text{-}O) \quad (4)$$

$$(mim)_2[(FPc)Fe]_2(\mu\text{-}O) \longrightarrow (mim)_2(FPc)Fe + (FPc)Fe{=}O \quad (5)$$

---

[7] B. A. Arndtsen, R. G. Bergman, T. A. Mobley, and T. H. Peterson, *Acc. Chem. Res.* **28**, 154 (1995).

[8] D. H. R. Barton and D. Doller, *Acc. Chem. Reson.* **28**, 504 (1992).

[9] B. Meunier, *Chem. Rev.* **25**, 504 (1992).

[10] M. J. Chen, L. Nunez, J. W. Rathke, and R. D. Rogers, *Organomet.* **15**, 2338 (1996).

[11] M. J. Chen and J. W. Rathke, *Organomet.* **13**, 4875 (1994).

$$(FPc)Fe{=}O + PPh_3 + 2\,mim \rightleftharpoons (mim)_2(FPc)Fe + OPPh_3 \qquad (6)$$

The complex (FPc)Fe=O has also been generated by the oxidation of $[(FPc)Fe]_2(\mu\text{-}O)$ with *tert*-butyl hydroperoxide.

We have not yet succeeded in oxidizing a hydrocarbon with the oxo atom of (FPc)Fe=O. However, $[(FPc)Fe]_2(\mu\text{-}O)$ has been used to catalyze the selective oxidation of 2,3-dimethyl-2-butene to its epoxide

(7)

and cyclohexene to 2-cyclohexene-1-one by iodosobenzene

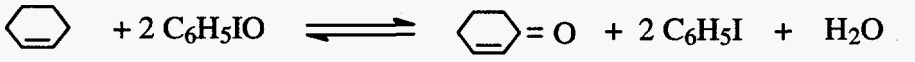

(8)

In both cases, only a single organic product is obtained. We found that (FPc)Fe=O does not oxidize these two substrates, while iodosobenzene, a known oxygen atom transfer reagent, does in the presence of $[(FPc)Fe]_2(\mu\text{-}O)$. These findings suggest that $[(FPc)Fe{=}O]^+$ may be involved in the oxidation with iodosobenzene.

As (FPc)Fe=O is among the most stable of $Fe^{IV}{=}O$ complexes, it is well suited for studying the spectroscopic and chemical properties of these complexes. This stability might be due to the presence of eight highly electronegative trifluoromethyl groups. In addition to continuing our study of (FPc)Fe=O, we will continue to search for $[(FPc)Fe{=}O]^+$ and will extend our study to use dioxygen as the oxygen source.

3. Electrochemical/Battery Research

This program uses *in situ* magnetic resonance imaging to investigate ion transport in lithium-polymer electrolyte batteries. Improved knowledge in this area may lead to lithium batteries that exhibit higher energy efficiencies by increasing the total ion conductivity and maximizing the fraction of the current that is carried by the electroactive lithium ions. In addition, the NMR imaging work is directed toward improving battery lifetime by reducing dendrite and passive film formation through investigation of the fundamental reaction chemistry that occurs at the electrode-electrolyte interface.

An important problem with the current generation of polymer electrolyte materials is that the lithium ion transference number is quite low[12,13] and, therefore, the bulk of the ionic current

[12] A. Hooper, M. Gauthier, and A. Belanger, "Polymer Electrolyte Batteries," in *Electrochemical Science and Technology of Polymers*, Vol. 2, Ed., R. G. Linford, Elsevier Applied Science, London (1990).

[13] P. G. Bruce, M. T. Hardgrave, and C. V. Vincent, *Solid State Ionics* **53-56**, 1087 (1992).

is carried by the anions. In that case, the electric field of the applied potential is inefficient at supplying the necessary lithium ions, and simple diffusion is exceedingly slow in these materials at room temperature. As a consequence, low lithium ion transference numbers result in rapid electrolyte depletion in the region adjacent to the electrode where the lithium ions are reduced. This electrolyte depletion severely limits the thickness of the polymer film that is effectively utilized and contributes to the difficulty in designing a battery with a uniform discharge voltage. These electrolyte depletion zones would be eliminated with an advanced electrolyte material that exhibits a lithium ion transference number of one, where the electric field would move only the lithium ions. Toward this end, new materials under investigation include conducting clays where the anions are part of the backbone of the clay, and where the only mobile species are the lithium cations. All of these activities to synthesize new solid-state electrolytes would benefit from a rapid *in situ* spectroscopic technique to measure the electrolyte depletion zones that form under normal battery operation. The direct determination of the lithium ion transference number by the Hittorf method previously has only been obtained by physically dissecting thin-layer cells with a razor blade and analyzing the extracted regions of the polymer electrolyte for their lithium content.[13] Consequently, it has been difficult to systematically study the effect of plasticizers, temperature, or alterations in the polymer backbone on the lithium ion transference number. In addition, the analytical requirements for the newer clay and composite polymer/clay electrolytes are even more demanding because of their inherent anisotropy.

As reported earlier,[14] we developed a new NMR-imaging method that has sufficient distance and signal sensitivity to rapidly quantify the electrolyte depletion zones that form adjacent to the cathode in an active electrolysis cell. In addition, we have recently developed a new method of measuring diffusion coefficients by using our NMR-electrochemical cell.[15] Importantly, our method for measuring diffusion coefficients is able to distinguish different regions of the sample because it is based on an NMR imaging technique. In contrast, the widely used pulsed field gradient (PFG) NMR method yields an average diffusion coefficient for the sample as a whole, and the ionic mobilities that have been determined by the PFG-NMR method are not in good agreement with the low lithium ion transference numbers that have been measured by the direct Hittorf method.[13] Our new imaging technique should make it possible to measure the lithium ion diffusion coefficient within the salt depletion zones that form adjacent to the electrode during normal battery operation; these values can then be compared with those for the lithium ion mobility in the bulk electrolyte. This information cannot be obtained by any other method for measuring diffusion coefficients.

The results in Fig. VII-3 depict the lithium ion profile in a polymer electrolyte material from 3M Corp. The sample was prepared by winding layers of the polymer electrolyte, separated by a polypropylene backing material, around a glass rod to yield approximately eleven alternating layers of polymer electrolyte and inert polypropylene film. The resulting ^{7}Li image clearly shows the lithium-containing layers at the expected 30-μm spacing. Significantly, by optimizing our cell design to minimize the distributed capacitance, we are able to divide each of the lithium-

[14] K. Woelk, J. W. Rathke, and R. J. Klingler, *J. Magn. Reson. A* **105**, 113 (1993).

[15] K. Woelk, R. E. Gerald II, R. J. Klingler, and J. W. Rathke, *J. Magn. Reson. A* **121**, 74 (1996).

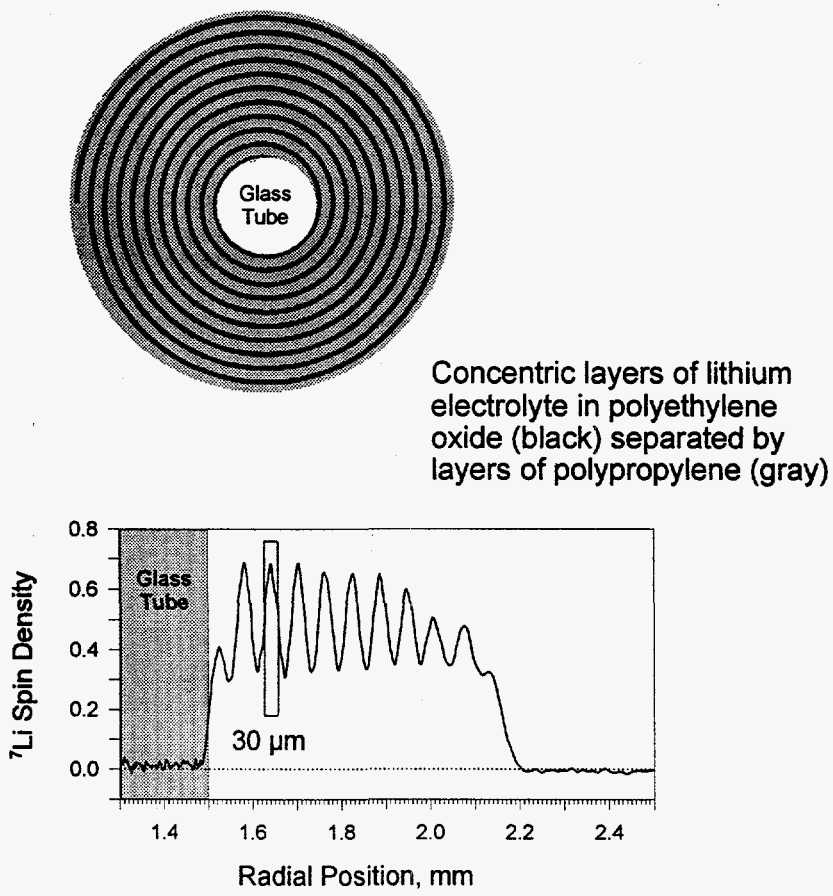

Fig. VII-3. Concentration Versus Radial Distance from Center of Eleven Layers of Lithium Electrolyte in Polyethylene Oxide, 30 µm, Separated by Inert Layers of Polypropylene, 30 µm, Wound Around Glass Tube. Schematic of sample design at top. Concentration (arbitrary units) measured with ^{7}Li NMR spin-labeling technique.

containing layers in Fig. VII-3 into ten sublayers and to achieve a distance resolution of 3 µm by using a spin-labeling technique that was developed for measuring diffusion coefficients.[15] These results demonstrate the feasibility of employing NMR imaging on polymer electrolyte films with thicknesses that are of interest in a practical battery design. Furthermore, the achievement of 3-µm distance resolution on a solid polymer sample attests to the power of the new toroid cavity NMR imager.[16] Since the spin-labeling technique measures motion perpendicular to the plane of the polymer film (along the radial position in Fig. VII-3), it should be capable of handling the anisotropy of new clay electrolyte materials that are available to us through a collaboration with researchers at Northwestern University.

[16] K. Woelk, J. W. Rathke, and R. J. Klingler, *J. Magn. Reson. A* **109**, 137 (1994).

Future efforts will focus on using our NMR-electrochemical cell to systematically measure the lithium ion transference numbers for a range of polymer electrolytes and plasticizers by directly imaging the salt depletion zones that form adjacent to the cathode during controlled electrolysis. We have recently added variable-temperature capability to our NMR-electrochemical cell, which should allow the temperature dependence of the lithium ion transfer coefficient to be determined. Efforts will continue to characterize the chemical composition of films that form at the electrode-electrolyte interface. In the ^{19}F NMR spectra of CF_3SO_3Li/polyethylene oxide electrolytes, we have observed a new species that forms within a thin layer adjacent to the cathode and will follow up on these observations by a combination of ^{7}Li, ^{1}H, ^{13}C, and ^{17}O NMR spectroscopic imaging.

B. Materials Sciences Research

The materials sciences program encompasses fundamental research on the characterization of electrochemical metal/solution interfaces (under conditions that are relevant to corrosion science and to electrochemical devices), the development of first-principle methods for computing molecular energies, and the study of materials properties by advanced computational methods.

1. Electrochemical and Corrosion Studies

Electrochemical processes occurring in aqueous media are of fundamental importance in many established and emerging energy-related technologies, including high-performance batteries for electric vehicles, large-scale fuel cells for primary electric power generation, and photoelectrochemical means of energy production. Also important is corrosion, an electrochemical process that cuts across practically all energy technologies. The purpose of our electrochemical and corrosion studies is to provide (1) experimental information on the structure and dynamics of metal/solution and metal oxide/solution interfaces as a function of temperature and solution chemistry and (2) theoretical models against which the experimental results can be tested. This research program employs *in situ* surface-sensitive synchrotron radiation methods, transient and steady-state electrochemical techniques, and theoretical modeling based on a combination of molecular dynamics and molecular orbital methods.

a. Synchrotron and Spectroelectrochemical Studies

The purpose of this activity is to elucidate the relationship between the structure of metal/solution interfaces and the mechanisms of interfacial reactions in various solutions. Synchrotron X-ray scattering (specular and diffuse), X-ray absorption spectroscopy, and far infrared spectroscopy techniques are employed for *in situ* determinations of the structure of the films on metals. Electrochemical techniques, such as dc polarization, ac impedance, and cyclic potentiodynamic scanning, are used to determine the energetics and mechanisms of the interfacial processes involved in the corrosion of metals.

Synchrotron far infrared spectroscopy (SFIRS) continues to be applied to the *in situ* identification of surface films and adsorbed layers on electrodes in various solution environments. During this reporting period, the spectroelectrochemical behavior of copper in dilute solutions of cyanate (OCN^-) and thiocyanate (SCN^-) in perchlorate-supporting electrolyte was investigated by SFIRS measurements at the U4IR beamline of the National Synchrotron Light Source (NSLS). Both OCN^- and SCN^- are pseudo halides that are of interest from the corrosion standpoint because of their ability to cause passive film breakdown, thus exacerbating metal corrosion. The SFIRS results indicated the formation of thin films of $Cu(SCN)_2$ and $Cu(OCN)_2$ at -0.05 V and -0.25 V (vs. standard calomel electrode), respectively. Spectra of the surface species showed bands at about 150 and 400 cm^{-1} for $Cu(OCN)_2$, which were assigned to the Cu-N-C bending and the Cu-N stretching vibrational modes, respectively. The corresponding bands for $Cu(SCN)_2$ appear at 120 and 380 cm^{-1}, suggesting a weaker interaction of SCN^- with copper compared to OCN^-. A study of adsorbed CN^- and H_2O at electrode surfaces is planned for the future. A polarization modulation-type spectrometer will be built to increase our detection sensitivity to the monolayer level. This work is being carried out in collaboration with the University of Auckland (New Zealand) and the University of Poitiers (France).

Synchrotron X-ray absorption spectroscopy (XAS) studies were carried out to examine the structure of thin nickel oxide films anodically deposited onto a graphite substrate from a nickel sulfate/sodium acetate aqueous solution. Adherent deposits could be obtained at a constant deposition potential of 1.1 V (vs. standard calomel electrode) with the film consisting of Ni^{2+} and Ni^{3+} oxides as deduced from the X-ray absorption near edge spectra. The material could be charged further in 1 M KOH solution to produce β- and γ-NiOOH. The capacitance of the electrodeposited material was measured to be about four times that of the pure graphite substrate. The material thus appears promising for use in the fabrication of ultracapacitors. Further studies on the structure of these films, as well as those prepared by the anodic oxidation of nickel thin films, will be undertaken. This research is being pursued with members of the Naval Surface Warfare Center.

Synchrotron X-ray scattering investigations (specular and diffuse) were carried out to further examine the electrodeposition of silver on a platinum substrate from acidic nitrate and sulfate solutions. The reflectivity data could be fitted with a two-layer model consisting of a dense silver underlayer and an overlayer of very low-density material. The amount of electrodeposited material was determined from the scattered X-ray intensity and found to be consistently higher compared with the coulometrically determined amount of electric charge passed. This may be due to additional scattering from Ag^+ species near the electrode surface. X-ray diffraction showed a pattern characteristic of a powder deposit. Scanning electron microscopy revealed microcrystals which have no spatial correlation. Further work on deposition at single-crystal surfaces is planned. This work is being pursued in collaboration with researchers from the Advanced Photon Source (APS) at Argonne.

b. Electrode Structure and Kinetics Studies

This research concentrates on understanding (1) the kinetic aspects and atomistic mechanism of heterogeneous charge-transfer reactions in aqueous solutions over a wide range of temperatures (25 to 300°C) and (2) the atomic level structure of electrified interfaces that

strongly influence the dynamics of these reactions. The electrode kinetics measurements of this study are carried out with relaxation techniques, such as galvanostatic, coulostatic, or potentiostatic pulse transients, ac-impedance measurements, and rotating-disk-electrode techniques, and the resulting data are evaluated with computerized data-evaluation methods. The interfacial structural studies use synchrotron X-ray scattering methods. Heterogeneous charge-transfer reactions are the essential chemical reactions in many energy-related technologies, such as high power-density and energy-density batteries and ultracapacitors for electrical vehicles and large-scale fuel cells for primary electrical power generation. They are also involved in corrosion, an insidious electrochemical process that is relevant to practically all energy technologies. Clearly, a fundamental understanding of the dynamics of electrode reactions could result in improvements in many energy technologies.

This past year, we continued our kinetic studies of the Cu^{2+}/Cu^{0} electrode reaction—an important but poorly understood cathodic reaction occurring during stress corrosion cracking in light water nuclear reactors. We have begun high-temperature/high-pressure kinetic measurements of the Cu^{2+}/Cu^{+} reaction, which is the rate-determining step in the overall copper deposition/dissolution process. We have carried out a large number of measurements in the temperature range from 25 to 100°C. An Arrhenius plot summarizing our results is shown in Fig. VII-4. From this plot, the activation energy for the reaction was calculated to be 30 kJ/mol. The rate of the Cu^{2+}/Cu^{+} charge-transfer reaction increased tenfold between 25 and 100°C, but the transfer coefficient was independent of temperature. Work at higher temperatures is in progress. This research is carried out in close coordination with the theoretical modeling effort described in Sec. VII.B.1.c.

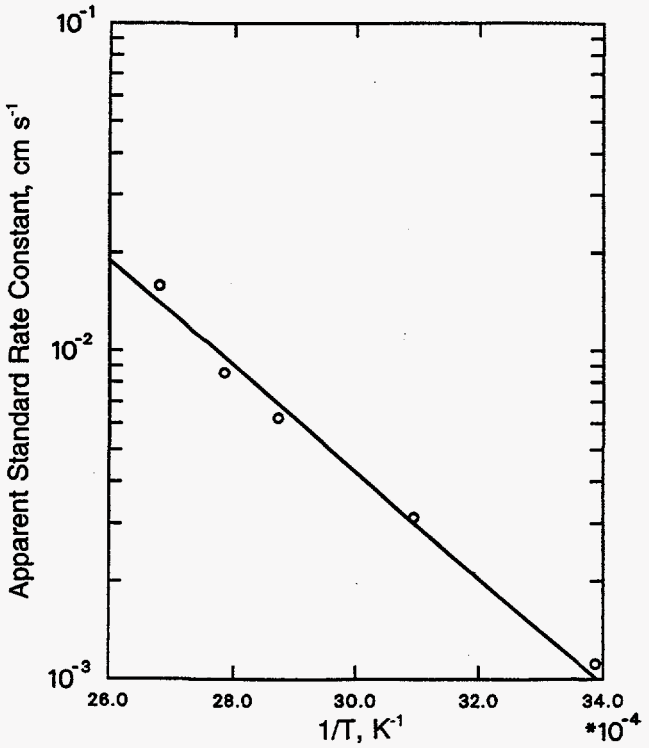

Fig. VII-4.

Arrhenius Plot of Cu^{2+}/Cu^{+} Reaction in Perchloric Acid Solution

In a collaborative effort with the Synchrotron Studies Group in the ANL Materials Science Division, we also continued the use of synchrotron X-ray techniques in probing the structure of electrified interfaces buried under or within condensed phases. We completed an investigation of structural changes at the Pt(111) single-crystal surface associated with incipient electrochemical oxidation/reduction (i.e., for a metal that is the most efficient electrocatalyst in fuel cell applications). On the basis of these results, we proposed a new mechanistic model that explains all our electrochemical and X-ray reflectivity observations. The model is based on dipole-dipole interaction considerations, resulting in nearest-neighbor-avoiding surface structures and a partial place exchange of platinum and oxygen atoms. We also initiated a new study on the underpotential deposition (UPD) of metals and the interaction of the UPD layer with coadsorbed anions on systems of electrocatalytic importance. Our initial measurements, carried out with the underpotential deposition of silver on platinum, have proven that (1) the UPD structure involves two complete silver monolayers (a very unusual structure for UPD), and (2) the first layer is fully completed before the deposition of the second layer. This project is being carried out in collaboration with the Chemistry Department at the University of Illinois, Urbana.

c. Theoretical Studies of Electrode Reactions

The accelerating effect of certain anions for electrode reactions has been known for a long time, but the fact that catalytic effects can sometimes be caused by traces of anions (present as unintended or unknown impurities) in the electrolyte solution is much less appreciated. Our theoretical studies are addressing the catalytic effect of halide anions on electron transfer rates, an important phenomenon occurring during stress corrosion. Using *ab initio* molecular orbital theory, we are investigating the homogeneous inner-shell electron transfer reaction $Fe^{3+} + e^- \rightarrow Fe^{2+}$ with bridging halide anions of F^-, Br^-, and I^-. These halide anions were found to give an increased electronic coupling due to a closer approach distance than is possible for an outer-sphere water bridge. This condition is similar to what we have previously found for the inner-shell chloride bridge of the Cu^{2+}/Cu^+ electron transfer reaction.[17] In addition, a model for the copper surface in the Cu^{2+}/Cu^+ reaction has been included in calculations of the distance dependence of electronic coupling in a hydrated copper ion. The surface is represented by a cluster of copper atoms. The distance dependence will be used in the calculation of electron transfer rates being carried out at the University of Minnesota. These calculations will then be compared with the experimental measurements described in Sec. VII.B.1.b.

2. Theoretical Studies of Materials

a. Gaussian-2 Theory Development

Critical evaluation of theoretical models for calculating molecular energies is essential if such methods are to become credible tools for chemical investigations. In this regard, our Gaussian-2 (G2) theory, developed in collaboration with workers at Northwestern University

[17] Z. Nagy, J.-P. Blaudeau, N. C. Hung, L. A. Curtiss, and D. J. Zurawski, *J. Electrochem. Soc.* **142**, L87-L89 (1995).

and AT&T Bell Laboratories, has become a cornerstone method for such calculations.[18] Originally, G2 theory was tested on a set of 125 reaction energies, chosen because they have well-established experimental values. All of the molecules contained only one or two non-hydrogen atoms with two exceptions (CO_2 and SO_2). In recent work, the test set has been expanded to include larger, more diverse molecules, with enthalpies of formation at 298 K being used for comparison between experiment and theory. This set, referred to as the "enlarged G2 neutral test set," includes the 55 molecules whose atomization energies were previously used to test G2 theory and 93 new molecules. The full set includes 29 radicals, 35 non-hydrogen systems, 22 hydrocarbons, 47 substituted hydrocarbons, and 15 inorganic hydrides. It also includes molecules containing up to six non-hydrogen atoms.

The enlarged G2 neutral test set of 148 molecules was used to assess the performance of G2 theory and two modified versions of it, G2(MP2)[19] and G2(MP2,SVP).[20] The mean absolute deviations between the theoretical and experimental enthalpies of formation at 298 K for the different methods are shown in Fig. VII-5. The results indicate that G2 theory is the most reliable of the methods, with a mean absolute deviation of 1.58 kcal/mol for the 148 enthalpies. This is slightly larger than for the atomization energies of the 55 small molecules in the original G2 test set but lower than the 2.0 kcal/mol needed for chemical accuracy. The modified versions of G2 theory, G2(MP2) and G2(MP2,SVP), have average absolute deviations of 2.04 and 1.93 kcal/mol, respectively. Since G2(MP2,SVP) theory uses considerably less computer time and disk storage than G2 theory, it may be a useful alternative for large hydrocarbons. The G2 neutral test set has also been used to assess density functional theory (DFT) methods for calculation of enthalpies of formation. The results are also shown in Fig. VII-5. Of the six methods tested, B3-LYP (the three-parameter exchange functional[21] and the correlation functional[22]) performed the best. It has an average absolute deviation of 3.12 kcal/mol, which is still nearly twice that of G2 theory, and a maximum deviation of 20 kcal/mol, which is more than double the maximum deviation of 8 kcal/mol for G2 theory. In future work we will use the G2 data set to help develop new methods that can handle larger systems with more accuracy. In addition we will include ions in the data set.

b. Computational Studies of Molecular Sieve Materials

Zeolites are solid acid catalysts that are widely used in the petrochemical industry for hydrocarbon cracking. We have extended our study of the interaction of a water dimer with the acid site in the zeolite ZSM-5 to a five-metal (T) atom cluster ($AlSi_4O_4H_{12}$) model. We have calculated the equilibrium geometries of the neutral [$ZH\cdots(OH_2)_2$] and ion-pair [$Z^-\cdots H(OH_2)_2^+$] adsorption complexes based on this 5 T model. In addition, we have calculated the transition-state geometry located between these two equilibrium structures on the potential surface. All of

[18] L. A. Curtiss, K. Raghavachari, G. W. Trucks, and J. A. Pople, *J. Chem. Phys.* **94**, 7221 (1991).
[19] L. A. Curtiss, K. Raghavachari, and J. A. Pople, *J. Chem. Phys.* **98**, 1293 (1993).
[20] L. A. Curtiss, P. C. Redfern, B. J. Smith, and L. Radom, *J. Chem. Phys.* **104**, 5148 (1996).
[21] A. D. Becke, *J. Chem. Phys.* **98**, 5648 (1993).
[22] C. Lee, W. Yang, and R. G. Parr, *Phys. Rev. B* **37**, 785 (1988).

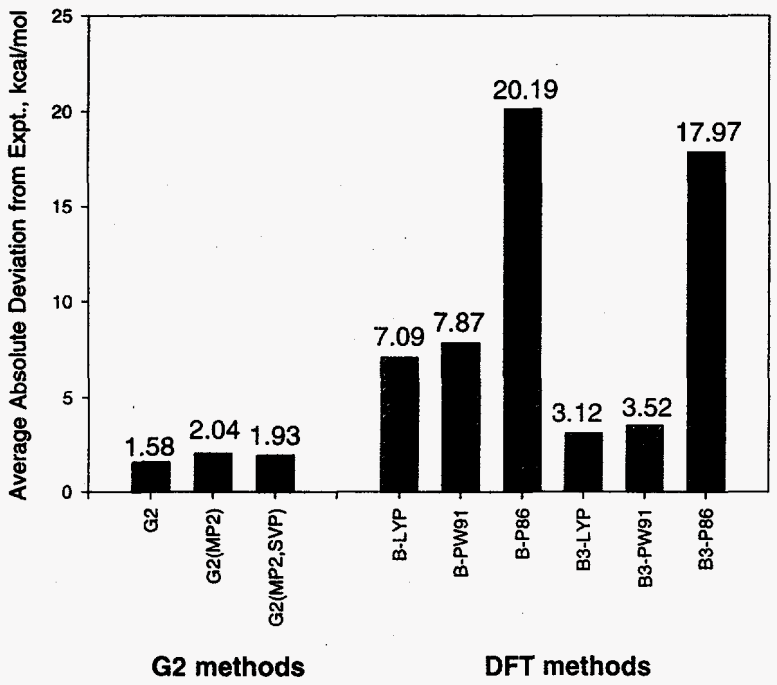

Fig. VII-5. Deviation from Experiment of Different Calculational Methods Evaluated with Enlarged G2 Neutral Test Set Containing 148 Molecules

the calculations were done with density functional theory. While density functional theory is not as accurate as G2 theory (see Sec. VII.B.2.a) it is a cost-effective way of including correlation effects, which are important in the water adsorption interactions. In tests on small model systems for water adsorption, it gave results in agreement with G2 theory for the types of bonding involved in the adsorption. The potential energy surface for this reaction is shown in Fig. VII-6. The figure shows the two minima in the potential energy surface corresponding to the neutral adsorbed complex $[ZH...(OH_2)_2]$ and the ionic complex $[Z^-...H(OH_2)_2^+]$. The barrier between the two minima corresponds to the transition state (TS). The relative energies ΔE_{rel} and ΔE_{TS} are small (less than 2 kcal/mol), indicating free movement of the proton. The results from this study indicate that the likelihood of proton transfer from the zeolitic acid site on an adsorbed molecule to form a stable intermediate may depend on the concentration of the adsorbate. In the case of H_2O, our results suggest that a loading of two or more molecules per acid site allows the proton to be transferred quite readily at room temperature. This finding has significance for our future study of the interactions of hydrocarbon molecules with the acid site in zeolites.

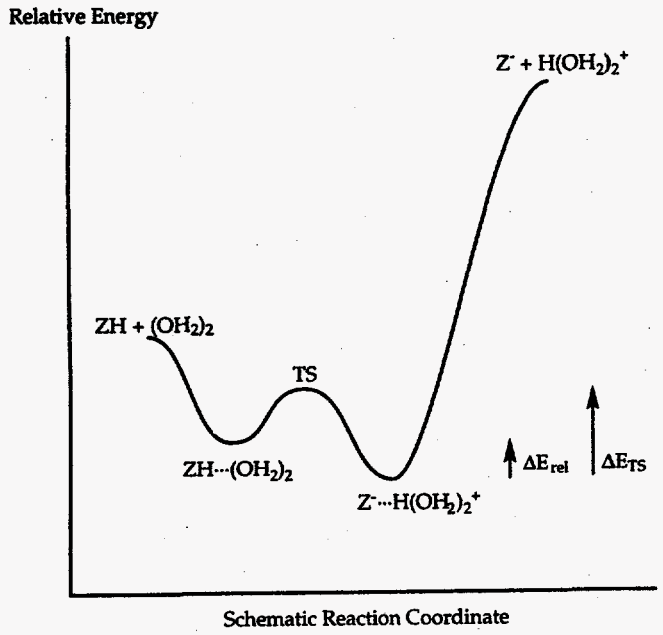

Fig. VII-6.

Potential Surface of Water Dimer Interacting with Acid Site in 5 T Cluster Model of Zeolite

VIII

Analytical Chemistry Laboratory

A. Introduction

The ACL operates in the ANL system as a full-cost-recovery center providing analytical support services, but has a mission that includes a complementary research and development component in analytical chemistry and its applications. Because of the diversity of research and development work at ANL, the ACL handles a wide range of analytical problems in its technical support role. Some routine or standard analyses are done, but the ACL usually works with commercial laboratories if our clients require high-volume, production-type analyses. It is common for ANL programs to generate unique problems that require significant development of methods and adaptation of techniques to obtain useful analytical data. Thus, much of the support work done by the ACL is very similar to our applied analytical chemistry research.

The ACL is administratively within the CMT, our principal ANL client, but provides technical support for many of the technical divisions and programs at ANL. The ACL has four technical groups—Chemical Analysis, Instrumental Analysis, Organic Analysis, and Environmental Analysis—which together include about 40 technical staff members. Talents and interests of staff members cross the group lines, as do many projects within the ACL. The ACL receives about 1500 different jobs annually, each of which could involve several samples.

The Chemical Analysis Group uses wet-chemical and instrumental methods for elemental, compositional, and isotopic determinations in solid, liquid, and gaseous samples and provides specialized analytical services. The Instrumental Analysis Group uses nuclear counting techniques to determine the radiochemical constituents in a wide range of sample types, from environmental samples with low radioactivity to samples with high radioactivity that require containment. The Organic Analysis Group uses a number of complementary techniques to separate organic compounds and measure them at trace levels and does development work in sensors, chemometrics, and detectors. The Environmental Analysis Group analyzes environmental, hazardous waste, and coal samples for the inorganic constituents and provides quality assurance support to DOE and other clients for various kinds of analytical data. Together,

the groups provide a full range of analytical capabilities to do inorganic, organic, and radiological analyses. (Additional information is available through the ACL's home page at http://www.cmt.anl.gov/acl/acl.htm.)

A major enhancement of ACL capabilities in 1996 occurred when a replacement for our inductively coupled plasma/atomic emission spectrometer was procured. It should be operational in early 1997.

B. Technical Highlights

The ACL provides analytical chemistry support to CMT, other ANL divisions and programs, other DOE sites, DOE's Chicago Operations Office, and DOE Headquarters. In addition, ACL conducts research and development programs funded by DOE and other sponsors. Selected accomplishments for 1996 are summarized here. In addition, the ACL did analytical work on many other projects, which are described in more detail elsewhere.[1]

1. Support for Nuclear Technology Programs

The ACL received samples from various experiments underway within the Nuclear Technology Department of CMT. Results from these determinations supported efforts that included development of a zeolite waste form that will trap fission products and transuranic elements, treatment of spent oxide fuel and simulated Three Mile Island fuel debris, treatment of spent metallic fuels, and treatment of fuels from the Molten Salt Reactor Experiment (MSRE).

The samples required a variety of dissolution techniques prior to measurement of the requested analytes. Analytical tools used included inductively coupled plasma/atomic emission spectrometry (ICP/AES), inductively coupled plasma/mass spectrometry (ICP/MS), X-ray diffraction (XRD), and thermal ion mass spectrometry (TIMS). Many of the samples that were submitted contained radioactive materials such as plutonium and were analyzed with instruments that had been modified for this purpose. Dissolution schemes were developed for hard-to-dissolve samples such as the fluoride salts used in the MSRE studies. Analytical results appear in Sections V and VI.

2. Continuous Monitoring of Plasma Arc Furnace at ANL-West

The continuous emission monitor (CEM) developed at ANL-East was used successfully to monitor the emissions from the first field test of the plasma arc furnace at ANL-West. The plasma system was developed to treat radioactive waste, including contaminated soils and resins, by thermally destroying volatile materials and converting the radioactive waste to nonleachable rocks. The initial test used nonradioactive material. The CEM was used to identify and quantify

[1] D. W. Green et al., *Analytical Chemistry Laboratory Progress Report for FY 1996*, Argonne National Laboratory Report ANL/ACL-96/6 (December 1996).

all volatile organic and selected inorganic species (CO, CO_2, and HCl). The results—obtained on-line during combustion—were used to optimize combustion of the surrogate materials as the test proceeded. Further testing is planned through 1997.

3. Characterization of Products and Residues from Automobile Shredder Fluff Recycling

About 25% of every junked car that is processed by automobile shredders to recover ferrous-metal scrap is made up of a mixture of plastics, glass, fibers, and foam. This mixture is referred to as "fluff." At present, shredder fluff is sent to landfills, but researchers in ANL's Energy Systems Division are testing technologies to segregate and recover the fluff components for recycling. The ACL has contributed to this process development by analyzing various intermediates and products to determine their composition and to measure potential contaminants in recovered oils, foams, and residual materials classified as "fines."

In a 1996 pilot-scale study, the Argonne researchers tested an approach to cleaning polyurethane foam so that it can be recycled into value-added products such as carpet padding. For this study, the ACL analyzed foam samples, as well as distillates and still bottoms generated during recovery of the solvent used in cleaning the foam. The data obtained from these analyses helped to establish the hazard classification of the still bottoms so that they could be properly disposed of and, in some cases, helped to guide improvements to the solvent recovery process. If the foam recycling process is commercialized, the methods and procedures ACL developed for these pilot samples should also help the emerging industry meet its analysis needs.

4. Support for High-Temperature Superconductor Development

The ACL continued to provide extensive analytical support to high-temperature superconductivity programs in ANL's Energy Technology (ET) and CMT Divisions. Much of this work involves analysis of starting materials, process samples, and products related to fabrication, as well as characterization studies on various ceramic compositions, including $YBa_2Cu_3O_{7-x}$ ("1,2,3-compound") and lead-doped bismuth/strontium/calcium/copper oxides ("BSCCO" ceramics). Our measurements include determining elemental composition by ICP/AES or classical methods, anions by ion chromatography, carbon with a LECO™ analyzer, and phase composition by X-ray powder diffraction. We also use an iodometric titration method to determine excess valence of the metals in a given ceramic (e.g., Cu^{3+}), which is related to the oxygen stoichiometry of the compound.

The ET researchers have been developing methods for fabricating practical component parts for devices that might use the BSCCO materials for high-current applications. Measurements by ACL for this development effort have included the characterization of impurities in different lots of silver tubing used in the process, as well as determination of the BSCCO-to-silver ratio in some tapes. More recently, ACL analysts have devised approaches for separating the BSCCO ceramic core from individual tape specimens to perform analyses on the ceramic in the core. These efforts have permitted evaluation of composition changes that might

have taken place when the ceramic was encapsulated in the silver sheath. Through these and related activities, the teamwork among chemists, ceramists, and analysts is helping to move the technology of superconducting ceramics toward practical applications.

5. Radon Remediation

In collaboration with ANL's Reactor Analysis (RA) and Reactor Engineering (RE) Divisions, the ACL is developing and testing a low-cost radon mitigation apparatus to be used for reducing radon levels in homes. Research personnel in RA had observed that vacuum pump oils concentrate noble gases. This observation led to the premise that oils may be useful for removing radon from air. The ACL tested numerous oils for radon solubility. We determined that, while most oils absorb radon to some degree, one of the better absorbers is corn oil. The RE and RA groups designed and constructed the radon-removal apparatus, which consists of an absorber and a desorber. The apparatus is being tested by the ACL. Under ideal conditions, the absorber removed up to 98% of radon. The desorber, which removes radon from the oil, is more difficult to optimize. At present, the best result obtained while operating both absorber and desorber simultaneously is 61% radon removal.

6. Development of "Smart" Chemical Sensors

Current ACL research efforts in chemometrics (the use of mathematics, statistics, and formal numerical methods for analysis of chemical data) are focused on the development of a software workbench for designing automated monitoring algorithms for spectroscopic, chromatographic, electrochemical, and radiochemical sensors of interest to DOE. The objective of this work is to produce "smart" chemical sensors, which implies that the sensor can (1) interpret multivariate data in real time; (2) perform data reduction and decision making; (3) communicate processed results to an end user, process control loop, or data fusion system; and (4) alter system operation on the basis of certain detection results. We have designed unique signal processing algorithms that combine digital filtering, pattern recognition, and multivariate calibration methods to provide enhanced qualitative and quantitative data analysis. These algorithms are initially developed using software; however, final versions of the algorithms can be implemented in hardware by encoding the algorithm onto a small digital signal processing board, which would become an integral part of the sensor electronics. Although the software workbench for designing these algorithms is still in the development phase, novel algorithms have been successfully generated for several applications. One application is qualitative processing of data from a passive-remote Fourier transform infrared (FTIR) sensor used for remote monitoring of chemical emissions. Another is quantitative processing of data from an extractive FTIR system used for continuous monitoring of incinerator emissions. In 1997, we expect to develop processing algorithms for hyperspectral image data. Such data provide a complete spectrum for any point or object in an image. Smart sensor algorithms have also been designed for automated analysis of multispectral image data and recognition of naval ships.

7. Preparation of Simulated Solidified Waste Samples for WIPP Performance Demonstration Program

The Waste Isolation Pilot Plant (WIPP) is a DOE installation consisting of large, interconnecting cavities hollowed out of deep geologic salt beds approximately 600 m underground. It is located approximately 26 mi (42 km) east of Carlsbad, NM. The facility is designed to demonstrate the safe handling, transportation, and disposal of transuranic (TRU) waste in the salt beds. The TRU waste destined for WIPP began to be generated during the 1940s from the nation's nuclear weapons programs at various DOE sites.

Wastes to be shipped to WIPP must first be characterized to identify the presence of any hazardous materials in the waste, in addition to any radioactive components. As part of the program to characterize TRU waste for WIPP, a Performance Demonstration Program (PDP) was established in 1995 for the analysis of Resource Conservation and Recovery Act (RCRA) constituents in Type I solidified waste. Type I waste is sludge from waste water treatment that consists of inorganic salt that has been solidified by adding Microcell E adsorbent and cemented. As part of Cycle 1 of the RCRA PDP in 1995, the ACL prepared and characterized simulated Type I solidified waste and developed methods for analysis of metals and volatile and semivolatile organic compounds in this matrix.

In 1996, for Cycles 2 and 3 of the PDP, the ACL's task was to prepare and characterize unspiked samples of simulated Type I solidified waste (cemented and uncemented) for metals analysis. The samples were provided to the PDP coordinator for spiking and shipment to the laboratories participating in the PDP.

8. Orphan Waste Projects

Many ANL facilities have "orphan" waste materials that have unknown origins or inadequate documentation or that remain from programs no longer funded. Wastes characterized by the ACL in 1996 included a substantial inventory of contaminated laboratory hoods, gloveboxes, equipment, and appliances (e.g., light fixtures). Chemical and radiological contamination on each item was assessed through smears and direct samples taken by ANL's Environmental Management Operations (EMO) personnel, who performed size-reduction and packaging operations on the waste. Other orphan waste projects involved hundreds of smaller waste items from various laboratories and storage areas, including unlabeled containers of solids, aqueous or organic liquids, oils, or sludges. For solids, X-ray fluorescence and X-ray diffraction analysis often gave the necessary information; for liquids and oils, several techniques, such as gas chromatography/mass spectrometry (GC/MS) and FTIR spectroscopy, were often employed. However, many wastes either could not be identified or contained complex mixtures of components; such wastes were evaluated for the RCRA characteristics of ignitability, corrosivity, toxicity, and reactivity. Wastes from radiological controlled areas required determination of the identity and quantity of radionuclides that might be present; these wastes were analyzed by gamma spectrometry, gas proportional counting, liquid scintillation counting, and/or alpha pulse height analysis. Through its orphan waste projects, EMO has helped ANL divisions dispose of tens of thousands of kilograms of waste materials.

9. Characterization of Used HEPA Filters for Disposal

Used HEPA filters removed from ANL laboratory exhaust systems represent a sizable waste stream from site operations. In the disposal process, EMO packages the used filters and takes composite samples, and the ACL characterizes the composite samples by chemical analysis to evaluate the waste against the waste acceptance criteria for disposal at DOE's Hanford Reservation. Samples shown to contain high concentrations of heavy metals are also processed by the Toxicity Characteristic Leaching Procedure to determine whether the metals exceed regulatory standards for mobility under landfill conditions.

During 1996, the ACL characterized approximately 25 composite HEPA filter samples. Each composite consisted of portions of approximately 12 filters. Thus, all filters replaced at ANL-East in 1996 (approximately 300 filters) were tested by this process. In addition, the filter-characterization methodology was applied to a historical accumulation of prefilter wastes. In a manner analogous to that used for the HEPA filters, EMO repackaged and sampled a collection of more than 8000 prefilters that had been stored over the years because no disposal facility would accept them without hazards classification information, which was not available. The volume of material in each prefilter composite required special efforts to homogenize the material for representative subsampling. Characterization of the composite samples from these packages will help ANL make a substantial reduction in its historical waste inventory.

10. Stand-Off Detection of Agent-Related Chemicals

The U.S. Army's Edgewood Research and Development and Engineering Center has an ongoing program in stand-off detection of gaseous chemical plumes, such as dimethyl methyl phosphonate and methanol, using FTIR technology. The ACL contributes to the objectives of this program by testing instrumentation. This testing includes determining the sensitivity of newly designed passive-remote FTIR spectrometers and enhancing the ability of existing spectrometers to detect chemical plumes in the presence of interferences.

Effort in 1996 focused on testing the "microFTIR" from Designs & Prototypes. This instrument weighs less than a pound and can be transported easily. Initial testing consisted of releasing quantitative amounts of methanol and dimethyl methyl phosphonate at the low parts-per-million-meter (concentration times pathlength) level both in the laboratory and the field. In the laboratory, calibrated blackbody backgrounds were used. In the field, low-sky, grass, and brick wall backgrounds were tested. The results were compared to those obtained by using a conventional Midac spectrometer. It was concluded that the microFTIR's performance was slightly less sensitive but comparable to the conventional spectrometer.

11. Analysis of Environmental Samples for U.S. Department of Agriculture

Over the past eight years, the ACL has participated in a collaborative effort with ANL's Environmental Research Division that involves monitoring the removal of carbon tetrachloride

and chloroform from groundwater under a former grain storage facility (in Waverly, NE) that is operated by the U.S. Department of Agriculture. Contaminants in the Waverly aquifer are being removed by groundwater extraction and air stripping. Carbon tetrachloride contamination in the Waverly aquifer remained fairly constant during the year, at approximately 20 ppb. The aquifer will continue to be sampled monthly in 1997 because the concentration of carbon tetrachloride is still above the Federal health standard of 5 ppb. In 1996, the ACL analyzed more than 100 aqueous samples for this project. All samples were analyzed within the allowed holding time, and reports were provided in a timely manner.

12. Transition Metal Speciation in Textile Mill Wastewater

Under Stream Quality Standards of the U.S. Environmental Protection Agency, discharges of certain metals present in industrial water effluents must be reduced. This reduction is especially significant to the U.S. textile industry because many of the important dyes used in textile processing contain Cu, Cr, or Co as part of the chromophore. With support from the AMTEX™ partnership (through a Cooperative Research and Development Agreement between DOE and the textile industry), ACL staff have developed a simple analytical procedure that will allow industrial facilities to determine the chemical lability of metals in their wastewater discharges. Chemically labile cations (e.g., divalent copper) are separated from the sample matrix by using a sodium sulfonate ion-exchange resin, and nonpolar species (e.g., certain dyes) are separated from the cation exchange effluent by using a nonionic polymer resin. When the two-column separation is combined with element-selective detection (e.g., ICP/AES), Co and Cu cations (labile species) are differentiated from their EDTA (ethylenediaminetetraacetic acid) complexes, and these species are further differentiated from Co and Cu dyes. Trivalent chromium, hexavalent chromium, and chromium dyes are also differentiated from one another.

Early work using metal-EDTA mixtures showed that the degree of Co(II) and Cu(II) retention on the cation column closely corresponded to that expected from the EDTA-to-metal ratios and the stability constant of the metal-EDTA complex. The procedure was tested more rigorously in 1996 by analyzing nearly 100 effluent samples taken from textile mills all over the southeastern United States. In general, the procedure performed as expected, with spike recoveries (for total metal) on the order of 95 to 100%, chemical recovery (for separated metal) on the order of 80 to 100%, method detection limits between 5 and 20 ng/mL, and excellent reproducibility. When the proper precautions are taken to avoid false positives (that is, careful and clean sample preparation), the procedure will facilitate realistic assessments of environmental impact due to metal discharges and also will provide information needed to develop appropriate water treatment processes.

13. Automated Data Cataloging Procedure for Objects in AMPS Multispectral Imagery

In the DOE Office of Nonproliferation and National Security Airborne Multispectral Pod System (AMPS) program, numerous images were collected that contain information about many kinds of targets, including buildings and vehicles. Different research groups are interested in

different types of targets, but searching through the large data set to find only those targets is time consuming. Therefore, a procedure is needed for automated retrieval of information on specified targets. The purpose of our project was to establish a database for cataloging the AMPS multispectral image data.

The ACL developed a procedure based on Microsoft Access to demonstrate the feasibility of establishing such a database. As the key element needed to uniquely identify data records, we chose Global Positioning System (GPS) information. Every target has a unique GPS value, and this GPS information is already collected by AMPS. The targets themselves are identified in the original image by the automatic target recognition algorithm developed under another ACL project, the Sensor Algorithm Generation Environment (Sec. VIII.B.6). Data obtained were target location, target type, and target image.

The establishment of this database makes it much easier for researchers to access the image data that contain targets of interest. In particular, the specific image of the target can be viewed without retrieving the whole image, which is usually at least 100 times as big as the target image itself. This feature is important because it allows researchers to pre-examine the targets quickly before they spend time retrieving the whole image for further research. We believe a similar type of database may be established for other sensors. Thus, a common framework may be created for performing multisensor data fusion.

14. Support of Counternarcotics Efforts

The ACL continued to provide analytical support to a collaborative program between ANL's Technology Development Division and the Office of the National Drug Control Policy. In addition, another program was initiated with the Houston Advanced Research Center (HARC) to recommend methods for the destruction of large quantities of seized illicit substances.

Primary support was given to testing commercially available instrumentation for narcotics detection and reporting the results to law enforcement agencies. Two reports have been issued and have provided important information on the applicability of each of the tested instruments. Instruments have also been field-tested on cargo containers at the Port of Miami to demonstrate how viable each instrument is under harsh conditions.

The second support area has been in the study of cocaine contamination and transfer. A legal issue has arisen concerning the correlation between the level of contamination of a defendant and the likelihood that the contamination was obtained through handling cocaine. In 1995, ACL research determined that almost 80% of all money is contaminated with cocaine, and that contamination was more prevalent in older and lower denomination bills. This year a study to determine the conditions that allow contamination to be transferred found that it is virtually impossible to transfer the contamination unless the contaminated money is vigorously rubbed onto someone. Other tests showed that, although a person would become contaminated by touching cocaine, that contamination could only be transferred immediately after contact with the cocaine. The contaminated individual may stay contaminated for several days, but the cocaine could not be transferred to another individual or to objects.

The third support area was to understand *why* contamination does not occur when innocent people handle highly contaminated money. Scanning electron microscopy studies were performed on both contaminated and uncontaminated money. Both had identical surfaces, and the contamination was clearly not evident on the surface of the bill. Investigation of the subsurface showed that contaminated bills have cocaine adhering to the fibers trapped in cages under the surface fibers. It appears that contamination does not transfer because when someone handles contaminated currency, that individual touches only the surface of the bill, while the cocaine is below the surface and, hence, cannot contaminate the individual.

15. Analysis of Samples from Process to Recycle Aluminum Salt Cake

When aluminum is recycled, it is melted in the presence of an alkali-metal-chloride flux, which serves to extract impurities from the molten scrap metal and to protect the metal from oxidation, which after it solidifies, is referred to as "salt cake." Composed of salt, aluminum metal, and oxide residues, the salt cake represents a substantial waste stream in the aluminum recycling industry, which is seeking ways to eliminate the environmental and economic disadvantages associated with disposing of salt cake waste. Researchers in ANL's Energy Systems Division are working with the Aluminum Recycling Association to develop cost-effective processes for treating salt cake to recycle the aluminum and salt fractions and convert the oxide-residue fraction to high-value-added products.

The ACL assisted this research by analyzing samples from a pilot-scale test of a process that converts the oxide residues into fiber insulation products. Materials from various stages of the process were analyzed to determine elemental composition, leachable salt content, total halide content, free-metal content, and phase composition. The determinations of total halides and free metal presented challenging opportunities for the analysts involved in this project. Special procedures had to be devised to permit measurement of low concentrations of these analytes because they had a profound effect on the product obtained from the manufacturing process. By providing expertise in compositional analysis of refractory materials (dissolutions and analysis by atomic emission or ion chromatography), X-ray diffraction, and gas-generation methods (free metals by hydrogen evolution), the ACL helped the Energy Systems Division team resolve product-quality problems in the pilot-plant operations. This success helped advance program goals to enhance the viability of the aluminum recycling industry and the environmental and economic benefits associated with it.

16. Development of Method for Radium Determination in Aqueous Samples

Under a Cooperative Research and Development Agreement initiated in 1994, ANL and the 3M Co., in conjunction with IBC Advanced Technologies, Inc., have developed a new technology based on solid-phase extraction for radiochemical analysis. The work resulted in a new product, Empore™ Rad Disks, which are thin membranes loaded with element-selective particles embedded in stable, inert polytetrafluoroethylene fibrils. The Empore™ Rad Disks

selectively separate target radioisotopes from aqueous samples, even in the presence of very large concentrations of other ions. Empore™ Rad Disks obviate the time-consuming preconcentration, precipitation, filtration, purification, elution, and evaporation steps associated with conventional sample preparation methods. The ACL and ANL's Environmental Research Division are collaborating to evaluate the performance of these disks and develop appropriate analytical procedures. Methods for separation of ^{99}Tc and $^{89/90}$Sr were developed in previous years.

In 1996, methods for separation of $^{226/228}$Ra were developed and disseminated to the radiochemistry community. The radium-selective disks resulting from this work lend themselves to a variety of approaches for determining the pertinent radium isotopes. The major radium isotopes, ^{226}Ra and ^{228}Ra, may be determined simultaneously by isolating radium on the disk, placing the disk in a sealed container, and then gamma-counting the sample by means of the least-squares gamma spectrometric method. Alternatively, the radium itself or its daughter products may be eluted from the disk and further processed according to prescribed EPA methods.

The team of ANL, 3M, and IBC received a 1996 R&D 100 Award from *Research and Development* magazine for the development of Empore™ Rad Disks.

17. Domestic Nuclear Smuggling Exercise

An exercise was carried out to demonstrate DOE's and other agencies' ability to respond to a nuclear smuggling scenario. "Intercepted" materials described in the scenario were sent to participating laboratories for forensic analysis. The ANL team consisted of personnel from the Technology Development, Energy Technology, and Chemical Technology Divisions.

The material consisted of radioactive metal together with nonradioactive substances. Various tests were used to identify and quantify the material. They included extensive photographic and metallographic examination by Energy Technology Division personnel and analyses performed by the ACL using ICP/AES, ICP/MS, gamma spectrometry, alpha pulse, FTIR microscopy, XRD, and TIMS techniques. The data were reported as the analysis proceeded, at intervals of 12, 24, 48, and 96 h. Interpretations of the data as to the origin and purpose of the material were also conveyed.

A post-exercise workshop was held at DOE Headquarters for the participants to share results, develop a consensus on measurements, and discuss source attribution issues. The workshop also addressed ways to improve the process and suggestions for future studies.

18. Development of a No-Moving-Parts Fourier Transform Infrared Sensor

Conventional FTIR sensors of the passive remote type are available from several commercial manufacturers. The term "passive" is used to indicate that these sensors, unlike laboratory FTIR spectrometers, do not contain an internal infrared (IR) radiation source. Instead,

the sensors are equipped with a special set of input optics which collect ambient IR energy. The term "remote" is used to indicate that gas-phase samples to be measured are located some distance away from the instrument. Passive remote IR sensing is based on the fact that most organic vapors absorb or emit IR radiation at characteristic frequencies and, therefore, have unique IR spectral signatures. The amount of energy absorbed or emitted at these characteristic frequencies is a function of the temperature of the analyte relative to the thermal background.

The fragile component of existing FTIR sensors is the interferometer, which consists of a beam splitter, a stationary mirror, and a moving mirror. To obtain good data, a critical requirement is precise alignment of the two mirrors with respect to the beam splitter. Another requirement is that the moving mirror must maintain constant velocity during the scan. Anything that causes a departure from these criteria can introduce phase errors and other artifacts, which will degrade the data.

The purpose of this ongoing project is to investigate the possibility of creating a novel FTIR sensor with *no moving parts* by creating an optical breadboard prototype. Unlike conventional FTIR sensors, which employ a moving mirror to temporally disperse interferometric information, the goal of this work is to produce an FTIR sensor design that spatially disperses interferometric patterns onto a two-dimensional focal-plane array detector. Since the new FTIR sensor design has no moving parts, the sensor is extremely rugged and immune to vibrations. To date, proof-of-principle has been demonstrated at visible wavelengths and infrared wavelengths of 3 to 5 μm, and data have been collected for carbon dioxide and hexane. Future work will involve demonstrating the prototype at longer IR wavelengths.

19. JANUS Reactor Characterization

The JANUS Biological Irradiation Facility, which operated at ANL-East from 1963 until 1992 to generate high neutron fluxes from highly enriched fuel, is scheduled for decommissioning. As part of the decommissioning process, the hazardous material and radiological characteristics of the facility had to be determined. The hazardous materials characterization provides data on the presence of inorganic and organic hazardous substances, their concentrations, and the potential regulatory status of materials to be disposed. The radiological characterization provides data to be used in assessing the impact of radioactivity on the facility and the surrounding area.

The ACL teamed with the Health Physics staff of ANL's Environment, Safety and Health Division (ESH-HP) in conducting the sampling and analysis needed for the facility characterization. The ESH-HP staff coordinated and conducted the sample collection. They also conducted on-site radioactivity surveys. The ACL was responsible for laboratory analysis of samples for inorganic, organic, and radiological constituents and selected parameters. The hazardous materials characterization included the analysis of soils, sludges, and waters for RCRA parameters, and target analytes and compounds such as pH, metals, volatile and semivolatile organic compounds, PCBs, and total cyanide and sulfide, as well as total organic carbon and phenols. The radiological characterization included the analysis of filters, smears, graphite powders and cores, concrete powders and cores, lead shavings and cores, hard board

cores, and steel and other metal cores for thorium, uranium, plutonium, and gamma-emitting radionuclides. Instrumental analysis techniques such as ICP/AES, atomic absorption spectrophotometry, and ultraviolet-visible spectrophotometry were used in the determinations of inorganic constituents. Gas chromatography and GC/MS were used to measure the organic compounds. Isotope-dilution alpha spectrometric and gamma spectrometric methods were used to determine the radionuclides. The ACL analyzed more than 150 samples in support of the characterization effort.

20. Study of Dry-Storage Casks for Spent Nuclear Fuel

Because available space in spent fuel storage pools is nearly exhausted at some nuclear power plants, commercial electric utilities are implementing dry-storage options to increase their capacity for storing spent fuel. In the dry-storage operations, spent fuel assemblies are loaded into a special cask in the storage pool, water is removed from the cask, and the cask is sealed for removal to aboveground storage. During one such operation at a power plant operated by the Wisconsin Electric Power Company (WEPCo), gas inside the cask ignited while the lid was being welded in place. This ignition was attributed to a buildup of hydrogen caused by chemical interaction between a zinc-based coating used on internal surfaces of the cask and the somewhat acidic storage pool water.

In following up on this incident, WEPCo enlisted ACL support to chemically characterize samples of slightly radioactive solid residues collected from the cask lid and other solids filtered from the water removed from the cask. This characterization included XRD analysis to identify crystalline phases, comprehensive elemental analysis by ICP/AES and other methods, and GC/MS analysis for possible organic constituents. The ACL also analyzed samples of the storage pool water to determine pH, total organic carbon, and metal concentrations. At about the same time, another utility, Entergy Arkansas Nuclear One (EANO), initiated a laboratory study of the interaction between the zinc coating and the water in their spent fuel pool. The ACL provided chemical analysis data to characterize and identify solid residues formed during the EANO tests. The ACL's data helped these utilities better understand the chemistry of the interaction between the storage pool water and the zinc coating inside their dry-storage casks. This understanding, in turn, allowed them to better address engineering and safety issues related to dry-storage operations.

IX

Publications and Presentations—1996

The Division's publications and oral presentations for 1996 were entered into a bibliographic data base. The pages that follow are a printout of this information sorted into six categories: (1) journal articles, books, and book chapters, (2) patents, (3) ANL progress and topical reports, as well as contributions to reports published by organizations other than ANL, (4) abstracts and papers published in proceedings of conferences, symposia, workshops, etc., (5) oral presentations at scientific meetings and seminars not referenced in the fourth category, and (6) papers accepted for publication but not yet published.

Chemical Technology Division Publications and Presentations—1996

A. Journal Articles, Books, and Book Chapters

Microstructure and Phase Identification in Type 304 Stainless Steel-Zirconium Alloys
D. P. Abraham, S. M. McDeavitt, and J. Y. Park
Metall. Mater. Trans. A **27A**, 2151–2159 (1996)

Treatment of Wastes in the IFR Fuel Cycle
J. P. Ackerman, T. R. Johnson, L. S. H. Chow, E. L. Carls, W. H. Hannum, and J. J. Laidler
Prog. Nucl. Energy **31**(1/2), 141–154 (1996)

Determination of Uranium by Flow Injection Inductively Coupled Plasma Mass Spectrometry
J. H. Aldstadt, J. K. Kuo, L. L. Smith, and M. D. Erickson
Anal. Chim. Acta **319**, 135–143 (1996)

Microwave Dissolution of Plant Tissue and the Subsequent Determination of Trace Lanthanide and Actinide Elements by Inductively Coupled Plasma-Mass Spectrometry
J. S. Alvarado, T. J. Neal, L. L. Smith, and M. D. Erickson
Anal. Chim. Acta **322**, 11–20 (1996)

Atomic Spectrometry Update—Atomic Mass Spectrometry
J. R. Bacon, J. S. Crain, A. W. McMahon, and J. G. Williams
J. Anal. At. Spectrom. **11**, 355R–393R (1996)

Containment Attachment for Mixed-Waste Analysis by Graphite Furnace AAS
D. A. Bass, L. B. TenKate, and A. M. Wroblewski
At. Spectrosc. **17**(2), 92–97 (1996)

Main Group Compounds as Amphoteric Ligands to Transition Metals. Synthesis and Molecular Structure of $Cr(CO)_5[PPh_2CH_2Ga(CH_2CMe_3)_2{\cdot}NMe_3]$
O. T. Beachley, M. A. Banks, J. P. Kopasz, and R. D. Rogers
Organometallics **15**, 5170–5174 (1996)

Lithium Ion Transport in a Model of Amorphous Polyethylene Oxide
P. T. Boinske, L. A. Curtiss, J. W. Halley, B. Lin, and A. Sutjianto
J. Computer-Aided Materials Design **3**, 385–402 (1996)

Pyrochemical Treatment of Metals and Oxides
M. C. Bronson and C. C. McPheeters
Chapter 7 in *Separation Techniques in Nuclear Waste Management*, Eds., T. E. Carleson, N. A. Chipman, and C. M. Wai, CRC Press, Boca Raton, FL, pp. 155–167 (1996)

Effect of α-Radiolysis on TRUEX-NPH Solvent
B. A. Buchholz, L. Nuñez, and G. F. Vandegrift
Sep. Sci. Technol. **31**(16), 2231–2243 (1996)

Radiolysis and Hydrolysis of Magnetically Assisted Chemical Separation Particles
B. A. Buchholz, L. Nuñez, and G. F. Vandegrift
Sep. Sci. Technol. **31**(14), 1933–1952 (1996)

Contaminant Uranium Phases and Leaching at the Fernald Site in Ohio
E. C. Buck, N. R. Brown, and N. L. Dietz
Environ. Sci. Technol. **30**(1), 81–88 (1996)

New Argonne Separation Process Cleans Contaminated Soil
D. J. Chaiko
Pollution Prevention Advisor **6**(4), 15 (1996)

Metal Separations Using Aqueous Biphasic Partitioning Systems
D. J. Chaiko, B. Zaslavsky, A. N. Rollins, Y. Vojta, J. Gartelmann, and W. A. Mego
Emerging Separation Technologies for Metals II, Ed., R. G. Bautista, The Minerals, Metals, and Materials Soc., Warrendale, PA, pp. 171–185 (1996)

Hydrido(1,4,8,11,15,18,22,25-octa-*n*-pentylphthalocyaninato)rhodium Dimers: Single-Crystal X-ray Structure and the Isomerization of the Four Isomers
M. J. Chen, L. Nuñez, J. W. Rathke, and R. D. Rogers
Organometallics **15**(9), 2338–2344 (1996)

Phthalocyanines in Hydrocarbon Activation
M. J. Chen and J. W. Rathke
Phthalocyanines: Properties and Applications, Eds., A. B. P. Lever and C. C. Leznoff, Vol. IV, VCH Publishers, Inc., New York, pp. 183–198 (1996)

Removal of Carbon Dioxide in Closed Loop Off-Gas Treatment Systems
M. K. Clemens, P. A. Nelson, and W. M. Swift
J. Environ. Sci. Health **A31**(7), 1801–1825 (1996)

Applications of Inductively Coupled Plasma/Mass Spectrometry in Environmental Radiochemistry
J. S. Crain
Spectrosc. **11**(2), 30–39 (1996)

Waste Reduction in Inductively Coupled Plasma Mass Spectrometry Using Flow Injection and a Direct Injection Nebulizer
J. S. Crain and J. T. Kiely
J. Anal. At. Spectrom. **11**, 525–527 (1996)

Gaussian-2 Theory: Reduced Basis Set of Requirements
L. A. Curtiss, P. C. Redfern, B. J. Smith, and L. Radom
J. Chem. Phys. **104**(13), 5148–5152 (1996)

Investigation of Pulping Effect on Pulp Yield and the Lignin Content of Black Liquor with a Central Composite Kraft Pulping Design

D. Dong and A. L. Fricke

Holzforschung **50**(1), 75–84 (1996)

Kinetics of Dissolution of Uranium Metal Foil by Alkaline Hydrogen Peroxide

D. Dong and G. F. Vandegrift

Nucl. Sci. Eng. **124**, 473–481 (1996)

X-ray Off-Specular Reflectivity Studies of Electrochemical Pitting of Cu Surfaces in Sodium Bicarbonate Solution

Y. P. Feng, S. K. Sinha, C. A. Melendres, and D. D. Lee

Physica B **221**, 251–256 (1996)

The Crystal Structure of Schoepite, $[(UO_2)_8O_2(OH)_{12}](H_2O)_{12}$

R. J. Finch, M. A. Cooper, F. C. Hawthorne, and R. C. Ewing

Can. Mineral. **34**, 1071–1088 (1996)

A Consistent Assessment of the Thermophysical Properties of Sodium

J. K. Fink and L. Leibowitz

High Temp. Mater. Sci. **35**, 65 (1996)

The Release of Uranium, Plutonium, Cesium, Strontium, Technetium and Iodine from Spent Fuel under Unsaturated Conditions

P. A. Finn, J. C. Hoh, S. F. Wolf, S. A. Slater, and J. K. Bates

Radiochim. Acta **74**, 65–71 (1996)

The Chemistry of the Light Rare Earth Elements as Determined by Electron Energy Loss Spectroscopy

J. Fortner and E. C. Buck

Appl. Phys. Lett. **68**(26), 3817–3819 (1996)

The Dreaded Lower Ten Percent

D. W. Green

Managing the Modern Laboratory **2**(1), 2A–3A (1996)

Feedback/Criticism/Praise

D. W. Green

Managing the Modern Laboratory **2**(2), 14A–15A (1996)

Forum on the Future of Chemists

D. W. Green

Managing the Modern Laboratory **2**(1), 11A–12A (1996)

Scientists as Managers

D. W. Green

Managing the Modern Laboratory **1**(4), 68A–69A (1995)

Secondary Waste Minimization in Analytical Methods

D. W. Green, L. L. Smith, J. S. Crain, A. S. Boparai, J. T. Kiely, J. S. Yaeger, and J. B. Schilling

Am. Environ. Lab. **8**(3), 28–29 (1996)

Alkali Carbonates: Raman Spectroscopy, *Ab Initio* Calculations, and Structures
N. Koura, S. Kohara, K. Takeuchi, S. Takahashi, L. A. Curtiss, M. H. Grimsditch, and M.-L. Saboungi
J. Mol. Struct. **382**, 163–169 (1996)

Ceramic Sealants for High Temperatures
M. Krumpelt
CHEMTECH **25**(10), 48 (1995)

Methanol Reformer for Vehicles
M. Krumpelt
CHEMTECH **25**(10), 48 (1995)

Rapid-Start Reformer for Methanol in Fuel-Cell Vehicles
R. Kumar, S. Ahmed, and M. Krumpelt
Electric & Hybrid Vehicle Technology '96, 123–127 (1996)

Development of Pyroprocessing Technology
J. J. Laidler, J. E. Battles, W. E. Miller, J. P. Ackerman, and E. L. Carls
Prog. Nucl. Energy **31**(1/2), 131–140 (1996)

Preliminary Evaluation of a FIBROSIC Candle Filter for Particulate Control in PFBC
S. H. D. Lee, P. Eggerstedt, and J. F. Zievers
J. Inst. Energy **69**(479), 87–95 (1996)

Glass-Ceramic Sealants for Solid Oxide Fuel Cells, Part I: Physical Properties
K. L. Ley, M. Krumpelt, R. Kumar, J. H. Meiser, and I. Bloom
J. Mater. Res. **11**(6), 1489–1493 (1996)

Mode of Lead Addition and Its Effects on Phase Formation and Microstructure Development in $Ag/(Bi,Pb)_2Sr_2Ca_2Cu_3O_x$ Composite Conductors
J. S. Luo, S. E. Dorris, A. K. Fischer, J. S. LeBoy, V. A. Maroni, Y. Feng, and D. C. Larbalestier
Supercond. Sci. Technol. **9**, 412–421 (1996)

Characterization of α-$Ni(OH)_2$ by XPS
A. N. Mansour and C. A. Melendres
Surf. Sci. Spec. **3**(3), 255–262 (1996)

Characterization of Electrochemically Prepared γ-NiOOH by XPS
A. N. Mansour and C. A. Melendres
Surf. Sci. Spec. **3**(3), 271–278 (1996)

Characterization of $KNiIO_6$ by XPS
A. N. Mansour and C. A. Melendres
Surf. Sci. Spec. **3**(3), 287–295 (1996)

Characterization of $Ni_2O_3 \cdot 6\ H_2O$ by XPS
A. N. Mansour and C. A. Melendres
Surf. Sci. Spec. **3**(3), 263–270 (1996)

Characterization of Slightly Hydrated $Ni(OH)_2$ by XPS
A. N. Mansour and C. A. Melendres
Surf. Sci. Spec. **3**(3), 247–254 (1996)

An X-ray Absorption Near-Edge Spectroscopic Study of the Structure of Passive Films on Amorphous Al-Fe-Ce Alloys
A. N. Mansour, C. A. Melendres, S. J. Poon, Y. He, and G. J. Shiflet
J. Electrochem. Soc. **143**(2), 614–619 (1996)

Use of Fourier Transform Infrared Spectroscopy as a Continuous Emission Monitor
Z. Mao, J. C. Demirgian, A. Mathew, and R. Hyre
Waste Manage. **15**, 567 (1995)

Hot-Isostatic Pressing of U-10Zr by a Coupled Grain Boundary Diffusion and Creep Cavitation Mechanism
S. M. McDeavitt and A. A. Solomon
J. Nucl. Mater. **228**, 184–200 (1996)

In-Situ Laser Raman and Infrared Spectroscopic Studies of Anodic Corrosion Films on Metals
C. A. Melendres
New Techniques for Characterizing Corrosion and Stress Corrosion, Eds., R. H. Jones and D. R. Baer, The Minerals, Metals, and Materials Soc., pp. 33–51 (1996)

In-Situ Far Infrared Spectroscopy of Electrode Surfaces with a Synchrotron Source
C. A. Melendres, G. A. Bowmaker, B. Beden, and J. M. Leger
New Directions in Electroanalytical Chemistry, Eds., J. Leddy and M. Wrightman, Electrochem. Soc., Pennington, NJ, Vol. 96-9, pp. 224–233 (1996)

Description and Classification of Uranyl Oxide Hydrate Sheet Anion Topologies
M. L. Miller, R. J. Finch, P. C. Burns, and R. C. Ewing
J. Mater. Res. **11**, 3048–3056 (1996)

Thermodynamics of (germanium + selenium): A Review and Critical Assessment
P. A. G. O'Hare, A. Zywocinski, and L. A. Curtiss
J. Chem. Thermodyn. **28**, 459–480 (1996)

Investigation of Through-Bond Coupling Dependence on Spacer Structure
B. P. Paulson, L. A. Curtiss, B. Bal, G. L. Closs, and J. R. Miller
J. Am. Chem. Soc. **118**(2), 378–387 (1996)

Phase Identification of a U-Zr/Ni-Cr Diffusion Couple Using Synchrotron Radiation
M. C. Petri, L. Leibowitz, M. H. Mueller, J. W. Richardson, Jr., and D. D. Keiser, Jr.
J. Mater. Res. **11**, 332 (1996)

NMR for Solids
J. W. Rathke
CHEMTECH **25**(10), 48 (1995)

Theoretical Studies of Growth of Diamond (110) from Dicarbon
P. C. Redfern, D. A. Horner, L. A. Curtiss, and D. M. Gruen
J. Phys. Chem. **100**(28), 11654–11663 (1996)

Oxygen Tracer Diffusion in $La_{1-x}Sr_xCoO_3$
J. L. Routbort, R. Doshi, and M. Krumpelt
Solid State Ionics **90**(1–4), 21–27 (1996)

Electron Binding Energy and Long-Range Electronic Coupling. A Theoretical Study
B. Sengupta, L. A. Curtiss, and J. R. Miller
J. Chem. Phys. **104**(24), 9888–9896 (1996)

Surface-Enhanced Raman Spectroelectrochemical Studies of Corrosion Films on Iron in Aqueous Carbonate Solutions
L. J. Simpson and C. A. Melendres
J. Electrochem. Soc. **143**(7), 2146–2152 (1996)

Temperature Dependence of the Surface Enhanced Raman Spectroelectrochemistry of Iron in Aqueous Solutions
L. J. Simpson and C. A. Melendres
Electrochim. Acta **41**(10), 1727–1730 (1996)

Application of Empore^{TM} Strontium Rad Disks to the Analysis of Radiostrontium in Environmental Water Samples
L. L. Smith, K. A. Orlandini, J. S. Alvarado, K. M. Hoffmann, D. C. Seely, and R. T. Shannon
Radiochim. Acta **73**, 165–170 (1996)

High-Pressure Microwave Digestion: A Waste Minimization Tool for the Radiochemistry Laboratory
L. L. Smith and J. S. Yaeger
Radioact. Radiochem. **7**(2), 35–38 (1996)

Geochemical Characteristics of the Yufuin Outflow Plume, Beppu Hydrothermal System, Japan
N. C. Sturchio, S. Ohsawa, Y. Sano, G. B. Arehart, K. Kitaoka, and Y. Yusa
Geothermics **25**(2), 215–230 (1996)

Oxygen Stoichiometry, Phase Stability, and Thermodynamic Behavior of the Lead-Doped and Lead-Free Bi-2212 Systems
M. Tetenbaum, M. C. Hash, B. S. Tani, and V. A. Maroni
Physica C **270**, 114–128 (1996)

Some Aspects of the Thermodynamic Behavior of the Lead-Doped Bi-2223 System
M. Tetenbaum and V. A. Maroni
Physica C **260**, 71–80 (1996)

The Thermal Stability of Lithium-Manganese-Oxide Spinel Phases
M. M. Thackeray, M. F. Mansuetto, D. W. Dees, and D. R. Vissers
Mater. Res. Bull. **31**, 133 (1996)

Thermal Stability of $Li_4Mn_5O_{12}$ Electrodes for Lithium Batteries
M. M. Thackeray, M. F. Mansuetto, and C. S. Johnson
J. Solid State Chem. **125**, 274–277 (1996)

Materials for Electrochemical Energy Storage

D. R. Vissers, V. S. Battaglia, D. W. Dees, A. N. Jansen, C. S. Johnson, A. J. Kahaian, M. F. Mansuetto, K. M. Myles, J. Prakash, and M. M. Thackeray

Electric & Hybrid Vehicle Technology '96, 119–121 (1996)

Imaging Diffusion in Toroid Cavity Probes

K. Woelk, R. E. Gerald, R. J. Klingler, and J. W. Rathke

J. Magn. Reson. A **121**, 74–77 (1996)

Ten-Year Results from Unsaturated Drip Tests with UO_2 at 90°C: Implications for the Geologic Disposal of Spent Nuclear Fuel

D. J. Wronkiewicz, J. K. Bates, S. F. Wolf, and E. C. Buck

J. Nucl. Mater. **238**, 78–95 (1996)

Computational Studies of Water Adsorption in the Zeolite H-ZSM-5

S. A. Zygmunt, L. A. Curtiss, L. E. Iton, and M. K. Erhardt

J. Phys. Chem. **100**(16), 6663–6671 (1996)

B. Patents

Corrosion-Resistant Ceramic Materials
T. D. Kaun
Patent No. 5,538,810, issued July 23, 1996

Li-Alloy Electrode for Li-Alloy/Metal Sulfide Cells
T. D. Kaun
Patent No. 5,536,600, issued July 16, 1996

Molten Salt Electrolyte Separator
T. D. Kaun
Patent No. 5,534,367, issued July 19, 1996

Advanced Electrorefiner Design
W. E. Miller, E. C. Gay, and Z. Tomczuk
Patent No. 5,531,868, issued July 2, 1996

Electrochemical Cell
L. Redey, K. M. Myles, and D. R. Vissers
Patent No. 5,532,078, issued July 2, 1996

Electrochemical Cell
L. Redey, D. R. Vissers, and J. Prakash
Patent No. 5,536,593, issued July 16, 1996

Nuclear Resonance Tomography with a Toroid Cavity Detector
K. Woelk, J. W. Rathke, and R. J. Klingler
Patent No. 5,574,370, issued November 12, 1996

C. Reports

Arsenic Speciation in Soil Using High Performance Liquid Chromatography/Inductively Coupled Plasma/Mass Spectrometry

D. A. Bass, Y. S. Yaeger, K. J. Parish, J. S. Crain, J. T. Kiely, M. J. Gowdy, G. B. Mohrman, and M. G. Besmer

ANL/ACL-96/2 (February 1996)

ANL Technical Support Program for DOE Office of Environmental Management Annual Report, October 1994–September 1995

J. K. Bates, E. C. Buck, N. L. Dietz, T. DiSanto, W. L. Ebert, J. W. Emery, J. Fortner, L. D. Hafenrichter, J. C. Hoh, J. S. Luo, L. Nuñez, M. T. Surchik, S. F. Wolf, and D. J. Wronkiewicz

ANL-96/11 (July 1996)

Electric Vehicle Battery Testing and Development Project at Argonne National Laboratory

W. H. DeLuca, J. E. Kulaga, A. F. Tummillo, and C. E. Webster

Electric Power Research Institute Report EPRI RP3150-01 (May 1996)

Analysis of Components from Drip Tests with ATM-10 Glass

J. Fortner, J. K. Bates, and T. J. Gerding

ANL-96/16 (September 1996)

Comparison of SW-846 Method 3051 and SW-846 Method 7471A for the Preparation of Solid Waste Samples for Mercury Determination

J. M. Giaquinto, A. M. Essling, and J. M. Keller

Oak Ridge National Laboratory Report ORNL/TM-13236 (1996)

Analytical Chemistry Laboratory Progress Report for FY 1996

D. W. Green, A. S. Boparai, D. L. Bowers, D. G. Graczyk, and P. C. Lindahl (with contributions from ACL staff)

ANL/ACL-96/6 (December 1996)

Chemical Technology Division Annual Technical Report, 1995

J. J. Laidler et al.

ANL-96/10 (June 1996)

Fuel Contaminant Removal and Methanol Burners for Reformer and Thermal Management System Start-Up

S. H. D. Lee, S. Ahmed, and R. Kumar

International Fuel Cells Corporation Report, ANL Contract No. 85E04 (December 1996)

Measurement of Alkali Vapor/Aerosol in PFBC Exhaust Gas at 71 MWe Wakamatsu PFBC Demonstration Plant

S. H. D. Lee and W. M. Swift

Final Report for ANL Contract 85976. Prepared for Ishikawajima-Harima Heavy Industry Co., Ltd., Tokyo, Japan (March 1996)

Development of the Vitrification Compositional Envelope to Support Complex-Wide Application of MAWS Technology

J. J. Mazer (editor)

DOE/CH-9601 (September 1996)

Evaluation of Three Analytical Techniques Used to Determine High Levels of Volatile Organic Compounds in Type IV Sludge from Rocky Flats Plant

K. J. Parish, D. V. Applegate, Y. Tsai, A. S. Boparai, and G. T. Reedy

ANL/ACL-96/3 (January 1996)

Rapid Determination of Radiostrontium Using Empore^{TM} Strontium Rad Disks

L. L. Smith, K. A. Orlandini, J. A. Alvardo, K. M. Hoffmann, D. C. Seely, and R. T. Shannon

DOE/EM-0089T, Method RP515, DOE Methods for Evaluating Environmental and Waste Management Samples (September 1996)

Separation Science and Technology Semiannual Progress Report, April–September 1993

G. F. Vandegrift, D. B. Chamberlain, C. Conner, J. M. Copple, K. Foltz, B. Gebby, J. C. Hutter, R. A. Leonard, L. Nuñez, M. C. Regalbuto, A. Rozeveld, J. Sedlet, B. Srinivasan, D. Taylor, and D. G. Wygmans

ANL-95/43 (January 1996)

D. Abstracts and Proceedings Papers

Metal Waste Forms from the Electrometallurgical Treatment of Spent Nuclear Fuel

D. P. Abraham, S. M. McDeavitt, and J. Y. Park

Proc. of the Embedded Topical Meeting on DOE Spent Nuclear Fuel and Fissile Material Management, Am. Nucl. Soc., Reno, NV, June 16–20, 1996, pp. 123–128 (1996)

Transportation Fuel Cell Research at Argonne National Laboratory

R. K. Ahluwalia, S. Ahmed, H. K. Geyer, G. L. Henriksen, M. Krumpelt, R. Kumar, and K. M. Myles

Preprints of the Annual Automotive Technology Development Customers' Coordination Meeting, Dearborn, MI, October 28–November 1, 1996

Processing of LEU Targets for ^{99}Mo Production—Demonstration of a Modified Cintichem Process

Z. Aliludin, A. Mutalib, A. Sukmana, Kadarisman, A. H. Gunawan, G. F. Vandegrift, B. Srinivasan, J. L. Snelgrove, D. Wu, and S. Landsberger

Proc. of the 18th Int. Meeting on Reduced Enrichment for Research and Test Reactors, Ed., A. Ballagny, Paris, France, September 17–21, 1995, French Atomic Energy Commission, Section 3–4 (1996)

Glass as a Waste Form for the Immobilization of Plutonium

J. K. Bates, A. J. G. Ellison, J. W. Emery, and J. C. Hoh

Mater. Res. Soc. Symp. Proc. **412**, 57–64 (1996)

Alternative Cathodes for Molten Carbonate Fuel Cells

I. Bloom, M. T. Lanagan, M. F. Roche, and M. Krumpelt

Proc. of the EPRI/GRI Fuel Cell Workshop on Fuel Cell Technology Research and Development, Tempe, AZ, April 2–3, 1996, Section 21 (1996)

Processing of LEU Targets for ^{99}Mo Production—Dissolution of U_3Si_2 Targets by Alkaline Hydrogen Peroxide

B. A. Buchholz and G. F. Vandegrift

Proc. of the 18th Int. Meeting on Reduced Enrichment for Research and Test Reactors, Ed., A. Ballagny, Paris, France, September 17–21, 1995, French Atomic Energy Commission, Section 3–6 (1996)

Neutron Powder Diffraction of Operating Electrochemical Cells Containing $LaNi_{5-y}Al_yD_x$ Electrodes

G. L. Burr, J. W. Richardson, J. M. Carpenter, W. Peng, L. Redey, and A. N. Jansen

Abstracts, Int. Union of Crystallography: XVII Congress and General Assembly, Seattle, WA, August 8–17, 1996, p. C-413 (1996)

Progress in Alkaline Peroxide Dissolution of Low-Enriched Uranium Metal and Silicide Targets

L. Chen, D. Dong, B. A. Buchholz, G. F. Vandegrift, and D. Wu

Proc. of the 19th Int. Meeting on Reduced Enrichment for Research and Test Reactors (RERTR), Seoul, Korea, October 7–10, 1996, pp. 180–188 (1996)

Alkali-Vapor Measurements in the Wakamatsu PFBC Plant

Y. Daijou, S. H. D. Lee, K. Suzuki, T. Ishinomori, T. Yanagisawa, and Y. Tsumita

High Temperature Gas Cleaning, Eds., E. Schmidt, P. Gäng, T. Pilz, and A. Dittler, Proc. of the Third Int. Symp. and Exhibition on Gas Cleaning at High Temperatures, University of Karlsruhe, Karlsruhe, Germany, September 18–20, 1996, pp. 664–683 (September 1996)

Processing of LEU Targets for ^{99}Mo Production—Dissolution of Metal Foil Targets by Alkaline Hydrogen Peroxide

D. Dong, G. F. Vandegrift, S. Amini, J. B. Hersubeno, H. Nasution, and Y. Nampira

Proc. of the 18th Int. Meeting on Reduced Enrichment for Research and Test Reactors, Ed., A. Ballagny, Paris, France, September 17–21, 1995, French Atomic Energy Commission, Section 3–5 (1996)

Ceria-Based SOFC Development

R. Doshi and M. Krumpelt

Proc. of the EPRI/GRI Fuel Cell Workshop on Fuel Cell Technology Research and Development, Tempe, AZ, April 2–3, 1996, Section 13 (1996)

Characterization of Ceria-Based SOFCs

R. Doshi, J. Rautbort, and M. Krumpelt

Extended Abstracts, Fuel Cell Seminar, Kissimmee, FL, November 17–20, 1996, p. 151 (1996)

Measurement of the Glass Dissolution Rate in the Presence of Alteration Phases

W. L. Ebert, A. J. Bakel, and N. R. Brown

Proc. of the Spectrum '96 Meeting, Nuclear and Hazardous Waste Management Int. Topical Meeting, Am. Nucl. Soc., Seattle, WA, August 18–23, 1996, pp. 569–575 (1996)

The Long-Term Corrosion Behavior of Environmental Assessment Glass

W. L. Ebert and J. K. Bates

Proc. of the Seventh Annual Int. High-Level Radioactive Waste Management Conf., Am. Nucl. Soc., Las Vegas, NV, April 29–May 3, 1996, pp. 399–401 (1996)

The Release of Technetium from Defense Waste Processing Facility Glasses

W. L. Ebert, S. F. Wolf, and J. K. Bates

Mater. Res. Soc. Symp. Proc. **412**, 221–227 (1996)

The Crystal Structure of Schoepite, $[(UO_2)_8O_2(OH)_{12}](H_2O)_{12}$

R. J. Finch, M. A. Cooper, F. C. Hawthorne, and R. C. Ewing

Abstracts, Joint Annual Meeting of the Geologic Association of Canada and the Mineralogical Association of Canada, Winnipeg, Manitoba, Canada, May 27–29, 1996, Vol. 21 (1996)

Phase Transformations and Crystallographic Relations among Schoepite, Metaschoepite, and Dehydrated Schoepite

R. J. Finch, F. C. Hawthorne, and R. C. Ewing

Abstracts, Joint Annual Meeting of the Geologic Association of Canada and the Mineralogical Association of Canada, Winnipeg, Manitoba, Canada, May 27–29, 1996, Vol. 21 (1996)

Schoepite and Dehydrated Schoepite
R. J. Finch, F. C. Hawthorne, and R. C. Ewing
Mater. Res. Soc. Symp. Proc. **412**, 361–368 (1996)

U-Series Ages of Secondary Uranium Minerals with Applications to the Long-Term Evolution of Spent Nuclear Fuel
R. J. Finch, J. Suksi, K. Rasilainen, and R. C. Ewing
Mater. Res. Soc. Symp. Proc. **412**, 823–830 (1996)

The Release of Cesium and the Actinides from Spent Fuel under Unsaturated Conditions
P. A. Finn, J. C. Hoh, S. F. Wolf, S. A. Slater, and J. K. Bates
Mater. Res. Soc. Symp. Proc. **412**, 75–81 (1996)

The Release of Uranium, Plutonium, Cesium, Strontium, Technetium, and Iodine from Spent Fuel under Unsaturated Conditions
P. A. Finn, J. C. Hoh, S. F. Wolf, S. A. Slater, and J. K. Bates
Proc. of the Fifth Int. Conf. on the Chemistry and Migration Behaviour of Actinides and Fission Products in the Geosphere, MIGRATION '95, Saint-Malo, France, September 10–15, 1995, pp. 65–71 (1996)

Radionuclide Release for Unsaturated Spent Fuel Tests—First 1.6 Years
P. A. Finn, S. F. Wolf, and J. K. Bates
Proc. of the Seventh Annual Int. High-Level Radioactive Waste Management Conf., Am. Nucl. Soc., Las Vegas, NV, April 29–May 3, 1996, pp. 390–392 (1996)

Long-Term Results from Unsaturated Durability Testing of Actinide-Doped DWPF and WVDP Waste Glasses
J. Fortner and J. K. Bates
Mater. Res. Soc. Symp. Proc. **412**, 205–211 (1996)

A Glovebox Design Checklist
A. A. Frigo
Proc. of the Ninth Annual Conf. and Equipment Display of the Am. Glovebox Soc., Minneapolis, MN, July 19–22, 1995, pp. 100–107 (1995)

Storage- and Furnace-Well Design for Large, User-Friendly Gloveboxes
A. A. Frigo, R. F. Malecha, J. L. Bailey, R. L. Tollner, and S. G. Wiedmeyer
Proc. of the Tenth Annual Conf. and Equipment Display of the Am. Glovebox Soc., San Diego, CA, July 22–25, 1996, pp. 36–68 (1996)

Dynamic Response of Steam-Reformed, Methanol-Fueled, Polymer Electrolyte Fuel Cell Systems
H. K. Geyer, R. K. Ahluwalia, and R. Kumar
Proc. of the 31st Intersoc. Energy Conversion Eng. Conf., Washington, DC, August 11–16, 1996, pp. 1101–1106 (1996)

Secondary Phase Formation and the Microstructural Evolution of the Surface Layer during Vapor Phase Alteration of the French SON 68 Nuclear Waste Glass at 200°C
W. L. Gong, R. C. Ewing, L.-M. Wang, E. Vernaz, J. K. Bates, and W. L. Ebert
Mater. Res. Soc. Symp. Proc. **412**, 377–384 (1996)

A Survey of Continuous Emission Monitoring Technologies for Volatile Organic Compounds, HCl, and Ammonia

W. J. Haas, N. French, J. C. Demirgian, and C. T. Snyder

Proc. of the Int. Incineration Conf. on Incineration and Thermal Treatment Technologies, Savannah, GA, May 6–10, 1996, pp. 409–414 (1996)

Investigation of CoS_2 as an Additive in a Rechargeable $LiAl/FeS_2$ Cell

A. N. Jansen, T. D. Kaun, M. C. Hash, D. R. Vissers, and G. L. Henriksen

Abstracts, 190th Electrochem. Soc. Meeting, San Antonio, TX, October 6–11, 1996, Vol. 96–2, pp. 153–154 (1996)

Thermodynamic Considerations for the Use of Vanadium Alloys with Ceramic Breeder Materials

C. E. Johnson, I. Johnson, and J. P. Kopasz

Proc. of the Fourth Int. Workshop on Ceramic Breeder Blanket Interactions, Kyoto, Japan, October 9–11, 1995, pp. 249–258 (1996)

Lithium-Oxide-Stabilized Alpha Manganese Dioxide for Rechargeable Lithium Batteries

C. S. Johnson, D. W. Dees, M. F. Mansuetto, M. M. Thackeray, D. R. Vissers, D. Argyriou, C.-K. Loong, and L. Christensen

Abstracts, 190th Electrochem. Soc. Meeting, San Antonio, TX, October 6–11, 1996, Vol. 96–2, pp. 1076–1077 (1996)

Treatment of Oxide Spent Fuel Using the Lithium Reduction Process

E. J. Karell, R. D. Pierce, and T. P. Mulcahey

Proc. of the Embedded Topical Meeting on DOE Spent Nuclear Fuel and Fissile Material Management, Am. Nucl. Soc., Reno, NV, June 16–20, 1996, pp. 352–358 (1996)

Sulfide Ceramics in Molten-Salt Electrolyte Batteries

T. D. Kaun, M. C. Hash, and D. R. Simon

Ceram. Trans. **65**, 293–310 (1996)

Development of a High-Rate, Rechargeable Bipolar $LiAl/FeS_2$ Battery

T. D. Kaun, A. N. Jansen, M. C. Hash, J. Prakash, R. L. Turner, and G. L. Henriksen

Proc. of the 37th Power Sources Symp., Cherry Hill, NJ, June 17–20, 1996, pp. 338–341 (1996)

Modification of LiCl-LiBr-KBr Electrolyte for $LiAl/FeS_2$ Batteries

T. D. Kaun, A. N. Jansen, G. L. Henriksen, and D. R. Vissers

Extended Abstracts, 189th Electrochem. Soc. Meeting, Los Angeles, CA, May 5–10, 1996, Vol. 96–1, p. 1178 (1996)

Modification of LiCl-LiBr-KBr Electrolyte for $LiAl/FeS_2$ Batteries

T. D. Kaun, A. N. Jansen, G. L. Henriksen, and D. R. Vissers

Proc. of the Tenth Symp. on Molten Salts, Electrochem. Soc. Meeting, Los Angeles, CA, May 5–10, 1996, Vol. 96–7, p. 342 (1996)

Actinide-Containing Metal Disposition Alloys

D. D. Keiser and S. M. McDeavitt

Proc. of the Embedded Topical Meeting on DOE Spent Nuclear Fuel and Fissile Material Management, Am. Nucl. Soc., Reno, NV, June 16–20, 1996, pp. 178–182 (1996)

Investigation of the Interactions of $H_2O_{(g)}$ with Li_2ZrO_3

J. P. Kopasz and C. E. Johnson

Proc. of the Fourth Int. Workshop on Ceramic Breeder Blanket Interactions, Kyoto, Japan, October 9–11, 1995, pp. 224–234 (1996)

In Situ NMR Spectroscopy Studies of Hydroformylation Catalysts Using High Pressure Toroid Probes

K. W. Kramarz, R. J. Klingler, and J. W. Rathke

Abstracts, Sixth Int. Conf. on the Chemistry of the Platinum Group Metals, University of York, England, July 21–26, 1996, p. 48 (1996)

Partial Oxidation Reforming of Methanol

M. Krumpelt, S. Ahmed, and R. Kumar

Proc. of the EPRI/GRI Fuel Cell Workshop on Fuel Cell Technology Research and Development, Tempe, AZ, April 2–3, 1996, Section 24 (1996)

Sealants for Solid Oxide Fuel Cells

T. W. Kueper, I. Bloom, and M. Krumpelt

Proc. of the EPRI/GRI Fuel Cell Workshop on Fuel Cell Technology Research and Development, Tempe, AZ, April 2–3, 1996, Section 17 (1996)

The Low-Temperature Partial-Oxidation Reforming of Fuels for Transportation Fuel Cell Systems

R. Kumar, S. Ahmed, and M. Krumpelt

Extended Abstracts, Fuel Cell Seminar, Kissimmee, FL, November 17–20, 1996, p. 750 (1996)

Lithium-Ferrate-Based Cathodes for Molten Carbonate Fuel Cells

M. T. Lanagan, I. Bloom, T. D. Kaun, J. Wolfenstine, and M. Krumpelt

Extended Abstracts, Fuel Cell Seminar, Kissimmee, FL, November 17–20, 1996, p. 402 (1996)

Removal of Sulfur Contaminants in Methanol for Fuel Cell Applications

S. H. D. Lee, R. Kumar, and R. Sederquist

Extended Abstracts, Fuel Cell Seminar, Kissimmee, FL, November 17–20, 1996, pp. 690–693 (1996)

Progress in Dissolving Modified LEU Cintichem Targets

R. A. Leonard, L. Chen, C. J. Mertz, and G. F. Vandegrift

Proc. of the 19th Int. Meeting on Reduced Enrichment for Research and Test Reactors (RERTR), Seoul, Korea, October 7–10, 1996, pp. 189–197 (1996)

Lead-Rich Phases in Partially Processed Ag/Bi-2223 Composite Conductors

J. S. Luo, N. Merchant, V. A. Maroni, M. C. Hash, and M. W. Rupich

Proc. of the Symp. on High Temperature Superconductors: Synthesis, Processing, and Large-Scale Applications, 125th Annual Meeting and Exposition of the Minerals, Metals, and Materials Soc., Anaheim, CA, February 4–8, 1996, pp. 33–42 (1996)

Large, User-Friendly Glovebox Design

R. F. Malecha, A. A. Frigo, R. L. Tollner, and S. G. Wiedmeyer

Proc. of the Tenth Annual Conf. and Equipment Display of the Am. Glovebox Soc., San Diego, CA, July 22–25, 1996, pp. 99–117 (1996)

Glovebox Window Seal Test

R. F. Malecha, D. E. Preuss, and S. G. Wiedmeyer

Proc. of the Ninth Annual Conf. and Equipment Display of the Am. Glovebox Soc., Minneapolis, MN, July 19–22, 1995, p. 99 (1995)

Alloy Waste Forms for Metal Fission Products and Actinides Isolated by Spent Nuclear Fuel Treatment

S. M. McDeavitt, D. P. Abraham, D. D. Keiser, and J. Y. Park

Proc. of the Second Int. Symp. on Extraction and Processing for the Treatment and Minimization of Wastes, Scottsdale, AZ, October 27–30, 1996, pp. 177–189 (1996)

Stainless Steel-Zirconium Alloy Waste Forms for Metallic Fission Products and Actinides Isolated during Treatment of Spent Nuclear Fuel

S. M. McDeavitt, D. P. Abraham, D. D. Keiser, and J. Y. Park

Proc. of the Spectrum '96 Meeting, Nuclear and Hazardous Waste Management Int. Topical Meeting, Am. Nucl. Soc., Seattle, WA, August 18–23, 1996, pp. 2477–2484 (1996)

Synchrotron Far Infrared Spectroscopy for the *In-Situ* Study of Surface Films on Metals

C. A. Melendres, G. A. Bowmaker, B. Beden, and J. M. Leger

Abstracts, 190th Electrochem. Soc. Meeting, San Antonio, TX, October 6–11, 1996, Vol. 96–2, p. 329 (1996)

In-Situ Far Infrared Spectroscopy of Electrode Surfaces with a Synchrotron Source

C. A. Melendres, G. A. Bowmaker, B. Beden, and J. M. Leger

Extended Abstracts, 189th Electrochem. Soc. Meeting, Los Angeles, CA, May 5–10, 1996, Vol. 96–1, p. 1301 (1996)

Decontamination of Actinides and Fission Products from Stainless Steel Surfaces

C. J. Mertz, D. B. Chamberlain, L. Chen, C. Conner, G. F. Vandegrift, D. Drockelman, M. D. Kaminski, S. Landsberger, and J. Stubbins

Proc. of the Am. Nucl. Soc. Topical Meeting on Decontamination and Decommissioning, Chicago, IL, April 14–17, 1996, pp. 125–131 (1996)

Description and Classification of Uranium Oxide Hydrate Sheet Topologies

M. L. Miller, R. J. Finch, P. C. Burns, and R. C. Ewing

Mater. Res. Soc. Symp. Proc. **412**, 369–376 (1996)

In Situ Investigation of the Electrode/Electrolyte Interface by Synchrotron X-ray Scattering

Z. Nagy and H. You

Extended Abstracts, 189th Electrochem. Soc. Meeting, Los Angeles, CA, May 5–10, 1996, Vol. 96–1, pp. 1348–1349 (1996)

Electrochemical and *In Situ* Neutron Diffraction Investigations of La-Ni-Al-H Alloys

W. Peng, L. Redey, D. R. Vissers, K. M. Myles, J. E. Carpenter, J. W. Richardson, and G. Burr

Extended Abstracts, 189th Electrochem. Soc. Meeting, Los Angeles, CA, May 5–10, 1996, Vol. 96–1, pp. 81–82 (1996)

Fission Product Removal from Molten Salt Using Zeolite

C. Pereira, B. D. Babcock, and J. C. Hutter

Proc. of the Second Int. Symp. on Extraction and Processing for Treatment and Management of Wastes, Scottsdale, AZ, October 27–30, 1996, pp. 139–151 (1996)

Overview of Mineral Waste Form Development for the Electrometallurgical Treatment of Spent Nuclear Fuel

C. Pereira, M. A. Lewis, and J. P. Ackerman

Proc. of the Embedded Topical Meeting on DOE Spent Nuclear Fuel and Fissile Material Management, Am. Nucl. Soc., Reno, NV, June 16–20, 1996, pp. 129–136 (1996)

Future of High Temperature Systems for EVs

J. Prakash, L. Redey, P. A. Nelson, and D. R. Vissers

Abstracts, 190th Electrochem. Soc. Meeting, San Antonio, TX, October 6–11, 1996, Vol. 96–2, pp. 754–755 (1996)

Calculations of Heat Evolution for a Lithium-Polymer/Metal Oxide Cell Based on Thermodynamic Parameters

J. Prakash, R. L. Turner, D. W. Dees, M. M. Thackeray, and D. R. Vissers

Abstracts, 190th Electrochem. Soc. Meeting, San Antonio, TX, October 6–11, 1996, Vol. 96–2, pp. 106–107 (1996)

Solubility of Li_2S in $LiAl/FeS_2$ Battery Type Cells

J. Prakash, R. L. Turner, G. L. Henriksen, and D. R. Vissers

Abstracts, 190th Electrochem. Soc. Meeting, San Antonio, TX, October 6–11, 1996, Vol. 96–2, pp. 149–150 (1996)

Toroid NMR Studies

J. W. Rathke, R. J. Klingler, M. J. Chen, K. W. Kramarz, and R. E. Gerald

Proc. of the Tenth DOE/BES Heterogeneous Catalysis and Surface Chemistry Research Conf., Lake Conroe, TX, May 21–24, 1996, pp. 121–124 (1996)

Spectroscopy of Plutonium-Organic Complexes

M. K. Richmann and D. T. Reed

Mater. Res. Soc. Symp. Proc. **412**, 623–630 (1996)

Comparison of Instrumental Methods Used in the Determination of Uranium and Plutonium

C. S. Sabau, D. L. Bowers, and F. P. Smith

Proc. of the Second Argonne National Laboratory Technical Women's Symp., Argonne, IL, April 29–30, 1996, p. 113 (1996)

Intercalation Compounds Used as Anodes in Lithium Secondary Batteries

G. Sandi, R. E. Winans, C. S. Johnson, P. C. Stair, and C. Li

Abstracts, 190th Electrochem. Soc. Meeting, San Antonio, TX, October 6–11, 1996, Vol. 96–2, p. 1061 (1996)

Evaluation of Standard Durability Tests towards the Qualification Process for the Glass-Zeolite Ceramic Waste Form

L. J. Simpson and D. J. Wronkiewicz

Abstracts, Fall Meeting of the Materials Research Soc., Boston, MA, December 2–5, 1996, p. 744 (1996)

Development and Processing of LEU Targets for ^{99}Mo Production—Overview of the ANL Program

J. L. Snelgrove, G. L. Hofman, T. C. Wiencek, C. T. Wu, G. F. Vandegrift, S. B. Aase, B. A. Buchholz, D. Dong, R. A. Leonard, B. Srinivasan, D. Wu, A. Suripto, and Z. Aliluddin

Proc. of the 18th Int. Meeting on Reduced Enrichment for Research and Test Reactors, Ed., A. Ballagny, Paris, France, September 17–21, 1995, French Atomic Energy Commission, Section 3–1 (1996)

Processing of LEU Targets for ^{99}Mo Production—Dissolution of Metal Foils by Nitric-Acid/Sulfuric-Acid Mixtures

B. Srinivasan, R. A. Leonard, S. B. Aase, G. F. Vandegrift, A. A. Rauf, H. Lubis, A. Hardi, S. Amini, and Y. Nampira

Proc. of the 18th Int. Meeting on Reduced Enrichment for Research and Test Reactors, Ed., A. Ballagny, Paris, France, September 17–21, 1995, French Atomic Energy Commission, Section 3–2 (1996)

The Russian American Fuel Cell Consortium

A. Sylvester, R. Baker, and M. Krumpelt

Extended Abstracts, Fuel Cell Seminar, Kissimmee, FL, November 17–20, 1996, p. 421 (1996)

Services Design for Large, User-Friendly Gloveboxes

R. L. Tollner, R. F. Malecha, A. A. Frigo, and S. G. Wiedmeyer

Proc. of the Tenth Annual Conf. and Equipment Display of the Am. Glovebox Soc., San Diego, CA, July 22–25, 1996, p. 204 (1996)

Alkali Emission Measurement in Atmospheric Circulating Fluidized Bed Combustors

J. Tuncay, K. M. Sellakumar, and S. H. D. Lee

Proc. of the Fifth Int. Conf. on Circulating Fluidized Beds, May 28–June 1, 1996, Beijing, People's Republic of China, pp. CSNA9-1 to -6 (1996)

High-Performance Iron Sulfide Electrode Development Studies

R. L. Turner, J. Prakash, J. Henzi, G. L. Henriksen, and D. R. Vissers

Abstracts, 190th Electrochem. Soc. Meeting, San Antonio, TX, October 6–11, 1996, Vol. 96–2, pp. 147–148 (1996)

Charge Transfer Mechanisms in LiAl/FeS_2 Cells

R. L. Turner, J. Prakash, E. Skinner, D. R. Vissers, and G. L. Henriksen

Abstracts, 190th Electrochem. Soc. Meeting, San Antonio, TX, October 6–11, 1996, Vol. 96–2, pp. 151–152 (1996)

Material Movement in Large, User-Friendly Gloveboxes

S. G. Wiedmeyer, R. F. Malecha, A. A. Frigo, and R. L. Tollner

Proc. of the Tenth Annual Conf. and Equipment Display of the Am. Glovebox Soc., San Diego, CA, July 22–25, 1996, pp. 217–240 (1996)

Radionuclide Content of Simulated and Fully Radioactive SRL Waste Glasses: Comparison of Results from ICP-MS, Gamma Spectrometry, and Alpha Spectrometry

S. F. Wolf and J. K. Bates

Mater. Res. Soc. Symp. Proc. **412**, 107–111 (1996)

Safety Considerations in the Design and Use of Gloveboxes

R. D. Wolson

Proc. of the Tenth Annual Conf. and Equipment Display of the Am. Glovebox Soc., San Diego, CA, July 22–25, 1996, p. 241 (1996)

Alteration Paragenesis of Uraninite under Oxidizing Conditions: Accelerated Corrosion Tests versus Natural Analogue Occurrences

D. J. Wronkiewicz, J. K. Bates, and E. C. Buck

Abstracts, Joint Annual Meeting of the Geological Association of Canada and the Mineralogical Association of Canada, Winnipeg, Manitoba, Canada, May 27–29, 1996, Vol. 21 (1996)

Apatite- and Monazite-Bearing Glass-Crystal Composites for the Immobilization of Low-Level Nuclear and Hazardous Wastes

D. J. Wronkiewicz, S. F. Wolf, and T. DiSanto

Mater. Res. Soc. Symp. Proc. **412**, 345–352 (1996)

Processing of LEU Targets for ^{99}Mo Production—Testing and Modification of the Cintichem Process

D. Wu, S. Landsberger, B. A. Buchholz, and G. F. Vandegrift

Proc. of the 18th Int. Meeting on Reduced Enrichment for Research and Test Reactors, Ed., A. Ballagny, Paris, France, September 17–21, 1995, French Atomic Energy Commission, Section 3–3 (1996)

Progress in Chemical Treatment of LEU Targets by the Modified Cintichem Process

D. Wu, S. Landsberger, and G. F. Vandegrift

Proc. of the 19th Int. Meeting on Reduced Enrichment for Research and Test Reactors (RERTR), Seoul, Korea, October 7–10, 1996, pp. 172–179 (1996)

Structure and Morphology of Electrodeposited $CaCO_3$: X-ray Diffraction and Microscopy Studies

S. Xu, M. A. Kamrath, and C. A. Melendres

Abstracts, 190th Electrochem. Soc. Meeting, San Antonio, TX, October 6–11, 1996, Vol. 96–2, p. 365 (1996)

In Situ Synchrotron X-ray Scattering Study of Incipient Formation of Porous Silicon

H. You, K. Huang, S. S. Yoo, and Z. Nagy

Proc. of the Int. Symp. on Advanced Luminescent Materials, Eds., D. J. Lockwood, P. M. Fauchet, N. Koshida, and S. R. J. Brueck, The Electrochem. Soc., Pennington, NJ, Vol. 95-25, pp. 230–239 (1996)

Place-Exchange Mechanism of Pt(111) Oxidation/Reduction as Observed by Synchrotron X-ray Scattering

H. You, Z. Nagy, D. J. Zurawski, and R. P. Chiarello

Proc. of the Sixth Int. Symp. on Electrode Process, Eds., K. Itaya and A. Wieckowski, Electrochem. Soc., Pennington, NJ, Vol. 96–8, pp. 136–149 (1996)

X-ray Absorption and Electrochemical Studies of Direct Methanol Fuel Cell Catalysts
D. J. Zurawski, A. J. Aldykiewicz, S. F. Baxter, and M. Krumpelt
Extended Abstracts, Fuel Cell Seminar, Kissimmee, FL, November 17–20, 1996, pp. 674–677 (1996)

Comparison of Sodium Zirconium Phosphate and Synroc Matrices of HLW Immobilization
V. N. Zyryanov and E. R. Vance
Abstracts, Fall Meeting of the Materials Research Soc., Boston, MA, December 2–5, 1996, p. 743 (1996)

E. Papers Presented at Scientific Meetings

Fuel Processor Development

S. Ahmed

Presented at the DOE Fuel Cells for Transportation—Exploratory R&D Program, Washington, DC, September 24–25, 1996

X-ray Absorption and Electrochemical Studies of Direct Methanol Fuel Cell Catalysts

A. J. Aldykiewicz, S. F. Baxter, D. J. Zurawski, R. Kumar, M. Krumpelt, G. Bunker, C. Segre, and E. Smotkin

Presented at the Electrochem. Soc. Symp. on the Electrochemistry of Surfaces and Interfaces, Argonne, IL, March 14, 1996

Determination of Water-Soluble Volatile Organic Compounds in WIPP Sludges

D. V. Applegate

Presented at the 26th Annual Analytical Chemistry Laboratory Technical Talks, Argonne, IL, November 1996

Determination of Water-Soluble Volatile Organic Compounds in Solid Matrices

D. V. Applegate, K. J. Parish, and A. S. Boparai

Presented at the 47th Pittsburgh Conf. and Exposition on Analytical Chemistry and Applied Spectroscopy, Chicago, IL, March 3–8, 1996

Performance of a Zeolite Column System in Removing Fission Products from Molten Salt

B. D. Babcock, C. Pereira, and J. C. Hutter

Presented at the 211th Am. Chem. Soc. National Meeting, Industrial and Engineering Chemistry Division, New Orleans, LA, March 24–28, 1996

Glass Dissolution at 20, 40, 70, and 90°C

A. J. Bakel, W. L. Ebert, D. M. Strachan, and N. R. Brown

Presented at the Am. Ceram. Soc. Meeting, Indianapolis, IN, April 14–17, 1996

High Performance Liquid Chromatography-Inductively Coupled Plasma-Mass Spectrometry (HPLC-ICP-MS) for Measurement of Arsenic Species in Environmental Samples

D. A. Bass, J. S. Yaeger, J. T. Kiely, J. S. Crain, M. J. Gowdy, L. M. Shem, H. J. O'Neill, G. B. Mohrman, and M. Besmer

Presented at the 47th Pittsburgh Conf. and Exposition on Analytical Chemistry and Applied Spectroscopy, Chicago, IL, March 3–8, 1996

The Chemistry and Kinetics of Waste Glass Corrosion

J. K. Bates

Presented at the National Academy of Sciences Conf. on Glass as a Waste Form and Vitrification Technology—An International Workshop, Washington, DC, May 13–15, 1996

Cleanup of Radioactive Mixed Waste Sample Extracts

A. S. Boparai, T. Henning, Y. Tsai, L. L. Smith, and E. L. Coleman

Presented at the 47th Pittsburgh Conf. and Exposition on Analytical Chemistry and Applied Spectroscopy, Chicago, IL, March 3–8, 1996

Chemical-Shift Selective Imaging of Molecular Probes Used in Porosity Determinations

R. E. Botto and R. E. Gerald

Presented at the 37th Experimental Nuclear Magnetic Resonance Conf., Pacific Grove, CA, March 17–22, 1996

Chemical-Shift Selective Imaging of Molecular Probes Used in Porosity Determinations

R. E. Botto and R. E. Gerald

Presented at the 38th Rocky Mountain Conf. on Analytical Chemistry, Denver, CO, July 21–26, 1996

Reduced Enrichment Research and Test Reactor (RERTR) Program at ANL

B. A. Buchholz

Presented at the University of Illinois Department of Engineering Seminar, Champaign-Urbana, IL, March 19, 1996

Corrosion Behavior of Zirconolite-Rich Synroc

E. C. Buck, A. J. Bakel, and J. K. Bates

Presented at the Fall Meeting of the Materials Research Soc., Boston, MA, December 2–5, 1996

Corroded Spent Nuclear Fuel Examined with EELS

E. C. Buck, N. L. Dietz, and J. K. Bates

Presented at the 30th Annual Meeting of the Microbeam Analysis Soc., Minneapolis, MN, August 11–15, 1996

Characterization of a Pu-Bearing Zirconolite-Rich Synroc

E. C. Buck, B. Ebbinghaus, A. J. Bakel, D. B. Chamberlain, and J. K. Bates

Presented at the Fall Meeting of the Materials Research Soc., Boston, MA, December 2–5, 1996

Low Level Detection of Transuranics with Electron Energy Loss Spectroscopy

E. C. Buck and J. Fortner

Presented at the Sixth Conf. on the Frontiers of Electron Microscopy in Materials Science, Oakbrook, IL, June 4–7, 1996

The Crystal Structure of Ianthinite, a Mixed-Valence Uranium Oxide Hydrate

P. C. Burns, R. J. Finch, F. C. Hawthorne, M. L. Miller, and R. C. Ewing

Presented at the Fall Meeting of the Materials Research Soc., Boston, MA, December 2–5, 1996

Resonance Ionization of Sputtered Atoms: Quantitative Analysis in the Near-Surface Region of Silicon Wafers

W. F. Calaway

Presented at the 14th Int. Conf. on the Application of Accelerators in Research and Industry, Denton, TX, November 6–9, 1996

Unambiguous Elemental Analysis at Trace Levels with Resonance Ionization Spectroscopy: Quantitative Analysis with Minimum Sample Consumption

W. F. Calaway, C. S. Hansen, and M. J. Pellin

Presented at the Fifth Int. Conf. and Workshop on Postionization Techniques in Surface Analysis, Argonne, IL, October 7–11, 1996

Detection of Calcium on Silicon with Monolayer Resolution Using Postresonance Ionization in Secondary Neutral Mass Spectrometry

W. F. Calaway, D. R. Spiegel, A. H. Marshall, S. W. Downey, and M. J. Pellin

Presented at the 47th Pittsburgh Conf. and Exposition on Analytical Chemistry and Applied Spectroscopy, Chicago, IL, March 3–8, 1996

Analysis of FTIR Sensor Data Using Multiple Bandpass Digital Filtering Algoithms

S. E. Carpenter

Presented at the 47th Pittsburgh Conf. and Exposition on Analytical Chemistry and Applied Spectroscopy, Chicago, IL, March 3–8, 1996

Evolution of Solution Microstructure during Third Phase Formation in a Reactive Microemulsion System

D. J. Chaiko and C. J. Mertz

Presented at the Annual AIChE Meeting, Chicago, IL, November 10–15, 1996

Metal Separations Using Aqueous Biphasic Partitioning Systems

D. J. Chaiko, B. Zaslavsky, A. N. Rollins, Y. Vojta, J. Gartelmann, and W. A. Mego

Presented at the Engineering Foundation Conf. on Emerging Separation Technologies for Metals, Kona, HI, June 16–21, 1996

Development and Testing of a Glass Waste Form for the Immobilization of Plutonium

D. B. Chamberlain, J. M. Hanchar, J. W. Emery, J. C. Hoh, S. F. Wolf, R. J. Finch, J. K. Bates, A. J. G. Ellison, and D. B. Dingwell

Presented at the Fall Meeting of the Materials Research Soc., Boston, MA, December 2–5, 1996

A Review of Chemical Decontamination Systems for Nuclear Facilities

L. Chen, D. B. Chamberlain, C. Conner, and G. F. Vandegrift

Presented at the Am. Nucl. Soc. Topical Meeting on Decontamination and Decommissioning, Chicago, IL, April 14–17, 1996

Solution Properties of Acidic Fluoride Wastes Complexed with Aluminum or Zirconium

L. Chen, D. B. Chamberlain, and G. F. Vandegrift

Presented at the AIChE Spring National Meeting, New Orleans, LA, February 25–29, 1996

Development of Processes and Equipment for Alkaline Peroxide Dissolution of Uranium-Foil Targets for Mo-99 Production

L. Chen, D. Dong, and G. F. Vandegrift

Presented at the 20th Annual Actinide Separations Conf., Itasca, IL, June 10–13, 1996

Metallophthalocyanines for Hydrocarbon Activation: Rhodium Phthalocyanine Radicals

M. J. Chen and J. W. Rathke

Presented at the Catalysis Club of Chicago, Spring Symp., Argonne, IL, May 14, 1996

Development of Pyrochemical Centrifugal Contactors

L. S. Chow and J. K. Basco

Presented at the 20th Annual Actinide Separations Conf., Itasca, IL, June 10–13, 1996

Testing of Pyrochemical Centrifugal Contactors

L. S. Chow, J. K. Basco, E. L. Carls, T. R. Johnson, and J. P. Ackerman

Presented at the Embedded Topical Meeting on DOE Spent Nuclear Fuel and Fissile Material Management, Am. Nucl. Soc., Reno, NV, June 16–20, 1996

Electronic Structure of Quinone Radical Anions

A. R. Cook, L. A. Curtiss, and J. R. Miller

Presented at the 20th DOE Solar Photochemistry Research Conf., French Lick, IN, June 8–12, 1996

Actinides at the Crossroads: ICP-MS or Alpha Spectrometry?

J. S. Crain, L. L. Smith, F. P. Smith, J. T. Kiely, J. S. Yaeger, D. G. Graczyk, and J. A. Alvarado

Presented at the Atomic Spectroscopy Symp., Howth, County Dublin, Ireland, March 28–29, 1996

ICP-MS and the Determination of Environmental Uranium: A Match Made in Heaven?

J. S. Crain, L. L. Smith, J. S. Yaeger, J. T. Kiely, F. P. Smith, D. G. Graczyk, and J. S. Alvarado

Presented at the U. S. Army Center for Health Promotion and Preventive Medicine, Aberdeen Proving Ground, MD, April 25, 1996

Basis for Acceptance Specifications for Solidified Low-Activity Waste from the Hanford Tanks

J. C. Cunnane and N. R. Brown

Presented at the 89th Annual Meeting of the Air and Waste Management Association, Nashville, TN, June 23–28, 1996

Computational Methods for Calculation of Accurate Bond Energies, Electron Affinities, and Ionization Energies

L. A. Curtiss

Presented at the 212th National Meeting of the Am. Chem. Soc., Computational Thermochemistry, Orlando, FL, August 25–30, 1996

Reaction Mechanisms for Growth of Diamond Thin Films from Buckyball Precursors

L. A. Curtiss

Presented at the 49th Annual Gaseous Electronic Conf., Argonne, IL, October 20–24, 1996

EPRI Battery Issues Workshop: Session III, Third Party Testing and Evaluation

W. H . DeLuca

Presented at the EPRI Battery Issues Workshop, Dallas, TX, September 18–19, 1996

Remote Detection of Environmental Pesticide Spray Using FTIR Spectroscopy

J. C. Demirgian, G. F. Busse, and J. Ditillo

Presented at the 47th Pittsburgh Conf. and Exposition on Analytical Chemistry and Applied Spectroscopy, Chicago, IL, March 3–8, 1996

Cocaine Contamination Studies on Chicago Currency

J. C. Demirgian, E. Y. Hwang, J. M. Ewing, B. S. Tani, C. T. Roche, S. Ulvick, T. Kunz, C.-W. Su, and S. W. Rigdon

Presented at the 47th Pittsburgh Conf. and Exposition on Analytical Chemistry and Applied Spectroscopy, Chicago, IL, March 3–8, 1996

Examining Cash for Cocaine Using SEM

J. C. Demirgian, B. S. Tani, E. Y. Hwang, C. T. Roche, J. M. Ewing, and S. Ulvick

Presented at the INTER/MICRO-'96 Meeting, Chicago, IL, July 22–25, 1996

Energies and Structures of Germanium Clusters

P. W. Deutsch and L. A. Curtiss

Presented at the Second Int. Symp. on Theory of Atomic and Molecular Clusters, Fontana, WI, September 15–20, 1996

Alkaline Peroxide Processing of LEU Metal Targets for ^{99}Mo Production

D. Dong and G. F. Vandegrift

Presented at the 211th Am. Chem. Soc. National Meeting, New Orleans, LA, March 24–28, 1996

Microengineered Cathode Interface Studies

R. Doshi, T. W. Kueper, and M. Krumpelt

Presented at the Fuel Cells '96 Review Meeting, Morgantown, WV, August 20–21, 1996

Dissolution Rates of DWPF Glasses from Long-Term PCT

W. L. Ebert and S.-W. Tam

Presented at the Fall Meeting of the Materials Research Soc., Boston, MA, December 2–5, 1996

Analytical Methods for Environmental Radionuclides

M. D. Erickson, J. H. Aldstadt, J. S. Alvarado, J. S. Crain, K. A. Orlandini, and L. L. Smith

Presented at the 47th Pittsburgh Conf. and Exposition on Analytical Chemistry and Applied Spectroscopy, Chicago, IL, March 3–8, 1996

Thermodynamic Stabilities of U(VI) Minerals: Estimated and Observed Relationships

R. J. Finch

Presented at the Fall Meeting of the Materials Research Soc., Boston, MA, December 2–5, 1996

Spent Fuel Reaction—The Behavior of the ϵ-Phase over 3.1 Years

P. A. Finn, J. C. Hoh, S. F. Wolf, M. T. Surchik, E. C. Buck, R. J. Finch, and J. K. Bates

Presented at the Fall Meeting of the Materials Research Soc., Boston, MA, December 2–5, 1996

The Chemistry of the Light Rare Earth Elements Determined by Electron Energy Loss Spectroscopy

J. Fortner and E. C. Buck

Presented at the Am. Phys. Soc. Meeting, St. Louis, MO, March 18–22, 1996

Chemical Effects of Lanthanides and Actinides in Glasses Determined with Electron Energy Loss Spectroscopy

J. Fortner, E. C. Buck, A. J. G. Ellison, and J. K. Bates

Presented at the 30th Annual Meeting of the Microbeam Analysis Soc., Minneapolis, MN, August 11–15, 1996

EELS Analysis of Cerium Redox in Glasses for Plutonium Immobilization

J. Fortner, E. C. Buck, A. J. G. Ellison, and J. K. Bates

Presented at the Sixth Conf. on the Frontiers of Electron Microscopy in Materials Science, Oakbrook, IL, June 4–7, 1996

Solution-Borne Colloids from Drip Tests Using Actinide-Doped and Fully-Radioactive Waste Glasses

J. Fortner, S. F. Wolf, E. C. Buck, C. J. Mertz, and J. K. Bates

Presented at the Fall Meeting of the Materials Research Soc., Boston, MA, December 2–5, 1996

Quality Assurance for Glovebox Design, Fabrication, Installation, Operation, Maintenance, and Decommissioning

A. A. Frigo

Presented at the Tenth Annual Conf. and Equipment Exhibit of the Am. Glovebox Soc., San Diego, CA, July 22–25, 1996

Proposed High Throughput Electrorefining Treatment for Spent N-Reactor Fuel

E. C. Gay, W. E. Miller, and J. J. Laidler

Presented at the Embedded Topical Meeting on DOE Spent Nuclear Fuel and Fissile Material Management, Am. Nucl. Soc., Reno, NV, June 16–20, 1996

In Situ Diffusion Measurements in an Electrochemical Cell

R. E. Gerald, R. J. Klingler, J. W. Rathke, and K. Woelk

Presented at the 37th Experimental Nuclear Magnetic Resonance Conf., Pacific Grove, CA, March 17–22, 1996

Status Summary of Argonne National Laboratory

D. W. Green

Presented at the DOE Analytical Manager's Meeting, Ames, IA, October 8–10, 1996

Synthesis and Rare-Earth Element Doping of Zircon with Implications for Trace Element Partitioning in Natural Zircons

J. M. Hanchar

Presented at the University of New Mexico, Albuquerque, NM, July 24, 1996

Cluster Ejection from Calcium during Energetic Ar^+ Ion Bombardment

C. S. Hansen, W. F. Calaway, and M. J. Pellin

Presented at the Fifth Int. Conf. and Workshop on Postionization Techniques in Surface Analysis, Argonne, IL, October 7–11, 1996

Calcium Cluster Ejection during Ar^+ Ion Bombardment: An Examination of Energy Distributions and Partial Sputter Yields

C. S. Hansen, W. F. Calaway, M. J. Pellin, and D. M. Gruen

Presented at the Particle Solid Interactions Gordon Conf., Plymouth, NH, July 21–26, 1996

Three-Color Resonance Ionization Spectroscopy of Zr in Si

C. S. Hansen, W. F. Calaway, M. J. Pellin, R. C. Wiens, and D. S. Burnett

Presented at the Eighth Int. Symp. on Resonance Ionization Spectroscopy and Its Applications (RIS '96), State College, PA, June 30–July 5, 1996

Hot Isostatic Pressing of Glass-Zeolite Composites

M. C. Hash, C. Pereira, M. A. Lewis, R. J. Blaskovitz, V. N. Zyryanov, and J. P. Ackerman

Presented at the 20th Annual Actinide Separations Conf., Itasca, IL, June 10–13, 1996

Hot Isostatic Pressing of Glass-Zeolite Composites

M. C. Hash, C. Pereira, M. A. Lewis, R. J. Blaskovitz, V. N. Zyryanov, and J. P. Ackerman

Presented at the Am. Ceram. Soc. Meeting, Indianapolis, IN, April 14–17, 1996

High Temperature Method for Conversion of Chlorinated Organics to CH_3Cl and CO_2 for Isotopic Analyses of Chlorine and Carbon

B. D. Holt and N. C. Sturchio

Presented at the 212th National Meeting of the Am. Chem. Soc., Orlando, FL, August 25–30, 1996

Computational Studies of Growth of Diamond (110) from Dicarbon

D. A. Horner, P. C. Redfern, L. A. Curtiss, and D. M. Gruen

Presented at the Spring Meeting of the Materials Research Soc., San Francisco, CA, April 8–12, 1996

Effects of CoS_2 in the Positive Electrode of a Rechargeable FeS_2 Cell

A. N. Jansen, T. D. Kaun, D. R. Vissers, G. L. Henriksen, and M. C. Hash

Presented at the Electrochem. Soc. Symp. on the Electrochemistry of Surfaces and Interfaces, Argonne, IL, March 14, 1996

Irradiation Performance of Lithium Ceramic Breeder Materials

C. E. Johnson

Presented at the Fifth Int. Workshop on Ceramic Breeder Blanket Interactions, Rome, Italy, September 23–25, 1996

Advanced Understanding of the Tritium Recovery Process from the Ceramic Breeder Blanket

C. E. Johnson, J. P. Kopasz, and S.-W. Tam

Presented at the Int. Workshop on Interfacial Effects in Quantum Engineering Systems, Mito, Ibaraki-keu, Japan, August 21–23, 1996

Structural and Electrochemical Studies of Alpha Manganese Dioxide (α-MnO_2)

C. S. Johnson, D. W. Dees, M. F. Mansuetto, M. M. Thackeray, D. R. Vissers, D. Argyriou, C.-K. Loong, and L. Christensen

Presented at the Eighth Int. Meeting on Lithium Batteries, Nagoya, Japan, June 16–21, 1996

Estimation Methods for Thermodynamic Quantities

I. Johnson

Presented at the 16th Annual Pyrochemical Workshop, St. Charles, IL, October 28–31, 1996

Light Element Thermodynamics Related to Actinide Separations

I. Johnson and C. E. Johnson

Presented at the 14th IUPAC Conf. on Chemical Thermodynamics, Osaka, Japan, August 25–30, 1996

Treatment of TMI-2 Fuel Debris Using the Lithium Reduction Process

E. J. Karell

Presented at the 16th Annual Pyrochemical Workshop, St. Charles, IL, October 28–31, 1996

Analysis of Polymer Plastics by Fourier Transform Infrared Microscopy

S. D. Kent, C. T. Snyder, and S. E. Carpenter

Presented at the 47th Pittsburgh Conf. and Exposition on Analytical Chemistry and Applied Spectroscopy: Releasing the Power of Imagination, Chicago, IL, March 3–8, 1996

Sputtering of Single-Crystal Alloys

B. V. King, C. Zimmerman, D. E. Riederer, N. Winograd, C. S. Hansen, W. F. Calaway, M. J. Pellin, and R. Smith

Presented at the Fifth Int. Conf. and Workshop on Postionization Techniques in Surface Analysis, Argonne, IL, October 7–11, 1996

In Situ NMR Investigations of Hydroformylation in Supercritical Carbon Dioxide and Polarity Effects of Organic Solvents on Precatalytic Species

K. W. Kramarz, R. J. Klingler, and J. W. Rathke

Presented at the Catalysis Club of Chicago, Spring Symp., Argonne, IL, May 14, 1996

Non-Segregating Electrolytes for Molten Carbonate Fuel Cells

M. Krumpelt, T. D. Kaun, and M. T. Lanagan

Presented at the Fuel Cells '96 Review Meeting, Morgantown, WV, August 20–21, 1996

Sealants for Solid Oxide Fuel Cells

T. W. Kueper, I. Bloom, and M. Krumpelt

Presented at the InterUniversity Research Workshop, Joining of Advanced Engineered Materials, University of Illinois at Chicago, Chicago, IL, June 26, 1996

Fuel Cell Technology: A Tutorial Overview

R. Kumar

Presented at the Partnership for a New Generation of Vehicle (PNGV) Manufacturing Workshop on Fuel Cells, Dearborn, MI, July 23–24, 1996

Overview of the U.S. Contribution to the Polymer Electrolyte Fuel Cell Annex

R. Kumar

Presented at the Int. Energy Agency's PEFC Annex VIII Workshop, KFA-Jülich, Germany, May 9–10, 1996

Electrometallurgical Treatment of Metallic Spent Nuclear Fuel Stored at the Hanford Site

J. J. Laidler and E. C. Gay

Presented at the Spectrum '96 Meeting, Nuclear and Hazardous Waste Management Int. Topical Meeting, Am. Nucl. Soc., Seattle, WA, August 18–23, 1996

Using the Centrifugal Contactor for Solvent Extraction Processes

R. A. Leonard, D. B. Chamberlain, and C. Conner

Presented at the Annual AIChE Meeting, Chicago, IL, November 10–15, 1996

Dissolution of Metal Foils for ^{99}Mo Production

R. A. Leonard, L. Chen, C. J. Mertz, B. Srinivasan, and G. F. Vandegrift

Presented at the 20th Annual Actinide Separations Conf., Itasca, IL, June 10–13, 1996

Effect of Different Glass and Zeolite A Compositions on the Leach Performance of Ceramic Waste Forms

M. A. Lewis, M. C. Hash, and D. Glandorf

Presented at the Fall Meeting of the Materials Research Soc., Symposium II: *Scientific Basis for Nuclear Waste Management XX*, Boston, MA, December 2–5, 1996

Thermal Stability of Salt-Occluded Zeolite

M. A. Lewis, M. C. Hash, and C. Pereira

Presented at the Am. Ceram. Soc. Meeting, Indianapolis, IN, April 14–17, 1996

Effects of Heating on Salt-Occluded Zeolite

M. A. Lewis, M. C. Hash, C. Pereira, and J. P. Ackerman

Presented at the Am. Ceram. Soc. Meeting, Indianapolis, IN, April 14–17, 1996

Pollution Prevention/Waste Minimization in the Analytical Chemistry Laboratory: Efficiency Factors and Source Reduction

J. Lu, M. D. Erickson, D. P. Peterson, E. A. Huff, J. T. Kiely, and J. S. Crain

Presented at the 47th Pittsburgh Conf. and Exposition on Analytical Chemistry and Applied Spectroscopy, Chicago, IL, March 3–8, 1996

Reproduction of Natural Corrosion by Vapor Hydration Test: Seven-Year Results

J. S. Luo, W. L. Ebert, J. J. Mazer, and J. K. Bates

Presented at the Fall Meeting of the Materials Research Soc., Boston, MA, December 2–5, 1996

Simulation of Natural Corrosion by Vapor Hydration Test: Seven-Year Results

J. S. Luo, W. L. Ebert, J. J. Mazer, and J. K. Bates

Presented at the Fall Meeting of the Materials Research Society, Boston, MA, December 2–5, 1996

SEM/EDS Analysis of Boron in Waste Glasses with Ultrathin Window Detector and Digital Pulse Processor

J. S. Luo, S. F. Wolf, W. L. Ebert, and J. K. Bates

Presented at the 30th Annual Meeting of the Microbeam Analysis Soc., Minneapolis, MN, August 11–15, 1996

Reproduction of Natural Corrosion by Accelerated Laboratory Testing Methods

J. S. Luo, D. J. Wronkiewicz, J. J. Mazer, and J. K. Bates

Presented at the National Academy of Sciences Conf. on Glass as a Waste Form and Vitrification Technology—An International Workshop, Washington, DC, May 13–15, 1996

X-ray Absorption Spectra and the Local Structure of Nickel in Some Oxycompounds and Fluorides

A. N. Mansour and C. A. Melendres

Presented at the Ninth Int. XAFS Conf., Grenoble, France, August 26–30, 1996

Rietveld Refinements of α-MnO_2 from Neutron Data

M. F. Mansuetto, D. W. Dees, C. S. Johnson, M. M. Thackeray, D. R. Vissers, D. Argyriou, and L. Christensen

Presented at the Int. Union of Crystallography Meeting, Seattle, WA, August 8–17, 1996

Analysis of Carbon Species in High Temperature Superconducting Ceramics Using Infrared Spectroscopy

P. D. Maroni, V. A. Maroni, and K. T. Wu

Presented at the 47th Pittsburgh Conf. and Exposition on Analytical Chemistry and Applied Spectroscopy, Chicago, IL, March 3–8, 1996

John and I: Application of Infrared and Raman Spectroscopy to Problems in Chemical and Materials Science

V. A. Maroni

Presented at the Eastern Analytical Symp. as Part of a Special Session Honoring Dr. John R. Ferraro, Somerset, NJ, November 17–22, 1996

Influence of Lead on Phase Formation and Microstructure Development in Ag/Bi-2223 Composite Conductors

V. A. Maroni, N. Merchant, J. S. Luo, J. S. Leboy, A. K. Fischer, K K. T. Wu, W. Zhong, and S. E. Dorris

Presented at the Symp. on High Temperature Superconductors, 125th Annual Meeting and Exposition of the Minerals, Metals, and Materials Soc., Anaheim, CA, February 4–8, 1996

Examination of Phase Evolution in High-T_c Superconducting Tapes Using Raman Microscopy

V. A. Maroni, K. T. Wu, and A. K. Fischer

Presented at the Fall Meeting of the Materials Research Soc., Boston, MA, December 2–5, 1996

High-Temperature Interaction Studies to Screen Melt Crucible Materials for Stainless Steel—Zirconium Alloys and Uranium

S. M. McDeavitt and G. W. Billings

Presented at the Symp. on High Temperature Superconductors, 125th Annual Meeting and Exhibition of the Minerals, Metals, and Materials Soc., Anaheim, CA, February 4–8, 1996

Application of Spent Fuel Treatment Technology to Plutonium Immobilization

C. C. McPheeters, J. P. Ackerman, E. C. Gay, and G. K. Johnson

Presented at the Embedded Topical Meeting on DOE Spent Nuclear Fuel and Fissile Material Management, Am. Nucl. Soc., Reno, NV, June 16–20, 1996

Synchrotron Far Infrared Spectroscopy of Electrode Surfaces and Interfaces

C. A. Melendres, G. A. Bowmaker, B. Beden, and J. M. Leger

Presented at the First Int. Conf. on Synchrotron Radiation in Materials Science, Chicago, IL, July 29–August 2, 1996

Identification and Quantification of Phases Formed during the Processing of $(Bi,Pb)_2Sr_2Ca_2Cu_3O_x$/Ag Composite Conductors

N. Merchant, A. K. Fischer, V. A. Maroni, W. L. Carter, and R. Parrella

Presented at the Applied Superconductivity Conf., Pittsburgh, PA, August 25–30, 1996

Colloid Formation during Waste Glass Corrosion

C. J. Mertz, E. C. Buck, J. Fortner, and J. K. Bates

Presented at the National Academy of Sciences Conf. on Glass as a Waste Form and Vitrification Technology—An International Workshop, Washington, DC, May 13–15, 1996

In-Situ Decontamination Technologies for Actinides and Fission Products in DOE Nuclear Facilities

C. J. Mertz, D. B. Chamberlain, L. Chen, C. Conner, and G. F. Vandegrift

Presented at the Am. Nucl. Soc. Topical Meeting on Decontamination and Decommissioning, Chicago, IL, April 14–17, 1996

In-Situ Decontamination Technologies for Actinides and Fission Products in DOE Nuclear Facilities

C. J. Mertz, D. B. Chamberlain, L. Chen, C. Conner, G. F. Vandegrift, D. Drockelman, M. D. Kaminski, S. Landsberger, and J. Stubbins

Presented at the Annual Society of Women Engineers National Convention, Portland, OR, June 25–29, 1996

Foreign Activities in Fuel Cells

J. F. Miller

Presented at the National Research Council Peer Review Panel Session on Fuel Cell R&D Activities in the Partnership for a New Generation of Vehicles (PNGV) Program, South Windsor, CT, October 17, 1996

Global Developments in Fuel Cells for Transportation Applications

J. F. Miller

Presented at the Soc. of Automotive Engineers (SAE) Meeting, Chicago Section, Willowbrook, IL, January 9, 1996

Major System Level Milestones for Fuel Cells in the Partnership for a New Generation of Vehicles

J. F. Miller

Presented at the DOE/Industry Planning Workshop for National Program Plan on Fuel Cells in Transportation, Golden, CO, April 16–17, 1996

National Laboratory Fuel Cell Stack R&D Overview

J. F. Miller

Presented at the National Research Council Peer Review Panel Session on Fuel Cell R&D Activities in the Partnership for a New Generation of Vehicles (PNGV) Program, South Windsor, CT, October 17, 1996

Status of PEM Fuel Cell R&D for Transportation

J. F. Miller

Presented at the AIST/DOE Technical Meeting, Orlando, FL, November 21, 1996

Government Role in PEM Fuel Cell R&D and Opportunities for R&D Funding

J. F. Miller and P. G. Patil

Presented at the Conf. on Commercializing Fuel Cell Vehicles, Chicago, IL, September 17–19, 1996

Transuranium Element Incorporation into the β-U_3O_8 Uranyl Sheet

M. L. Miller, R. J. Finch, P. C. Burns, and R. C. Ewing

Presented at the Fall Meeting of the Materials Research Soc., Boston, MA, December 2–5, 1996

Synchrotron X-ray Investigations of the Incipient Oxidation/Reduction of the Pt(111) Surface

Z. Nagy

Presented at the DOE/BES Corrosion Contractors' Meeting, Argonne, IL, September 26–27, 1996

Trace Anion Catalysis of Elementary Charge Transfer–Steps in Metal Deposition

Z. Nagy

Presented at the Gordon Research Conf. on Electrodeposition, New London, NH, August 11–16, 1996

Laser Desorption and Resonant Ionization Mass Spectroscopy for Trace Elemental Analysis of μm-Sized Samples

G. Nicolussi, M. J. Pellin, W. F. Calaway, R. S. Lewis, A. M. Davis, and R. N. Clayton

Presented at the Fifth Int. Conf. and Workshop on Postionization Techniques in Surface Analysis, Argonne, IL, October 7–11, 1996

Analysis of Multispectral Image Data Utilizing a Neural Network Based on Adaptive Resonance Theory (ART2A)

Y. X. Noyes and S. E. Carpenter

Presented at the 47th Pittsburgh Conf. and Exposition on Analytical Chemistry and Applied Spectroscopy, Chicago, IL, March 3–8, 1996

Comparison of the Corrosion Behavior of Tank 51 Sludge-Based Glass and a Nonradioactive Homologue Glass

L. Nuñez, W. L. Ebert, S. F. Wolf, and J. K. Bates

Presented at the Fall Meeting of the Materials Research Soc., Boston, MA, December 2–5, 1996

Leachability of Radionuclides and Hazardous Metals from a Cement-Based Low Level Waste Form

L. Nuñez, S. F. Wolf, T. R. Johnson, R. Weasley, and G. A. Genslinger

Presented at the 211th Am. Chem. Soc. National Meeting, New Orleans, LA, March 24–28, 1996

Isotopic Analysis of Samples of Micron Dimensions: A Case for Laser Photoionization of Secondary Neutrals

M. J. Pellin, G. Nicolussi, W. F. Calaway, A. M. Davis, R. S. Lewis, R. N. Clayton, and D. M. Gruen

Presented at the Todai Int. Symp. on Cosmochronology and Isotope Geoscience, Tokyo, Japan, January 17–20, 1996

Electrochemical and *In Situ* Neutron Diffraction Studies of NiOOD/$LaNi_{5-y}Al_yD_x$ Cells

W. Peng, L. Redey, A. N. Jansen, D. W. Dees, J. R. Selman, J. M. Carpenter, J. W. Richardson, and G. Burr

Presented at the 28th Am. Chem. Soc. Central Regional Meeting on Metal-Hydrogen Systems, Dayton, OH, June 9–12, 1996

Mixing of Zeolite Powders and Molten Salt

C. Pereira, V. N. Zyryanov, M. A. Lewis, and J. P. Ackerman

Presented at the Am. Ceram. Soc. Meeting, Indianapolis, IN, April 14–17, 1996

Application of Quantum Beams to Analysis of Radioactive Materials

M. Petri, L. Leibowitz, and C. E. Johnson

Presented at the Int. Workshop on Interfacial Effects in Quantum Engineering Systems, Mito, Ibaraki-keu, Japan, August 21–23, 1996

Fuel Cell Systems R&D Program

W. F. Podolski

Presented at the Hydrogen Technical Advisory Panel Review Meeting, Denver, CO, October 15, 1996

High-Temperature Sodium Nickel Chloride Battery for Electric Vehicles

J. Prakash, L. Redey, P. A. Nelson, and D. R. Vissers

Presented at the 190th Electrochem. Soc. Meeting, San Antonio, TX, October 6–11, 1996

New Methods of Evaluating Battery Cell Performance

L. Redey

Presented at the 47th Annual Meeting of the Int. Soc. of Electrochemistry, Budapest, Hungary, September 1–6, 1996

Performance-Stabilizing Processes in Sodium/Metal-Chloride Cells

L. Redey, J. Prakash, and D. R. Vissers

Presented at the 47th Annual Meeting of the Int. Soc. of Electrochemistry, Budapest, Hungary, September 1–6, 1996

Reduction of U(VI), Np(VI), and Pu(VI) by WIPP-Relevant Organic Complexants

D. T. Reed and M. K. Richmann

Presented at the 212th National Meeting of the Am. Chem. Soc., Orlando, FL, August 25–30, 1996

Stability/Solubility of U(VI), Np(VI), and Pu(VI) in Synthetic WIPP Brine

D. T. Reed, D. G. Wygmans, and R. C. Moore

Presented at the 212th National Meeting of the Am. Chem. Soc., Orlando, FL, August 25–30, 1996

Identification and Quantitative Determination of Congeners in Unresolved Chromatographic Peaks Using Gas Chromatography and Matrix Isolation Infrared Spectrometry

G. T. Reedy

Presented at the 47th Pittsburgh Conf. and Exposition on Analytical Chemistry and Applied Spectroscopy, Chicago, IL, March 3–8, 1996

Use of Process Modeling to Design Cost-Effective Cleanup Technologies

M. C. Regalbuto

Presented at the Annual Society of Women Engineers National Convention, Portland, OR, June 25–29, 1996

An Overview of the Generic TRUEX Model Validation Studies Using Data from TRUEX Demonstrations from the Power Reactor and Nuclear Fuel Development Corp. of Japan

M. C. Regalbuto and G. F. Vandegrift

Presented at the Second Argonne National Laboratory Technical Women's Symp., Argonne, IL, April 29–30, 1996

TRUEX Process Model Verification Studies: Comparison of Simulated and Experimental Results from Demonstrations at PNC of Japan and ORNL

M. C. Regalbuto, G. F. Vandegrift, and R. A. Leonard

Presented at the 20th Annual Actinide Separations Conf., Itasca, IL, June 10–13, 1996

Anion Diffusion in $La_{1-x}Sr_xCoO_3$

J. L. Routbort and R. Doshi

Presented at the Am. Ceram. Soc. Meeting, Indianapolis, IN, April 14–17, 1996

A Simple and Robust Precipitation Method for Treating Transuranic Waste Solutions

J. Sedlet, S. B. Aase, C. Conner, S. A. Slater, and G. F. Vandegrift

Presented at the Ninth World Congress of the Int. Protection Assoc., Vienna, Austria, April 14–19, 1996

Electron Binding Energy and Long-Range Electronic Coupling. A Theoretical Study

B. Sengupta, L. A. Curtiss, and J. R. Miller

Presented at the 20th DOE Solar Photochemistry Research Conf., French Lick, IN, June 8–12, 1996

Microstructural Control during the Redox Synthesis of Electrochemically Active Alpha MnO_2

Y. Shao, S. Hackney, C. S. Johnson, and M. M. Thackeray

Presented at the Tenth Int. Battery Association Meeting, Materials Symp., Tucson, AZ, October 1–4, 1996

Evaluation of Standard Durability Tests towards the Qualification Process for the Glass-Zeolite Ceramic Waste Form

L. J. Simpson and D. J. Wronkiewicz

Presented at the Fall Meeting of the Materials Research Soc., Boston, MA, December 2–5, 1996

Decontamination of MSRE Salt Using Nitride Formation

S. A. Slater, W. E. Miller, and J. L. Willit

Presented at the Second Argonne National Laboratory Technical Women's Symp., Argonne, IL, April 29–30, 1996

Precipitation of Metal Nitrides from Chloride Melts

S. A. Slater, W. E. Miller, and J. L. Willit

Presented at the Annual AIChE Meeting, Chicago, IL, November 10–15, 1996

Scrubbing Metals from Molten Salts via Nitride Formation

S. A. Slater, W. E. Miller, and J. L. Willit

Presented at the 20th Annual Actinide Separations Conf., Itasca, IL, June 10–13, 1996

Waste Minimization in Analytical Chemistry Methods

L. L. Smith, D. W. Green, J. S. Crain, J. B. Schilling, J. S. Yaeger, J. T. Kiely, and A. S. Boparai

Presented at the IEPA Office of Pollution Prevention Seventh Annual Pollution Prevention Conf., Lisle, IL, October 7, 1996

CO Fluxes in the Northern Hemisphere Temperature Zone in 1971

C. M. Stevens

Presented at the Fall Meeting of the Am. Geophys. Union, San Francisco, CA, September 11, 1996

The Uses and Abuses of Kinetics-Glass Dissolution in Perspective

D. M. Strachan and C. L. Liotta

Presented at the Fall Meeting of the Am. Ceram. Soc., San Antonio, TX, October 30–November 2, 1996

Theoretical Study of Diethylene Oxide Dimethylether

A. Sutjianto and L. A. Curtiss

Presented at the 29th Midwest Theoretical Chemistry Conf., Indiana University—Purdue University, Indianapolis, IN, May 30–June 1, 1996

Transport through Low Porosity Media—Microstructure and Uncertainty Analysis

S.-W. Tam and M. J. Steindler

Presented at the Seventh Annual Int. High-Level Radioactive Waste Management Conf., Am. Nucl. Soc., Las Vegas, NV, April 29–May 3, 1996

Thermodynamic and Nonstoichiometric Behavior of Pb-Doped and Pb-Free Bi-2212 and Pb-Doped Bi-2223 Systems

M. Tetenbaum

Presented at the High Temperature Superconductor Phase Diagrams Workshop, Santa Fe, NM, November 17–20, 1996

Lithium Insertion into Transition Metal Oxides

M. M. Thackeray

Presented at Illinois Institute of Technology, Chicago, IL, February 14, 1996

Manganese Oxides for Electric Vehicle Batteries

M. M. Thackeray

Presented at the 190th Electrochem. Soc. Meeting, San Antonio, TX, October 6–11, 1996

Structural Stability of $LiMn_2O_4$ Electrodes for Lithium Batteries

M. M. Thackeray and M. F. Mansuetto

Presented at the Eighth Int. Meeting on Lithium Batteries, Nagoya, Japan, June 16–21, 1996

Treatment of Salt from Molten Salt Reactor Experiment

Z. Tomczuk, W. E. Miller, J. L. Willit, and J. J. Heiberger

Presented at the 20th Annual Actinide Separations Conf., Itasca, IL, June 10–13, 1996

ANL Progress in Developing the Modified Cintichem Process

G. F. Vandegrift

Presented at PUSPIPTEK, Serpong, Indonesia, April 26–May 4, 1996

Modification of Current Processes for Fission-Product ^{99}Mo Production by Substitution of Low-Enriched for High-Enriched Uranium

G. F. Vandegrift, S. B. Aase, B. A. Buchholz, L. Chen, C. Conner, D. Dong, R. A. Leonard, C. J. Mertz, J. Sedlet, B. Srinivasan, D. Wu, and L. Landsberger

Presented at the 20th Annual Actinide Separations Conf., Itasca, IL, June 10–13, 1996

Discussion Notes: ^{99}Mo

G. F. Vandegrift and R. A. Leonard

Presented at PUSPIPTEK, Serpong, Indonesia, August 19–23, 1996

Potential Role of the National Laboratories in a Fuel Cell Alliance

D. Watkins and R. Kumar

Presented at the DOE/Industry Fuel Cell Planning Meeting, Golden, CO, April 16–17, 1996

Electrometallurgical Treatment of Aluminum-Matrix Fuels

J. L. Willit, E. C. Gay, W. E. Miller, C. C. McPheeters, and J. J. Laidler

Presented at the Embedded Topical Meeting on DOE Spent Nuclear Fuel and Fissile Material Management, Am. Nucl. Soc., Reno, NV, June 16–20, 1996

Electrometallurgical Treatment of Aluminum-Based Fuel

J. L. Willit, S. A. Slater, and W. E. Miller

Presented at the 16th Annual Pyrochemical Workshop, St. Charles, IL, October 28–31, 1996

Imaging of Diffusion and T_1 Relaxation Using Asymmetric Magnetization Grids in Toroid Cavity Probes

K. Woelk, R. E. Gerald, R. J. Klingler, and J. W. Rathke

Presented at the 37th Experimental Nuclear Magnetic Resonance Conf., Pacific Grove, CA, March 17–22, 1996

Grain Boundary Corrosion and Alteration Phase Formation during the Oxidative Dissolution of UO_2 Pellets

D. J. Wronkiewicz, E. C. Buck, and J. K. Bates

Presented at the Fall Meeting of the Materials Research Soc., Boston, MA, December 2–5, 1996

Application of High-Pressure Microwave Digestion to Radiochemical Analyses

J. S. Yaeger and L. L. Smith

Presented at the 47th Pittsburgh Conf. and Exposition on Analytical Chemistry and Applied Spectroscopy, Chicago, IL, March 3–8, 1996

Place Exchange during Surface Oxidation of Platinum

H. You and Z. Nagy

Presented at the 212th National Meeting of the Am. Chem. Soc., Orlando, FL, August 25–30, 1996

X-ray Absorption and Electrochemical Studies of Direct Methanol Fuel Cell Catalysts

D. J. Zurawski, A. J. Aldykiewicz, R. Kumar, M. Krumpelt, G. Bunker, C. Segre, and E. Smotkin

Presented at the First Int. Conf. on Synchrotron Radiation in Materials Science, Chicago, IL, July 29–August 2, 1996

Computational Studies of Water Adsorption in the Zeolite H-ZSM-5

S. A. Zygmunt, L. A. Curtiss, L. E. Iton, and M. K. Erhardt

Presented at the Catalysis Club of Chicago, Spring Symp., Argonne, IL, May 14, 1996

Theoretical and Experimental Studies of Water Adsorption in Zeolites

S. A. Zygmunt, M. K. Erhardt, D. H. Olson, L. A. Curtiss, and L. E. Iton

Presented at the Discussions in Catalytic Chemistry Workshop, Baltimore, MD, July 6, 1996

Incorporation of Actinide-Simulating Rare Earth Elements in NZP Ceramic Waste Form

V. N. Zyryanov and E. R. Vance

Presented at the 20th Annual Actinide Separations Conf., Itasca, IL, June 10–13, 1996

F. Papers Accepted for Publication

Formation of the $Fe_{23}Zr_6$ Phase in an Fe-Zr Alloy
D. P. Abraham, J. W. Richardson, and S. M. McDeavitt
To be published in Scr. Mater. J.

Stability of Low-Concentration Calibration Standards for Graphite Furnace Atomic Absorption Spectroscopy
D. A. Bass and L. B. TenKate
To be published in At. Spectrosc.

Optimized Gaussian Basis Sets for Use with Relativistic Effective (Core) Potentials: K, Ca, Ga–Kr
J.-P. Blaudeau and L. A. Curtiss
To be published in Int. J. Quantum Chem.

Assessment of Gaussian-2 and Density Functional Theories for the Computation of Enthalpies of Formation
L. A. Curtiss, K. Raghavachari, P. C. Redfern, and J. A. Pople
To be published in J. Chem. Phys.

Phase Transformations and Structural Relations among Schoepite, Metaschoepite, and Dehydrated Schoepite
R. J. Finch, F. C. Hawthorne, and R. C. Ewing
To be published in Can. Mineral.

Distinguishing among Schoepite, $[(UO_2)_8O_2(OH)_{12}](H_2O)_{12}$, and Related Uranyl Oxide Hydrates with X-ray Powder Diffraction
R. J. Finch, F. C. Hawthorne, M. L. Miller, and R. C. Ewing
To be published in Powder Diffr.

Structural and Electrochemical Studies of Alpha Manganese Oxide (α-MnO_2)
C. S. Johnson, D. W. Dees, M. F. Mansuetto, M. M. Thackeray, D. R. Vissers, D. Argyriou, C.-K. Loong, and L. Christensen
To be published in J. Power Sources

Stabilized α-MnO_2 Electrodes for Rechargeable 3-V Lithium Batteries
C. S. Johnson, M. F. Mansuetto, M. M. Thackeray, Y. Shao-Horn, and S. A. Hackney
To be published in J. Electrochem. Soc.

Electrochemical Energy Conversion
M. Krumpelt
To be published in the Seventh Edition of *Perry's Handbook of Chemical Engineering*, Ed., D. Green, McGraw-Hill, New York

Centrifugal Contactors for Laboratory-Scale Solvent Extraction Tests
R. A. Leonard, D. B. Chamberlain, and C. Conner
To be published in Sep. Sci. Technol.

Meteoroid Streams as Sources for Meteorite Falls: A Status Report
M. E. Lipschutz, S. F. Wolf, and R. T. Dodd
To be published in Plan. Space Sci.

Application of the Pyrochemical Process to Recycle of Actinides from LWR Spent Fuel
C. C. McPheeters, R. D. Pierce, and T. P. Mulcahey
To be published in Prog. Nucl. Energy

X-ray Absorption Spectroelectrochemical Cell for *In-Situ* Studies of Thin Films
C. A. Melendres and A. N. Mansour
To be published in Electrochim. Acta

Identification and Quantification of Phases Formed during the Processing of $(Bi,Pb)_2Sr_2Ca_2Cu_3O_x$/Ag Composite Conductors
N. Merchant, A. K. Fischer, V. A. Maroni, W. L. Carter, and R. Parrella
To be published in IEEE Trans. on Applied Superconductivity

Applicability of DC Relaxation Techniques to Multistep Reactions
Z. Nagy, N. C. Hung, K. C. Liddell, M. Minkoff, and G. K. Leaf
To be published in J. Electroanal. Chem.

Energy, Resources, Conversion, and Utilization
W. F. Podolski, S. A. Miller, D. K. Schmalzer, A. G. Fonseca, V. Conrad, D. E. Lowenhaupt, J. D. Bacha, L. D. Bacha, L. K. Rath, H. P. Loh, E. B. Klunder, H. G. Mcllvried, G. J. Stiegel, R. D. Srivastava, P. J. Loftus, C. E. Benson, J. M. Wheeldon, and M. Krumpelt
To be published in the Seventh Edition of *Perry's Handbook of Chemicl Engineering*, Ed., D. Green, McGraw-Hill, New York, Section 27

Toroids in NMR Spectroscopy
J. W. Rathke, R. J. Klingler, R. E. Gerald, K. W. Kramarz, and K. Woelk
To be published in Prog. Nucl. Magn. Reson. Spectrosc.

Off-Specular X ray Scattering Studies of the Morphology of Thin Films
S. K. Sinha, Y. P. Feng, C. A. Melendres, D. D. Lee, T. P. Russel, S. K. Satija, E. B. Sirota, and M. K. Sanyal
To be published in Phys. B

Theoretical Study of the Potential Energy Surface of Diglyme
A. Sutjianto and L. A. Curtiss
To be published in Chem. Phys. Lett.

The Structural Stability of Transition Metal Oxide Insertion Electrodes for Lithium Batteries
M. M. Thackeray
To be published in *Handbook of Energy Materials*, VCH Verlagsgesellschaft mbH, Germany

Physical and Chemical Characterization of Actinides in Soil from Johnston Atoll
S. F. Wolf, J. K. Bates, E. C. Buck, N. L. Dietz, J. Fortner, and N. R. Brown
To be published in Environ. Sci. Technol.

Chemical Studies of H Chondrites—VIII. On Contemporary Meteoroid Streams
S. F. Wolf, M.-S. Wang, R. T. Dodd, and M. E. Lipschutz
To be published in J. Geophys. Res.—Planets

Application of Neutron Activation Analysis in a Fission Molybdenum Separation Study
D. Wu, S. Landsberger, and G. F. Vandegrift
To be published in J. Radioanal. Nucl. Chem.

Raman Microscopy Examination of Phase Evolution in Bi(Pb)-Sr-Ca-O Superconducting Ceramics
K. T. Wu, A. K. Fischer, V. A. Maroni, and M. W. Rupich
To be published in J. Mater. Res.

X-ray Scattering Study of Porous Silicon Growth during Anodic Dissolution
H. You, Z. Nagy, and K. Huang
To be published in Phys. Rev. Lett.

Distribution for ANL-97/13

Internal:

J. P. Ackerman
J. G. Asbury
A. J. Bakel
J. K. Bates
J. E. Battles
P. R. Betten (5)
I. D. Bloom
A. S. Boparai
D. L. Bowers
L. M. Boxberger
E. C. Buck
F. A. Cafasso
D. J. Chaiko
D. B. Chamberlain
Y. I. Chang
L. D. Chipman
J. C. Cunnane
D. W. Dees
L. W. Deitrich
W. H. DeLuca
H. Drucker
B. D. Dunlap
D. E. Eastman
W. L. Ebert
P. A. Finn
J. Fortner
S. C. Foster
F. Y. Fradin
E. C. Gay
D. G. Graczyk
D. W. Green
D. M. Gruen
J. E. Harmon (5)
J. E. Helt
G. L. Henriksen
C. E. Johnson
G. K. Johnson
L. R. Johnson
E. J. Karell
T. D. Kaun
T. R. Krause
M. Krumpelt
R. Kumar
J. J. Laidler (75)
L. Leibowitz
R. A. Leonard
L. G. LeSage
M. A. Lewis
P. C. Lindahl
M. J. Lineberry
J. S. Luo
R. F. Malecha
V. A. Maroni
S. M. McDeavitt
W. D. McFall
C. C. McPheeters
J. F. Miller
W. E. Miller
T. P. Mulcahey
K. M. Myles
L. Nuñez
C. A. Osolin
C. Pereira
W. H. Perry
W. F. Podolski
R. B. Poeppel
J. W. Rathke
D. T. Reed
N. F. Sather
W. W. Schertz
D. K. Schmalzer
J. A. Smaga
D. L. Smith
M. J. Steindler
D. M. Strachan
W. M. Swift
S.-W. Tam
M. Thackeray
M. C. Thurnauer
C. E. Till
Z. Tomczuk
G. F. Vandegrift
D. R. Vissers
D. C. Wade
L. C. Walters
R. W. Weeks
C. L. Wilkinson
J. L. Willit
S. F. Wolf
A. M. Wolsky
R. D. Wolson
D. J. Wronkiewicz
TIS Files

External:

DOE-OSTI , per distribution per UC-400 and -500 (74)
ANL-E Library
ANL-W Library
Manager, Chicago Operations Office, DOE
R. C. Baker, DOE-CH
A. Bindokas, DOE-CH
J. C. Haugen, DOE-CH

A. L. Taboas, DOE-CH
S. L. Webster, DOE-CH
J. R. LaFevers, DOE-UC
S. Ludwig, DOE-ARG
Chemical Technology Division Review Committee Members:
H. U. Anderson, University of Missouri-Rolla, Rolla, MO
E. R. Beaver, Monsanto Company, St. Louis, MO
D. L. Douglas, Consultant, Bloomington, MN
R. K. Genung, Oak Ridge National Laboratory, Oak Ridge, TN
J. G. Kay, Drexel University, Philadelphia, PA
R. A. Osteryoung, North Carolina State University, Raleigh, NC
G. R. St. Pierre, The Ohio State University, Columbus, OH
R. C. Alkire, University of Illinois, Champaign, IL
J. Allison, Westinghouse Savannah River Company, Aiken, SC
T. D. Anderson, USDOE, Office of Science and Technology, Germantown, MD
R. A. Bajura, USDOE, Federal Energy Technology Center, Morgantown, WV
S. Barker, Lockheed Martin Hanford Company, Richland, WA
S. E. Berk, USDOE, Office of Fusion Energy, Germantown, MD
E. Beyma, USDOE, Office of Special Technologies, Germantown, MD
A. L. Boldt, Lockheed Martin Hanford Company, Richland, WA
S. S. Borys, Gas Research Institute, Chicago, IL
D. F. Bowersox, Los Alamos National Laboratory, Los Alamos, NM
E. Brueckner, US CAR, Dearborn, MI
S. A. Butter, USDOE, Office of Basic Energy Sciences, Washington, DC
L. Camara, MC Power Corporation, Burr Ridge, IL
M. H. Campbell, MACTECH, Richland, WA
K. A. Chacey, USDOE, Office of Environmental Management, Germantown, MD
S. G. Chalk, USDOE, Office of Transportation Technologies, Washington, DC
L. Christensen, Process Technologies Lab., 3M/Corporate Research Laboratories, St. Paul, MN
S. W. Chun, USDOE, Federal Energy Technology Center, Pittsburgh, PA
J. D'Ambrosia, EnviroTech Associates, Inc., Rockville, MD
P. Davis, USDOE, Office of Transportation Technologies, Washington, DC
C. Donnelly, 3M Center, St. Paul, MN
J. J. Eberhardt, USDOE, Office of Transportation Technologies, Washington, DC
R. E. Erickson, USDOE, Office of Environmental Management, Germantown, MD
G. Escobar, LATO Office, Rocky Flats Plant, Golden, CO
R. C. Ewing, University of Michigan, Ann Arbor, MI
R. J. Fiskum, USDOE, Building Equipment Division, Washington, DC
C. W. Frank, USDOE, Office of Science and Technology, Washington, DC
M. W. Frei, USDOE, Office of Waste Management, Germantown, MD
T. Fryberger, Pacific Northwest National Laboratory, Richland, WA
D. R. Funk, USDOE, Office of Nuclear Energy, Germantown, MD
D. Geiser, USDOE, Office of Technology Development, Germantown, MD
M. R. Ghate, USDOE, Federal Energy Technology Center, Morgantown, WV
R. Gilchrist, Pacific Northwest National Laboratory, Richland, WA

R. Goldstein, Electric Power Research Institute, Palo Alto, CA
Government Documents Department, University of California, Berkeley, CA
T. J. Gross, USDOE, Office of Transportation Technologies, Washington, DC
H. Haskins, Ford Motor Company, Dearborn, MI
D. Haught, USDOE, Nevada Operations Office, Las Vegas, NV
K. L. Heitner, USDOE, Office of Transportation Technologies, Washington, DC
T. M. Hohl, Lockheed Martin Hanford Company, Richland, WA
R. A. Hunter, USDOE, Office of Nuclear Energy, Washington, DC
G. Jansen, Lockheed Martin Hanford Company, Richland, WA
L. J. Jardine, Lawrence Livermore National Laboratory, Livermore, CA
E. F. Johnson, Princeton University, Princeton, NJ
E. Jones, Pacific Northwest National Laboratory, Richland, WA
F. Kane, University of Idaho, Moscow, ID
R. D. Kelley, USDOE, Office of Basic Energy Sciences, Germantown, MD
C. Kincaid, USDOE, Office of Nonproliferation and National Security, Washington, DC
R. Kinney, 3M Industrial and Electronic Sector Research Laboratory, 3M Center, St. Paul, MN
R. S. Kirk, USDOE, Office of Transportation Technologies, Washington, DC
B. Knutson, Lockheed Martin Hanford Company, Richland, WA
L. J. Krause, 3M Industrial and Electronic Sector Research Laboratory, 3M Center, St. Paul, MN
K. Krist, Gas Research Institute, Chicago, IL
A. R. Landgrebe, USDOE, Office of Transportation Technologies, Washington, DC
S. C. T. Lien, USDOE, Office of Technology Development, Germantown, MD
G. J. Lumetta, Pacific Northwest National Laboratory, Richland, WA
J. E. Lytle, USDOE, Office of Nuclear Materials and Facility Stabilization, Washington, DC
T. Marechaux, USDOE, Office of Transportation Technologies, Washington, DC
P. Marpin, USDOE, Office of Energy Research, Germantown, MD
B. P. McGrail, Pacific Northwest National Laboratory, Richland, WA
J. Milliken, USDOE, Office of Transportation Technologies, Washington, DC
A. C. Muscatello, LATO Office, Rocky Flats Plant, Golden, CO
C. Nalezny, USDOE, Office of Environmental Management, Germantown, MD
R. J. Nowak, DARPA/DSO, Defense Sciences Office, Arlington, VA
J. B. O'Sullivan, Electric Power Research Institute, Palo Alto, CA
A. L. Olson, Lockheed Idaho Technology Company, Idaho Falls, ID
J. Owendoff, USDOE, Office of Environmental Restoration, Washington, DC
P. G. Patil, USDOE, Office of Transportation Technologies, Washington, DC
R. Paur, Army Research Office, Research Triangle Park, NC
D. Pepson, USDOE, Office of Waste Management, Germantown, MD
L. Petrakis, Brookhaven National Laboratory, Upton, NY
S. T. Picraux, Sandia National Laboratories, Albuquerque, NM
W. M. Polansky, USDOE, Division of Advanced Energy Projects, Germantown, MD
C. Purdy, USDOE, Office of Technology Development, Germantown, MD
G. Reddick, Lockheed Martin Hanford Company, Richland, WA
S. Rogers, USDOE, Office of Transportation Technologies, Washington, DC
P. Rosenfeld, Chrysler Corporation, Auburn Hills, MI
G. Rudins, USDOE, Office of Fossil Energy, Germantown, MD

R. L. San Martin, USDOE, Dep. Asst. Secy. for Renewable Energy, Washington, DC
P. S. Schaus, Lockheed Martin Hanford Company, Richland, WA
W. C. Schutte, USDOE, Office of Technology Development, Germantown, MD
L. H. Schwartz, National Institute of Standards and Technology, Gaithersburg, MD
A. W. Searcy, Lawrence Berkeley Laboratory, Berkeley, CA
R. W. Shivers, USDOE, Div. of Energy Utilization Research, Washington, DC
R. R. Shockley, Illinois Clean Coal Institute, Carterville, IL
J. S. Siegel, USDOE, Office of Fossil Energy, Germantown, MD
W. A. Siegel, USDOE, Office of Transportation Technologies, Washington, DC
A. Simmons, USDOE, Las Vegas, NV
M. I. Singer, USDOE, Advanced Research/Special Technologies, Washington, DC
S. Singhal, Westinghouse Electric Corporation, Pittsburgh, PA
E. Slaathug, Lockheed Martin Hanford Company, Richland, WA
C. Sloane, GM Research and Development Center, Warren, MI
F. D. Stevenson, USDOE, Office of Basic Energy Sciences, Germantown, MD
R. B. Stout, Lawrence Livermore National Laboratory, Livermore, CA
J. P. Strakey, USDOE, Pittsburgh Energy Technology Center, Pittsburgh, PA
R. A. Sutula, USDOE, Office of Transportation Technologies, Washington, DC
R. Swaroop, Electric Power Research Institute, Palo Alto, CA
J. C. Tseng, USDOE, Office of Environmental Management, Germantown, MD
G. P. Turi, USDOE, Office of Environmental Management, Germantown, MD
J. A. Turi, USDOE, Office of Environmental Management, Germantown, MD
M. P. Whelan, Gas Research Institute, Chicago, IL
M. Williams, USDOE, Federal Energy Technology Center, Morgantown, WV
R. Witschonke, Ford Motor Company, Dearborn, MI
K. Yeager, Electric Power Research Institute, Palo Alto, CA
R. E. York, General Motors Corporation, Warren, MI
R. J. Harrison, Atomic Energy of Canada, Ltd., Chalk River, Ontario, CANADA
M. Ozawa, Tokai-Works, Ibaraki-ken, JAPAN